ST.PETERSBURG STATE UNIVERSITY

Akimova Ekaterina Yurjevna

Mineralogical and geochemical characteristics and fluid regime of corundum-bearing metasomatites of the Belomorian mobile belt (Eastern Fennoscandia)

Scientific specialty 1.6.4. Mineralogy, crystallography.
Geochemistry, geochemical methods of prospecting for mineral resources

DISSERTATION
submitted for the degree of the candidate
of geological and mineralogical sciences

Translation from Russian

Scientific advisor:
Doctor of Geological and Mineralogical
Sciences, Assoc. Prof., S.G. Skublov

Saint-Petersburg
2023

Contents

Introduction

The relevance of research

Corundum is formed in a variety of geological settings, but it is quite rare, because it requires a silica-depleted (otherwise, aluminum is included in aluminosilicates - feldspars, micas) and alumina-saturated environment. According to the modern classification, primary (associated with igneous, metamorphic, and metasomatic rocks) and secondary (associated with placers) corundum deposits are distinguished (Giuliani et al., 2020). Among the primary deposits of corundum, magmatic deposits (deposits of sapphire in alkaline basalts, syenites, and lamprophyres) have been most thoroughly studied. Models for the formation of other types of primary deposits – metamorphic and metasomatic – have not been developed in such detail.

In metamorphic rocks, corundum is formed at high temperatures (amphibolite, granulite, eclogite facies), usually as a result of the transformation of sedimentary rocks rich in alumina - bauxite (emery deposits), as well as basic and ultrabasic rocks (during their metamorphism, basic granulites with corundum are formed), marbles etc. (Chowdhury et al., 2013; Awalt, Whitney, 2016; Giuliani et al., 2020 and references there; Karmakar et al., 2020). Migmatization processes also contribute to the formation of corundum during metamorphism. In this case, associations with corundum usually form in restite (Altherr et al., 1982), but sometimes corundum-containing leucosomes without quartz also form (Raith et al., 2010); corundum in this case is formed as a result of incongruent melting of plagioclase in the presence of aqueous fluid (Kullerud et al., 2012; Karmakar et al., 2017) or as a result of decompression melting of muscovite in the absence of quartz (Li et al., 2020).

Metasomatites with corundum are formed as a result of bimetasomatic desilication of granite-pegmatites or other vein rocks, or granulites with the participation of postmagmatic solutions at contact with ultramafic rocks (Korzhinsky, 1955; Keulen et al., 2014; Fernando et al., 2017). In this case, specific rocks are formed – corundum plagioclasites: plumazites (corundum + intermediate plagioclase) and kyshtymites (corundum + basic plagioclase) (Kolesnik, 1976; Nasedkina, 1977; Vakhrusheva et al., 2016, references in Filina et al., 2019). Contact interaction explains, in particular, the occurrence of corundum in metapelites around ultramafic bodies (Riesco et al., 2005; Yakymchuk, Szilas, 2018; Keulen et al., 2020 and references there).

Corundum is known in products of hydrothermal processing of oceanic basalts (blackwall) (Bucher et al., 2005; Owens et al., 2013; Nozaka et al., 2016 and references therein).

Some manifestations of corundum are associated with the seepage of metasomatizing fluid through permeable zones and its subsequent impact on host gneisses (Beach, 1973; Pajunen, Poutiainen, 1999; Raith et al., 2008; Van Hinsberg et al., 2021), ultramafics (Berger et al., 2010), metacarbonates (Dutrow et al., 2019; Dufour et al., 2007, Terekhov, Akimov, 2013; Kisin et al., 2020 and references therein), but the fluid source in this case often remains debatable.

As can be seen even from a brief review, conditions favorable for the growth of corundum (oversaturation of rocks with alumina and their depletion in silica) can be created in very different conditions. Therefore, the nature of corundum-bearing rocks often turns out to be disputable, as in the case of occurences of corundum-bearing rocks in the Belomorian mobile belt.

Some authors consider the corundum-bearing rocks of the Belomorian belt to be high-alumina metamorphic rocks (Lebedev et al., 1974; Korikovsky, 1979), but most authors support the hypothesis of the metasomatic genesis of rocks with corundum (Bukanov, Lipovsky, 1980; Glebovitsky, Bushmin, 1983; Volodichev, 1990; Drugova, 1999; Serebryakov and Rusinov, 2004; Terekhov, 2007; Khodorevskaya, Varlamov, 2018; Astafiev, Voinova, 2020; Skublov et al., 2020).

In addition, an interesting feature of corundum-bearing rocks of most occurrences is the unusual isotopic composition of oxygen and hydrogen in minerals and rocks in general (Ustinov et al., 2008; Krylov et al., 2011; Vysotsky et al., 2014; Bindeman, Serebryakov, 2011; Bindeman et al., 2014; Herwartz et al., 2015; Zakharov et al., 2019 and references therein).

The largest and most studied occurrence of corundum-bearing rocks in the Belomorian mobile belt is at the Khitoostrov occurrence. Here, the anomaly in the isotopic composition of oxygen and hydrogen is most pronounced: $\delta^{18}O$ in them is up to -27‰, and δD reaches -235‰ (Baksheev et al., 2006; Ustinov et al., 2008, etc.). Therefore, it was the Khitoostrov occurrence that was chosen as the object of research.

Purpose and objectives of the study

The aim of the work was the mineralogical and geochemical characterization of the rocks of the Khitoostrov occurrence with subsequent reconstruction of the physicochemical parameters of their formation (temperature, pressure, composition and source of the fluid involved in mineral formation).

To achieve this goal, the following tasks were identified:

1) Mineralogical and geochemical study of metasomatites and host rocks, establishing relationships between minerals.

2) Characterization of the chemical composition of minerals (major and rare earth elements) and its evolution in the process of metasomatism.

3) Determination of the composition and genesis of the fluid according to the study of fluid inclusions in minerals, the isotope composition of noble gases, Sr-Nd isotope systematics of apatite.

4) Analysis of the information received by the methods of physical and chemical petrology using computer programs.

Actual material

The collection of studied material includes 49 samples collected by the author during field work in 2015-2022, from which 70 transparent polished sections were made. Also, the work also used the materials of P.Ya. Azimov and N.S. Serebryakov, including 20 transparent polished sections. Partly thin sections of Khitoostrov rocks were provided by S.A. Bushmin (153 sections). The collection also includes monomineral fractions from Khitoostrov rocks (25 samples), including 6 apatite samples for geochemical and isotope-geochemical studies, 14 petrochemical samples, 11 samples for noble gas isotope analysis, 6 of which were provided by P.Ya. Azimov.

The personal contribution of the author includes direct participation in field work and selection of stone material, independent petrographic description of thin sections, processing of microprobe and other analytical data, study of fluid inclusions, work with computer programs for thermodynamic modeling, processing of isotope-geochemical data, interpretation of the results and their presentation in the form of oral presentations and articles in scientific periodicals.

Research methodology

Field geological mapping with the selection of reference samples, including with the help of a diamond petrol cutter.

The composition of the rocks. The content of petrogenic (main) elements in the rocks was analyzed by X-ray spectral fluorescence (XRF) on an ARL-9800 multichannel spectrometer according to the standard method (VSEGEI, St. Petersburg). The lower limit of determination of oxides of petrogenic elements is 0.01–0.05%. Bulk analyzes of rocks for trace and rare earth elements (REE) were carried out by inductively coupled plasma mass spectrometry (ICP-MS) on an ELAN-DRC-6100 quadrupole mass spectrometer according to the standard method (VSEGEI). In this case, the relative error in determining the elements does not exceed 5–10%. Rock compositions are given in Appendix 2.

Mineral diagnostics. Primary diagnostics of minerals was carried out using optical microscopy. To determine the compositions of the minerals of the studied rocks, transparent polished thin sections were made. Mineral compositions were determined on a Hitachi S-3400N scanning electron microscope with an AzTec Energy 350 energy-dispersive spectrometer and a set of standard samples at the Geomodel Research Center of St. Petersburg State University

(analysts V.V. Shilovskikh and N.S. Vlasenko) and on a JSM-6510LA scanning electron microscope with a JED-2200 (JEOL) energy-dispersive spectrometer and a set of reference materials at the IPGG, Russian Academy of Sciences (analyst O.L. Galankina). The compositions of minerals are given in Appendix 3. The calculation of crystal chemical formulas of minerals from microprobe analyzes was carried out using the Minal3 program (author – D.V. Dolivo-Dobrovolsky), which implements well-known methods for calculating crystal chemical formulas of minerals (Bulakh et al., 2014). Mineral symbols are from Whitney and Evans (2010).

The content of REE in minerals was measured in the same areas (crater diameter of about 20 μm) as the oxides of the main elements, using the Cameca IMS-4f ion microprobe at the JB PTIAS (analysts S.G. Simakin, E.V. Potapov) using the standard method. Shooting conditions: the primary ion beam is used, the diameter of which is approximately 15–20 μm; ion current 5–7 nA; accelerating voltage of the primary beam 15 keV. Each measurement consisted of three cycles, which made it possible to evaluate the reproducibility of the measurement results. The total time of analysis of one point averaged 30 min. The size of the studied area of the mineral did not exceed 15–20 μm in diameter; the relative measurement error for most elements was 10–15%; the element detection threshold is on average 10 ppb. When constructing the distribution spectra of REE, their composition was normalized to the composition of CI chondrite (McDonough, Sun, 1995).

Analysis of apatite samples for trace and rare earth elements (REE) was carried out by inductively coupled plasma mass spectrometry (ICP-MS) on an ELAN-DRC-6100 quadrupole mass spectrometer according to the standard method (VSEGEI). In this case, the relative error in determining the elements does not exceed 5–10%. To plot the REE distribution spectra, the composition of apatites was normalized to PAAS (Pourmand et al., 2012), and for other geochemical constructions, to the composition of chondrite CI (McDonough, Sun, 1995). The results of the analyzes are given in Appendix 4.

Microthermometric studies were carried out using a Linkam THMSG 600 thermocryometric setup and an Olympus BX51 microscope operating in the temperature range from –196 to +600°C. Temperature changes were monitored using the Linksys 32 software module. Cryometric studies make it possible to determine the phase, including the salt composition of fluid inclusions (eutectic temperature), as well as to determine the salt concentration (melting temperature of the last ice crystal) (Rödder, 1987). The table in (Borisenko, 1977) was used to identify the salt composition of water-salt fluid inclusions. For salinity calculation - software tools (Steele-MacInnis et al., 2011, Bakker, 2018). A summary table of microthermometric data is given in Appendix 5.

Raman spectrometry has been used to diagnose some minerals, as well as to establish the phase composition of the content of fluid inclusions in minerals of corundum-bearing and associated rocks. In addition to transparent polished sections, fluid inclusions were studied in plates about 0.3 mm thick, polished on both sides. The study was carried out at the Geomodel resource center on a Horiba Jobin-Yvon LabRam HR800 Raman spectrometer with an Olympus BX41 microscope, a 50x objective, an argon ion laser was used, notch filters were used to work at 488 nm and 514 nm with a power of up to 50 mW (analyst – Bocharov V.N.). The spectra of minerals were identified by comparison with the database in the Crystal Sleuth program, and fluid inclusions were identified using data from Frezzotti (Frezzotti et al., 2012). Partly data on fluid inclusions was also obtained using a RamMix M532 Raman spectral analyzer with a microscope at the IPGG RAS.

The isotope composition of noble gases from fluid inclusions in minerals of corundum-bearing rocks of the Khitoostrov occurrence was determined in bulk samples and in monomineral fractions (corundum, garnet, calcium amphibole, and staurolite). The isotopic composition of light noble gases in bulk samples was determined at the Central Research Institute of VSEGEI using the vacuum crushing technique to extract trapped gases from fluid inclusions and subsequent measurements on a Micromass NG-5400 isotope gas static mass spectrometer (Prasolov et al., 2011) (analyst – K .A. Gruzdov). This technique makes it possible to carry out crushing in glass ampoules on a separate vacuum unit, after which the ampoules are transferred to the mass spectrometer sample preparation system and opened using a revolving ampoule breaker. The initial size of rock fractions was 0.3 mm; after crushing, it was less than 10 microns. After purification of the released gases from reactive gases using two NuproNP-50 getter pumps, the cryogenic separation of the He+Ne and Ar+Kr+Xe fractions was carried out on activated carbon at liquid nitrogen temperature. In the isolated fractions, the isotope ratio $^{3}He/^{4}He$, elemental $^{4}He/^{20}Ne$, and isotope ratio $^{40}Ar/^{36}Ar$, respectively, were measured. Correction for mass discrimination and estimation of the amount of gases were carried out by comparison with an atmospheric noble gas standard. The peak intensities of the ^{4}He, ^{20}Ne, and ^{40}Ar ion currents were measured using a Faraday collector with an error no worse than 10%. The $^{40}Ar/^{36}Ar$ isotope ratio was measured using a Faraday collector with an error no worse than 1.5%, the intensity of the ^{3}He ion current was measured using a Daly detector, the error in measuring the $^{3}He/^{4}He$ isotope ratio at the atmospheric isotope composition of helium was no worse than 5%, with the isotope ratio about 5×10^{-8} – no worse than 20%.

The isotopic composition of light noble gases and some volatiles (CO_2 and N_2) in monomineral fractions was determined using the Finesse mass spectrometer system at The Open

University, Milton Keynes, UK using stepwise crushing and stepwise heating techniques (temperature range 200 – 1400°C) (Verchovsky et al, 2002).

When studying *Rb-Sr and Sm-Nd systematics of apatite*, worn samples were preliminarily treated with 0.1N hydrochloric acid solution and dissolved in 1N HCl. Rb and Sr were isolated by ion exchange on a Dowex AG50Wx8 cation exchanger (Gorokhov et al., 1998, 2016). The concentrations of these elements were determined by isotopic dilution mass spectrometric method using a mixed indicator ^{87}Rb-^{84}Sr. The isotopic compositions of Rb, Sr, as well as Sm, Nd were measured on a Triton TI multicollector mass spectrometer in static mode. The average values of $^{87}Sr/^{86}Sr$ in the NIST SRM-987 and USGS EN-1 standard samples, normalized to the ratio $^{86}Sr/^{88}Sr = 0.1194$, were, respectively, 0.710281 ± 0.000004 (2σcp, n = 26) and 0.709211 ± 0.000005 (2σcp, n = 20).

Physicochemical analysis of parageneses was carried out using the Perple_X software package (version Perple_X 6.9.0) (Connolly, 2005). The petrochemical data used for the calculation (see Appendix 1) were previously recalculated for a dry sample, MnO, TiO_2, P_2O_5 and part of CaO corresponding to apatite were subtracted from the composition to simplify the calculation; Fe_2O_3, if present in the composition, was converted to FeO. The thermodynamic database of minerals and fluids hp02ver.dat (Holland and Powell, 1991, 1998) was used in all calculations. Solid solution models were selected (file solution_model.dat): for monoclinic amphibole – Amph(DPW), for orthorhombic amphibole – o-Amph, for garnet – Gt(HP), for staurolite – St(HP), for biotite – Bio(HP), for feldspar – feldspar, for spinel – Sp(HP), for orthopyroxene – Opx(HP), for clinopyroxene – Cpx(HP), for cordierite – hCrd, for muscovite – Mica(M), for chlorite – Chl(HP), for carbonates – Do(HP) and M(HP), for melt – melt(HP) (see description http://www.perplex.ethz.ch/). The chemical potentials of SiO2, Na2O were preliminarily calculated using the frendly thermodynamic calculator included in the software package. Isolines of mineral compositions (isopleths) were constructed using the Werami program included in the Perple_X software package. The technique for constructing diagrams for systems with perfectly mobile components is given in (Goncalves et al., 2012, Manning, 2013). A certain (insignificant) minus of the software package is the incompleteness of thermodynamic data for amphiboles; for example, ferrogedrite, sodic gedrite, and barroisite are absent from the databases.

Theoretical and practical significance

The results obtained by the author can be used in the study of metasomatites in metamorphic complexes, in the study of the geological history of the Belomorian mobile belt, and in regional geological mapping. Information about the physicochemical state of fluids in deep conditions is

important for solving the problems of sources and mechanisms for the transfer of matter, including ore.

Scope and structure of work

The dissertation with a total volume of 158 pages consists of an introduction, seven chapters, a conclusion, a list of references (out of 255 titles), as well as appendices on 17 pages. The dissertation contains 9 tables and 102 figures, as well as 17 tables in 5 appendices.

Approbation of work

On the topic of the dissertation, 5 articles were published in scientific journals indexed in the Scopus and Web of Science databases, as well as 29 conference papers.

The main results of the work were reported at the All-Russian Conference dedicated to the 120th anniversary of the birth of the outstanding Russian scientist Academician D.S. Korzhinsky "Physical and chemical factors of petro- and ore genesis: new frontiers", XXI and XXII symposium on geochemistry of isotopes named after V.I. acad. A.P. Vinogradov, V Russian Conference on the Problems of Geology and Geodynamics of the Precambrian "Geodynamic Settings and Thermodynamic Conditions of Regional Metamorphism in the Precambrian and Phanerozoic", EGU-2020, XIX All-Russian Conference on Thermobarogeochemistry, XIII All-Russian Petrographic Conference and at various youth conferences.

Acknowledgement

The author is grateful to the supervisor S.G. Skublov for valuable comments and constant attention to the work. A.B. Kuznetsov and K.I. Lokhov for help in isotope-geochemical studies. V.A. Glebovitsky and A.B. Kol’tsov for advice and recommendations. E.N. Kozlov (GI KSC RAS), P.Ya. Azimov (IPGG RAS), N.S. Serebryakov (IGEM RAS) for assistance in organizing and conducting field seasons. V.N. Bocharov, N.S. Vlasenko, V.N. Shilovskikh (RC Geomodel, St. Petersburg State University), O.L. Galankina (IPGG RAS) for help in analytical work. Thanks to K.A. Gruzdov and E.M. Prasolov (CIR VSEGEI) made it possible to study the isotopic composition of noble gases. Various aspects of the work were also discussed with A.I. Brusnitsyn (St. Petersburg State University), P.Ya. Azimov, D.V. Dolivo-Dobrovolsky, S.A. Bushmin (IPGG RAS), A.B. Verchovsky (The Open University, UK), A.I. Buikin (GEOKHI RAS), E.A. Vapnik (Ben-Gurion University, Israel). This work was partially supported by the St. Petersburg State University grant 3.42.973.2016 from the funds of Activity 6 and the RFBR grant 17-05-00265.

List of main works on the topic of the dissertation

Articles

1. Akimova E.Yu., Skublov S.G. (2023) Mineralogy of clinozoisite amphibolites in the Khitoostrov occurrence of corundum-bearing rocks (Fenno-Scandinavian shield). Zapiski RMO. V. CLII. № 3. P. 59–81.

2. Akimova E.Yu., Kol'tsov A.B. (2022) Thermodynamic modeling of the formation of corundum-bearing metasomatic rocks in the Belomorian mobile belt, Fennoscandian shield. Petrology. V. 30. № 1. P. 60–81.

3. Akimova E.Yu., Skublov S.G. (2021) Distribution of rare earth elements in rock-forming minerals of corundum-bearing rocks of the Khitoostrov deposit (Northern Karelia). Bulletin of St. Petersburg State University. Earth Sciences. V. 66. № 4. P. 686–705.

4. Akimova E.Yu., Kozlov E.N., Lokhov K.I. (2017) Origin of corundum rocks of the Belomorian mobile belt: Evidence from noble gas isotope geochemistry. Geochemistry International. V. 55. № 11. P. 1000–1009.

5. Lokhov K.I., Prasolov E.M., Akimova E.Yu., Lokhov D.K., Bushmin S.A. (2016) Isotopic and elemental fractionated He, Ne, and Ar in the fluid Inclusions of minerals from metamorphic rocks of the Northern Karelia with anomalous isotopic light oxygen: isotopic fractionation in endogenous fluid by thermodiffusion with cascading. Bulletin of St. Petersburg State University. Series 7: Geology and geography. № 1. P. 29–47.

Conference papers

1. Akimova E.Yu. Fluid inclusions in corundum-bearing and host rocks of the Khitoostrov occurrence (Northern Karelia) // Proceedings of the XIX All-Russian Conference on Thermobarogeochemistry. IGM SB RAS. Novosibirsk. 2022. P. 5–6.

2. Akimova E.Yu., Koltsov A.B. Genesis of corundum-bearing rocks of the Belomorian mobile belt of Eastern Fennoscandia // Petrology and Geodynamics of Geological Processes: Proceedings of the XIII All-Russian Petrographic Meeting (with the participation of foreign scientists). Irkutsk: Publishing House of the Institute of Geography. V.B. Sochavy SB RAS. 2021. V. 1. P. 26–28.

3. Akimova E.Yu., Koltsov A.B. Thermodynamic modeling of desilication during the metamorphism of kyanite-garnet-biotite gneisses of the Chupa sequence (Belomorian mobile belt of Eastern Fennoscandia) // XII International School of Earth Sciences named after Professor L.L. Perchuk. IVS FEB RAS, Petropavlovsk-Kamchatsky. 2020. P. 10.

4. Akimova E., Kol'tsov A. Thermodynamic modeling of the formation of corundum-bearing rocks within the Belomorian mobile belt using Perple_x software // EGU-2020. https://doi.org/10.5194/egusphere-egu2020-327

5. Akimova E.Yu., Azimov P.Ya., Serebryakov N.S. Rare and unusual minerals of corundum-bearing rocks of Khitoostrov (Northern Karelia) // Proceedings of the Kola Scientific Center of the Russian Academy of Sciences. 2019. V. 6 (1). P. 9–15.

6. Akimova E.Yu., Koltsov A.B. Experience in the study of metasomatic processes using the Perple_X software package // Physico-chemical factors of petro- and ore genesis: new frontiers. All-Russian conference dedicated to the 120th anniversary of the birth of the outstanding Russian scientist Academician D.S. Korzhinsky. Conference materials. Moscow: IGEM RAN. 2019. P. 15–17.

7. Akimova E.Yu., Koltsov A.B. Conditions for the formation of corundum-bearing metasomatites of the Khitoostrov occurrence (North Karelia) // X All-Russian School of Young Scientists "Experimental Mineralogy, Petrology and Geochemistry". Chernogolovka, Moscow Region, IEM RAS. 2019. P. 34–36.

8. Akimova E.Yu., Verkhovsky A.B., Lokhov K.I. Helium and argon isotopes from rocks with anomalously isotopically light oxygen (Khitoostrov, North Karelia): data on stepwise fragmentation of corundum crystals // XXII Symposium on Isotope Geochemistry named after academician A.P. Vinogradov. Extended abstracts of reports. GEOKHI RAN. M: Akvarel. 2019. P. 19–23.

9. Akimova E.Yu., Prasolov E.M., Kozlov E.N., Gruzdov K.A., Lokhov K.I. Origin of corundum rocks with ultralight oxygen (Northern Karelia) according to the geochemistry of noble gas isotopes // Proceedings of the XXI Symposium on Geochemistry of Isotopes named after Academician A.P. Vinogradov, Moscow. 2016. P. 321–324.

10. Akimova E., Lokhov K., Helium and argon isotopes in corundum rocks from the Nothern Karelia as indicators of mass-dependent isotopic fractionation in the endogenic fluid // Goldschmidt Conference Abstracts. 2016.

Main scientific results

In corundum-bearing rocks, calcium (tschermakite) and sodium-calcium (barroisite) amphiboles, sodium phlogopite (aspidolite), and paragonite are described for the first time. The clinozoisite amphibolites associated with them contain calcium amphiboles of the tschermakite-pargasite-sadanagaite and margarite series. For the first time, data on the distribution of rare earth elements in rock-forming minerals have been obtained. It has been established that rare earth elements in the process of metasomatism, which led to the formation of corundum-bearing and associated rocks, became mobile: in the case of corundum-bearing rocks, LREE was introduced, and in the case of clinozoisite amphibolites, local redistribution occurred. The substance of fluid inclusions in minerals of corundum-bearing and host rocks was studied for the first time by microthermometry and Raman spectrometry. The isotopic

composition of noble gases was studied by crushing the bulk fractions of rocks and corundum crystals. Data on the isotopic composition of Sr and Nd in apatite have been obtained for the first time. The methods of isotope geochemistry substantiate the deep nature of the fluid that participated in the mineral formation. For the first time, physical and chemical modeling of the metasomatic process that led to the formation of corundum-bearing rocks and associated clinozoisite amphibolites was performed: temperature, pressure, and the regime of perfectly mobile components were quantitatively estimated.

Propositions submitted for defense

1. The zoning of corundum-bearing metasomatites of the Khitostrov occurrence is represented by a regular change of mineral parageneses due to the disappearance of quartz (zone 1) and the successive appearance of reaction minerals: staurolite (zone 2), corundum (zone 3a) or Ca-amphibole (zone 3b) and corundum together with sodic gedrite and Ca-amphibole (zone 4). aspidolite, Ca-amphiboles of the tschermakite-sadanagaite series, and Na-Ca-amphibole (barroisite) were found for the first time in the composition of corundum-bearing rocks.

2. Corundum-bearing metasomatites were formed after the kyanite-garnet-biotite gneisses of the Chupa sequence by its desilication during regional metamorphism (lga_{SiO2} decreases from -0.06 to -0.2) with increased Na activity (A_{Na} increases from 4.38 to 4.88) and decreased K (A_K decreases from 3.35 to 3.11), with the participation of a deep carbon dioxide-water fluid ($X(CO_2)$ about 0.3) containing Na and Ca chlorides.

3. In a number of minerals of corundum-bearing metasomatites (garnet, calcium amphibole, apatite), enrichment in light rare earth elements (LREE) is recorded, which is not manifested in the minerals of host rocks. In clinozoisite metasomatites associated with corundum rocks, the effect of inheritance of the REE distribution was established when garnet was replaced by Ca-amphibole and clinozoisite. The mobility of the LREE was provided by the specific composition of the fluid involved in the mineral formation.

Chapter 1. Geological conditions of occurrence and mineralogical and petrographic diversity of corundum-bearing rocks in the Belomorian mobile belt

1.1. General features of the geological structure of the Belomorian mobile belt

The Belomorian mobile belt (or Belomorian zone, megazone) is a complex linear nappe-thrust structure with a length of more than 1500 km, which is part of the Belomorian–Lapland collisional orogen of the Fennoscandian Shield (Fig. 1). Works of N.G. Sudovikov, K.A. Shurkin, Yu.V. Nagaitsev, V.A. Glebovitsky, O.I. Volodichev, etc. devoted to the study of the Belomorian mobile belt. In early works, the belt was considered as a huge monocline composed of stratified sequences of metamorphosed sedimentary and volcanic rocks (Shurkin et al., 1962). However, later in the works of V.A. Glebovitsky and Yu.V. Miller et al. have shown that the previously distinguished "formations" are in fact covers: Khetolambinsky, Oriyarvinsky, Mayozersky, Keretsky, Kovdozersky and Chupinsky (Miller, Milkevich, 1995; Glebovitsky et al., 1996; Miller, 1997, 2006; Lobach-Zhuchenko et al., 1998).

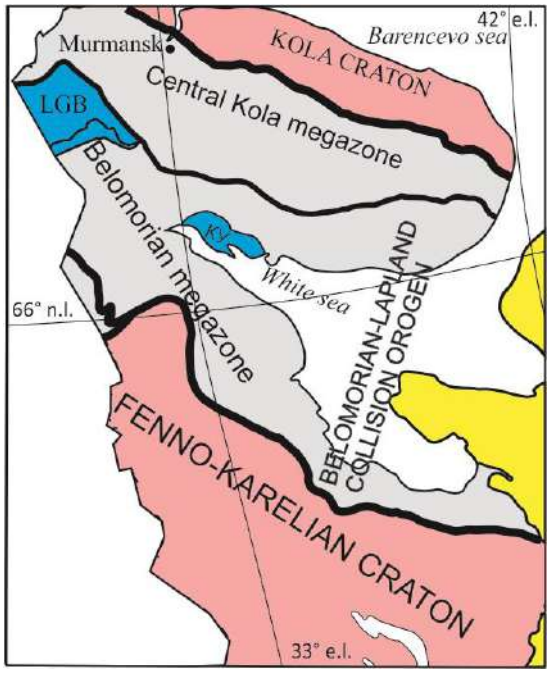

Fig. 1. Location of the Belomorian megazone on the scheme of the tectonic structure of the Russian part of the Fennoscandian Shield (Bushmin and Glebovitsky, 2016).

The Belomorian mobile belt includes greenstone complexes (metamorphosed volcanics, sedimentary-volcanogenic, hypabyssal formations, metasediments and intrusive rocks of the Keretsky, Tiksheozersky, Pebozersky, Ensky, Voche-Lambinsky, Central Belomorsky greenstone belts) and paragneiss complexes (Chupinsky paragneiss belt) (Slabunov, 2008). The latter (Chupinskaya sequence) is located in the axial part of the Belomorian belt and is

represented mainly by supracrustal formations – migmatized garnet-biotite, kyanite-garnet-biotite (aluminous) gneisses. They contain rare interlayers of biotite gneisses (metadacites) and amphibolites (Slabunov, 2008).

There are several varieties of aluminous gneisses: non-migmatized fine-grained garnet-biotite gneisses (“sukhari”), kyanite-garnet-biotite-orthoclase gneisses with microscopic kyanite, kyanite-garnet-biotite gneisses with macroscopic kyanite, kyanite-garnet-biotite gneisses with muscovite (Volodichev, 1975; Ruchyev, 1998, 2005, 2010). Kyanite-bearing gneisses are considered as restite formed during migmatization of the original garnet-biotite gneisses (during migmatization, gneiss restite becomes more aluminous) (Myskova et al., 2000; Early Precambrian…, 2005). According to other authors, kyanite appears due to the “deoxidation” of plagioclase during diaphthoresis (Bibikova et al., 1993; Drugova, 1999). Some researchers associate the formation of small fine needle-shaped kyanite with high pressures during metamorphism, and the appearance of large "cut-off" crystals with acid leaching zones (Shcherbakova, Terekhov, 2004). All authors agree that the kyanite-garnet-biotite gneisses were formed as a result of the superposition of kyanite on the original garnet-biotite gneisses.

The protolith of aluminous gneisses was immature, weakly differentiated graywacke (Balaganskii et al., 1986; Volodichev, 1990; Miller, 1999; Myskova, 2001, 2002; Ruchev, 2000). For some varieties of rocks, tholeiitic basalts were the protolith (Myskova et al., 2003). The age interval of sedimentation within the Belomorian belt is 2.88–2.82 billion years ago, according to U-Pb zircon geochronology (Bibikova et al., 2004). In aluminous gneisses, relict primary sedimentary textures are occasionally preserved (Precambrian…, 2014).

The rocks of the Belomorian complex in general and the Chupa sequence in particular have been repeatedly metamorphosed (Balagansky et al., 1986; Drugova, 1996, 1999; Early Precambrian…, 2005). In works (Bibikova et al., 1993, 1997, 2001, 2004; Bogdanova and Bibikova, 1993; Bibikova et al., 1996; Skublov et al., 2017), several stages of metamorphism were distinguished based on the results of isotope dating:

1. Early Rebol metamorphism 2.88–2.82 Ga associated with subduction under the margin of the Karelian granite–greenstone region. Conditions of metamorphism: T = 700–730ºC, P = 6–7 kbar (Volodichev et al., 2011). Non-migmatized garnet-biotite gneisses (“sukhari”) are classified as rocks of the pre-collision period in the Belomorian mobile belt (Volodichev, 1975).

2. Late Rebol metamorphism 2.74–2.69 Ga from amphibolite to eclogite facies associated with the collision of the Belomorian terranes towards the Karelian granite-greenstone region. Metamorphism conditions: T = 700–780ºC, P = 9–11 kbar (Slabunov et al., 2016). Migmatized garnet-kyanite-biotite-orthoclase gneisses belong to this period (Volodichev, 1975).

3. Svecofennian stage (1.95 - 1.75 billion years). Within it, the Early Svecofennian (1.95–1.85 Ga) high-pressure metamorphism associated with the formation of the Lapland-Kola collisional orogen (Daly et al., 2006) and the Late Svecofennian (1.85–1.75 Ga) low- and moderate-pressure metamorphism of the epidote-amphibolite to granulite facies with diaphthoresis to greenschist facies are distinguished (Grodnitsky, Sibelev, 1995; Sibelev, 1998). Conditions of Early Svecofennian metamorphism: T = 640–765ºC, P = 8–11.7 kbar (Kozlovsky et al., 2016, 2018, 2020). At the late stage of Svecofennian metamorphism (1.78 Ga), pegmatite fields formed (Grodnitskii, 1982; Bibikova et al., 2001).

Rocks of the Belomorian mobile belt, including the Chupa sequence, were repeatedly subjected to migmatization under conditions of amphibolite and granulite metamorphism of elevated pressures (Migmatization and granite formation ..., 1985). The first episode of migmatization (2.73–2.68 Ga) is associated with the formation of the Belomorian collisional orogen, and the second episode (1.97–1.89 Ga) is associated with the development of the Lapland–Kola collisional orogen (Sedova, Glebovitskii, 2005; Glebovitskii, Sedova, 2005; Slabunov et al., 2016). Recently, migmatites with an age of 2.49 billion years have been described in the area of the Tupaya Bay (Glebovitsky et al., 2017).

Two episodes are separated by the stage of intrusion of multiple bodies of magnesian peridotites, norites, gabbroids, traditionally combined into a "drusite" complex. Now it has been subdivided in more detail: complexes of gabbro-anorthosites, lherzolites-gabbronorites, and coronitic gabbro have been identified (Stepanov, 1981; Stepanova et al., 2003, 2011, 2017; Stepanova, Stepanov, 2005; Stepanova, Stepanov, 2010). The implementation of these intrusions occurred in an extension setting at the initial stage of rifting (Rybakov et al., 2000) during the period of 2.5–2.1 Ga. Literature data on whether it was accompanied by metamorphism are contradictory: some authors believe that it was not accompanied (Bibikova et al., 2004), while other authors distinguish the Seletsk stage of metamorphism, synchronous with the emplacement of intrusions (Geology..., 1985; Kolodyazhny, 2006, 2007; Volodichev et al., 2011). During cover plastic deformations associated with the formation of the Lapland-Kola collisional orogen, some of the intrusions were transformed into tectonic plates and boudins (Babarina et al., 2017). The complex of basic intrusions is a reliable benchmark separating the Archean and Paleoproterozoic stages of development of the Belomorian belt.

A number of authors believe that Svecofennian metamorphic processes are mostly nonisochemical due to the interaction of rocks with metamorphic fluids (Kozlovsky, Bychkova, 2016). In addition, the Svecofennian stage of transformation of Belomorian mobile belt rocks is characterized by the wide development of local metasomatism zones associated with shear zones (Bushmin, 1987; Levitsky, 2005; Shcherbakova, Terekhov, 2008; Shevchenko et al., 2009).

Hornblende-staurolite-kyanite-quartz and staurolite-kyanite-quartz acidic, associated with hornblende-staurolite-garnet and staurolite-garnet basic metasomatites (Khizovara type), as well as kyanite-muscovite-quartz, hornblende-anorthite metasomatites are described in the junction zone of Belomorian mobile belt and the Karelian craton (Khizovaara, Vincha, Sharivara, Ryabovaara, Stepanova Lamba, Kukasozero, Lekhta structure, etc.) (Moskovchenko, Turchenko, 1975; Glebovitsky, Bushmin, 1983; Facies of metamorphism…, 1990). Kyanite-gedrite-garnet, hornblende-garnet-kyanite-quartz, garnet-kyanite-quartz metasomatites (Shueretsky type) are known in the area of Shueretskaya Bay (Shurkin et al., 1962; Glebovitsky and Bushmin, 1983; Facies of metamorphism…, 1990). In the mentioned manifestations of metasomatism during acid leaching of amphibolites unusual mineral associations are formed – kyanite + hornblende, staurolite + hornblende (Pinaeva, 1970). The age interval for the formation of metasomatites is 1.9–1.8 Ga (Astafiev et al., 2020; Skublov et al., 2009).

1.2. Mineralogical and petrographic types of corundum-bearing rocks in the Belomorian mobile belt

More than a dozen occurrences of corundum-bearing rocks are known within the Belomorian mobile belt: Khitoostrov, Dyadina Gora, Varatskoye, Kulezhma, Height 128 (Nigrozero), Plotina, Lyagkomina, Mironova Bay (Notozero), Kiy-ostrov, Pulonga, Peruselka, Vazhenka, Klimovskoye, that described in many works (Shurkin et al., 1962; Lebedev et al., 1974; Nagaitsev, 1974; Kievlenko et al., 1983; Terekhov, Levitsky, 1991; Gromov, 1993; Moiseeva, 2002; Serebryakov et al., 2001 ; Serebryakov, Aristov, 2004; Serebryakov, 2004, 2007; Serebryakov, Korpechkov, 2009; Korpechkov, 2009; Kulikov, Kulikova, 1990, etc.). Probably, they also include the occurrence of corundum-bearing rocks of Kittila, located in Finnish Lapland (Haapala et al., 1971).

For the most part, occurrences are located among the rocks of the Chupa sequence or near its contacts, but some (for example, Kiy-ostrov) are located at a considerable distance, including among the amphibolites of the Khetolambinsky sequence (Klimovskoye, Peruselka). Corundum-bearing rocks form lenses, vein-like and sheet-like bodies up to 75 m thick, with uneven, tortuous boundaries. Manifestations are controlled by shear zones; often they are located at the contact of rocks with contrasting compositions: felsic (garnet-biotite and kyanite-garnet-biotite gneisses) and mafic (metagabbro, amphibolites) (Terekhov, Levitsky, 1991).

Within the Belomorian mobile belt, corundum is found in two types of associations (Terekhov, Levitsky, 1991; Serebryakov, 2004):

1. Corundum-bearing rocks after coarse-grained lenticular-banded kyanite-garnet-biotite gneisses (apogneiss type) (Khitoostrov, Varatskoye, Vysota 128, Dam). In rocks of the apogneiss type, in association with corundum, staurolite, which is uncharacteristic of aluminous gneisses of the Chupa sequence, has been described (Shurkin et al., 1962; Yuzhanova, 1975) and the rare mineral sodic gedrite (Serebryakov, 2004). Reactionary relationships between minerals are typical: plagioclase rims between kyanite and quartz in the outer zones, staurolite-plagioclase and corundum-staurolite-plagioclase pseudomorphs after kyanite (Lebedev et al., 1974; Serebryakov, 2004). Based on the analysis of mineral zoning and thermobarometric studies, N.S. Serebryakov and co-authors believe that corundum-bearing rocks were formed as a result of high-temperature high-pressure (600–700ºC, 7–8 kbar) metasomatism, which was accompanied by rock desilication and the addition of Ca and Na (Serebryakov, Rusinov, 2004). The age of corundum-bearing rocks of the apogneiss type, determined by local U-Pb dating of zircon, is 1894±17 Ma (Khitoostrov), 1931±54 Ma (Varatskoe) (Serebryakov et al., 2007; Astafiev, Voinova, 2020).

2. Corundum-bearing rocks after amphibolites and amphibole schists, metaultrabasites (apobasite type) (Dyadina Gora, Varatskoe, Vysota 128, Kulezhma, Peruselka, Vazhenka, Kiy-ostrov, Klimovskoye, Mironova Bay, Pulonga). In rocks of the apobasite type, cordierite, spinel, högbomite, and high-alumina sapphirine occur together with corundum (Sengupta et al, 2004; Serebryakov, 2006). Sapphirine and kornerupine are known in the Kittila occurrence in association with corundum (Haapala et al, 1971). These rocks are also characterized by reactive relationships between minerals: corundum-staurolite-plagioclase pseudomorphs after kyanite, sapphirine-orthoamphibole rims between hornblende and spinel, corundum fouling of sapphirine, högbomite and spinel (Serebryakov, 2004). It is assumed that corundum-bearing rocks of the apobasite type were also formed as a result of high-temperature high-pressure (600–700ºC, 7–8 kbar) metasomatism, accompanied by rock desilication, but with the addition of Mg and K (Serebryakov, 2004). The age of corundum-bearing rocks of the apobasite type coincides within the error with the age of the rocks of the apogneiss type: 1897±23 Ma (Klimovskoye), 1937±23 Ma (Kiy-island) (Serebryakov et al., 2007; Astafiev, Voinova, 2020).

Corundum is also known in completely different rocks of the Belomorian mobile belt – in eclogites and in dumortierite- and phengite-bearing kyanite-biotite-feldspar-quartz "pegmatoid" veins among them (for example, Dokukina et al., 2017), but this type will not be considered in detail.

A characteristic feature of rocks of both types are rare associations of kyanite + hornblende, staurolite + hornblende, which were already mentioned earlier when discussing the

metasomatites of the junction zone of the Belomorian mobile belt and the Karelian craton, are noted at most occurrences of corundum: Khitoostrov, Dyadina Gora, Varatskoe, Vysota 128, Kulezhma, Klimovskoe, Kiy-ostrov, Peruselka (Serebryakov, 2004; Korpechkov, 2009; Khodorevskaya and Varlamov, 2018 and references there). Thus, occurrences of kyanite and staurolite amphibolites in the Belomorian mobile belt (Volodichev, 1990) are associated either with zones of acid and associated metasomatites, or with occurrences of corundum-bearing rocks. The kyanite amphibolites of the large Lyagkomina occurrence (Lutkovskaya, 1971) are similar to the rocks of corundum occurrences (Serebryakov, 2004).

In addition to kyanite and staurolite amphibolites, epidote- and zoisite-bearing metasomatites are closely associated with corundum-bearing rocks of most occurrences (Khitoostrov, Dyadina Gora, Varatskoye, Kulezhma, Vysota 128) (Serebryakov, Korpechkov, 2009). They develop mainly at the expense of corundum-bearing rocks containing calcium amphibole (Serebryakov, Korpechkov, 2009). The authors distinguish zoisite-epidote, zoisite-quartz, less often epidote and quartz-epidote rocks with hornblende, garnet and plagioclase, as well as zoisitized and epidotized varieties of host rocks (the amount of zoisite and epidote in the rock is about 20–40%) (Serebryakov, Korpechkov, 2009). It is assumed that these rocks were formed by acid leaching of rocks at elevated Ca activity (Serebryakov and Korpechkov, 2009). In association with corundum-bearing rocks, chloritites (Dyadina Gora, Peruselka), gedritites (Kulezhma, Varatskoye), and plagioclasites (on all occurrences of corundum-bearing rocks of the apogneissic type) are also known (Serebryakov, 2004, 2006).

Corundum-bearing rocks of most occurrences in the Belomorian mobile belt are characterized by an unusual isotopic composition of oxygen and hydrogen: $\delta^{18}O$ in them reaches -27‰, $\Delta^{17}O$ up to -14‰, and δD drops to -235‰ (Khitoostrov occurrence) (Baksheev et al., 2006, Ustinov et al., 2008, etc.) (Fig. 2).

$\delta^{18}O$ (and, accordingly, δD) is rarely negative in rocks, and therefore it is of interest. A pronounced anomaly ($\delta^{18}O<-10$ ‰) characterizes only single geological objects of the world. For example, UHP – eclogites (eclogites of ultra-high pressures) of Dabi-Sulu in China (up to -10.4‰) (Fu et al., 2013 and references there); skarns from the lead-zinc deposit of Baiyinnuo in Inner Mongolia (-12.5‰) (Baolei et al., 1997); jade rocks of the Chuncheon deposit (-13.6‰) (Yui, Kwon, 2002). Relatively recently, an oxygen isotope anomaly was established in metamorphosed high-alumina rocks of southwestern Transbaikalia (up to -13‰) (Izbrodin, 2014) and in rocks of jade deposits in Eastern Siberia (up to -20‰) (Burtseva et al., 2015).

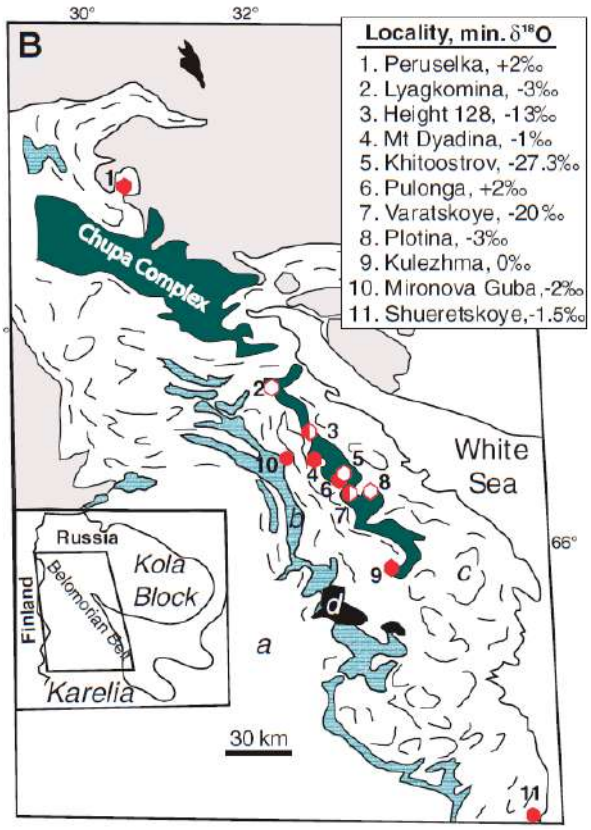

Fig. 2. $\delta^{18}O$ for occurrences of corundum in Belomorian mobile belt (Bindeman et al., 2014).

Negative $\delta^{18}O$ values are typical for high-latitude meteoric and glacial melt waters (Hoefs, 2018). Therefore, when faced with negative $\delta^{18}O$ in rocks, researchers usually postulate the interaction of such rocks with meteoric and glacial melt waters (Hoefs, 2018 and references there). Corundum-bearing rocks of Belomorian mobile belt are no exception. Let us briefly consider the hypotheses put forward by various authors about their origin:

1. The anomaly of the oxygen isotope composition was inherited from the protolith of corundum-bearing rocks, i.e., peculiar weathering crust rocks enriched in the light oxygen isotope due to surface interaction with meteoric waters. Further, weathering crust rocks were buried together with captured meteoric fluid and underwent Svecofennian metamorphism, which had little effect on the oxygen isotopic composition and chemical composition of the rocks (Krylov, Glebovitsky, 2007, 2017; Krylov, 2008; Krylov et al., 2011, 2012; Herwartz et al, 2015).

2. Corundum-bearing rocks represent a fumarole field reworked during the Svecofennian metamorphism, which existed under the glacier. The protolith of corundum rocks in this case are hydrothermal rocks of the propylite type, i.e. a

metasomatic genesis of the protolith of corundum-bearing rocks is assumed (Vysotsky et al., 2008, 2011, 2012, 2014; Yakovenko, 2013).

3. The protolith of corundum-bearing rocks was formed under the influence of fluid formed as a result of the interaction of glacial melt waters with the main intrusions during rifting 2.45 billion years ago. Because in the Paleoproterozoic the White Sea region was in the equatorial region (Lubnina, 2015, 2016), researchers conclude that the Earth was globally glaciated at that time (the Snowball Earth or Slushball Earth hypothesis) (Bindeman et al, 2010, 2014; Bindeman, Serebryakov, 2011; Zakharov et al, 2017, 2019).

Some alternative hypotheses allow the participation of endogenous fluid in the formation of rocks with anomalously isotopically light oxygen (Dubinina et al., 2012).

1.3. Geological characteristics and composition of the rocks of the Khitoostrov occurrence

Khitoostrov is an occurrence of metasomatic corundum-bearing rocks of the apogneiss type (Serebryakov, 2004), located near the southwestern extremity of Upper Pulonga Lake, to the north of the settlement Chupa of Loukhsky district of the Republic of Karelia. The occurrence is located in the northern part of Khitoostrov Island and is controlled by a large flexure-like shear deformation zone, within which the strike of rocks varies from northeast to northwest. In the lock of this flexure, rocks with corundum form a lenticular body 300 × 120 m in size with uneven, tortuous boundaries near the contact of migmatized gneisses of the Chupa sequence with intensely amphibolized gabbros (Fig. 3), whose bodies are turned into boudins (Stepanova et al., 2022; Babarina et al., 2017).

The strata of the host metamorphic rocks are quite homogeneous and are characterized by a relatively simple mineral composition; they are represented by the following varieties: metamorphosed gabbro, migmatized garnet and garnetless amphibolites, migmatized garnet-biotite and kyanite-garnet-biotite gneisses, sometimes with muscovite. The garnet and garnetless amphibolites at the Khitoostrov occurrence probably formed after gabbros as a result of their metamorphism: the degree of amphibolization of gabbroids increases towards the edges of boudins, up to the transformation into migmatized garnet amphibolites without the preservation of igneous minerals.

The body of corundum-bearing rocks is located among the kyanite-garnet-biotite gneisses of the Chupa sequence to the northwest of their contact with a large boudin of amphibolized metagabbro.

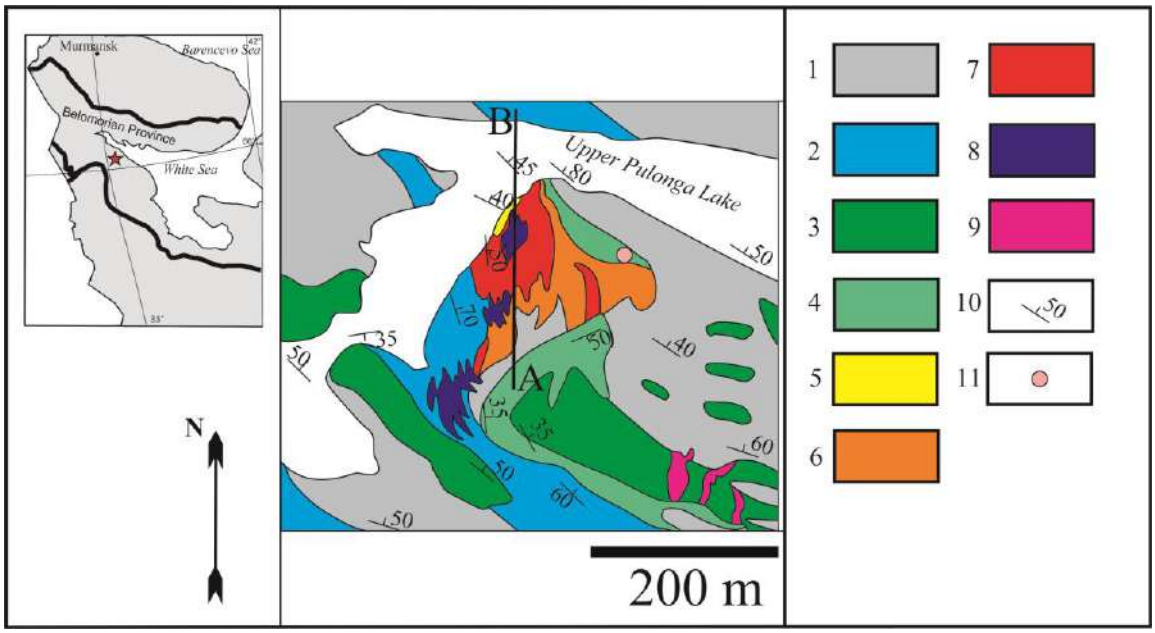

Fig. 3. Schematic map of the geological structure of the Khitoostrov occurrence (after Bindeman et al, 2014, with modifications) with sampling points. 1, 2 – gneisses of the Chupa sequnce (1 – garnet-biotite, 2 – kyanite-garnet-biotite); 3 – metamorphosed gabbro; 4 – migmatized garnet amphibolites; 5 – rocks with parageneses *Pl + Grt + Bt + Ky*, *Pl + Grt + Bt + Crn* (zones 1, 3a) (Akimova and Koltsov, 2022); 6 – rocks with parageneses *Pl + Grt + Bt + St*, *Pl + Grt + St + Cam* (zones 2, 3b); 7 – rocks with *Pl + Grt + Cam + Crn* paragenesis (zone 4); 8 – plagioclasites; 9 – pegmatites; 10 – occurrence elements, 11 – occurrence of clinozoisite amphibolites.

The contacts of the body of corundum-bearing rocks with kyanite-garnet-biotite gneisses are gradual. At contact with the body of corundum-bearing rocks, quartz disappears in gneisses, and kyanite crystals become much larger. No direct contact of corundum-bearing rocks with amphibolites was observed.

The body of corundum-bearing rocks is characterized by a complex zonal structure (Fig. 3, 4). In the marginal part of the body of corundum-bearing rocks on the western flank of the manifestation, in the form of a small lens with fuzzy contours, mesocratic kyanite-garnet-biotite-plagioclase rocks (hereinafter referred to as zone 1) are found, a characteristic feature of which is large kyanite crystals, the absence of quartz. Leucocratic garnet-biotite-plagioclase rocks with staurolite-plagioclase pseudomorphs after kyanite and corundum-staurolite-plagioclase pseudomorphs after kyanite (zone 2) on the southeastern flank are common, as well as leucocratic amphibole-garnet-biotite-plagioclase rocks with similar reaction structures (zone 3b). The northwestern flank also contains mesocratic amphibole-free rocks with large corundum crystals (zone 3a), which then pass into mesocratic gedrite-bearing, two-amphibole (sodicgedrite

+ calcium amphibole) rocks with large corundum crystals (zone 4). The largest crystals of pink translucent corundum (up to 6 cm long, about 1–2 cm wide) are confined to the rocks of zone 4. In addition to corundum, porphyroblasts of garnet (up to 1 cm) and staurolite (up to 2 cm) are found in the rocks of zone 4.

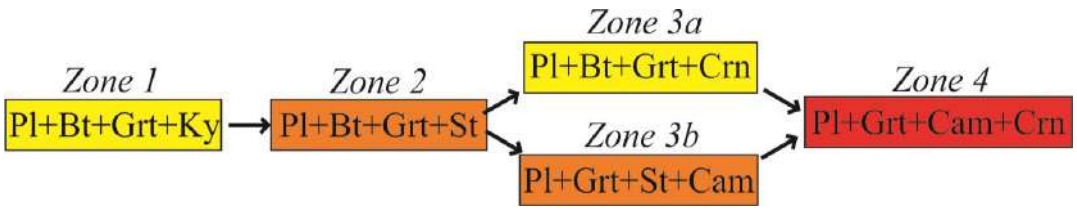

Fig. 4. Scheme of mineral zoning of the body of corundum-bearing rocks at the Khitoostrov occurrence.

The contacts of the zones are, as a rule, gradual and blurry. Thus, at the contact of zones 3a and 4 (observed at point EA22-08), the amount of calcium amphibole gradually increases, which first appears in the form of small lenses located along plagioclase bands.

The rocks of all zones are highly heterogeneous: they are characterized by banding (Fig. 5), which is very similar to migmatite banding in kyanite-garnet-biotite gneisses, but these bands lack quartz and are almost entirely composed of plagioclase.

Often, corundum crystals are located at the contact of these light bands composed of plagioclase and the ground mass; in this case, the growth direction of corundum crystals is from the ground mass towards the leucocratic band. It should be noted that kyanite crystals in zone 1, as well as incomplete plagioclase – staurolite pseudomorphs after kyanite in zones 2, 3b, are also located at the contact of the groundmass and leucocratic bands, and are oriented along the banding.

Fig. 5. Banding of corundum-bearing rocks.

Often, the thickness of these light bands, composed of plagioclase, greatly increases, up to the formation of bodies of anchymonomineral plagioclasites (Fig. 6). The thickness of the bodies of anchymonomineral plagioclasites reaches 20 m, their contacts with the surrounding rocks are often secant, the shape of the bodies is complex, and the boundaries are uneven and winding. Plagioclasites are common among all zones of corundum-bearing rocks. Probably, plagioclasites, like light plagioclase bands, are desilicated leucosomes.

Among migmatized garnet amphibolites in the northern part of the island there is a small body of clinozoisite amphibolites with unclear contours (Khi-008D site). In a small outcrop (about 1.5 meters across), approximately 2 meters north of the body of corundum-bearing rocks, there is a gradual transition from host garnet amphibolites to clinozoisite rocks: first, quartz disappears in garnet amphibolites, the amount of plagioclase sharply decreases, and large differently oriented clinozoisite crystals appear. Below we will refer to these rocks as clinozoisite amphibolites.

Fig. 6. Contact of corundum-bearing rocks (top right) with anchymonomineral plagioclasites (bottom left).

Chemical composition of rocks

The migmatized kyanite-garnet-biotite gneisses of the Chupa Unit, hosting corundum-bearing rocks, the Khitoostrov occurrence are characterized by wide variations in the content of SiO_2 (60–70 wt. %), Al_2O_3 (12–22 wt %), and $MgO + FeO_{tot}$ (4–14 wt. %) at a low CaO content (1.5–5.5 wt. %) (Volodichev, 1975, 1990; Myskova et al., 2001). Wide variations in the composition of kyanite-garnet-biotite gneisses are largely due to varying degrees of migmatization of rocks.

Compared to the host kyanite-garnet-biotite gneisses, the corundum-bearing rocks of Khitoostrov are characterized by a significantly lower content of SiO_2 with a higher content of

Al_2O_3 and MgO + Fe_{tot}. At the same time, in corundum-bearing rocks, as well as in host gneisses, the content of these components varies - in this case, depending on the amount of leucocratic plagioclase layers in the rocks.

If we consider a series of rocks from kyanite-garnet-biotite gneisses and corundum-bearing rocks (from zone 1 to zone 4) to plagioclasites, one can see a regular, directed change in the rock compositions in this series (Fig. 7).

In zone 1 of corundum-bearing rocks (paragenesis *Pl+Bt+Grt+Ky*), there is a sharp decrease in the content of SiO_2, which then remains almost constant in the rocks of zones 2–4 (Fig. 7a). At the same time, the content of Al_2O3 and Na_2O sharply increases in the rocks of zone 1. The content of Na_2O, after a sharp jump in the rocks of zone 1, then somewhat decreases, but still remains higher than in the enclosing kyanite-garnet-biotite gneisses and naturally increases from the rocks of zone 2 to the rocks of zone 4.

The content of CaO in corundum-bearing rocks, namely, in the rocks of zones 1-3a, remains the same as in the enclosing kyanite-garnet-biotite gneisses of the Chupa sequence. In zone 3b, there is a sharp jump-like increase in the content of CaO in the rocks, simultaneously with an equally sharp decrease in the content of K_2O (Fig. 7b).

Plagioclasites are distinguished by a significantly lower content of MgO, FeO_{tot}, and TiO_2, and a higher content of SiO_2, Al_2O_3, and Na_2O (Fig. 7).

Let us now consider variations in the composition of host garnet amphibolites after gabbro and clinozoisite amphibolites. As the degree of amphibolization of gabbroids increases, the content of Si (from 53.2 to 59.4 wt. % SiO_2), Mg (from 4.11 to 7.61 wt. % MgO), Ca (from 7.82 to 10.10 wt. % CaO) gradually increases in them, while Na content decreases (from 4.88 to 1.80 wt. % Na_2O). Thus, one can observe a gradual transition from amphibolized gabbro to garnet amphibolites. Garnet amphibolites are characterized by compositional variations caused by different degrees of migmatization: leucosomes are enriched in Si (74.6 *vs* 56.67 wt. % SiO_2), Na (3.21 wt. % *vs* 2.08 wt. % Na_2O) and, at the same time, depleted in Mg, Fe, and Ca against the background of mesosomes.

The composition of clinozoisite amphibolites significantly differs from the host garnet amphibolites in higher Al content (22 wt.% *vs* 14.44 wt.% Al_2O_3), while clinozoisite amphibolites contain less Si (44.5 wt.% *vs* versus 56.67 wt. % SiO_2), less Na (1.91 wt. % *vs* 2.08 wt. % Na_2O), and somewhat more MgO, FeO, CaO. In terms of Si and (Na + K), the studied rocks correspond to ultramafic igneous rocks of the normal series, but ultramafic rocks, consisting mainly of olivine and pyroxenes, contain much less Al. Aluminous basalts contain less Al, more Si and are not described in the Belomorian region. The igneous rocks closest in Al

content, anorthosites, consist of 90% or more of basic plagioclase and contain significantly less Mg and Fe than the studied rocks.

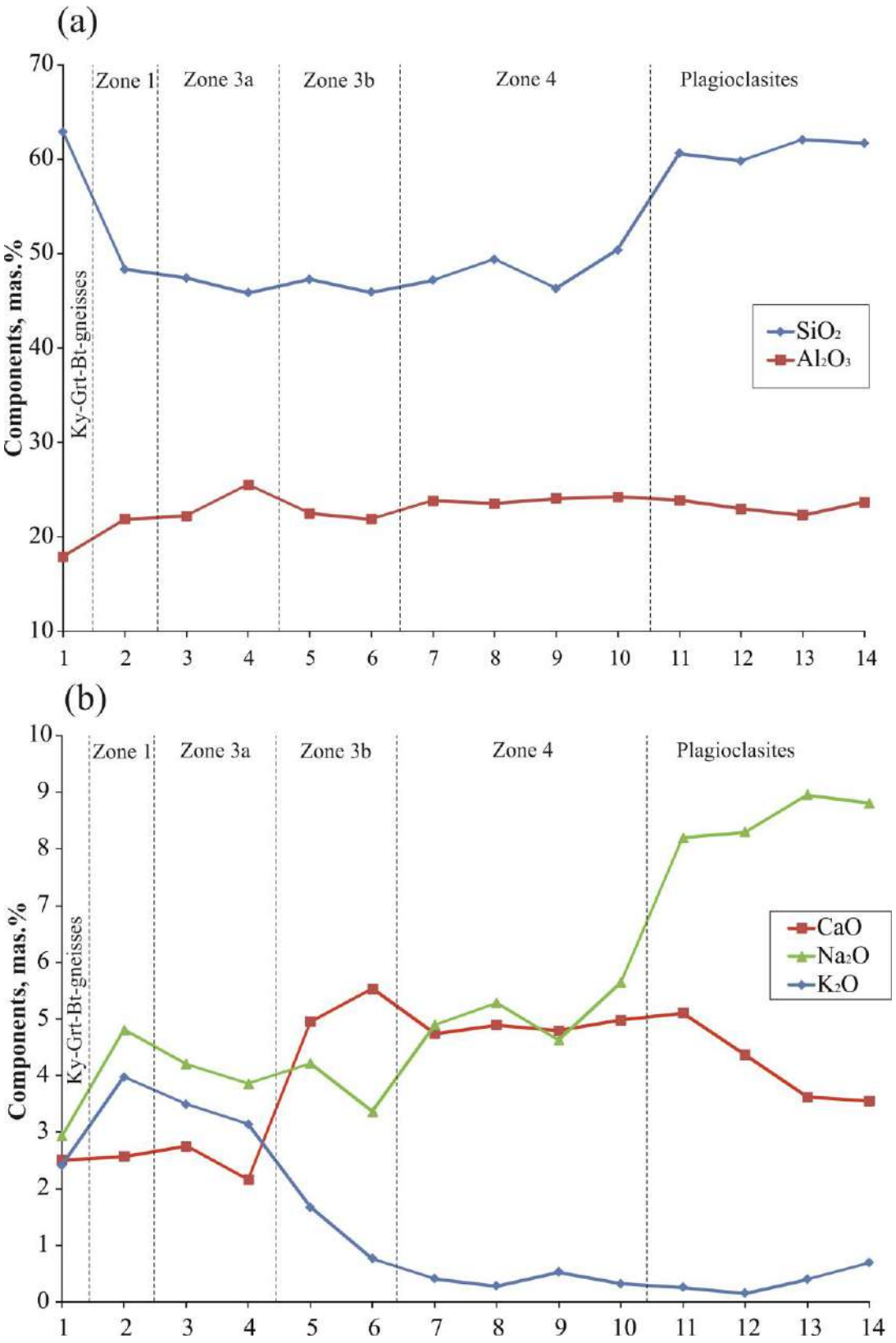

Fig. 7. Variations in the content of some components in the series from host kyanite-garnet-biotite gneisses to corundum-bearing rocks (zones 1–4) and plagioclasites. The numbers indicate the analyzes of the rocks in Table. 1 in Appendix 2.

Conclusions to chapter 1

1. From the review of the literature, it follows that the data on the genesis of corundum-bearing rocks of the Belomorian mobile belt are contradictory, petrological and isotope-geochemical models do not agree with each other; thus, petrological models suggest a deep origin of corundum-bearing rocks, while isotopic-geochemical ones allow the participation of surface waters in mineral formation. It is obvious that a more detailed and versatile study of occurrences of corundum-bearing rocks is necessary.

2. Geological observations lead to the conclusion that the corundum-bearing rocks of the Khitoostrov occurrence are an integral part of a complex zonal body confined to the kyanite-garnet-biotite gneisses of the Chupa sequence. On the northwestern flank of this body rocks with parageneses *Pl + Grt + Bt + Ky, Pl + Grt + Bt + Crn* (zones 1, 3a) are common; on the southeastern flank – rocks with parageneses *Pl + Grt + Bt + St, Pl + Grt + St + Cam* (zones 2, 3b); in the central part of the body – rocks with the *Pl + Grt + Cam + Crn* paragenesis (zone 4).

Chapter 2. Petrography of metasomatites and host rocks of Khitoostrov occurrence

2.1. Petrographic characterization of host rocks

According to the results of petrographic study of thin sections, the metamorphic rocks of the Khitoostrov occurrence are represented by the following varieties: metamorphosed gabbro, apogabbroic garnet and garnet-free amphibolites, garnet-biotite, kyanite-garnet-biotite gneisses, sometimes with muscovite.

(Kyanite)-garnet-biotite gneisses are banded, intensely migmatized fine-medium-grained rocks from dark gray to light gray (Fig. 8a, b), often with lenses of fine-grained garnet-biotite rocks.

a

b

Fig. 8. Gneisses of the Chupa sequence in the outcrop: a – garnet-biotite, b – kyanite-garnet-biotite.

(Kyanite)-garnet-biotite gneisses are composed of the following minerals: biotite – 20–50%, garnet – 10–25%, plagioclase – 15–25%, quartz – 15–35%, kyanite – up to 5%, muscovite, rutile, zircon, opq – single grains. The texture is gneissic, oriented (biotite leaves are oriented), it can also be spotty (light spots are accumulations of quartz and plagioclase), the structure of the rock is granoblastic to porphyroblastic (in places where garnet porphyroblasts are distributed), fine-medium-grained to coarse-grained, uneven-grained. Garnet, biotite are euhedral. Sometimes weak secondary changes in plagioclase (pelitization, sericitization) are diagnosed. Kyanite-garnet-biotite gneisses, in addition to the above minerals, sometimes contain muscovite (0–5%) or potassium feldspar (single grains).

The metamorphosed gabbro is homogeneous, massive, fine-medium-grained dark gray rocks (Fig. 9), slightly migmatized, with only single leucosomes.

Fig. 9. Metagabbro in the outcrop.

The following minerals are found in metamorphosed gabbro: garnet – 5–40%, clinopyroxene – 0–25%, calcium amphibole – 10–60%, plagioclase – 10–40%, biotite – 0–10%, quartz – 5–10%, ilmenite, titanite, allanite are single grains. The texture of the rocks is massive, in some places the primary magmatic (gabbroic) texture is preserved. The structure is granoblastic, medium-fine-grained, uneven-grained. Calcium amphibole, clinopyroxene, garnet, and biotite are euhedral. Calcium amphibole is sometimes observed in the form of clusters surrounding clinopyroxene, ilmenite; ilmenite is also often surrounded by titanite.

Amphibolites are banded, intensely migmatized, highly heterogeneous medium-coarse-grained rocks of light to dark gray color (Fig. 10, 11). They differ from metagabbro in the absence of relics of the primary gabbro structure, a banded texture, and a porphyronematoblast structure (the size of garnet porphyroblasts reaches 3 cm).

Fig. 10. Garnet amphibolites in outcrop (sampling site KHI-008B).

Fig. 11. Garnet-free amphibolites in outcrop

The mineral composition of amphibolites varies: calcium amphibole (40–60%), plagioclase (20–40%), garnet (10–20%), quartz (about 10%), biotite, zircon, titanite, opaque ore minerals – single grains. Sometimes large grass-green clinopyroxene (porphyroblasts up to 1 cm or more) is found in amphibolites. It should be noted that the rocks acquire heterogeneity due to migmatization: in the leucosome, the amount of quartz, plagioclase, and garnet increases significantly, while in the mesosome these minerals are significantly less, but the amount of calcium amphibole increases. The texture is gneissic, banding is pronounced. The structure is granoblastic to porphyroblastic (in varieties with very large garnet), fine-medium-grained to coarse-grained, uneven-grained. Calcium amphibole, garnet are euhedral.

2.2. Petrographic characterization of metasomatite bodies

Thin sections of corundum-bearing rocks contain the following minerals: plagioclase, amphiboles (monoclinic yellowish-green calcium amphibole and yellowish to colorless orthorhombic amphibole – gedrite), biotite, garnet, kyanite, staurolite, corundum, rutile, ilmenite, apatite, zircon, chlorite. According to the results of the petrographic study of thin sections, a number of petrographic varieties of metasomatites were revealed (Table 1). Further, where no clarification is required, we will combine all these varieties into a single complex of corundum-bearing rocks.

Tab. 1. Varieties of metasomatites and associated plagioclasites of the Khitoostrov occurrence. Relic minerals are indicated in parentheses.

Position in zoning	**Mineral associations**
Source gneiss	*Pl + Bt + Grt + Ky + Qz*
Zone 1	*Pl + Bt + Grt + Ky*
Zone 2	*Pl + Bt + Grt + St (no Ky)*
	Pl + Bt + Grt + St
	Pl + Bt + Grt + Ged + St
Zone 3a	*Pl + Bt + Grt + Crn + (St no Ky)*
	Pl + Bt + Crn + (St no Ky)
	Pl + Bt + Grt + Crn + (St)
	Pl + Grt + Crn + (St no Ky)
	Pl + Bt + Grt + Crn + (Ky)
Zone 3b	*Pl + Cam + (Bt) + Grt + St (no Ky)*
	Pl + Cam + (Bt) + Grt + Ged + St (no Ky)
	Pl + Cam + (Bt) + Grt + Ged + St
	Pl + Cam + (Bt) + Grt + St
Zone 4	*Pl + Cam + (Bt) + Grt + Ged + (St) + Crn*
	Pl + Cam + (Bt) + Grt + (St) + Crn
	Pl + Cam + (Bt) + Grt + Crn
	Pl + Cam + (Bt) + Grt + Ged
Plagioclasites	*Pl + Bt + Grt*
	Pl + Bt + Cam
	Pl + Bt + Ms
	Pl + Bt
	Pl + Grt

Note: hereinafter, mineral designations are according to Whitney and Evans, 2010.

According to the mineral composition and ratios of minerals, corundum-bearing rocks are very heterogeneous even on the scale of a thin section (Fig. 12).

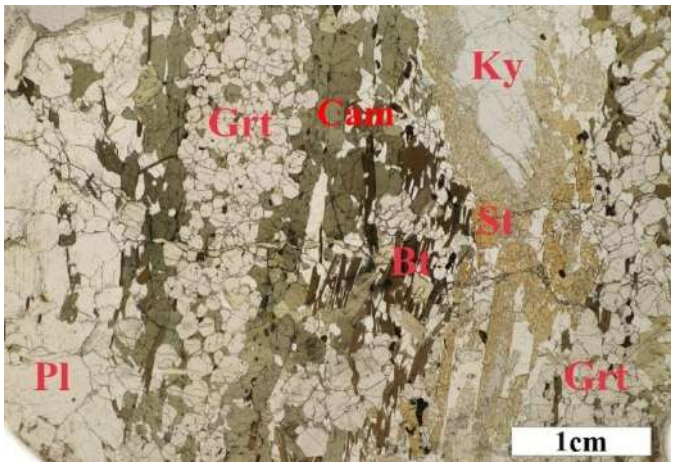

Fig. 12. Heterogeneity of distribution of minerals in thin section of corundum-bearing rock. Section X-26b from the collection of N.S. Serebryakov. Photo in transmitted light, without analyzer.

Zone 1. The rocks of this zone are dark gray banded kyanite-garnet-biotite-plagioclase rocks, similar in appearance to the migmatized kyanite-garnet-biotite gneisses of the Chupa sequence. Their features - the complete absence of quartz and large, up to giant, kyanite crystals (Fig. 13) - are much larger than in the host gneisses. The rocks of this zone are characterized by an oriented texture, granoblastic or porphyroblastic, fine-medium-grained, uneven-grained structure. The following minerals are present: garnet, biotite, kyanite, plagioclase, muscovite, rutile, zircon, opaque ore minerals. Percentages: biotite – 20–50%, garnet – 10–25%, plagioclase – 15–25%, kyanite (about 10%), other minerals – single grains. Garnet and biotite are euhedral.

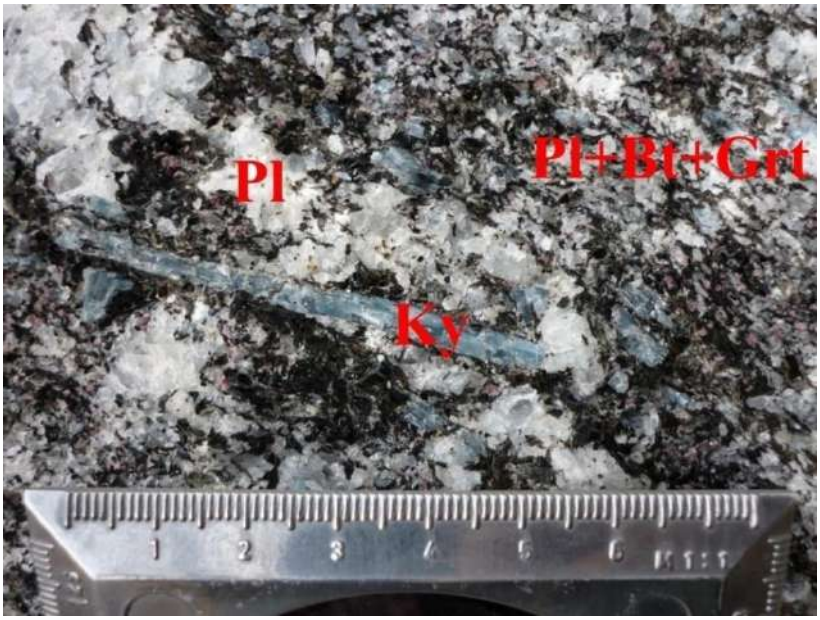

Fig. 13. Large crystal of kyanite in zone 1.

Zone 2. This zone contains garnet-biotite-plagioclase rocks with pseudomorphs of staurolite after kyanite (Fig. 14). The rocks of this zone are characterized by a spotted texture, porphyroblastic structure (porphyroblasts – staurolite, garnet), coarse-medium-grained, uneven-grained.

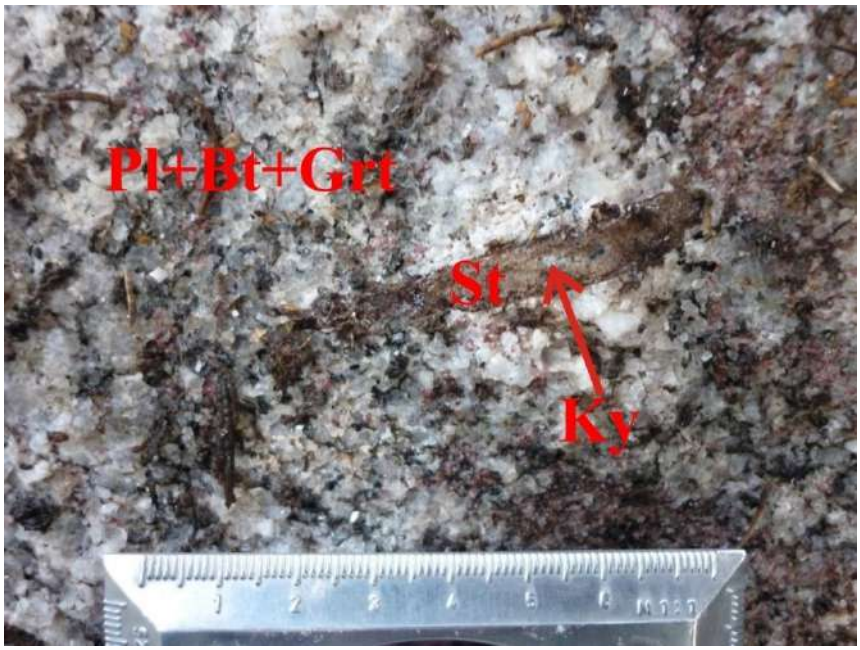

Fig. 14. Incomplete plagioclase-staurolite pseudomorph after kyanite in zone 2.

These rocks are composed of the following minerals: plagioclase – 50%, biotite – 20%, garnet – 15%, staurolite – 10%, kyanite – 5%, ilmenite, rutile, zircon – single grains. Biotite and garnet are euhedral in them. Plagioclase is zonal in places. Reactionary structures are observed in thin sections: large kyanite porphyroblasts are surrounded by plagioclase-staurolite symplectites (Fig. 15) or even completely transformed into them; garnet is separated from staurolite by a plagioclase rim.

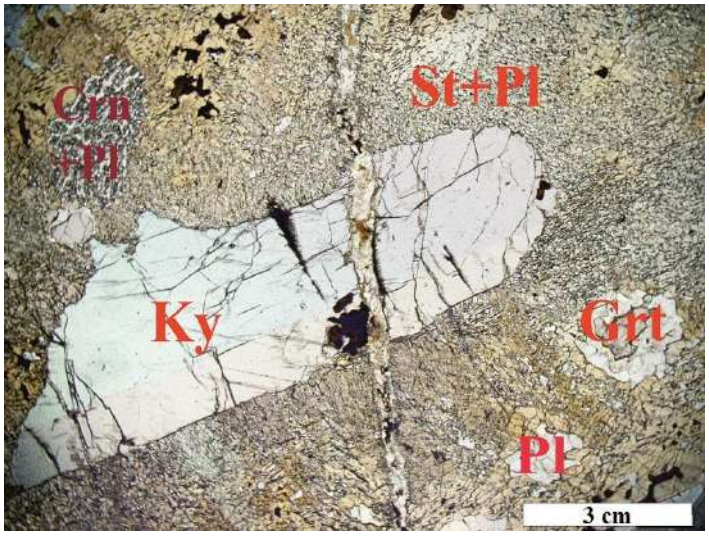

Fig. 15. Plagioclase-staurolite symplectites around a kyanite porphyroblast in zone 2

Zone 3a. The rocks of this zone are characterized by a spotty texture, porphyroblastic structure (porphyroblasts – staurolite, garnet, corundum), coarse–medium–grained, uneven–grained. The rocks are composed of the following minerals: plagioclase – about 50%, biotite – 15–20%, garnet – 10–15%, staurolite – 5–10%, corundum – 5–10%, kyanite – up to 5%, ilmenite, rutile, zircon - single grains. Biotite, garnet are euhedral. Plagioclase is zonal in places. Reaction structures: plagioclase-staurolite symplectites in place of large kyanite crystals, among which corundum-plagioclase symplectites occasionally begin to develop (Fig. 16).

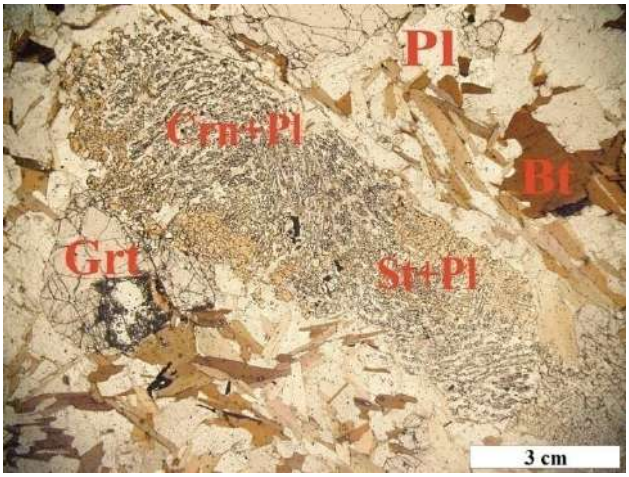

Fig. 16. Plagioclase-staurolite and corundum-plagioclase symplectites in place of a kyanite crystal in zone 3a. Photo in transmitted light, without analyzer.

In this zone, corundum can be present as porphyroblasts 1–2 cm in size. In this case, large corundums are often surrounded by a thin kyanite rim (Fig. 17).

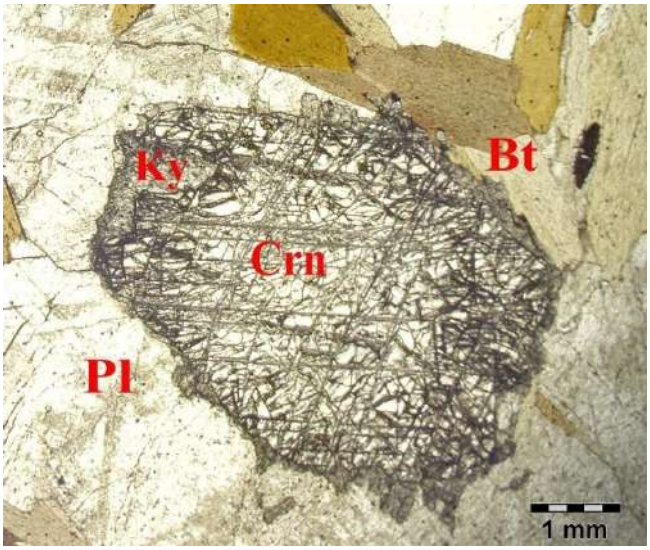

Fig. 17. Large corundum porphyroblast surrounded by a kyanite rim (zone 3a). Photo in transmitted light, without analyzer.

Zone 3b. The rocks of this zone are characterized by a spotted texture, porphyrogranoblastic structure (porphyroblasts – staurolite, garnet), coarse-medium-grained,

uneven-grained. The rocks are composed of the following minerals: plagioclase – 50%, biotite – 10–15%, garnet – 10–15%, staurolite – 5–10%, corundum – 5–10%, kyanite – up to 5%, ilmenite, rutile, zircon – single grains. Calcium amphibole appears in this zone, usually in small amounts (5–10%). Biotite, garnet and calcium amphibole are euhedral. Plagioclase is zonal in places. Reaction structures: large kyanite porphyroblasts are surrounded by plagioclase-staurolite symplectites or even completely transformed into them. Intergrowths of biotite and calcium amphibole are often noted (see below).

Zone 4. Rock texture varies from massive to banded and spotty. The structure is coarse-medium-grained, uneven-grained (the size of garnet grains varies especially strongly – from about 1 mm to 1 cm), granoblastic to porphyroblastic in the presence of large grains of corundum, staurolite, and garnet. Among the main minerals, as a rule, plagioclase prevails, but its amount is extremely variable – from 10 to 80%. Also characteristic are biotite (5–15%), garnet (about 20%), and the amount of calcium amphibole varies from 10 to 40%. Kyanite is absent here, but large corundum crystals appear. It also contains the rare mineral sodic gedrite (Fig. 18), described in the works of predecessors (Serebryakov, 2004). Staurolite occurs occasionally, often as part of symplectites. Garnet, biotite, amphiboles are euhedral. Staurolite porphyroblasts are up to 2 cm in size; there are elongated pink corundum crystals up to 6 cm long and about 1–2 cm wide. In the groundmass of the rock, they are often surrounded by accumulations of calcium amphibole and garnet.

The reaction structures include corundum-plagioclase and sodic gedrite-corundum-plagioclase symplectites around staurolite grains (Fig. 18). Staurolite in such reaction structures, as well as outside them, is sometimes found as relics among orthorhombic amphibole. Apparently, gedrite-corundum-plagioclase symplectites develop after staurolite.

Intergrowths of biotite and calcium amphibole are often noted (Fig. 19). Staurolite in such reaction structures, as well as outside them, is sometimes found as relics among sodic gedrite, as well as among calcium amphibole. Garnet is usually separated from symplectites by a plagioclase rim. Sometimes there are atoll garnets (Fig. 20).

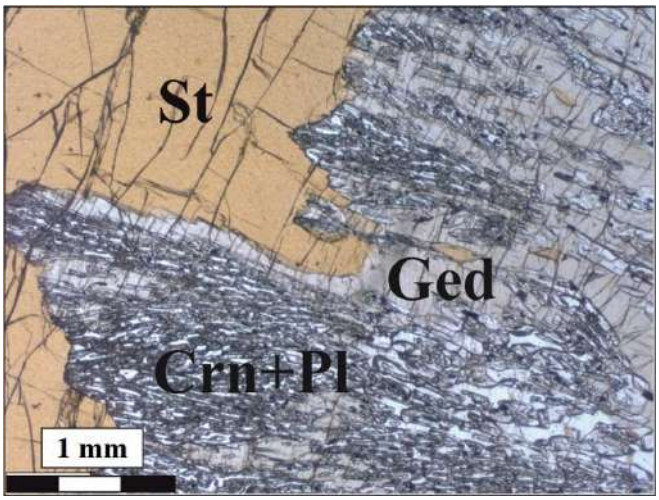

Fig. 18. Corundum-gedrite-plagioclase symplectites in zone 4. Photo in transmitted light, without analyzer.

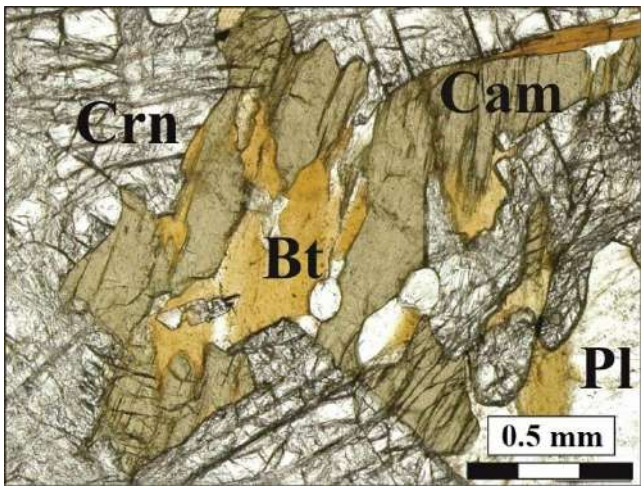

Fig. 19. Reaction intergrowths of biotite and calcium amphibole in corundum-bearing rocks (zone 4). Photo in transmitted light, without analyzer.

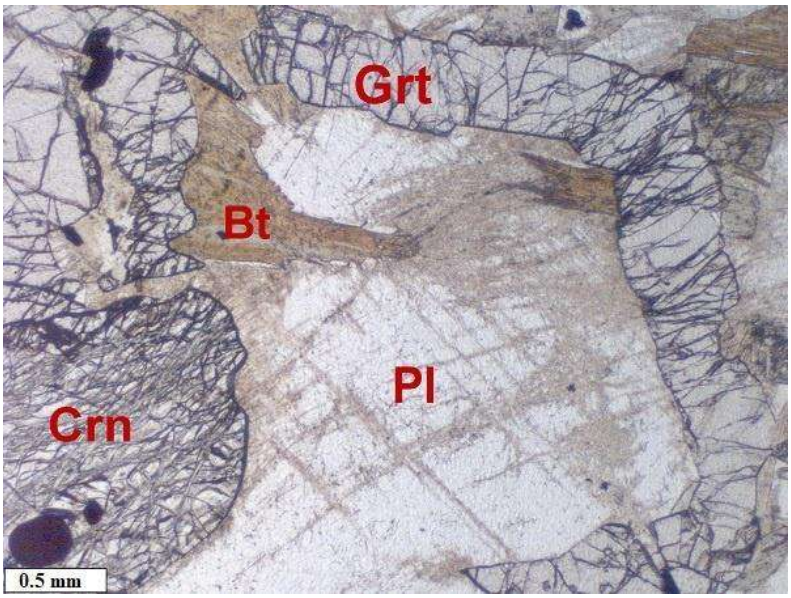

Fig. 20. Atoll garnet in rocks with corundum (zone 4). Photo in transmitted light, without analyzer.

Corundum can occur as large euhedral crystals. It is dissected by numerous fissures filled with diaspore, it also contains inclusions of paragonite, which is absent in the matrix of corundum-bearing rock (Fig. 21).

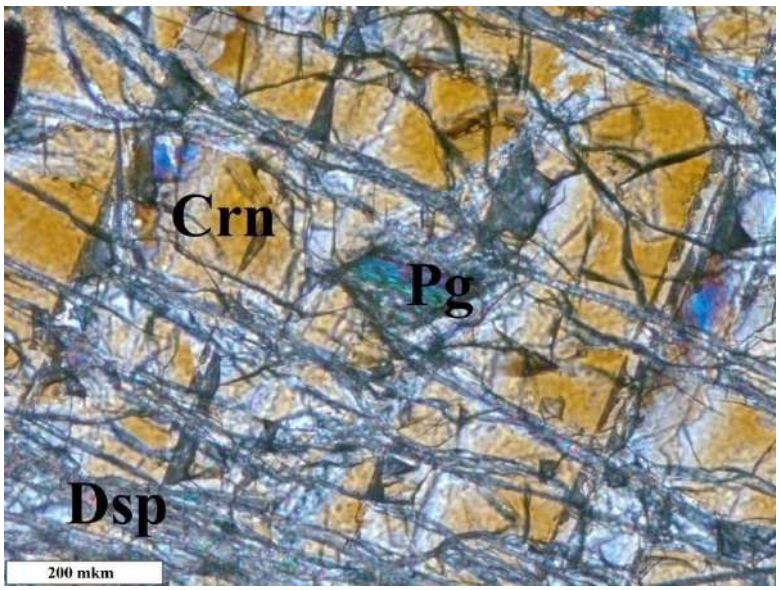

Fig. 21. Cracks filled with diaspore and inclusions of paragonite in corundum. Photo in transmitted light, with analyzer.

Corundum crystals in the groundmass of the rock are often surrounded by segregations of calcium amphibole and garnet (Fig. 22).

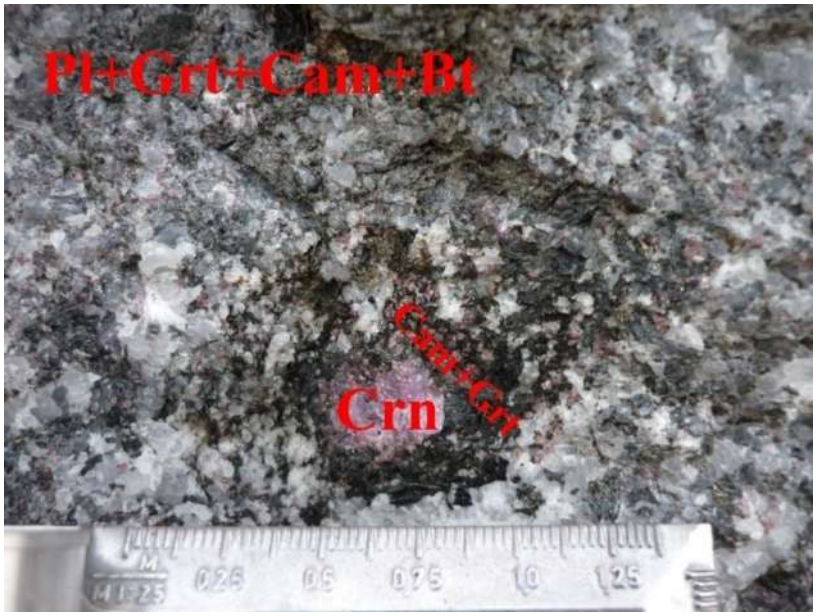

Fig. 22. Large crystal of corundum in the rock

Rutile is present in significant amounts in corundum-bearing metasomatites of all zones. Sometimes rutile is observed in the form of nests, where its idiomorphic crystals are adjacent to pyrite.

Ilmenite is less widely distributed than rutile, in the form of grains of various shapes, often located at the boundaries of staurolite grains, separated from it by a plagioclase rim. Sometimes ilmenite is found in the form of lamellae in gedrite (Fig. 23).

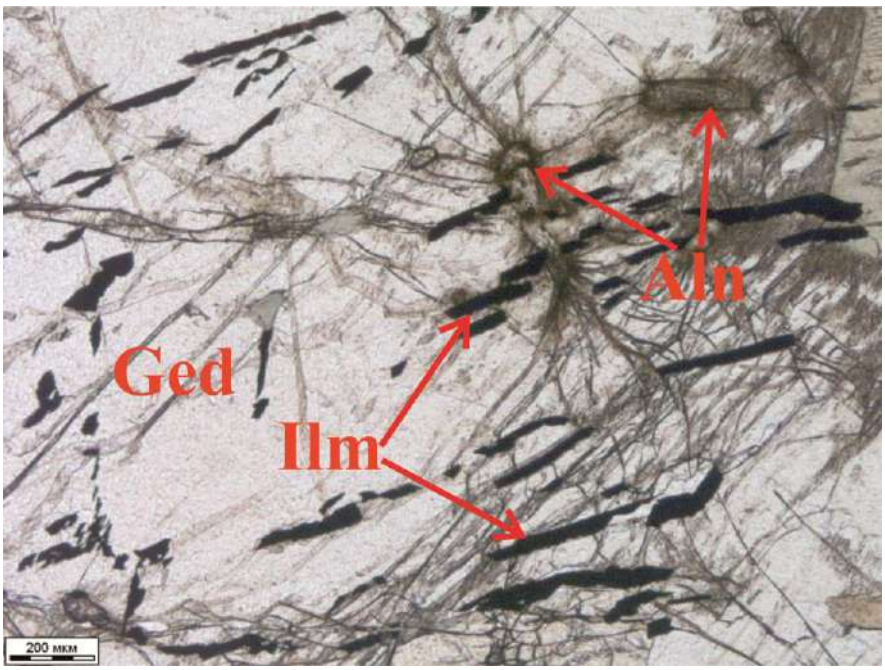

Fig. 23. Ilmenite in sodic gedrite. Photo in transmitted light, without analyzer.

In the rocks of all zones, late secondary changes are manifested to varying degrees: chloritization of biotite and amphiboles, development of muscovite after biotite, pelitization of plagioclase.

Plagioclasites are characterized by a spotted texture, granoblastic, medium-coarse-grained, uneven-grained structure. The main mineral is oligoclase (usually weakly zoned), the amount of which in the rocks is 90% or more. Garnet, biotite, calcium amphibole, muscovite, zircon, rutile, and opaque ore minerals can occur in small amounts. Reaction structures are not observed in plagioclasites. Secondary changes: pelitization and sericitization of plagioclase.

Clinozoisite amphibolites. Dark gray rocks with large garnet porphyroblasts and large differently oriented long prismatic clinozoisite crystals (Fig. 24). They contain the following minerals: bluish-green calcium amphibole (50–70%,), plagioclase (10–40%), garnet (10–30%), clinozoisite (10–20%), biotite, quartz, epidote, titanite, zircon, allanite, apatite are single grains. The texture is spotted, the structure is porphyroblastic (garnet porphyroblasts up to 3 cm), coarse-medium-grained, uneven-grained. Calcium amphibole, garnet, and clinozoisite are euhedral. Clinozoisite sometimes occurs as large ingrowths in garnet.

Fig. 24. Altered amphibolite with clinozoisite and large garnet

Reaction structures are sometimes observed: amphibole-plagioclase symplectites after garnet (Fig. 25), clinozoisite-plagioclase symplectites, replacement of calcium amphibole by clinozoisite. There are few secondary alterations after plagioclase and amphibole.

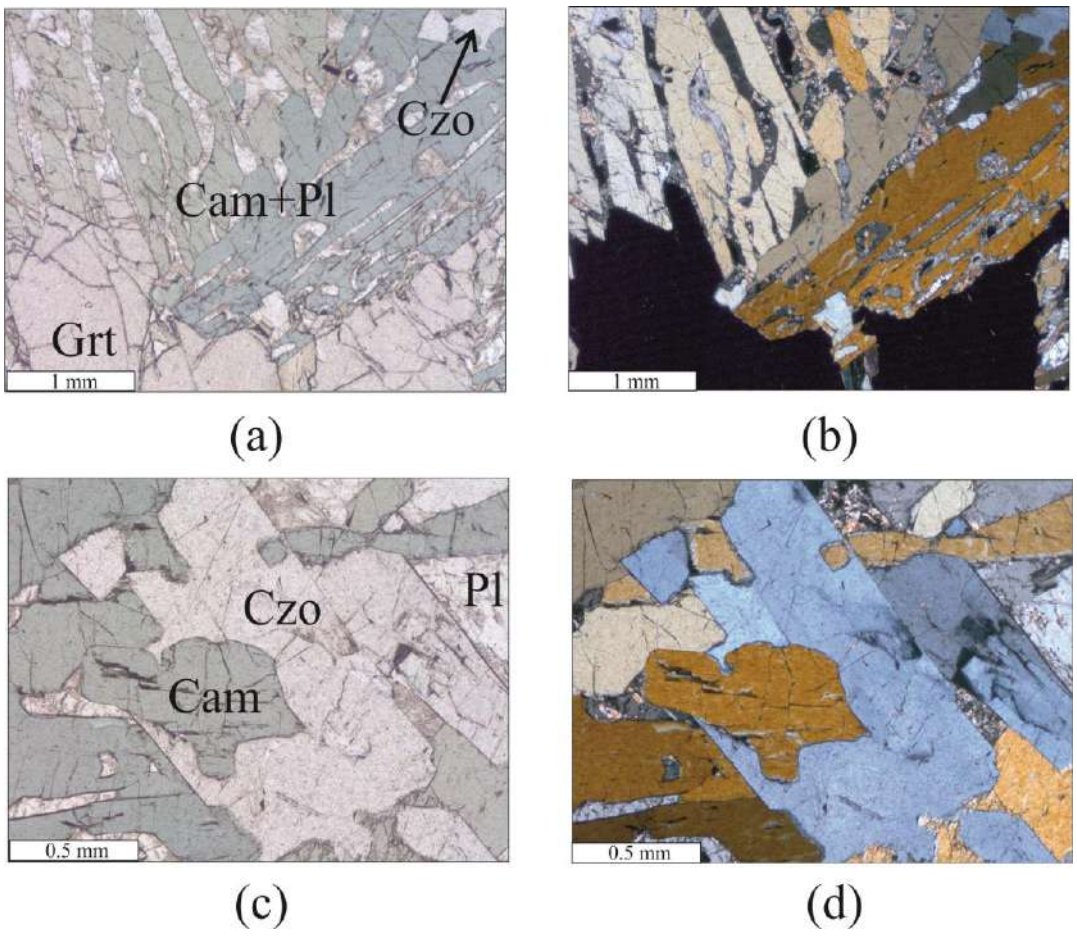

Fig. 25. Photographs of a transparent polished thin section of clinozoisite amphibolite (sample KHI-008D): a – development of plagioclase-amphibole symplectites around garnet, in

transmitted light, without an analyzer; b – the same, with the analyzer; c – replacement of calcium amphibole with clinozoisite, in transmitted light, without an analyzer; d – the same, with the analyzer.

Conclusions to chapter 2

1. According to the results of petrographic analysis, it was revealed that the zoning of the body of corundum-bearing rocks is due to a regular change in paragenesis: at first, quartz disappears in kyanite-garnet-biotite gneisses and kyanite crystals grow larger; then staurolite appears, developing as plagioclase-staurolite symplectites around kyanite, then corundum appears, first as corundum-plagioclase symplectites, and then as large porphyroblasts; biotite is replaced by calcium amphibole, and staurolite is replaced by sodic gedrite-corundum-plagioclase symplectites.

2. In association with corundum-bearing rocks, there are plagioclasites and clinozoisite amphibolites. The latter are also associated with the host rocks (garnet amphibolites) by a gradual transition: quartz disappears in garnet amphibolites, then amphibole-plagioclase symplectites after garnet and clinozoisite-plagioclase symplectites are formed, then calcium amphibole is replaced by clinozoisite.

Chapter 3. General characteristics of the mineral composition of the rocks of the Khitoostrov occurrence

Thirty mineral species were identified in the rocks of the Khitoostrov occurrence (Table 2).

Table 2. Distribution of minerals in the rocks of the Khitoostrov occurrence

№	Mineral	Formulae	Rocks			
			Ky-Grt-Bt gneisses	Crn rocks	Grt amphibolites	Czo amphibolites
1	Pyrite	FeS_2	×	×	×	×
2	Quartz	SiO_2	■		■	
3	Rutile	TiO_2	×	×	×	×
4	Corundum	Al_2O_3		×		
5	Ilmenite	$Fe^{2+}TiO_3$	×	×	×	×
6	Diaspore	$AlO(OH)$		×		
7	Kyanite	$Al_2(SiO_4)O$	●	●		
8	Zircon	$Zr(SiO_4)$	×	×	×	×
9	Almandine	$Fe^{2+}{}_3Al_2(SiO_4)_3$	■	■	■	■
10	Titanite	$CaTi(SiO_4)O$			×	×
11	Staurolite	$Fe^{2+}{}_2Al_9Si_4O_{23}(OH)$		●		
12	Clinozoisite	$(Ca_2)(Al_3)(Si_2O_7)(SiO_4)O(OH)$				■
13	Epidote	$Ca_2(Al_2Fe^{3+})(Si_2O_7)(SiO_4)O(OH)$				×
14	Ferriepidote	$Ca_2(Fe^{3+}{}_2Al)(Si_2O_7)(SiO_4)O(OH)$				×
15	Allanite-Ce	$(CaCe)(Al_2Fe^{2+})(Si_2O_7)(SiO_4)O(OH)$	×	×	×	×
16	Diopside	$CaMgSi_2O_6$			●	
17	Sodic gedrite	$NaMg_2(Mg_3Al_2)(Al_3Si_5O_{22})(OH)_2$		●		
18	Mg-hornblende	$□Ca_2(Mg_4Al)(Si_7Al)O_{22}(OH)_2$			■	
19	Tschermakite	$□Ca_2((Mg, Fe)_3Al_2)(Al_2Si_6O_{22})(OH)_2$		■		■
20	Pargasite	$NaCa_2((Mg, Fe)_4Al)(Si_6Al_2)O_{22}(OH)_2$				■
21	Sadanagaite	$NaCa_2((Mg, Fe)_3Al_2)(Si_5Al_3O_{22})(OH)_2$				■
22	Barroisite	$□(CaNa)(Mg_3Al_2)(AlSi_7O_{22})(OH)_2$		■		
23	Muscovite	$KAl_2(AlSi_3O_{10})(OH)_2$	×	×		

24	Paragonite	$NaAl_2(AlSi_3O_{10})(OH)_2$		×		
25	Phlogopite	$KMg_3(AlSi_3O_{10})(OH)_2$	■	■	■	●
26	Margarite	$CaAl_2(Al_2Si_2O_{10})(OH)_2$				×
27	Clinochlore	$Mg_5Al(AlSi_3O_{10})(OH)_8$	×	×	×	×
28	Plagioclase	$(Na,Ca)[Al(Si,Al)Si_2O_8]$	■	■	■	■
29	Calcite	$CaCO_3$		×	×	
30	Apatite-F	$Ca_5(PO_4)_3F$	×	×	×	×

Note. The table shows the ideal formulas of minerals. Minerals: ■ - major (>5 vol.%), ● - minor (1 - 5 vol.%), × - accessory (< 1 vol.%).

Tables of compositions of the main, minor and some ore and accessory minerals of Khitoostrov are placed in Appendix 3.

3.1. Composition of minerals of corundum-bearing rocks

Calcium and sodium-calcium amphiboles from corundum-bearing rocks exhibit wide variations in composition, forming a series of chermakite-sadanagaite-barroisite and ferrichermakite-ferrisadanagaite-ferribarroisite (high calculated content of Fe^{3+}). That is, according to the classification (Leake et al., 1997, 2004, Hawthorne et al., 2012), these are 6 different mineral species (Fig. 26, 27), which we will further combine under the names - calcium amphibole and soda-calcium amphibole, since the compositions of calcium amphiboles and sodium-calcium amphiboles form a single continuous series and no regularities in the distribution of different mineral species within the studied samples have been identified. Amphiboles have a high magnesium content ($x_{Mg} \geq 0.75$). Titanium content 0.05–0.18 f.c., $^{B}Ca/^{B}(Ca+Na)$ average 0.70–0.80, $^{C}(Al+Fe^{3+}+2Ti)$ average 2.22–2.63, $^{A}(Na+K+2Ca)$ average 0.23-0.52 (position A is partially filled).

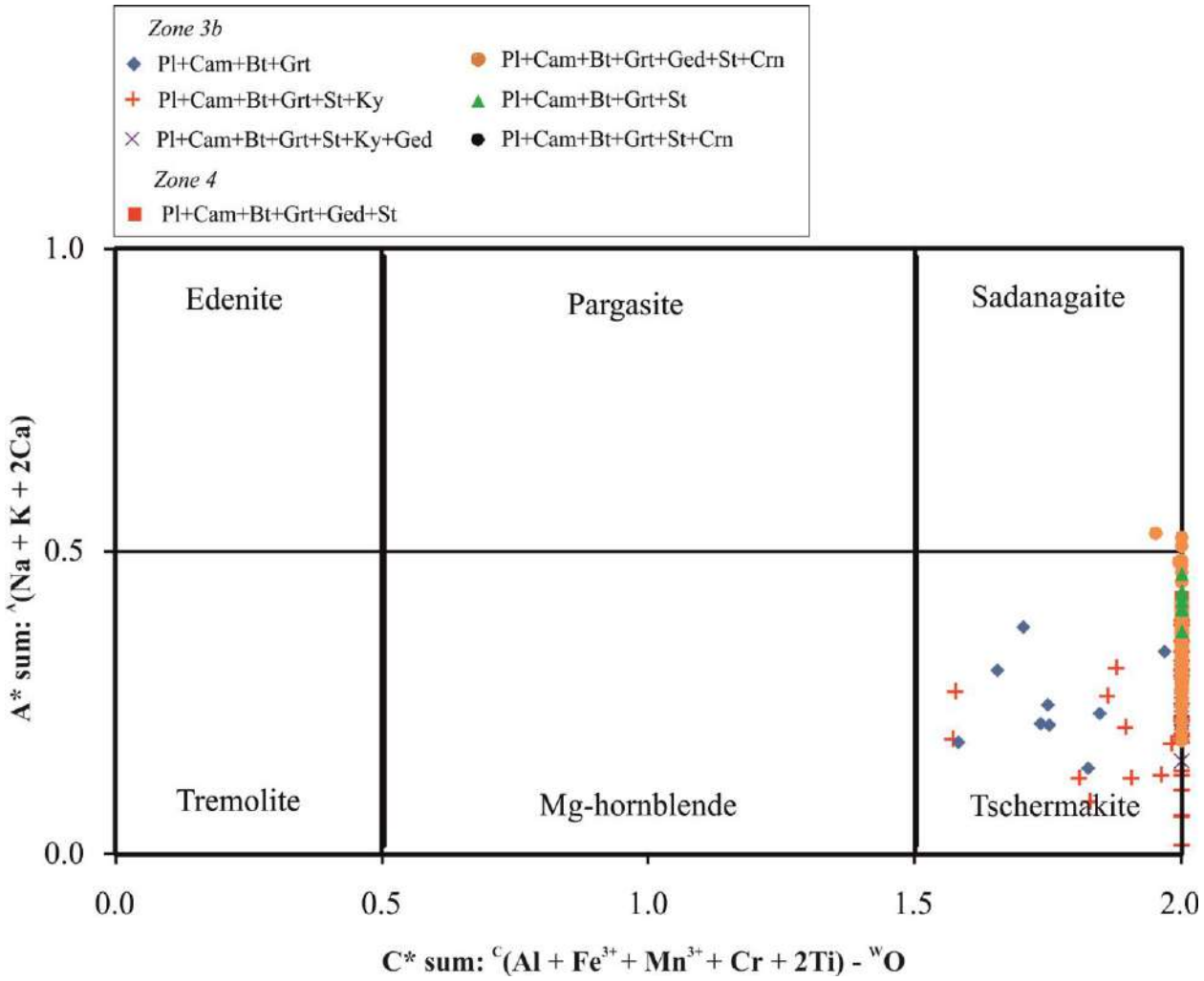

Fig. 26. Composition of calcium amphiboles from corundum-bearing rocks of Khitoostrov on the classification diagram (after Hawthorne et al., 2012).

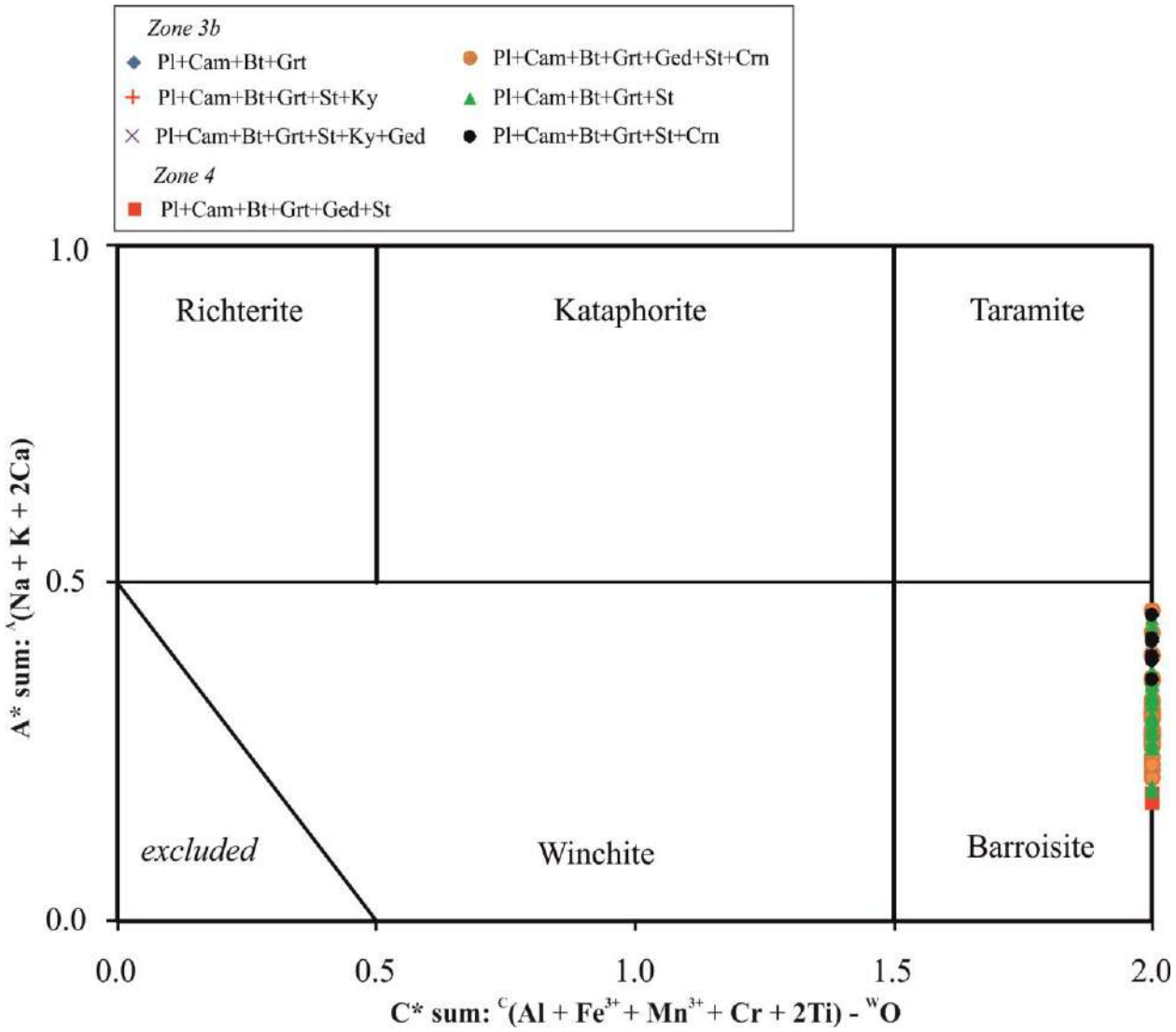

Fig. 27. Composition of sodium-calcium amphiboles from corundum-bearing rocks of Khitoostrov on the classification diagram (after Hawthorne et al., 2012).

The composition of calcium amphiboles varies greatly from zone 3b to zone 4: alumina content (namely, ^{C}Al) and alkali content naturally increase (Fig. 28 a, b). At the same time, the content of ^{B}Ca decreases, so Na enters position B (transition from chermakites to barroisites), while position A remains partially empty. Calcium amphiboles of garnet amphibolites (magnesiohornblendes) differ from calcium amphiboles in rocks with corundum by significantly lower alumina content (^{T}Al = 1.1–1.7 f.c., ^{C}Al = 0.7–0.9 f.c.).

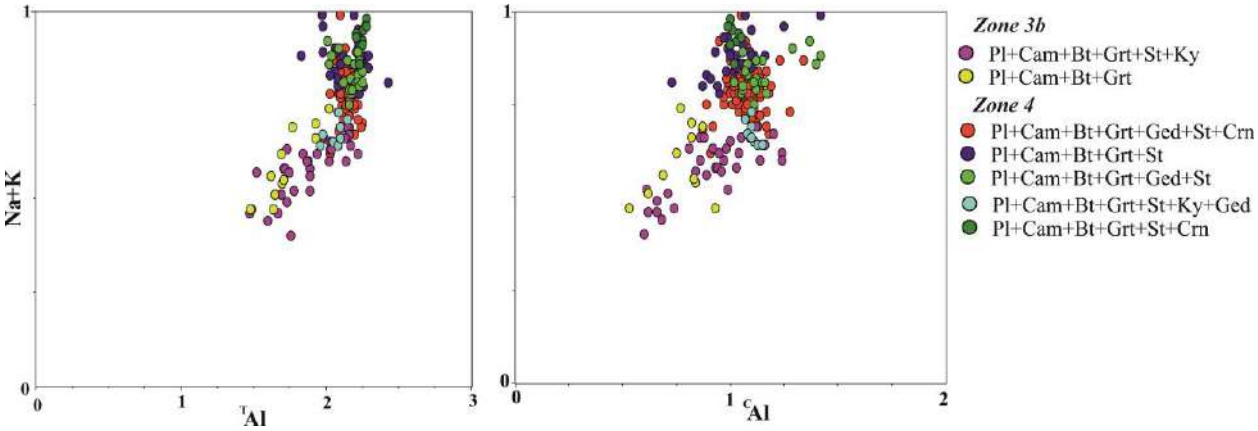

a b

Fig. 28. Dependence of ^{T}Al (a) and ^{C}Al (b) on the amount of alkalis in amphiboles from Khitoostrov rocks.

Sodic gedrite from corundum-bearing rocks of Khitoostrov is characterized by a high sodium content (0.67–0.98 f.c.) (Fig. 29), a relatively constant magnesian content: *x*Mg = 0.7–0.8, and high alumina content (^{T}Al = 2.0–2.5 f.c., ^{C}Al = 1.2 –1.8 f.c.), low content of Ti (0.02–0.07 f.c.) (however, we note that ilmenite lamellae are often observed in gedrite).

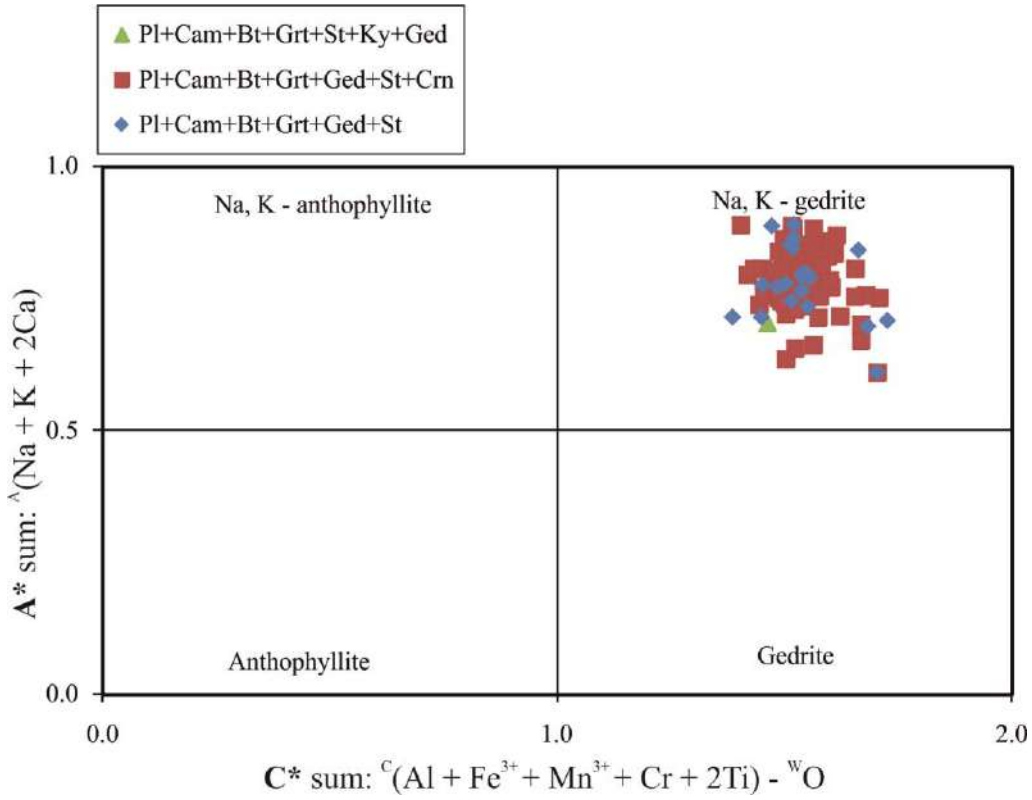

Fig. 29. Composition of gedrites from corundum-bearing rocks of Khitoostrov on the classification diagram (after Hawthorne et al., 2012).

Biotite in corundum-bearing rocks is represented by ferruginous phlogopite (^{T}Al = 1.1–1.5 f.c., ^{D}Al = 0.2–0.8 f.c.), it is magnesian (*x*Mg = 0.54–0.95, where *x*Mg = Mg/(Mg+Fe) (Mg, Fe – f.c.)) (Fig. 30), contains a significant amount of sodium (^{A}Na/^{A}(K+Na) up to 0.27) (Fig. 31).

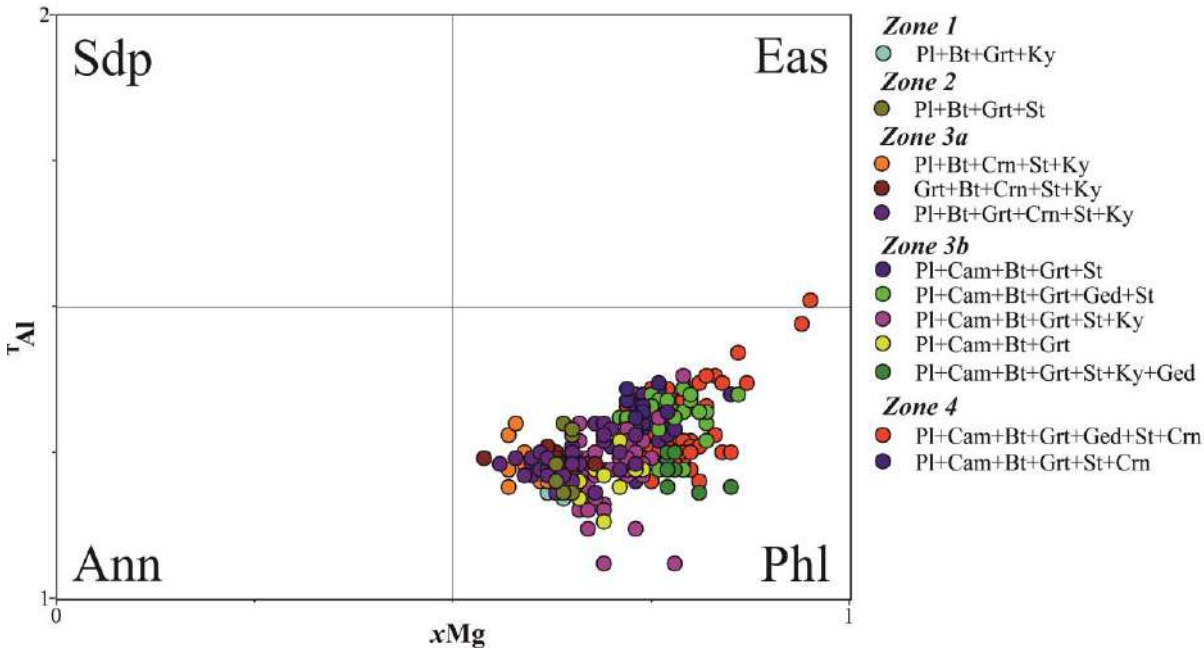

Fig. 30. Composition of biotites from corundum-bearing rocks of Khitoostrov on the classification diagram (after Rieder et al., 1998).

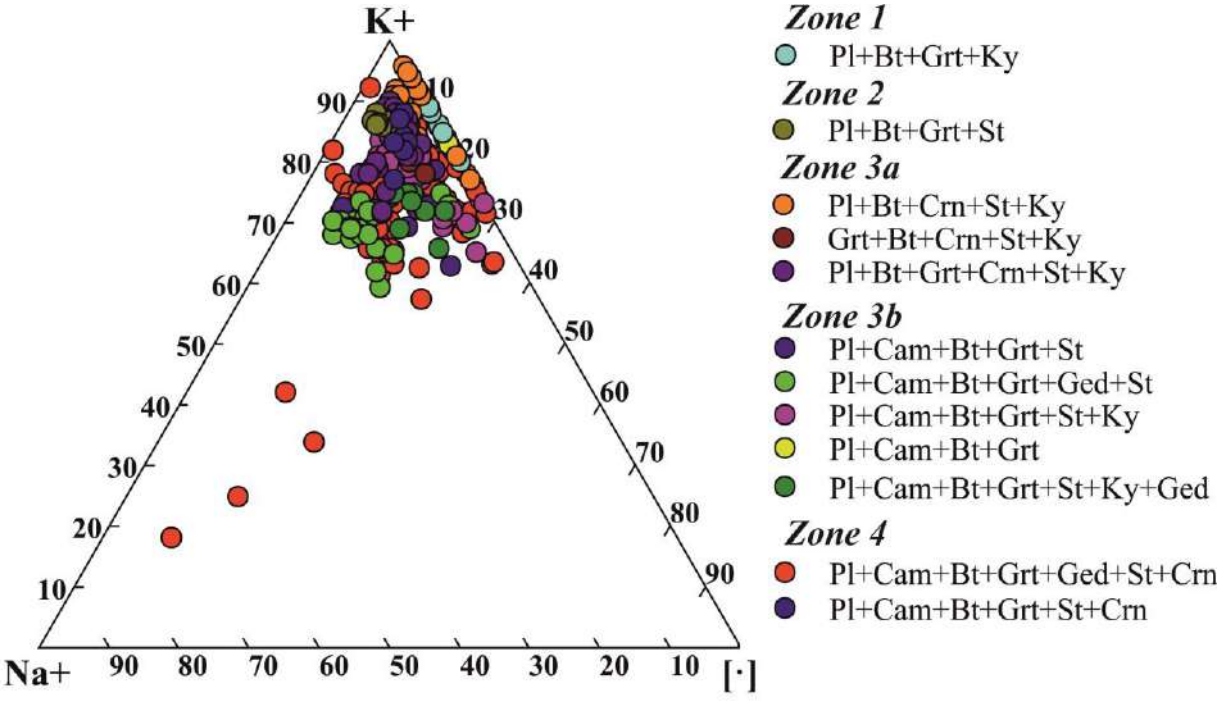

Fig. 31. Diagram K-Na-[•] ([•] – vacancy, [•] = 1 – (K+Na)) for biotites from corundum-bearing rocks of Khitoostrov.

Biotites of all varieties of corundum-bearing rocks are characterized by a relatively constant composition; they are more magnesian than the biotites of the host garnet-biotite gneisses of the Chupa sequence (in the latter, *x*Mg is in a rather narrow range from 0.57 to 0.62; the magnesian content of biotites from garnet amphibolites falls into the same range). The biotites of the host gneisses, in contrast to the biotites of corundum-bearing rocks, lack Na, and in the biotites from garnet amphibolites $^{A}Na/^{A}(K+Na) \leq 0.04$.

In one sample (KHI010-4), the biotites turned out to be inhomogeneous: on the BSE image, the biotite grains show bands (ingrowths?) of biotite with a different composition (Fig. 32). This biotite is distinguished by a high content of Na (0.44–0.72 f.c.), a reduced content of K (0.18–0.42 f.c.), and in composition corresponds to Na-biotite (aspidolite, after Anthony et al., 2001, Rieder et al., 1998).

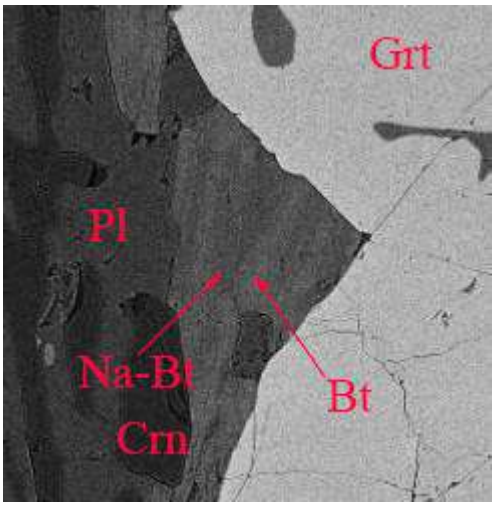

Fig. 32. Inhomogeneous grain of biotite in BSE (field of view 400 μm).

Plagioclase from corundum-bearing rocks of Khitoostrov varies greatly in composition ($An_{13–61}$) and forms a continuous series from oligoclase to andesine, some points even fall into the field of labrador (Fig. 33). Late albite ($An_{6–10}$) is also present, developing together with chlorite after biotite.

Plagioclase from host gneisses is represented by oligoclase №17–24, thus, in corundum-bearing rocks, and especially in rocks of zones 2-3, plagioclase is often more basic than in garnet-biotite gneisses.

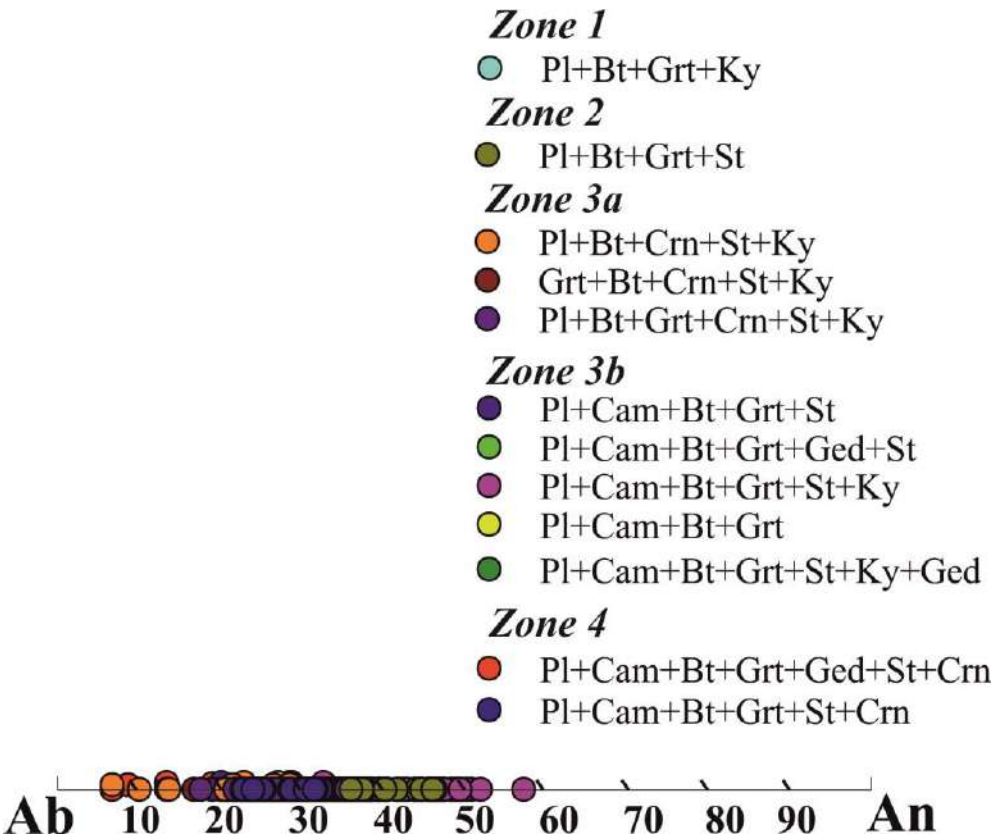

Fig. 33. Composition of plagioclases from corundum-bearing rocks of Khitoostrov.

Garnet from corundum-bearing rocks of Khitoostrov is quite rich in Mg and Ca ($Alm_{43-78}Prp_{12-46}Grs_{5-19}$) (Fig. 34), and is characterized by weak reverse zoning (the proportion of pyrope and grossular decreases from the center to the edge of the grains) (Fig. 35 a, b). In garnets from corundum-bearing rocks, the share of pyrope and grossular components increases in comparison with host gneisses, where in garnet $Alm_{66-79}Prp_{16-24}Grs_{5-10}$. The highest proportion of the grossular component is characteristic of garnets from the rocks of zone 2 (14–19% against the background of 5–7% in the rocks of zone 3a and 7–14% in the rocks of zone 4), but it is not higher in them than in the host garnet amphibolites, where the share of the grossular component in garnet reaches 30%. The pyrope component of garnets naturally increases from the outer zones to the inner ones, but its variations also become wider.

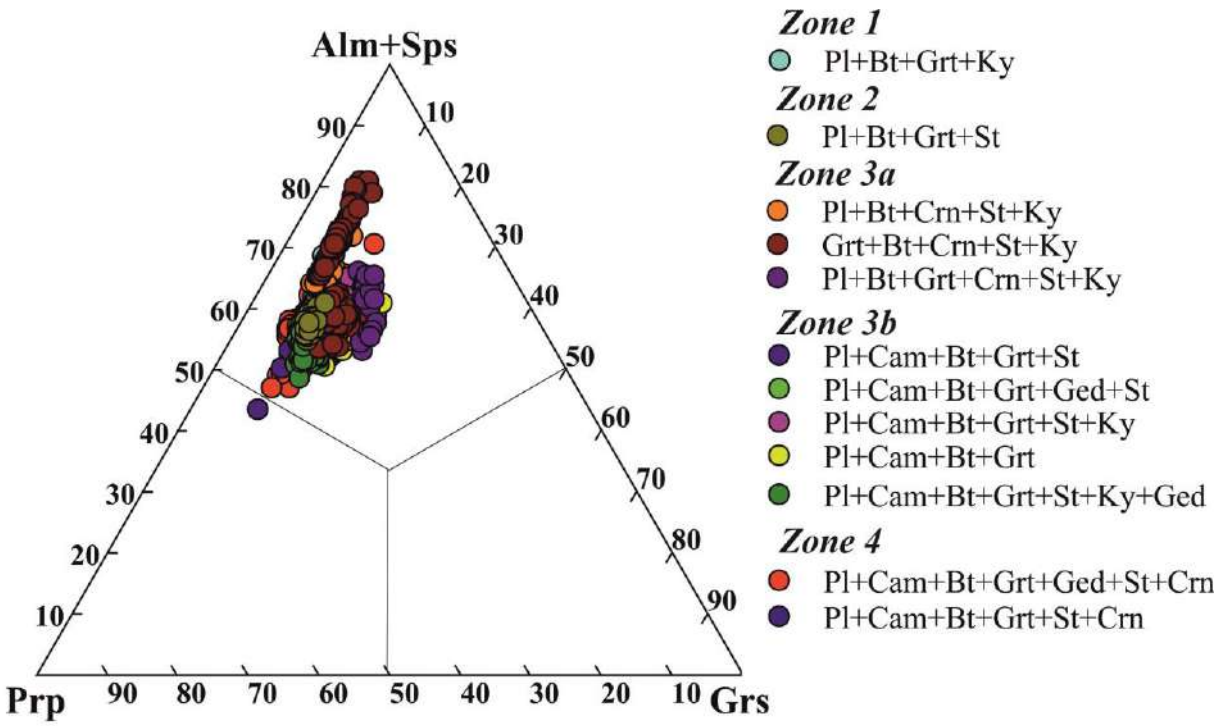

Fig. 34. Composition of garnets from corundum-bearing rocks of Khitoostrov.

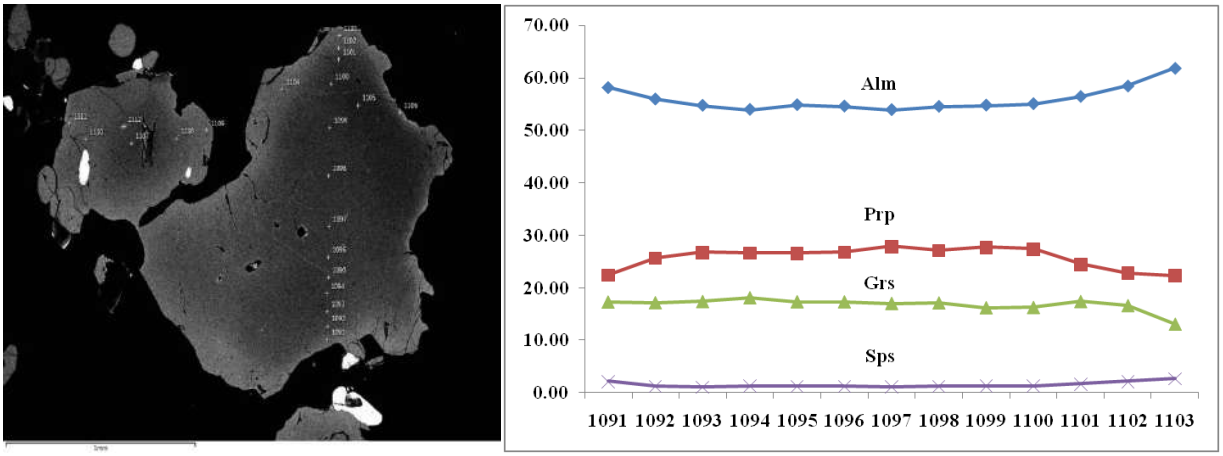

a b

Fig. 35. Zoning of chemical composition in garnets: a – illustration of zoning in a garnet grain from corundum-bearing rocks in the BSE; b – garnet composition zoning profile.

Staurolite from corundum-bearing rocks of Khitoostrov is characterized by wide variations in magnesian content (*x*Mg = 10–56%, where *x*Mg = Mg/(Mg + Fe) (Mg, Fe - f.c.)) - it is often much more magnesian than metapelite staurolites (Fedkin, 1975). Sometimes there is an admixture of Zn (up to 0.1 f.c.), Ti from 0.02 to 0.14 f.c., Al varies from 8.60 to 9.22 f.c. A significant amount of Fe^{3+} may be present (up to 0.75 f.c.).

White micas in the corundum-bearing rocks of Khitoostrov are represented by muscovite and paragonite (Fig. 36).

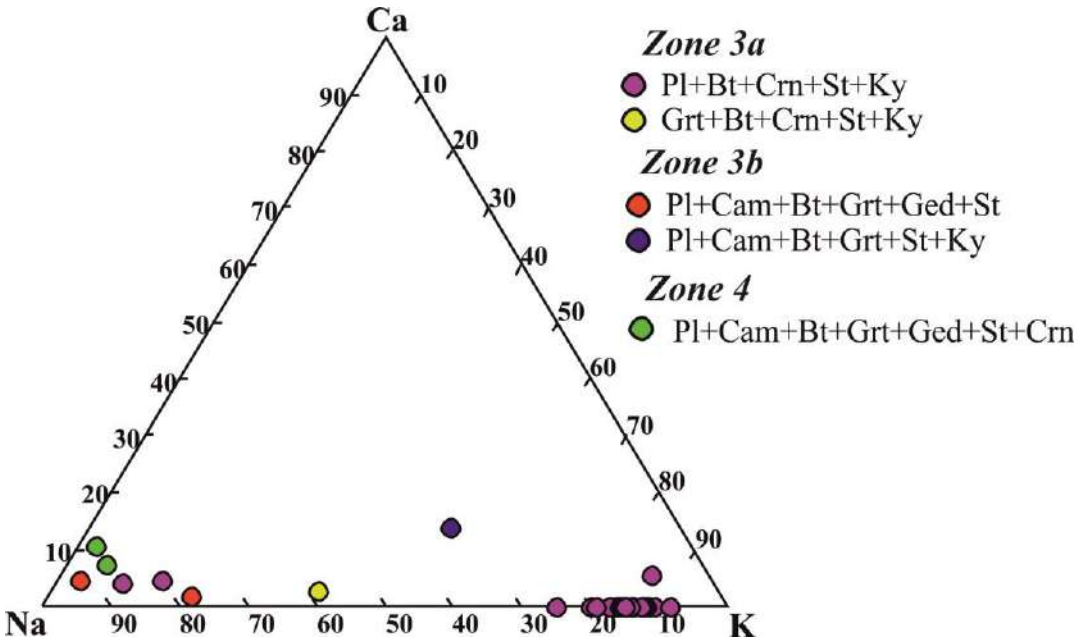

Fig. 36. Composition of light micas from corundum-bearing rocks of Khitoostrov.

Apatite in corundum-bearing rocks of Khitoostrov is represented by F-apatite containing OH (0.39–0.68 f.c.) (Fig. 37). The host kyanite-garnet-biotite gneisses also contain F-apatite, but it contains less OH (up to 0.21 f.c.).

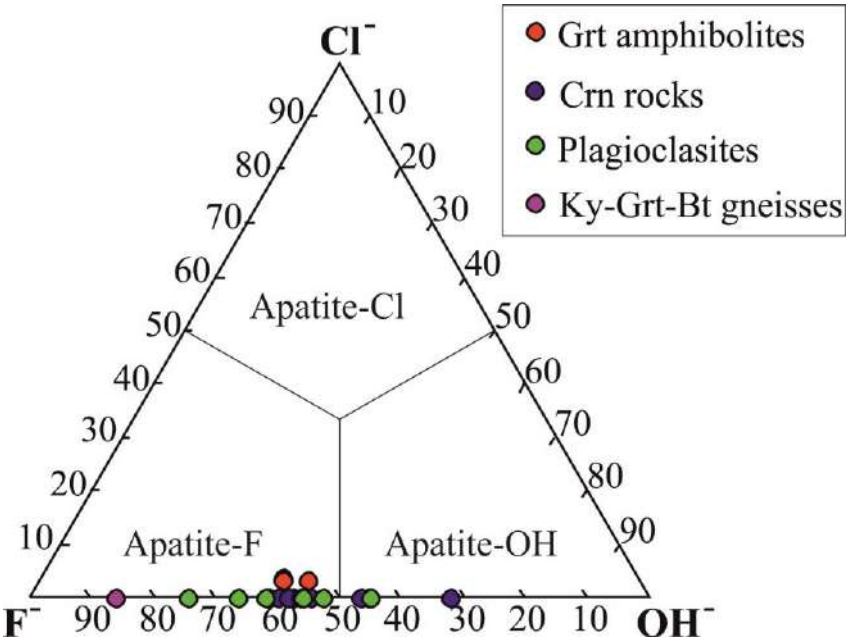

Fig. 37. Apatite from corundum-bearing and host rocks of Khitoostrov.

Ilmenite from the corundum-bearing rocks of Khitoostrov can also contain a small amount of Mg up to 0.14 f.c. and Fe^{3+} – up to 0.06 f.c.

3.2. Composition of minerals of clinozoisite amphibolites

Calcium amphiboles in host garnet amphibolites are represented by magnesiohornblende: $^{B}Ca/^{B}(Ca+Na)$ average 0.94, $^{C}(Al+Fe3^{+}+2Ti)$ average 1.34, $^{A}(Na+K+2Ca)$ average 0.43. Calcium amphiboles from clinozoisitic amphibolites exhibit wide compositional variations and form the series chermakite-pargasite-sadanagaite and ferrochermakite-ferropargasite-ferrosadanagaite (according to the classification (Hawthorne et al., 2012)): $^{B}Ca/^{B}(Ca+Na)$ average 0.93, $^{C}(Al+Fe^{3+}+2Ti)$ average 1.66, $^{A}(Na+K+2Ca)$ average 0.51 (Fig. 38). That is, according to the classification, these are 6 different mineral species, which we will further combine under one name - calcium amphibole, since the compositions of calcium amphiboles from clinozoisitic amphibolites form a single continuous series and no regularities in the distribution of different mineral species within the studied samples have been identified. It should be noted that the composition of calcium amphibole in plagioclase-amphibole symplectites (Cam2) is somewhat different from that of calcium amphibole in the rock matrix (Cam1). Cam2 contains more Al: both ^{T}Al (5.96 *vs* 6.16 f.c.) and ^{C}Al (1.14 *vs* 0.98 f.c.) are higher in it, while Mg is lower (^{C}Mg is 1.66 *vs* 2.18 f.c). Thus, calcium amphiboles from clinozozite amphibolites differ from magnesiohornblende from the host garnet amphibolites in having a lower content of Si and a higher content of Al and Mg.

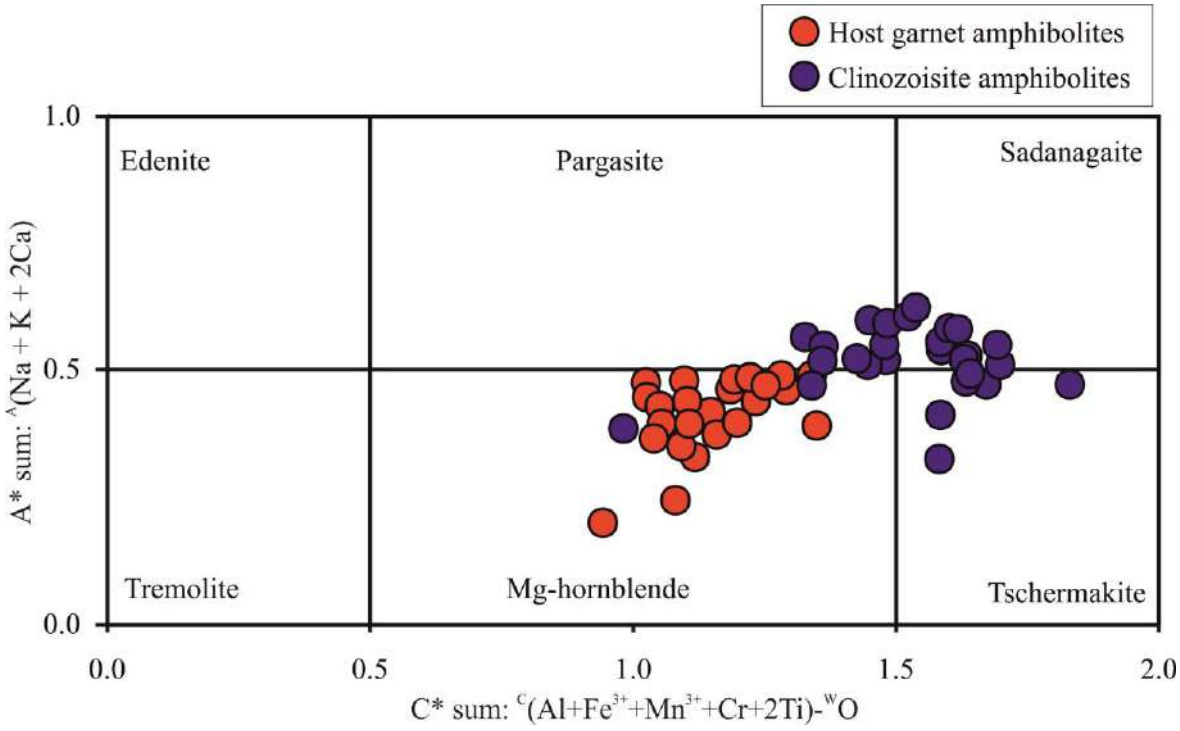

Fig. 38. Classification diagram for calcium amphibole from clinozoisite (sample Khi008D) and host (sample Khi008G) amphibolites. Composition fields after Hawthorne et al., 2012.

Biotite from the host garnet amphibolites is a ferruginous phlogopite and is characterized by a low Al content (after Rieder et al., 1988). The clinozoisite amphibolites also contain ferruginous phlogopite with *x*Mg = 0.50–0.64 (*x*Mg = Mg/(Mg+Fe), where Mg, Fe are f.c.), the Al content in it is somewhat higher (^{T}Al = 0.25–0.49) (Fig. 39). Sometimes there is an insignificant admixture of Na up to 0.05 f.c.; Ti ≤ 0.16 f.c.

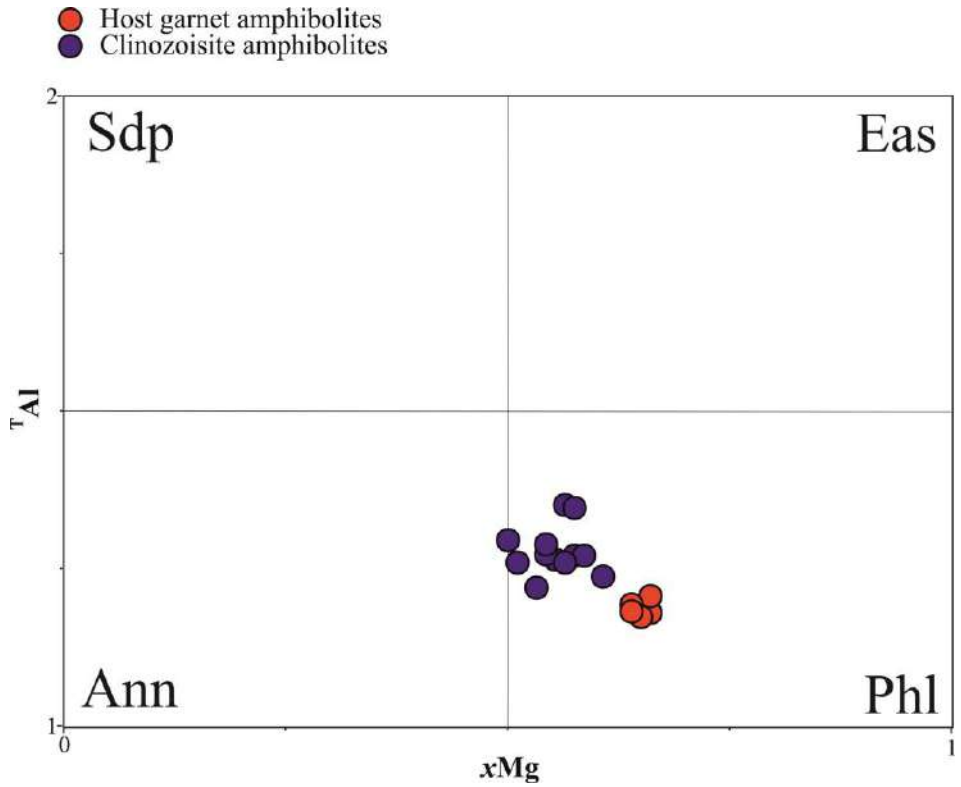

Fig. 39. Diagram of the composition of biotites from clinozoisite and host amphibolites.

Garnet from host garnet amphibolites is almandine with an Fe content of 1.37–1.76 f.a. and Mg 0.34–0.52 f.c., with a high content of Ca 0.65–0.98 f.c. Garnet from clinozoisite amphibolites is characterized by a similar chemical composition: Fe 1.35–1.66 f.c., Mg 0.22–0.60 f.c., Ca 0.88–0.94 f.c. Garnet is characterized by weak zoning (the Mg content decreases from the cores to the rims of the grains) (Fig. 40).

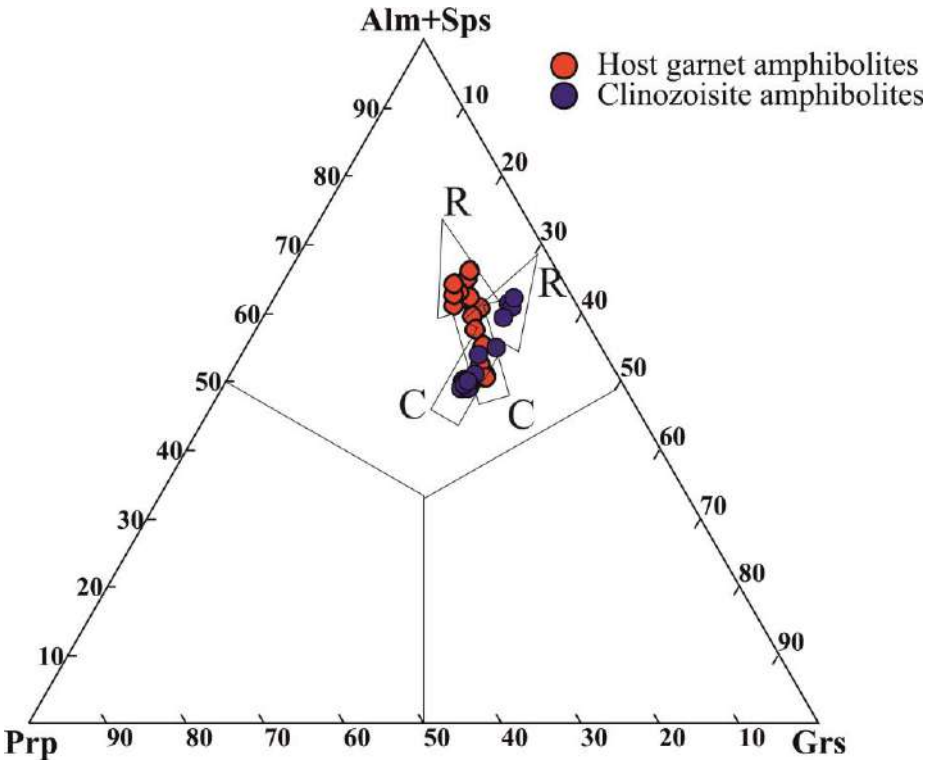

Fig. 40. Diagram of the composition of garnets from clinozoisite amphibolites. The letters C and R denote the cores and rims of the grains, respectively.

Plagioclase in host garnet amphibolites is from acidic to intermediate: An23-39 (Fig. 41). Plagioclases from clinozoisite amphibolites are clearly divided into two groups according to their composition: An_{45-67} and An_{78-90} (Fig. 41), both plagioclases are more or less evenly distributed throughout the rock without distinct regularities. There are also zonal plagioclases: for example, in the center of An_{51}, on the edge of An_{86} (i.e., plagioclase from the center and from the edge falls into two different groups), or in the center of An_{48}, at the edge of An_{64} (i.e., plagioclase from the center and from the edge belongs to the same group). While the matrix contains plagioclases from both groups, the plagioclase–amphibole symplectites contain only basic plagioclase.

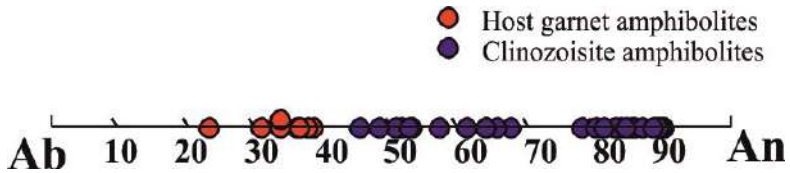

Fig. 41. Diagram of the composition of plagioclases from clinozoisite and host amphibolites.

Minerals of the epidote group in clinozoisite amphibolites are represented by clinozoisite; the content of Fe3+ in the M3 position is less than 0.5 (Armbruster et al., 2006), single analyzes turned out to be epidote (Fig. 42). Late ferriepidote develops after biotite.

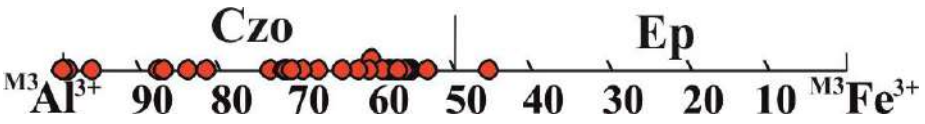

Fig. 42. Diagram of the composition of clinozoisite from clinozoisite amphibolites.

Titanite from host garnet amphibolites contains an admixture of Mg (up to 0.09 f.c.) and Fe^{2+} (up to 0.06 f.c.). In titanite from clinozoisite amphibolites, only an admixture of Fe^{2+} (up to 0.01 f.c.) was revealed.

Margarite contains an admixture of Fe^{2+} (up to 0.04 f.c.).

Conclusions to chapter 3

The conducted studies make it possible to significantly expand the data on the minerals of corundum-bearing and associated rocks of the Khitoostrov occurrence.

1. In the corundum-bearing rocks of the Khitoostrov occurence, in association with corundum pyrope-almandine garnet, plagioclase №26–39, phlogopite and aspidolite, Ca-amphiboles of the tschermakite-sadanagaite series, Na-Ca-amphibole (barroisite) and Mg-Fe orthorhombic amphibole – sodic gedrite, magnesian staurolite, paragonite, muscovite, ilmenite, rutile was found.

2. The clinozoisite amphibolites associated with corundum-bearing rocks contain ferruginous phlogopite containing more Al than the ferruginous phlogopite from the host garnet amphibolites; calcium amphibole of the tschermakite-pargasite-sadanagaite series; garnet, clinozoisite, epidote, titanite; basic plagioclase, which is absent in the host rocks, and margarite appear.

Chapter 4. Distribution of REE in minerals of metasomatites of Khitoostrov occurrence

4.1. Rare earth elements in minerals of corundum-bearing rocks

Garnet

The content of rare-earth elements in garnets was analyzed at 17 points: 9 - in apogabbroic garnet amphibolite, 8 - in the corundum-bearing rock of the Khitoostrov occurrence. Analyzes were carried out for grain cores (c), middle parts (m) and their rims (r).

The distribution spectra of REE in garnets from apogabbroic amphibolites are characterized by a clearly pronounced slope from light to heavy REE (Fig. 43a). The europium anomaly, as a rule, is not manifested, which is generally typical for high-calcium garnets (Skublov, 2005); two analyzes revealed a negative cerium anomaly. The zoning for rare earth elements is rather weak. The least magnesian central and middle parts of garnet grains are somewhat enriched in HREE, the least calcium marginal and middle parts of garnet grains are somewhat enriched in LREE.

The distribution spectra of REE in garnets from corundum-bearing rocks have a less pronounced positive slope (Fig. 43b), which is associated with a noticeable enrichment of LREE garnets and a slight depletion of HREE compared to garnets from apogabbroic amphibolites. A negative europium anomaly is noted, which is often characteristic of pyralspit garnets (Skublov, 2005); some analyzes also show a weak cerium anomaly. Zoning for rare earth elements is revealed. As in the case of apogabbroic amphibolites, the least magnesian central and middle parts of garnet grains are enriched in HREE, while the marginal parts of the grains are prone to some enrichment in LREE. Similar distribution spectra of rare earth elements have already been described earlier in garnets from the rocks of the Belomorian mobile belt (Skublov, 2005).

Amphiboles

The content of rare-earth elements in amphiboles was analyzed at 7 points: 2 - in apogabbroic garnet amphibolite, 5 - in the corundum-bearing rock of the Khitoostrov occurrence (2 of them - in sodic gedrite).

Calcium amphiboles from apogabbroic garnet amphibolites are characterized by a flat distribution spectrum of rare earth elements with a weakly pronounced positive Eu anomaly (Fig. 44a). Similar distribution spectra of rare earth elements are characteristic of calcium amphiboles

from rocks of the high-temperature amphibolite facies of metamorphism (Skublov, Drugova, 2003).

The distribution spectra of rare earth elements in calcium amphiboles from corundum-bearing rocks are completely different: they acquire a sinusoidal shape, which was not previously observed in amphiboles from metamorphic rocks (Fig. 44b). Calcium amphiboles of corundum-bearing rocks are significantly enriched in rare earth elements, compared with amphiboles from apogabbroic garnet amphibolites, especially LREE (more than an order of magnitude) and, to a lesser extent, MREE. A weakly pronounced negative europium anomaly is observed.

The distribution spectra of rare-earth elements in sodic gedrite resemble in shape the distribution spectra of rare-earth elements in garnets: they are characterized by a positive slope (but the spectrum is much flatter - the tendency to HREE enrichment in sodic gedrite is not as strong as in garnet), the presence of a negative europium anomaly to varying degrees (Fig. 44b).

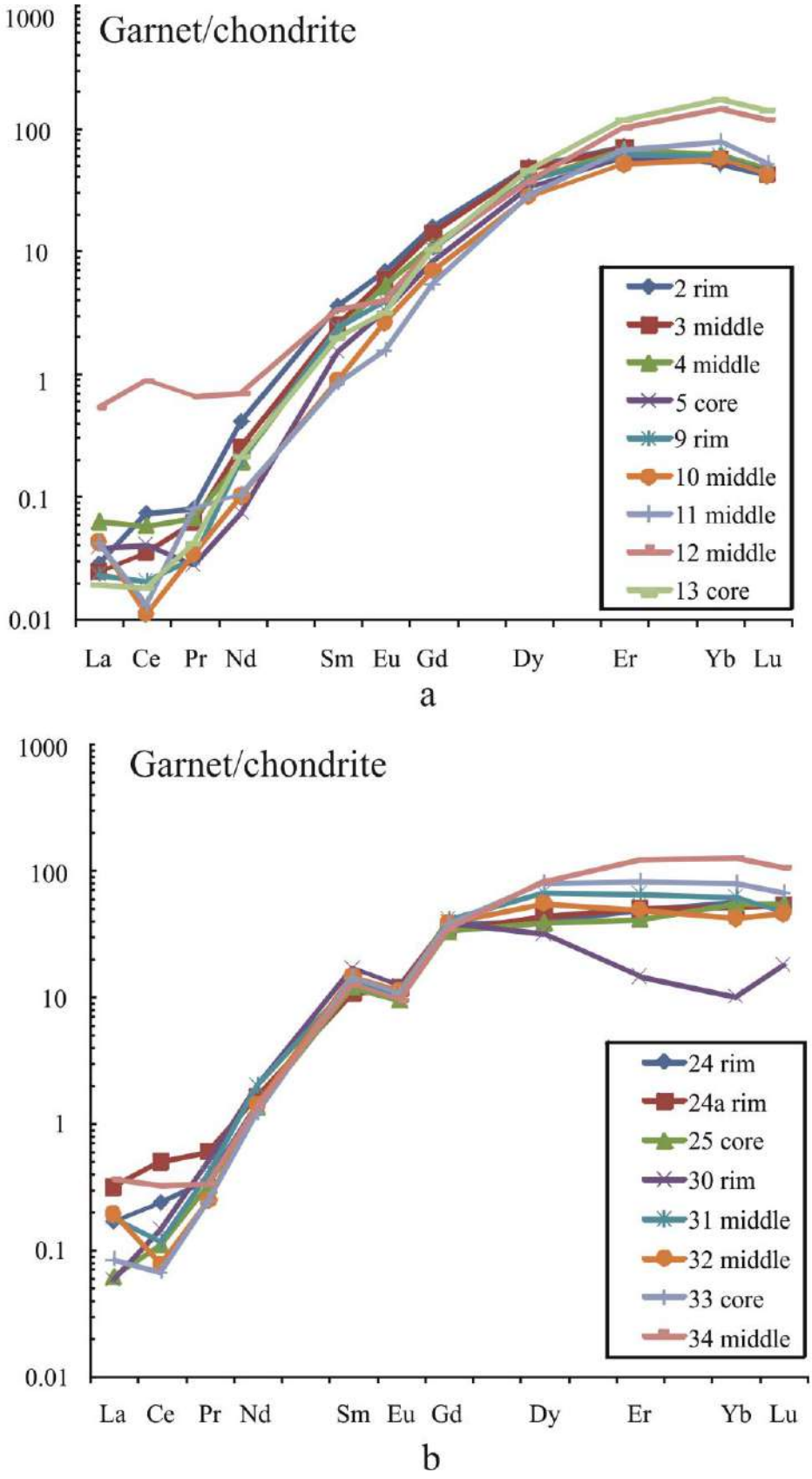

Fig. 43. Distribution spectra of rare-earth elements in garnet: a - from apogabbroic garnet amphibolites, b - from corundum-bearing metasomatites of the Khitoostrov occurrence.

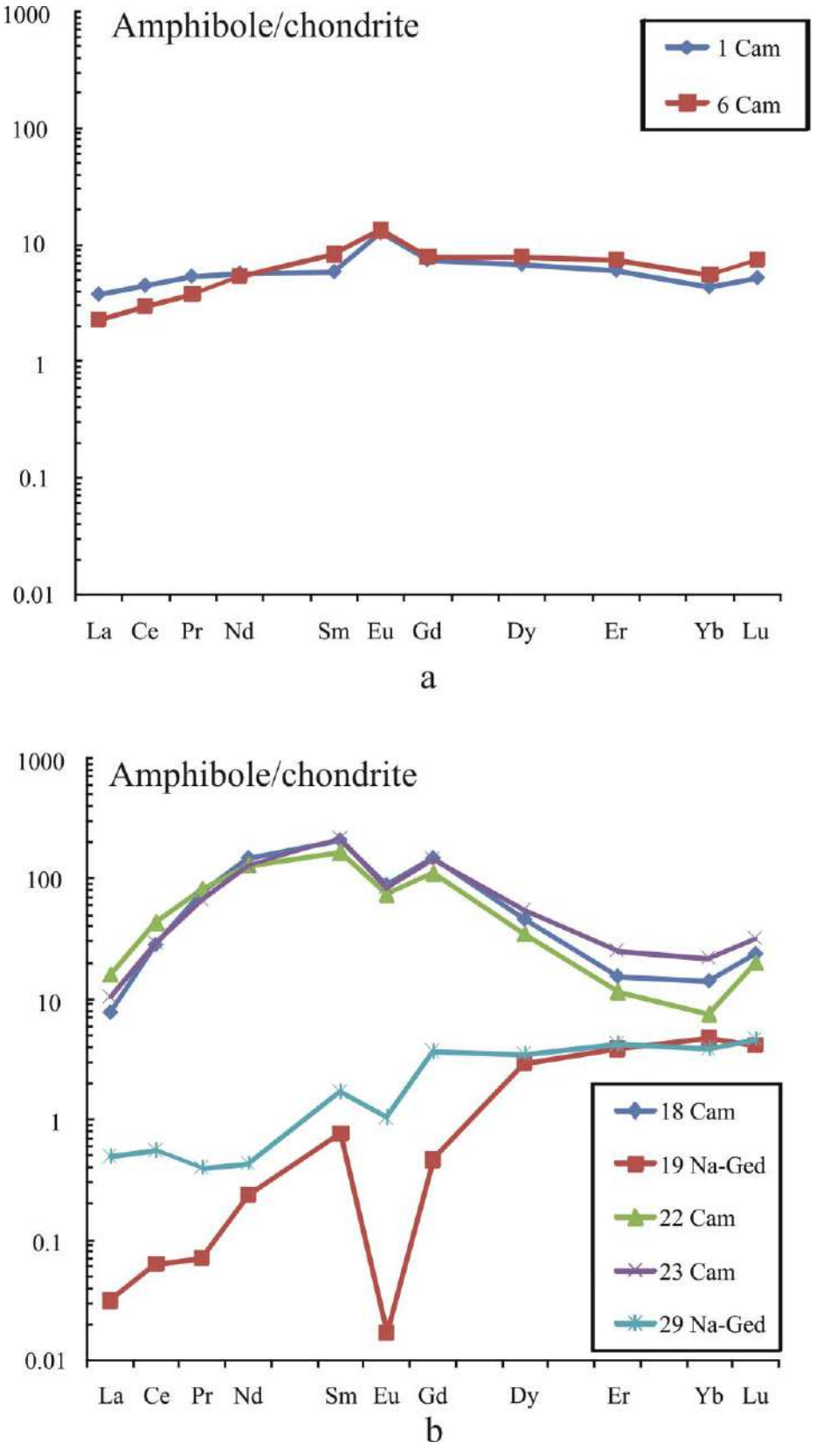

Fig. 44. Distribution spectra of rare-earth elements in amphiboles: (a) in calcium amphibole from apogabbroic garnet amphibolites, (b) in calcium amphibole and sodic gedrite from corundum-bearing metasomatites of the Khitoostrov occurrence.

Biotite

In corundum-bearing rocks, the content of rare earth elements in biotite was analyzed at 3 points. Biotites from corundum-bearing rocks are characterized by a curious feature - a convex spectrum for HREE, except for Yb (Fig. 45). Otherwise, the REE distribution spectra are the same as for other biotites from metamorphic rocks (Skublov, 2005).

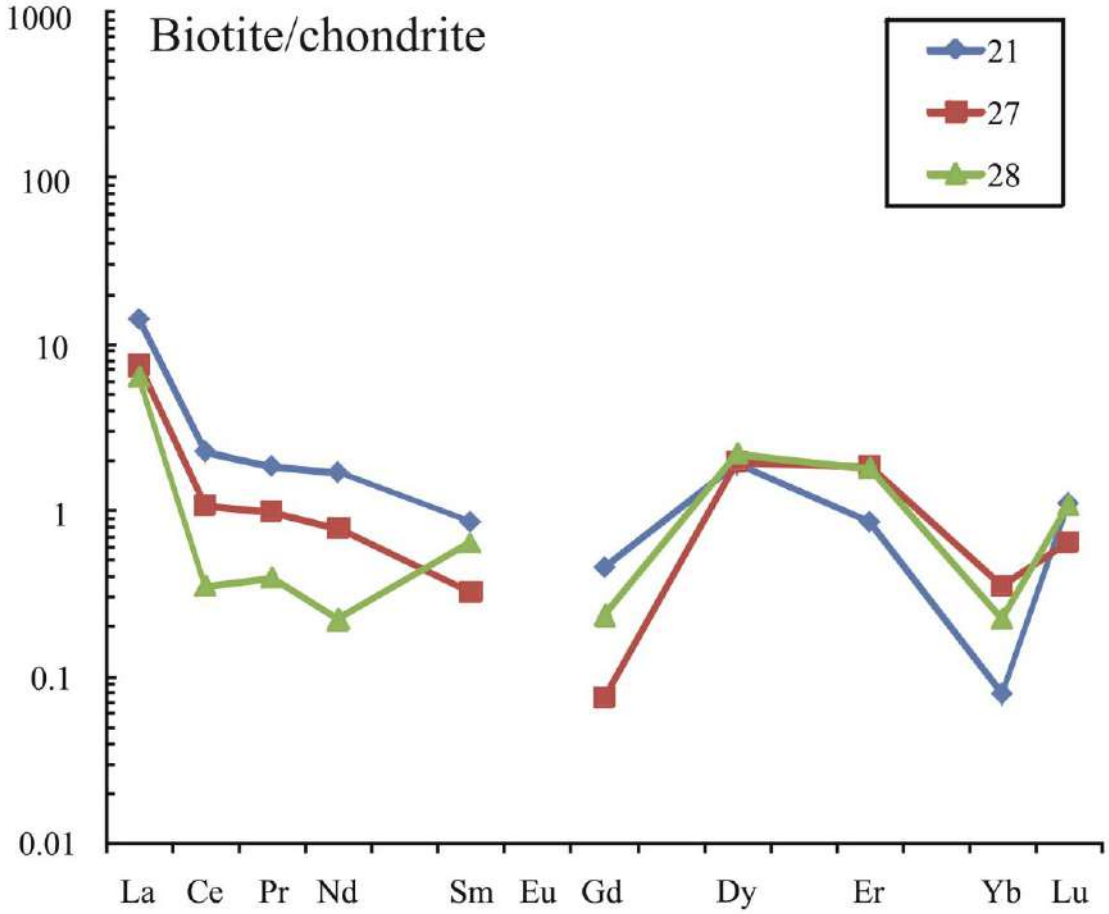

Fig. 45. Distribution spectra of rare earth elements in biotite from corundum-bearing metasomatites of the Khitoostrov occurrence.

Plagioclase

The content of rare-earth elements in plagioclase was analyzed at 4 points: 2 - in apogabbroic garnet amphibolite, 2 - in corundum-bearing rock.

Plagioclases from apogabbroic amphibolites are characterized by a flat REE distribution spectrum (Fig. 46a), while plagioclases from corundum-bearing rock are slightly enriched in LREE, which causes the spectrum to acquire a slight negative slope (Fig. 46b). Both of them are characterized by a pronounced positive europium anomaly, which is typical for plagioclases.

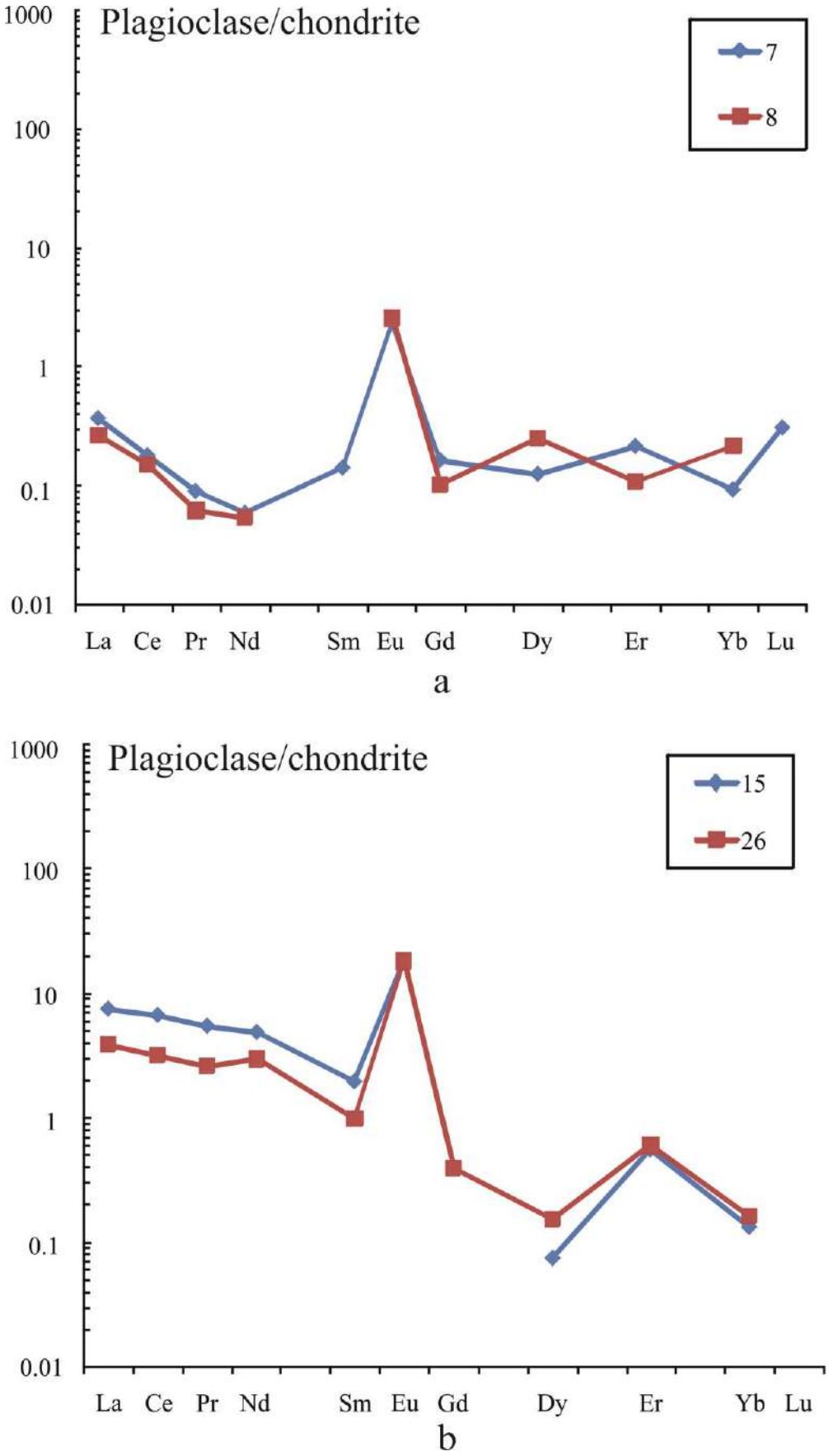

Fig. 46. Distribution spectra of rare earth elements in plagioclase: a - from apogabbroic garnet amphibolites, b - from corundum-bearing metasomatites of the Khitoostrov occurrence.

Apatite

Apatite from kyanite-garnet-biotite gneisses of the Chupa sequence (Fig. 47) is characterized by a convex REE distribution spectrum, the slope of which varies from positive in the LREE region to negative in the HREE region, with a pronounced negative Eu anomaly. Apatite from garnet amphibolites is characterized by a somewhat less convex REE distribution spectrum without a negative Eu anomaly; the content of all REEs, except for Eu, is slightly lower in it compared to apatite from host gneisses.

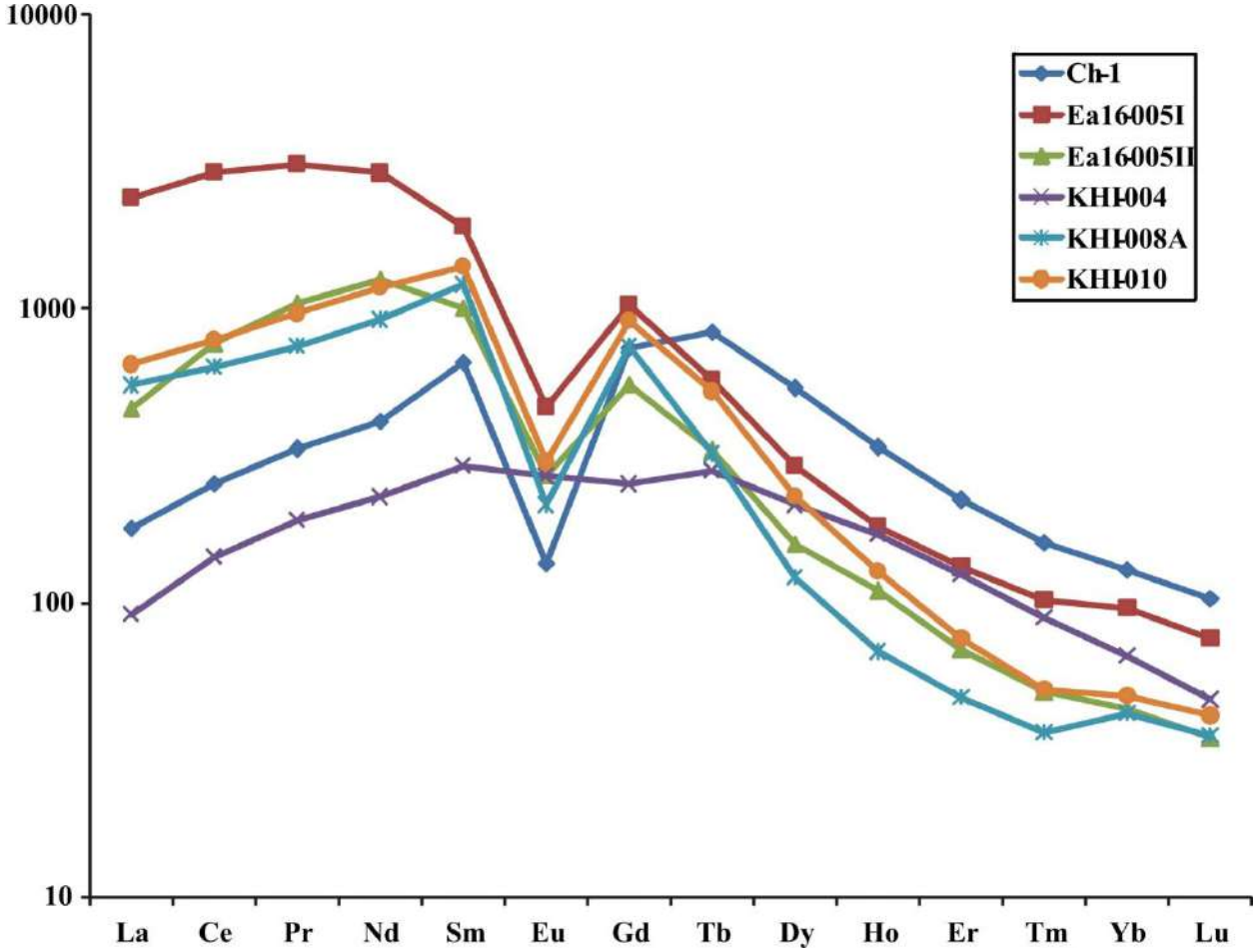

Fig. 47. Chondrite-normalized spectra of REE distribution in apatite from corundum-bearing metasomatites (zone 2 - KHI-008A, zone 4 - KHI-010, Ea16-005II), plagioclasites (Ea16-005I) and garnet amphibolites (KHI-004) of the Khitoostrov occurrence, kyanite-garnet-biotite gneisses of the Chupa sequence (Ch-1).

Apatite from corundum-bearing rocks of Khitoostrov is somewhat similar in REE distribution spectrum to apatite from host kyanite-garnet-biotite gneisses: here the slope of the spectrum also changes from positive in the LREE region to negative in the HREE region, and there is a pronounced negative Eu anomaly. But there are also differences: apatite from corundum-bearing rocks is significantly enriched in LREE and depleted in HREE. These features—higher LREE and lower HREE—distinguish it from apatite from garnet amphibolites.

Apatite from plagioclasites is similar in the REE distribution spectrum to apatite from corundum-bearing rocks, but differs in an even more pronounced enrichment in LREE, as well as a slightly higher content of HREE. The similarity of the REE distribution spectra in apatite from corundum-bearing rocks and from plagioclasites indicates their genetic relationship.

REE in apatite is a valuable source of information about the mineral formation environment. Thus, the REE content and the magnitude of the Eu and Ce anomalies are a marker of redox conditions in a magma or hydrothermal fluid (Drake, 1975; Cao et al., 2012; Mao et al., 2016); informative are also diagrams in coordinates Ce *vs* Th, REE *vs* La/Sm (Belousova et al., 2002). Since most of these diagrams are designed for igneous rocks, we can only rely on the relative position of the points on such diagrams. On the diagrams Ce/Ce* *vs* Eu/Eu* (Fig. 48), Ce *vs* Th, REE *vs* La/Sm (Fig. 49 a, b) it can be seen that apatite from corundum-bearing rocks crystallized under conditions of higher oxygen fugacity than apatite from host kyanite-garnet-biotite gneisses. The position of the point of garnet amphibolites is less informative, additional studies are required.

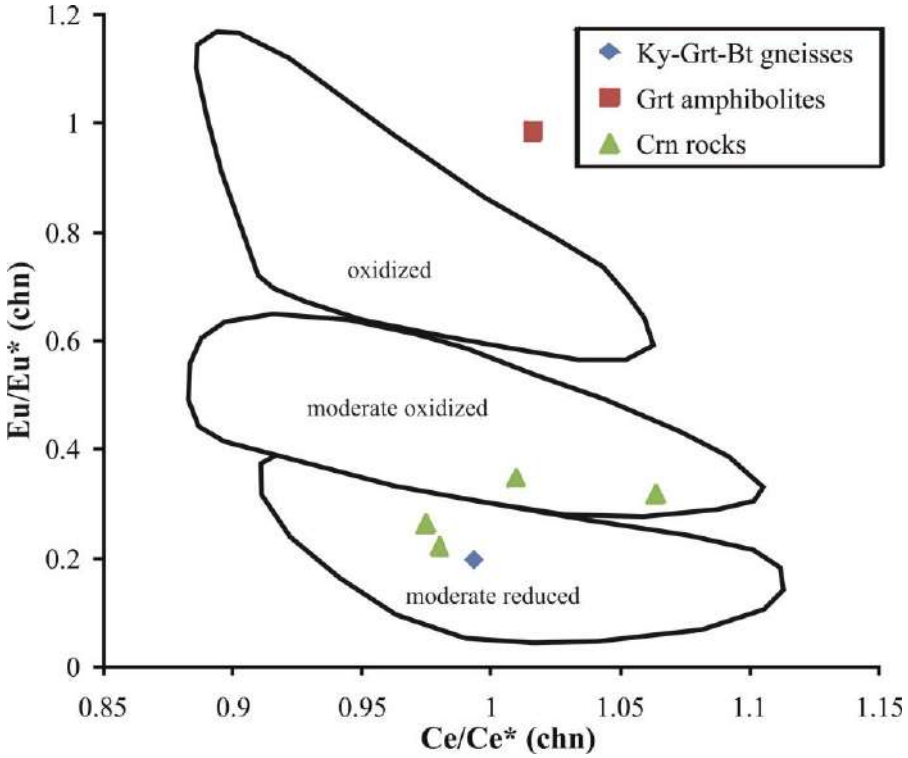

Fig. 48. Compositions of the studied apatites on the genetic diagram Ce/Ce* (chondrite normalized) vs Eu/Eu* (chondrite normalized) with plotted fields of different mineral formation settings (after Cao et al., 2011).

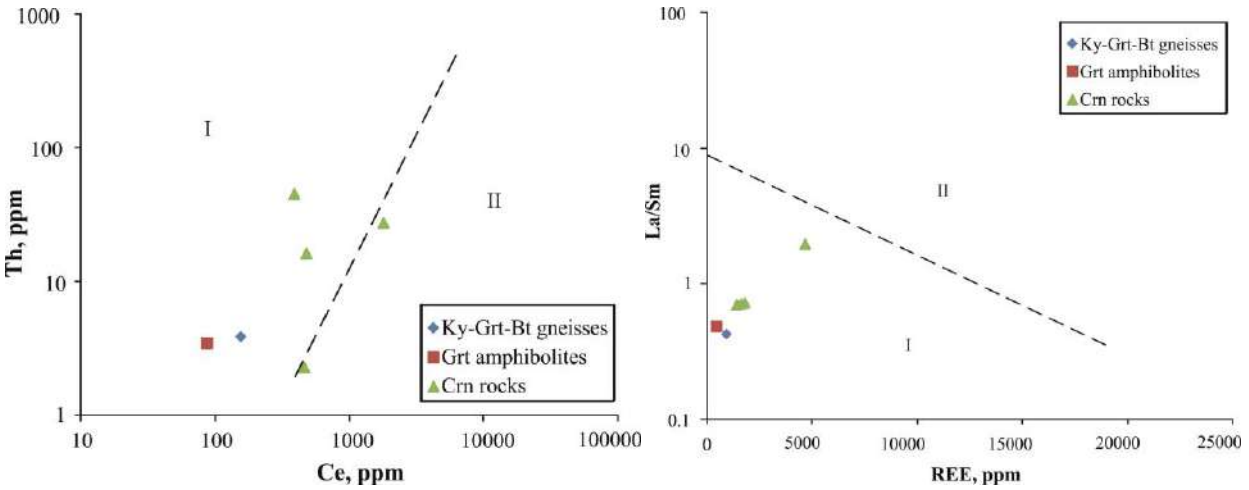

a b

Fig. 49. Compositions of the studied apatites in the diagrams: (a) Ce vs Th, (b) REE vs La/Sm used to assess redox conditions. Field I corresponds to rocks with $Fe_2O_3/FeO < 1$, field II corresponds to rocks with $Fe_2O_3/FeO>1$ (after Belousova et al., 2002).

The Th content and the Mn/Sr ratio in apatites from all studied rocks fall within the range characteristic of apatite from metamorphic rocks (Henrich et al., 2018), but due to higher Sr contents, apatite points from corundum-bearing rocks are somewhat to the left of apatite points from host rocks (Fig. 50). In the Sr/Y vs ∑LREE diagram (O'Sullivan et al., 2020), the apatite composition points from most of the analyzed rocks also fall into the apatite field of medium-temperature metamorphic rocks, but the apatite points from corundum-bearing rocks are slightly shifted up and to the right (Fig. 51), which is due to an increase in Sr and LREE contents. The excess of LREE in this case, apparently, indicates the mobile behavior (introduction) of LREE during metasomatism (Akimova, Skublov, 2021).

In addition to the above features, apatite from corundum-bearing rocks against the background of host rocks (gneisses and amphibolites) is distinguished by an increased content of Na_2O, MgO, Pb, Th, U, and a reduced content of SiO_2. It is also distinguished from apatite from host gneisses by an increased content of CaO, P_2O_5, TiO_2, Fe_2O_3, Sr, Nb, and a reduced content of Al_2O_3, K_2O, Cr, Mn, Ba, Y (see Appendix 4).

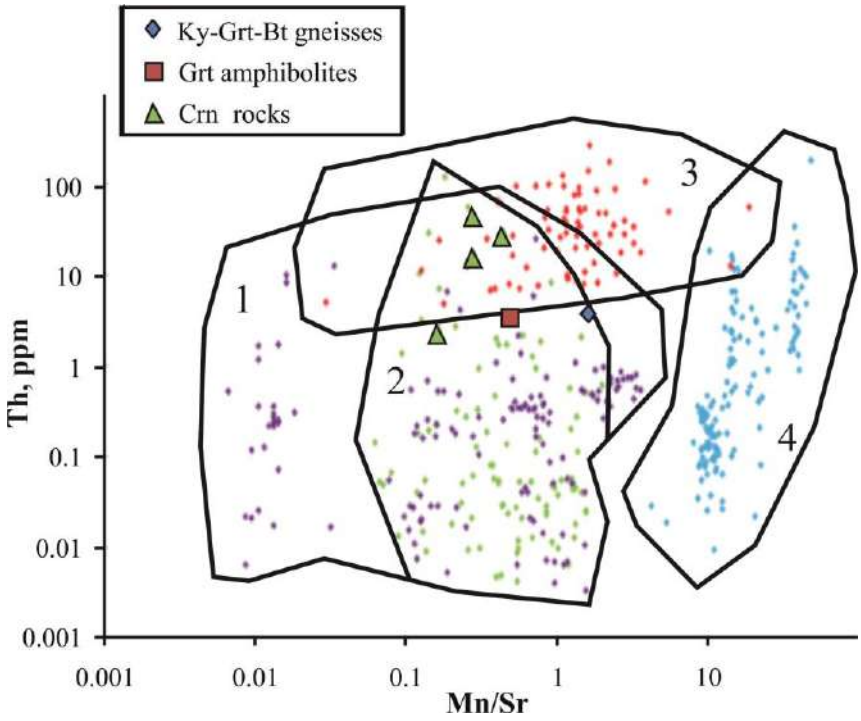

Fig. 50. Compositions of the studied apatites on the Mn/Sr vs Th genetic diagram with plotted fields and dots of varieties of metamorphic rocks (after Henrich et al., 2018). Symbols: 1 – metapelites, 2 – metabasites, 3 – orthogneisses, 4 – paragneisses.

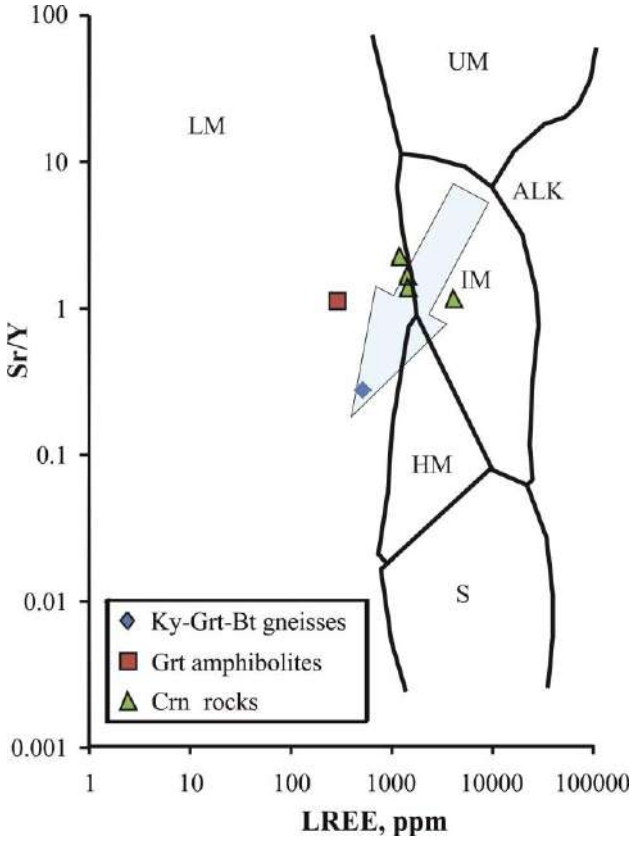

Fig. 51. Compositions of the studied apatites on the Sr/Y vs ∑LREE genetic diagram with plotted fields of the main rock types (after O'Sullivan et al., 2020). Legend: ALK – alkaline igneous rocks, HM – rocks of high metamorphic stages and migmatites, IM – I-type granitoids

and mafic igneous rocks, LM – rocks of low and middle stages of metamorphism, metasomatites, S – S-type granitoids, UM – ultramafic rocks, incl. carbonatites, lherzolites, pyroxenites. The arrow shows the expected trend in fluid processing.

4.2. Rare earth elements in minerals of clinozoisite amphibolites

The distribution pattern of REE in *garnets* was analyzed in one large garnet porphyroblast, at five points. The analysis was performed for the grain cores (c), middle parts (m) and rims (r). The distribution spectra of REE in garnet from clinozoisite amphibolites are characterized by a clearly pronounced positive slope from light to heavy REE (Fig. 52a). A slightly pronounced positive negative europium anomaly is noted, despite the high calcium content of the garnet. Zoning for rare earth elements is practically not manifested. The central parts of a garnet grain are slightly enriched in HREE and depleted in LREE compared to the marginal parts. Similar distribution spectra of rare earth elements have already been described earlier in garnets from the rocks of the Belomorian mobile belt (Skublov, 2005).

The distribution spectra of REE in *biotites* from clinozoisite amphibolites were estimated at two points in the distribution of plagioclase-amphibole symplectites around the garnet. Biotite is characterized by an unusual "sinusoidal" REE distribution spectrum with very pronounced positive anomalies in the content of lanthanum and samarium (Fig. 52b). At the same time, a negative europium anomaly is not recorded in them.

The distribution spectra of REE in *calcium amphiboles* from clinozoisite amphibolites were estimated at three points, both outside the area of distribution of plagioclase-amphibole symplectites (Cam1) and inside it (Cam2). A pronounced difference in the distribution spectra of REE in Cam1 and Cam2 is recorded (Fig. 52c). Calcium amphibole in the rock matrix is characterized by a flat spectrum with a very weakly pronounced negative europium anomaly. Similar distribution spectra of rare earth elements are characteristic of calcium amphiboles from rocks of the high-temperature amphibolite facies of metamorphism (Skublov and Drugova, 2003). At the same time, the spectrum of calcium amphibole from plagioclase-amphibole symplectites is more unusual – it acquires a significant positive slope, a rather pronounced negative cerium anomaly appears.

The content of rare earth elements in *plagioclase* was analyzed at two points outside the plagioclase-amphibole symplectites. It was not possible to establish the composition of plagioclase within symplectites, since it is strongly sericitized in them. Plagioclases from clinozoisite amphibolites are characterized by a flat REE distribution spectrum (Fig. 52d) and a clearly pronounced positive Eu anomaly, which is typical for plagioclases.

The distribution spectra of REE in *clinozoisite* from clinozoisite amphibolites were estimated at three points (Fig. 52e). Significant variability of the REE distribution spectrum in clinozoisite is noted: the total content of REE changes, the slope of the spectrum varies from almost flat to a significant positive slope, the degree of manifestation of a positive europium anomaly (from weakly pronounced for clinozoisite with a flat spectrum to significant in clinozoisite with a sloping spectrum). As a rule, minerals of the epidote group in different rocks act as a LREE concentrator; therefore, the REE distribution spectrum in them usually acquires a negative slope to varying degrees (Frei et al., 2004). Comparison with the known spectra of minerals of the epidote group suggests that clinozoisite in clinozoisite amphibolites acquires an uncharacteristic REE distribution spectrum.

The content of rare earth elements in *titanite* was analyzed in 2 grains within plagioclase-amphibole symplectites (Fig. 52f). Titanites are characterized by a convex REE distribution spectrum with a slight negative europium anomaly and a slightly increased lutetium content. This shape of the REE distribution spectrum indicates that titanite in clinozoisite amphibolites could not have been formed by replacing garnet; otherwise, titanite would have been characterized by a different distribution spectrum, convex in the HREE region.

The content of rare earth elements in rutile was also analyzed in 2 grains - inclusions in a large garnet porphyroblast. Rutile is high in niobium (2196–3046 ppm), while the chromium content is low (about 650 ppm), Nb/Ta = 38–42, Zr/Hf = 71–76. The high content of niobium and low content of chromium combine the analyzed rutile with rutiles from metapelites (Zack et al., 2004).

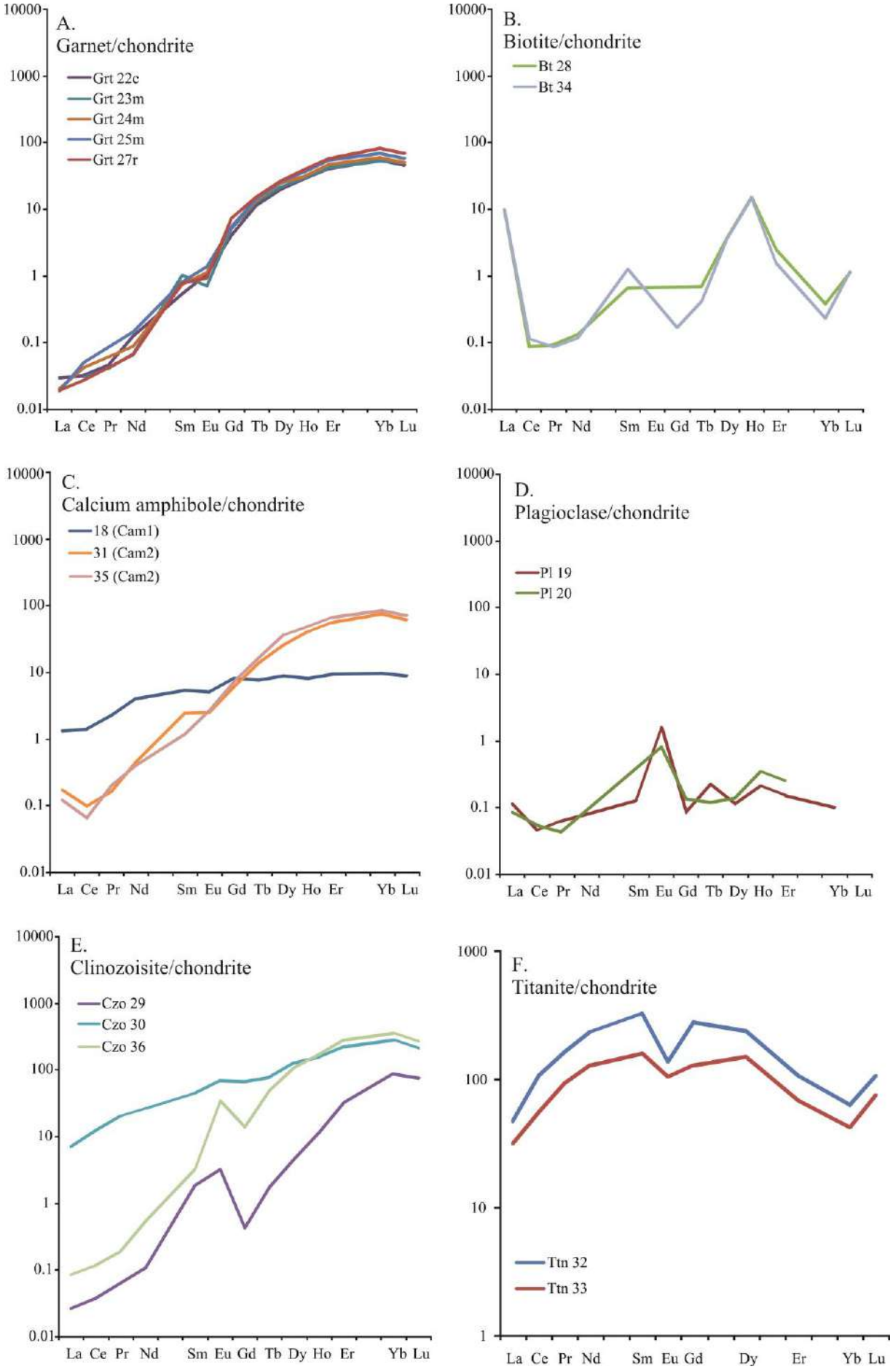

Fig. 52. REE distribution spectra in minerals from clinozoisite amphibolites

Of interest is the fact that some of the minerals (clinozoisite, calcium amphibole) acquire uncharacteristic REE distribution spectra (Akimova, Skublov, 2023). Thus, the spectrum of calcium amphibole from plagioclase-amphibole symplectites around garnet is very similar to the spectrum of garnet along which it develops (Fig. 53). When comparing the spectra of garnet and calcium amphibole from symplectites, it can be seen that the spectrum of calcium amphibole differs from the spectrum of garnet only by a slightly increased content of LREE, especially lanthanum; and in the region of heavy REE, its spectrum completely inherits the spectrum of garnet.

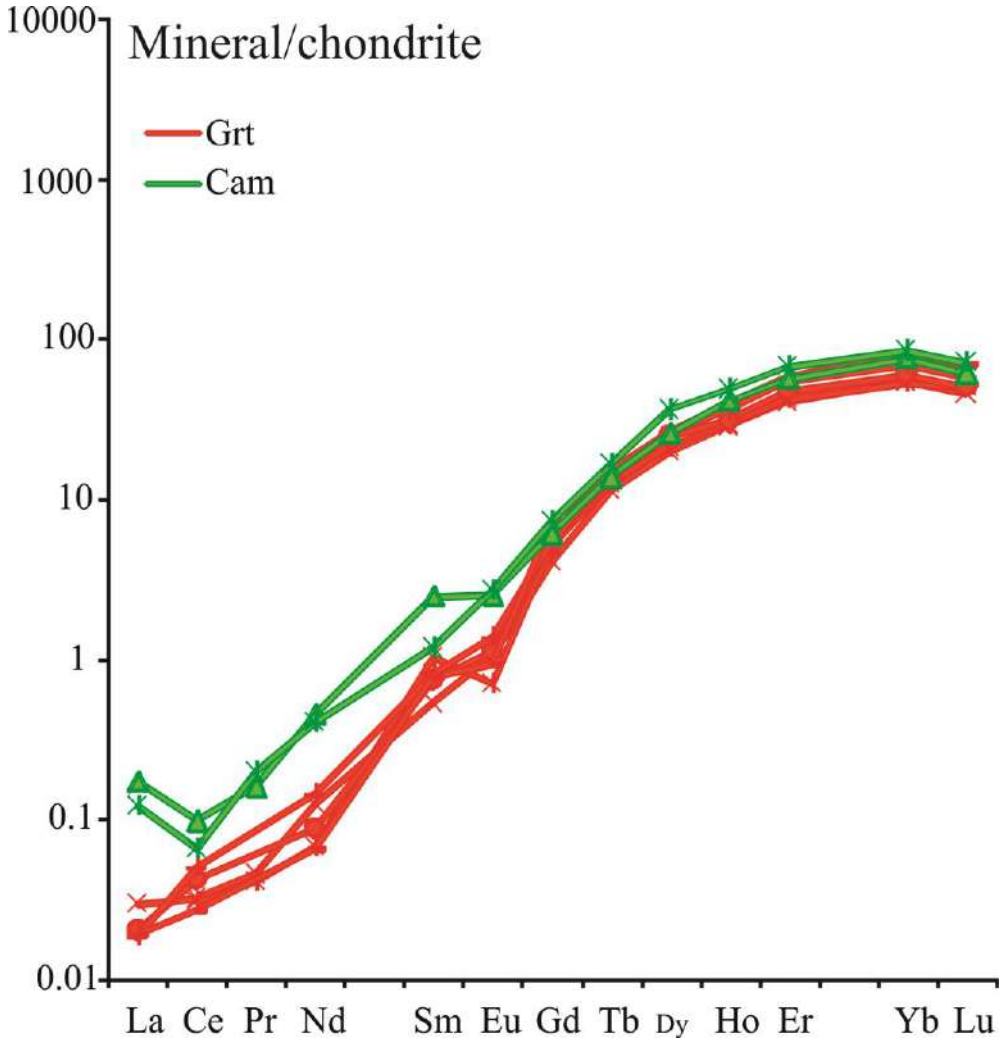

Fig. 53. Inheritance of garnet REE distribution (Grt) by calcium amphibole from plagioclase-amphibole symplectites (Cam2).

A similar picture is observed for clinozoisite. When comparing the spectrum of clinozoisite and the spectrum of calcium amphibole from the amphibolite matrix, it can be seen that although the content of all REEs in clinozoisite is higher, it partially copies the flat spectrum of calcium amphibole (Fig. 54).

Clinozoisite also develops after calcium amphibole in the area of plagioclase-amphibole symplectites around garnet, partially inheriting its spectrum, which calcium amphibole, in turn, inherited from garnet. At the same time, the spectrum is already inherited with significant differences: the REE content changes (and it can both decrease and increase), a positive europium anomaly is acquired, and sometimes the content of samarium also increases (Fig. 55).

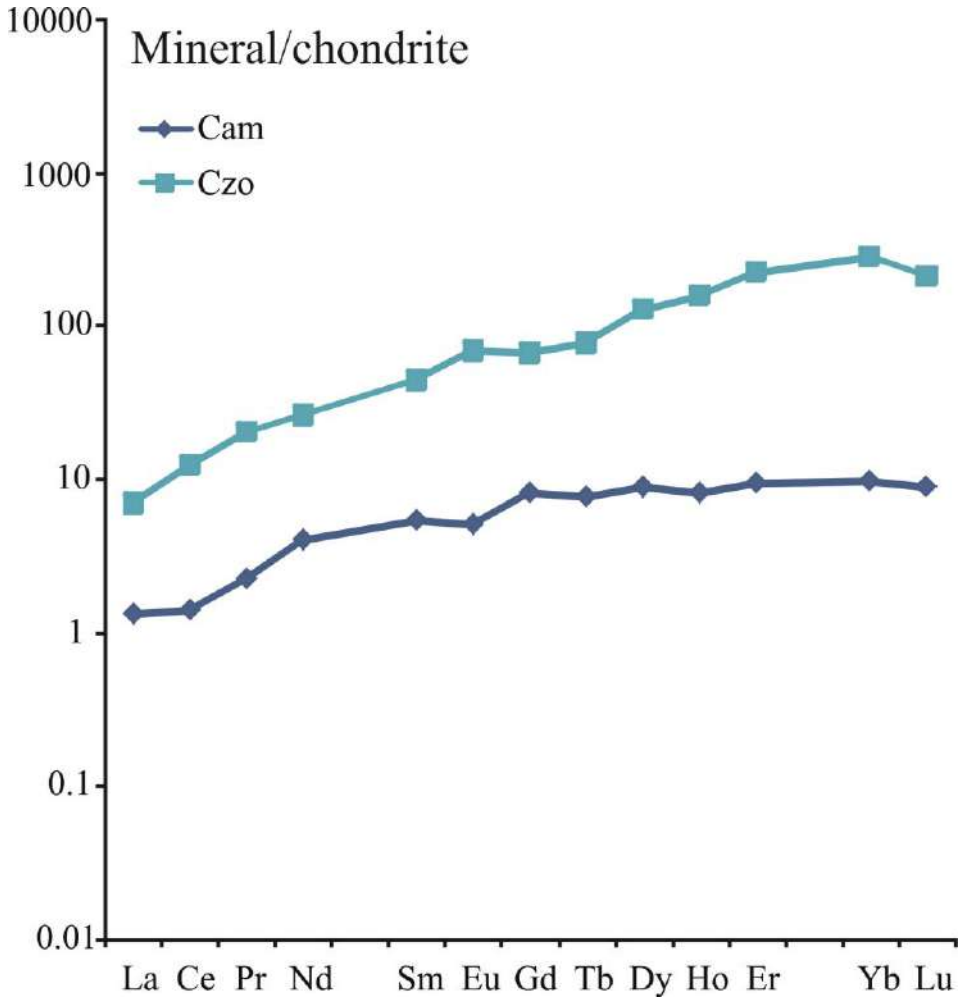

Fig. 54. Inheritance by clinozoisite (Czo) of the REE distribution spectrum of calcium amphibole from the rock matrix (Cam1).

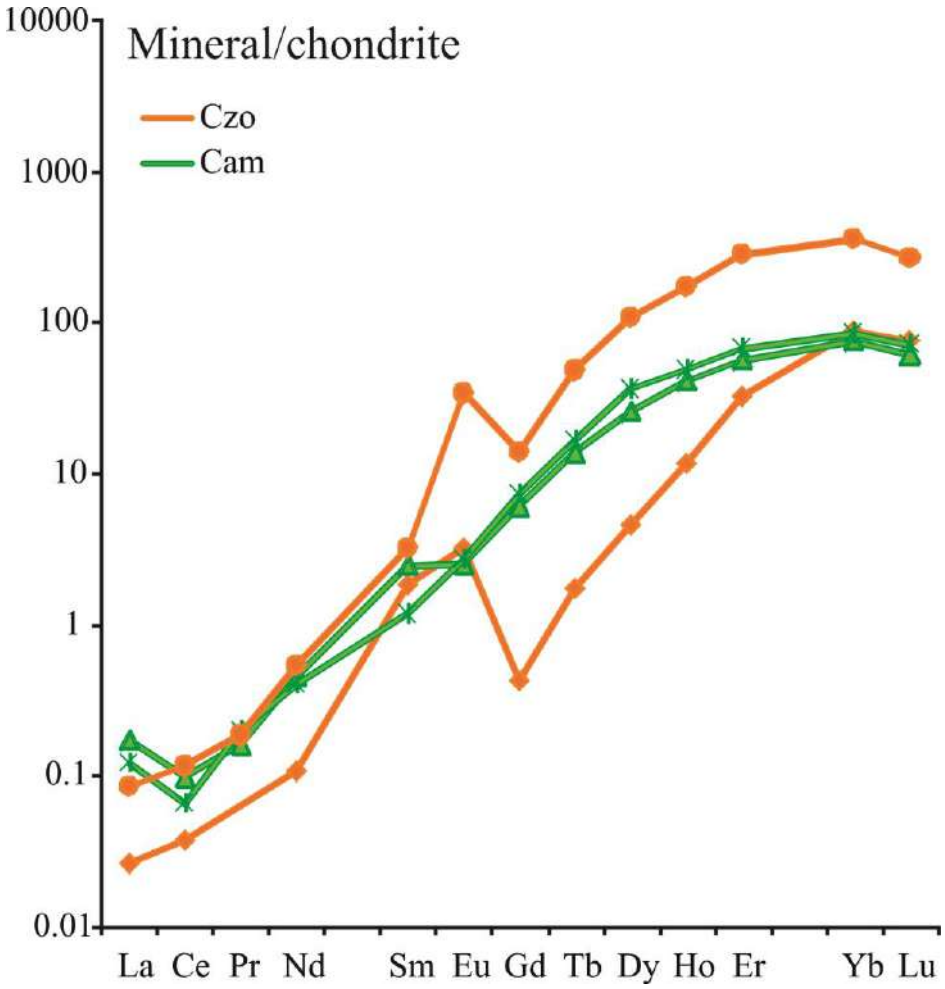

Fig. 55. Inheritance by clinozoisite (Czo) of the REE distribution spectrum of calcium amphibole from plagioclase-amphibole symplectites (Cam2), which inherits the spectrum of garnet.

Conclusions to chapter 4

Thus, it has been established that the minerals of corundum-bearing rocks (garnet, calcium amphibole, apatite) and the associated clinozoisite amphibolites are to some extent enriched in LREE against the background of host rocks – garnet amphibolites after gabbro, as well as kyanite-garnet-biotite gneisses of the Chupa sequence (Skublov, 2005). It should be noted that, in total, corundum-bearing rocks and clinozoisite amphibolites contain a higher LREE content than kyanite-garnet-biotite gneisses of the Chupa sequence (Myskova et al., 2000; Terekhov, 2007) and garnet amphibolites, respectively. In clinozoisite metasomatites associated with corundum ones, the effect of inheritance of the REE distribution was established when garnet was replaced by Ca-amphibole and clinozoisite.

Chapter 5. Fluid inclusions in minerals of metasomatites and host rocks of Khitoostrov occurrence

Among the host rocks, 3 samples of gneisses of the Chupa sequence and 2 samples of garnet amphibolites were studied. All varieties of these rocks contain quartz, which is why fluid inclusions were studied in it. As a rule, these are chains of irregularly shaped inclusions 5–20 μm in size.

In the migmatized kyanite-garnet-biotite gneisses at the contact with corundum-bearing rocks, there are chains of primary-secondary water-salt inclusions with average Tml = -33°C, Tmf = -21°C (corresponding to 17 wt.% $CaCl_2$ and 5 wt. % NaCl), there are also a few secondary water-salt inclusions with average Tml = -23°C, Tmf = -6°C (corresponding to 7 wt.% NaCl) (Fig. 56 a, b).

In migmatized kyanite-garnet-biotite gneisses at some distance from the occurrence of corundum-bearing rocks, there are chains of primary-secondary water-salt inclusions with average Tml = -49°C, Tmf = -13°C (which corresponds to 15 wt.% $CaCl_2$ and 1 wt.% NaCl), as well as less common chains of secondary water-salt inclusions with average Tml = -57°C, Tmf = -19°C (probably H_2O-NaCl-$CaCl_2$-$LiCl_2$ system) (Fig. 56d).

In migmatized garnet-biotite gneisses at some distance from the occurrence of corundum-bearing rocks, there are chains of primary-secondary water-salt inclusions with average Tml = -51°C, Tmf = -21°C (corresponding to 20 wt.% $CaCl_2$ and 1 wt.% NaCl), as well as chains of secondary water-salt inclusions with average Tml = -49°C, Tmf = -7°C (corresponding to 10 wt.% $CaCl_2$ and 1 wt.% NaCl) (Fig. 56c).

Migmatized garnet amphibolites contain single primary water-salt inclusions with mean Tml = -44°C, Tmf = -25°C (corresponding to 21 wt.% $CaCl_2$ and 2 wt.% NaCl), chains of primary-secondary inclusions with mean Tml = -40°C, Tmf = -9°C (corresponding to 12 wt.% $CaCl_2$ and 1 wt.% NaCl), as well as single secondary water-salt inclusions with average Tml = -12°C, Tmf = 0°C (corresponding to ≤5 wt. % NaCl equiv.) (Fig. 57).

In all varieties of rocks with water-salt inclusions, associations sometimes contain small gas (nitrogen) inclusions.

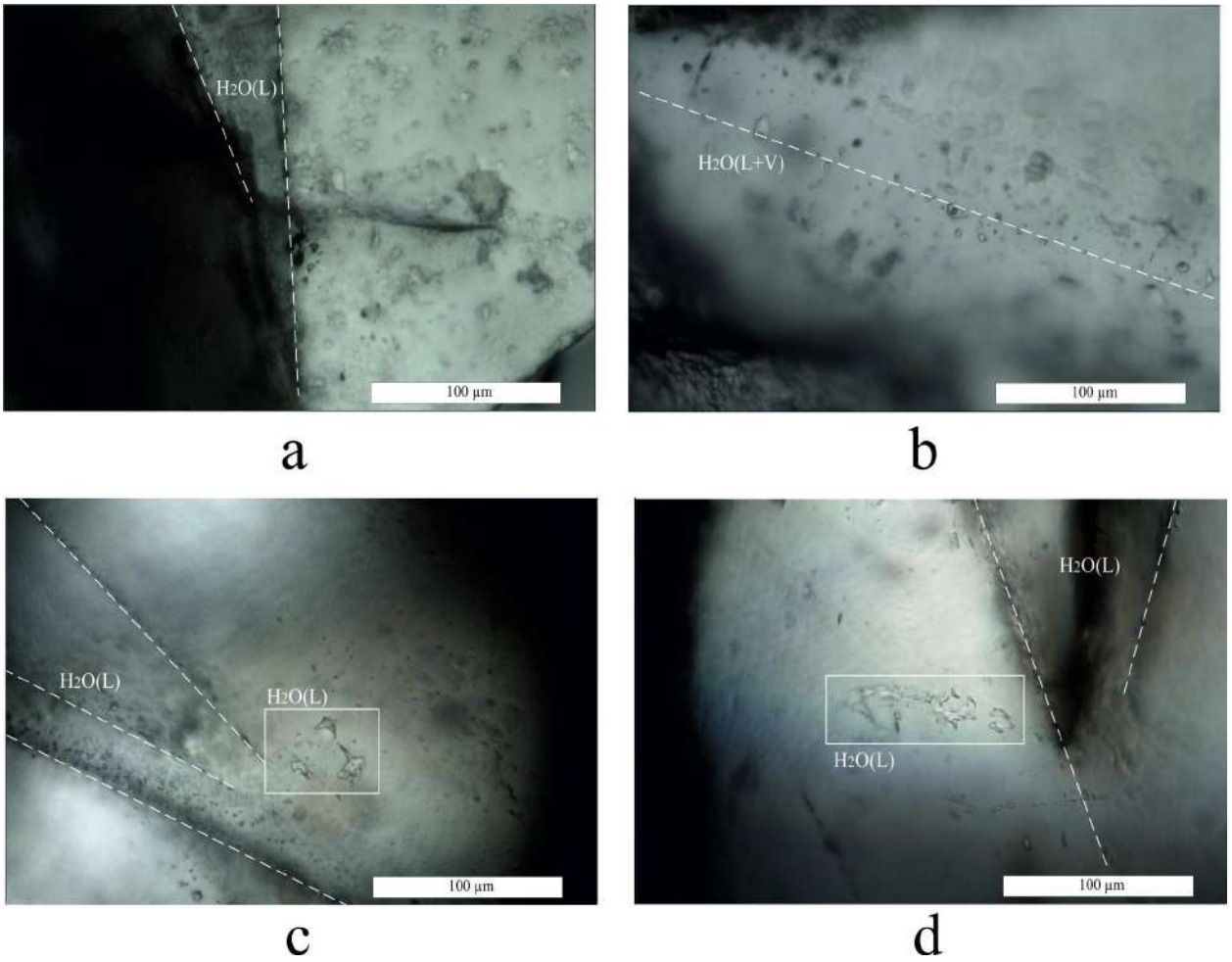

Fig. 56. Fluid inclusions in host rocks: a – chains of secondary water-salt inclusions in quartz from kyanite-garnet-biotite gneisses of the Chupa sequence at contact with corundum-bearing metasomatites, b – a chain of primary-secondary water-salt inclusions in quartz from kyanite-garnet-biotite gneisses of the Chupa sequence at the contact with corundum-bearing metasomatites, c – a group of primary-secondary and chains of secondary water-salt inclusions in quartz from garnet-biotite gneisses of the Chupa sequence at away from contact with corundum-bearing metasomatites, d – a group of primary-secondary and chains of secondary water-salt inclusions in quartz from kyanite-garnet-biotite gneisses of the Chupa sequence at a distance from contact with corundum-bearing metasomatites. L is liquid, V is gas. Dashed lines indicate chains of fluid inclusions, rectangles indicate groups of fluid inclusions.

Quartz is absent in corundum-bearing rocks (5 samples); therefore, inclusions were studied in other minerals. Corundum and kyanite contain only primary-secondary carbon dioxide fluid inclusions of a complex polygonal or round shape, 5 to 20 μm in size, less often up to 60 μm, arranged, as a rule, in chains (Fig. 58–60). In plagioclase and garnet, in addition to carbon dioxide inclusions (Fig. 61b), water-salt inclusions are also common.

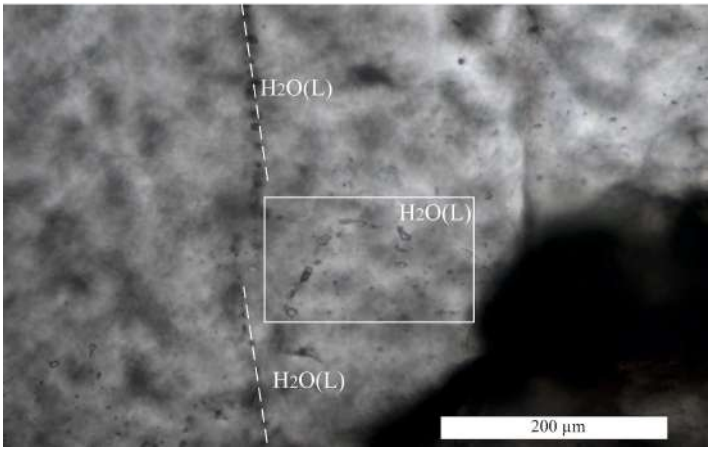

Fig. 57. Group of primary-secondary and chains of secondary water-salt inclusions in quartz from garnet amphibolites. Dashed lines indicate chains of fluid inclusions, rectangles indicate groups of fluid inclusions.

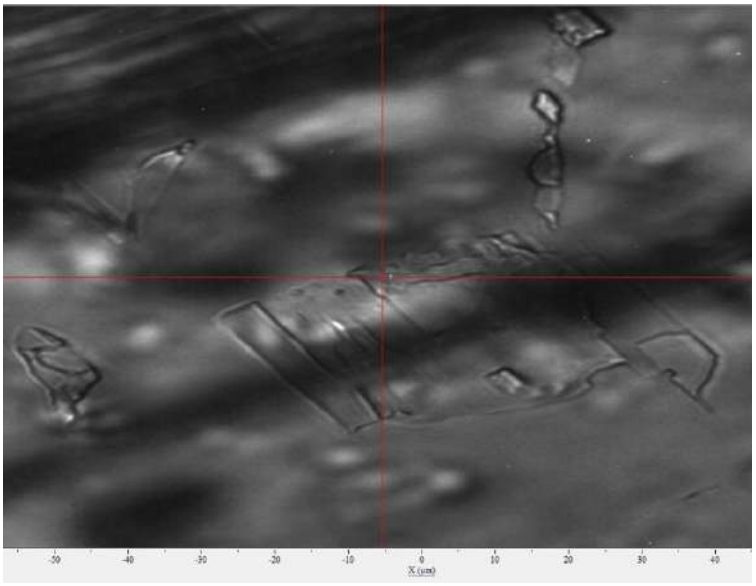

Fig. 58. Carbon dioxide inclusions in kyanite from zone 1 of corundum-bearing metasomatites (sample EA16-004).

In the rocks of zone 2, garnet contains water-salt inclusions of an elongated, rounded or more complex shape ranging in size from 1 to 10 µm. They are located in small groups far from individual fractures, so we assume that these are primary-secondary inclusions (Fig. 61a). Sometimes they are diagnosed with daughter phases represented by calcite. For them, the average Tml = -46°C, Tmf = -32°C (corresponding to 24 wt.% $CaCl_2$ and 2 wt.% NaCl).

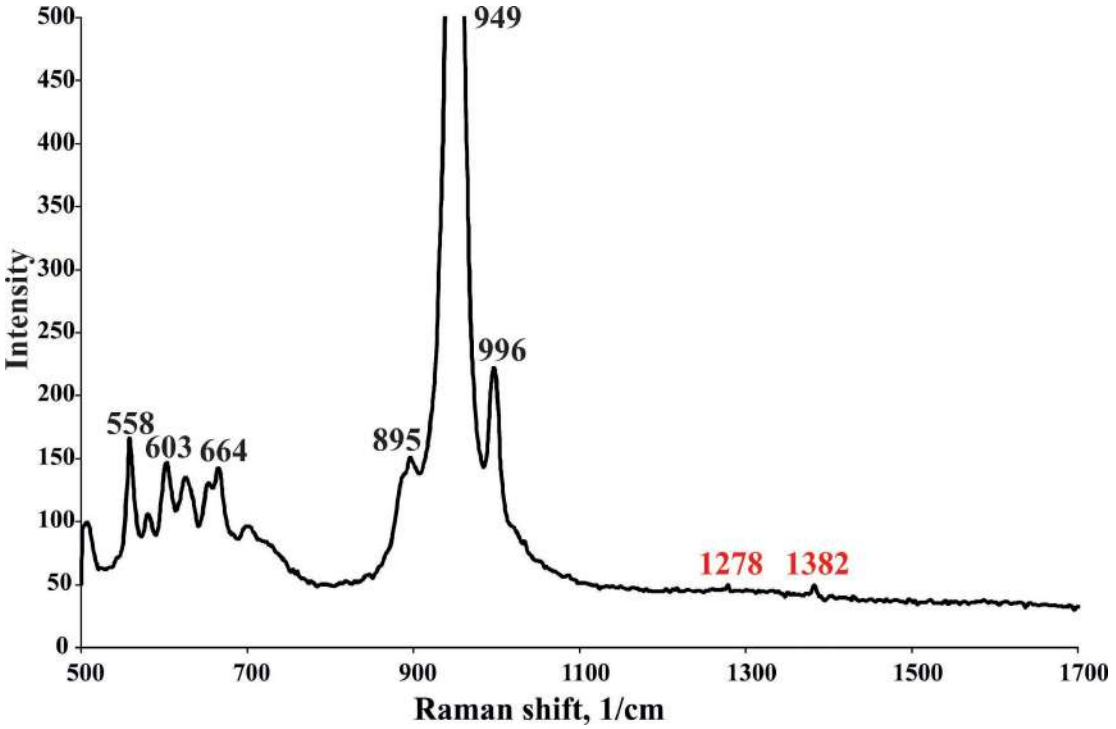

Fig. 59. Raman spectrum of kyanite (peaks are labeled in black) and carbon dioxide inclusions in it (peaks are labeled in red)

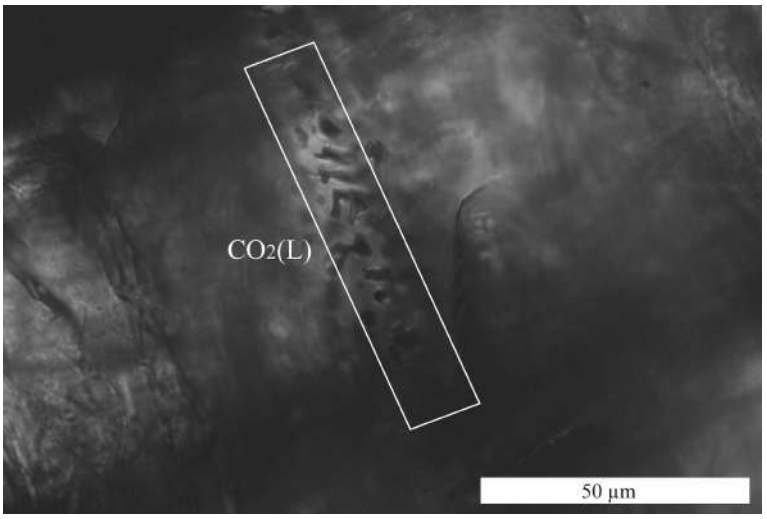

Fig. 60. A chain of primary-secondary carbon dioxide inclusions (indicated by a white rectangle) in corundum from amphibole-bearing corundum-bearing metasomatites, zone 4 (sample KHI-010).

In the rocks of zone 3a in garnet, only single primary-secondary water-salt inclusions of an elongated, rounded or more complex shape, ranging in size from 1 to 10 µm, were found. They are also sometimes diagnosed with daughter phases represented by calcite. For them, the average Tml = -49°C, Tmf = -33°C (corresponding to 24 wt.% $CaCl_2$ and 2 wt.% NaCl). In the rocks of this zone, water-salt inclusions in plagioclase are also common - most often small (about

5 μm), located along cleavage cracks, in sericitization zones, so we assume that these are secondary inclusions (Fig. 60c). For them, the average Tml = -27°C, Tmf = -13°C (corresponding to 11 wt.% $CaCl_2$ and 6 wt.% NaCl).

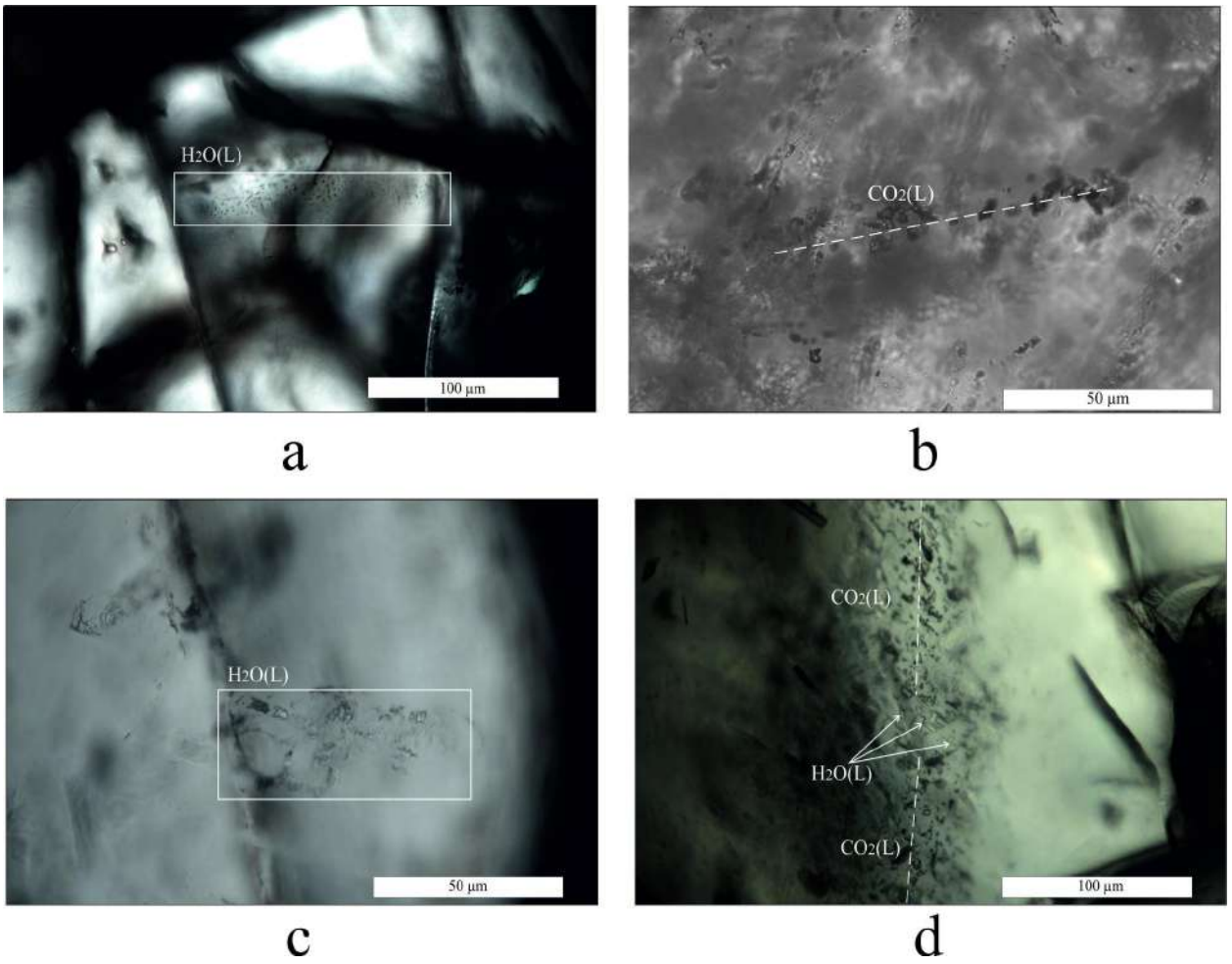

Fig. 61. Fluid inclusions in minerals of corundum-bearing metasomatites: a – a group of primary-secondary water-salt inclusions in garnet from amphibole-free corundum-bearing metasomatites, zone 2, b – a chain of primary-secondary carbon dioxide inclusions in plagioclase from amphibole-bearing corundum-bearing metasomatites, zone 4, c – chain of secondary water-salt inclusions in plagioclase from amphibole-free corundum-bearing metasomatites, zone 3a, d – a chain of primary-secondary water-salt and carbon dioxide inclusions in garnet from plagioclasites. Dashed lines indicate chains of fluid inclusions, rectangles indicate groups of fluid inclusions.

The rocks of zone 4 in garnet contain water-salt inclusions of elongated, polygonal shape ranging in size from 1 to 20 μm (Fig. 62 a–d, Fig. 63). They are located in chains or in small groups, but far from individual cracks, so we assume that these are primary-secondary inclusions. Sometimes they are diagnosed with daughter phases represented by calcite (Fig. 64,

65). For them, the average Tml = -42°C, Tmf = -32°C (corresponding to 23 wt.% $CaCl_2$ and 3 wt.% NaCl).

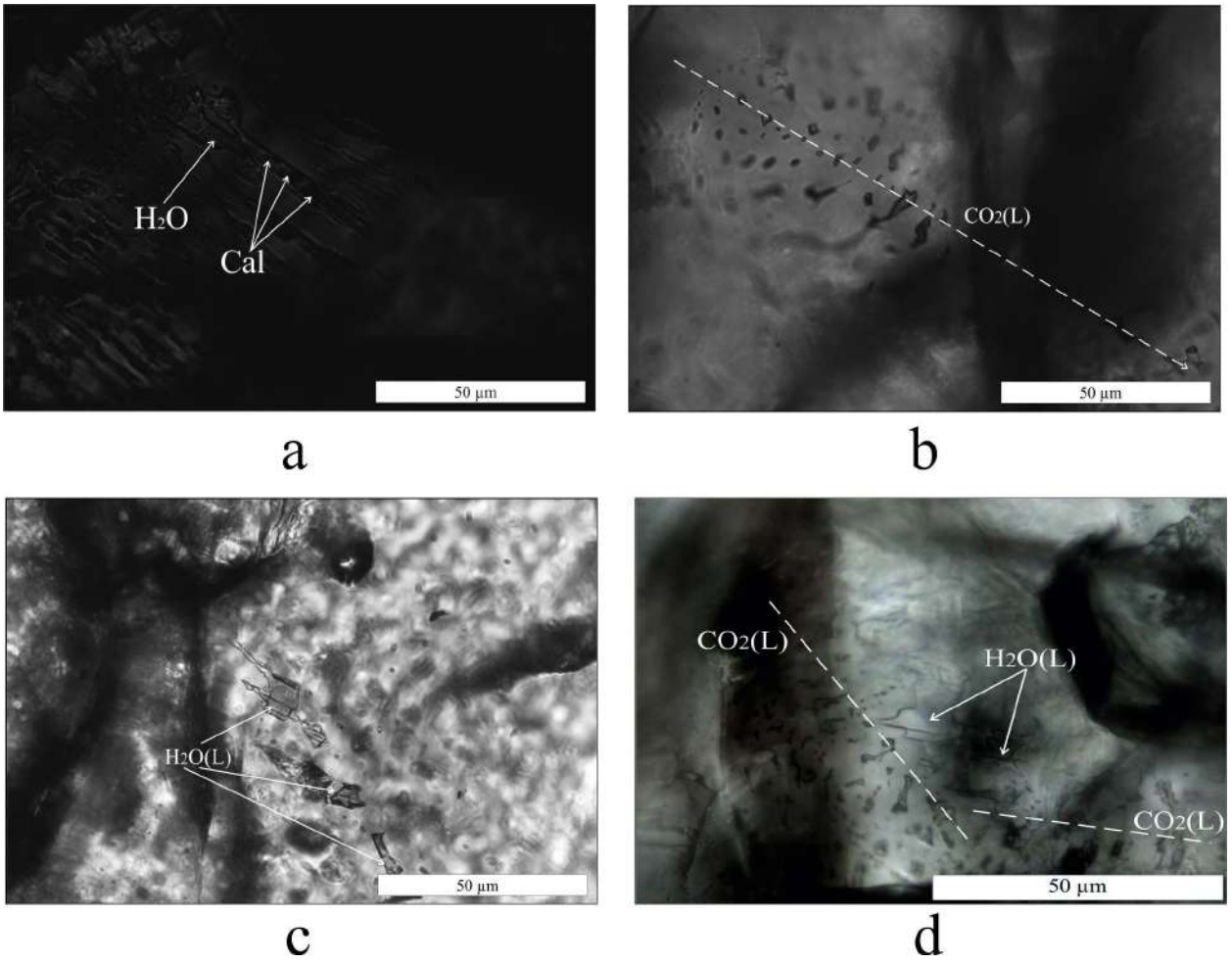

Fig. 62. Fluid inclusions in garnet from zone 4 of corundum-bearing metasomatites (sample KHI-010): a – primary-secondary water-salt inclusions with calcite crystals, b – chain of primary-secondary carbon dioxide inclusions, c – group of primary-secondary water-salt inclusions , d – group of primary-secondary water-salt and carbon dioxide inclusions. Dashed lines indicate chains of fluid inclusions.

The garnet-biotite plagioclasites in the garnet also contain primary-secondary water-salt inclusions of elongated, polygonal or more complex shapes ranging in size from 1 to 15 µm (Fig. 61d). Sometimes they are also diagnosed with daughter phases represented by calcite. For them, the average Tml = -45°C, Tmf = -34°C (corresponding to 25 wt.% $CaCl_2$ and 2 wt.% NaCl).

A summary table of microthermometric data is included in Appendix 5.

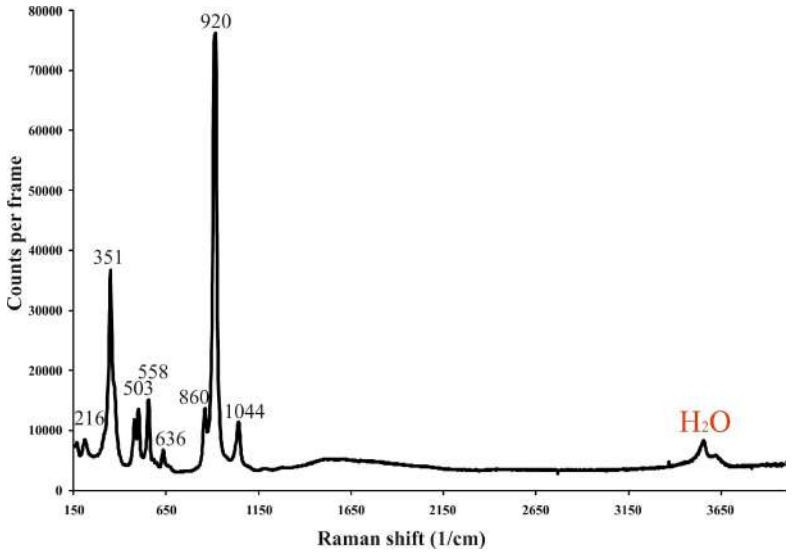

Fig. 63. Raman spectrum of a garnet (peaks in black) and a water-salt inclusion in it.

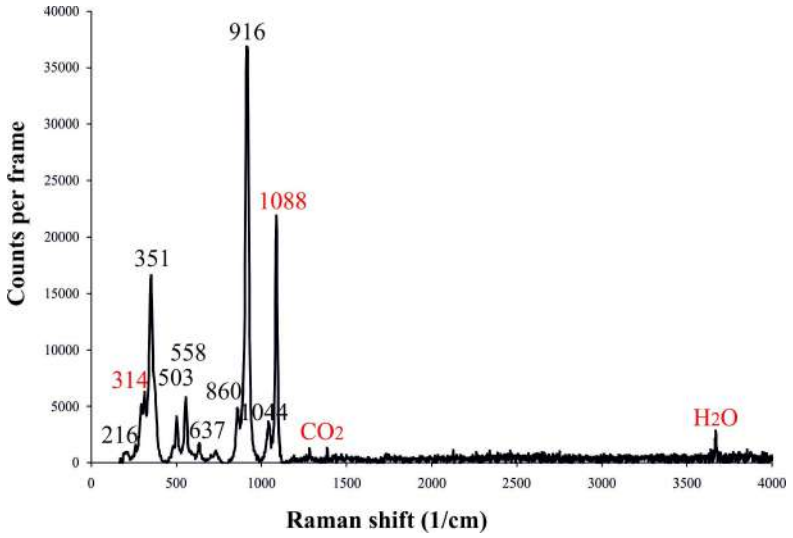

Fig. 64. Raman spectrum of a garnet (peaks in black) and a water-salt inclusion with CO2 and carbonate in it.

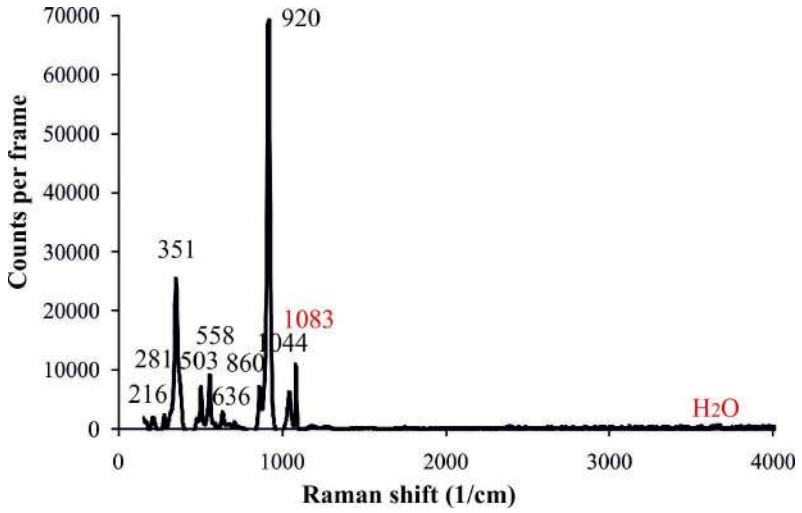

Fig. 65. Raman spectrum of a garnet (peaks are labeled in black) and a water-salt inclusion with carbonate in it.

Conclusions to chapter 5

Based on the results of the study of fluid inclusions in the minerals of corundum-bearing and host rocks, we can draw the following conclusions.

1. In the minerals of corundum-bearing and host rocks, water-salt inclusions similar in salt composition containing NaCl and $CaCl_2$ were found. Apparently, such inclusions are also characteristic of other rocks of the Belomorian mobile belt; additional studies are needed to resolve this issue. The similarity of the salt composition of fluid inclusions in corundum-bearing and host rocks indicates that these rocks were formed in a single process (the Svecofennian stage of regional metamorphism).

2. At the same time, fluid inclusions in the minerals of corundum-bearing rocks are characterized by a slightly higher total salinity. Apparently, a fluid (solution of Ca and Na chlorides) was in equilibrium with the minerals of corundum-bearing metasomatites, somewhat different in composition from the porous fluid of the host gneisses of the Chupa sequence and garnet amphibolites, being characterized by a higher concentration of salts, in particular, $CaCl_2$.

Chapter 6. Isotope-geochemical characteristics of the environment of mineral formation

6.1. Geochemistry of noble gas isotopes

Noble gases are reliable indicators of mineral formation conditions, since their isotopic ratios in different reservoirs of the Earth differ by orders of magnitude (Table 3) (Ozima, Podosek, 2002). The results of the study of the isotopic composition of noble gases are given in Table 4 (Akimova, Lokhov, 2015; Lokhov et al., 2016).

Table 3. Isotopic and elemental ratios of argon and helium in the main reservoirs of the Earth

Reservoir	**$^{3}He/^{4}He$**	**$^{40}Ar/^{36}Ar$**	**$^{4}He/^{40}Ar$**
Primitive mantle	$5*10^{-5}$	3000–5000	1–5
Depleted upper mantle	$1.4*10^{-5}$	20000–30000	5–10
Continental crust	10^{-7}–10^{-8}	5000–10000	0.01–10
Atmo- and hydrosphere	$1.2*10^{-6}$	296.5	0.002

Table 4. Results of the analysis of the isotopic composition of noble gases in samples of corundum-bearing and host rocks of Khitoostrov.

Sample	Description	$\delta^{18}O$	$^{4}He*10^{-6}$, cm^3/g	$^{3}He*10^{-6}$, cm^3/g	$^{3}He/^{4}He*10^{-6}$	$^{4}He/^{20}Ne$	$^{40}Ar*10^{-6}$, cm^3/g	$^{40}Ar/^{36}Ar$	$^{4}He/^{40}Ar$
Khi-001	Amphibolized gabbro	5.7	1.28	0.12	0.09	331	6.78	10700	0.19
Khi-002	Amphibolized gabbro	6	4.00	0.35	0.09	390	6.40	8186	0.63
NK13-006/10	Amphibolized gabbro	5.7	1.54	0.11	0.07	440	3.90	8154	0.39
NK13-069	Amphibolized gabbro	-5.5	7.06	0.51	0.07	805	7.00	7728	1.01
Khi-006	Grt-Bt gneiss	-7	0.48	0.07	0.15	155	7.69	4197	0.06
Khi-007a	Plagioclasite	-9	1.62	0.41	0.25	328	8.34	4895	0.19
Khi-007b	Pelitized plagioclasite	-9	2.96	0.34	0.12	171	23.60	1025	0.13
NK13-064/6	Grt-Bt-Hbl-Pl rock with Crn, St, Ged	-9.4	1.62	0.42	0.26	328	13.90	4786	0.12
Ea16-002	Grt-Bt-Hbl-Pl rock with Crn and St	-15	0.61	0.22	0.36	182	6.37	4640	0.10
Khi-008a	Hbl-Grt-Bt-Pl rock	-17	1.63	0.15	0.09	218	12.40	3769	0.13
Khi-008b	Amphibolite	-17	1.11	0.23	0.21	212	17.5	13780	0.06

							0		
NK13-065	Bt gneiss	8.8	1.54	0.29	0.19	478	7.90	5810	0.19
NK11-071/1	Ky-Grt-Bt gneiss	-7.3	0.72	0.19	0.26	131	6.20	4514	0.12
NK11-037B/1	Ky-Grt-Bt gneiss	8.1	48.10	4.67	0.10	353	8.20	5227	5.87
Ch-1	Ky-Grt-Bt gneiss	8	30.10	3.31	0.11	360	5.10	5420	5.90
blank			0.001			3.1	0.03	630	0.03

Note. Sample NK11-037B/1 was taken in the area of the settlement. Chupa, Ch-1 - in the area of the village Karelsky. $\delta^{18}O$ from the work of I.N. Bindeman et al. (Bindeman et al., 2014).

Primary analytical data needs to be corrected for some components that are an interfering factor in further reasoning.

1. *The correction of ^{3}He for the cosmogenic component* was made in all samples, except for corundum-bearing metasomatites, which were taken from a working with a fresh surface. The rates of cosmogenic helium generation (Niedermann, 2002; Farley et al., 2006) and the real exposure time of the glacial relief of northern Karelia, which is about 20 ka, were taken into account. The maximum possible amount of cosmogenic ^{3}He is $n \times 10^{-14}$ cm^3/g (≥10% of the observed values).

2. *Correction of ^{3}He for the nucleogenic component.* The contribution of nucleogenic ^{3}He was estimated taking into account the data (Ballentine, Burnard, 2002). In gneisses of the Chupa sequence with a metamorphic age of about 1900 Ma and contents of Li = 5–10 ppm, U, Th = 3–5 ppm (Bindeman, Serebryakov, 2011), the amount of nucleogenic ^{3}He is no more than $n \times 10^{-13}$ cm^3/g, and in metasomatites with Li < 1 ppm, U, Th = 1-2 ppm (Terekhov, Levitsky, 1991; Bindeman, Serebryakov, 2011) – much less. Thus, the contribution of nucleogenic helium is also ≥10% of the observed values.

3. *Correction of ^{40}Ar for the radiogenic component* released from the lattice of minerals during crushing (Buikin et al., 2018) and migrating from the lattice into fluid inclusions. Diffusion of radiogenic argon into fluid inclusions from the mineral lattice could be neglected, since the K-Ar age of micas and amphiboles (Budnitsky, 2013) coincides within the error with the U-Pb age from metamorphic zircon shells (Bindeman et al., 2014), although the sample preparation technique for K-Ar dating in this case involves fine abrasion of the samples. This means that there was no loss of radiogenic argon from potassium-containing minerals during crushing and its diffusion into fluid inclusions. The percentage of ^{40}Ar amphiboles released during crushing can also be quantified by comparing the data on stepwise heating and stepwise crushing of grains (monofraction 0.5–0.25 mm) of this mineral.

Stepwise heating of amphibole (6.75 mg sample). It can be seen that ^{40}Ar is released only at high temperatures (1100 - 1400°C) (Fig. 66). This temperature interval corresponds to the structural transformation of amphibole that occurs during its dehydration (Foldvari, 2011); therefore, it is obvious that all argon is released in this interval - which was in inclusions and in the amphibole lattice. In total, $2.7 * 10^{-5}$ g of radiogenic argon was released.

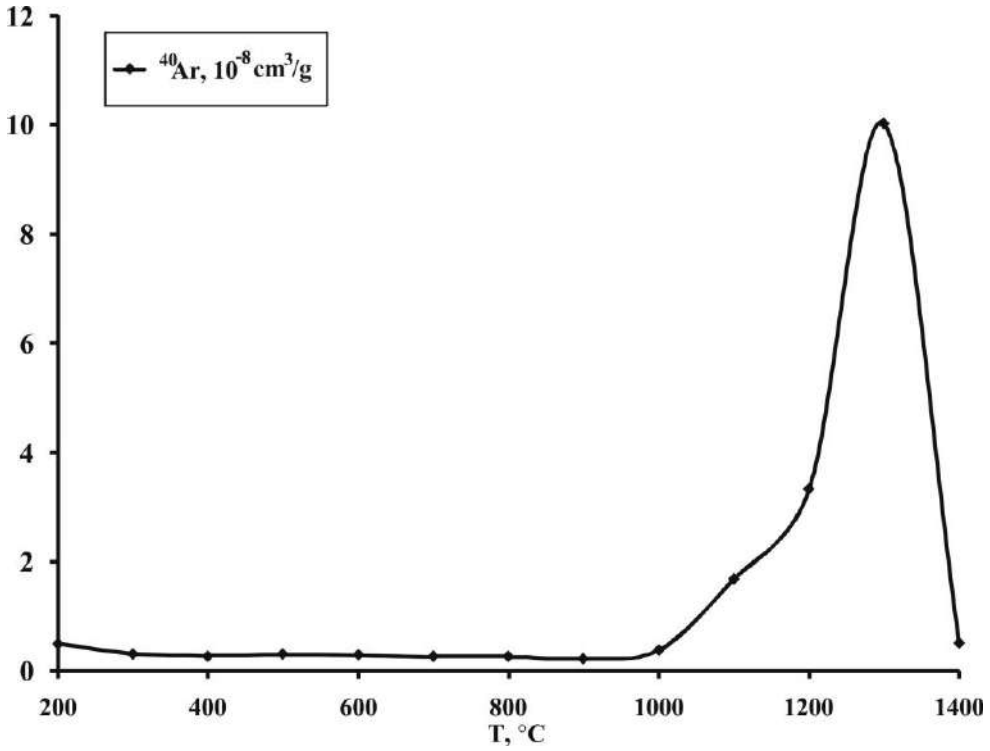

Fig. 66. Graph of the release of ^{40}Ar from amphibole during stepped heating

Stepwise crushing of amphibole (94.53 mg sample). With stepwise crushing, much less argon was released - $6 * 10^{-6}$ g. This is about 22% of the total argon released during heating. That is, the proportion of radiogenic argon released during stepwise crushing is 22% of the total argon released during stepwise heating. Since crushing in vacuum (a technique implemented at the CIR of VSEGEI) does not achieve such a number of impacts as with stepwise crushing, the amount of released radiogenic argon will be even less.

The corrected results of the study show that the isotopic compositions of noble gases differ little in fluid inclusions of minerals in rocks with normal and anomalously light oxygen isotopic compositions, but the elemental ratios are different.

Fig. 67 shows the ratios of non-radiogenic isotopes of helium, neon and argon. The rocks are characterized by wide variations in the correlated values of the $^{20}Ne/^{36}Ar$ and $^{3}He/^{36}Ar$ ratios with their decrease by more than two orders of magnitude in the direction from the original host gneisses to the rocks of the central part of the permeable zone, which have an anomalous oxygen isotopic composition. In fluid inclusions of all studied rocks, exceptionally high values of

$^{20}Ne/^{36}Ar$ and $^{3}He/^{36}Ar$ ratios are observed in relation to atmospheric gases (Akimova et al., 2017). Such significant effects of fractionation of helium and neon relative to argon can hardly be explained by the equilibrium fractionation of gases in the fluid-minerals system. Apparently, the diffusion of gases from the minerals of ancient rocks into the fluid played a significant role in the formation of metamorphic and metasomatic fluids. This effect is considered as the main mechanism of noble gas transport in crystalline lower and middle crustal rocks (Ballentine, Burnard, 2002).

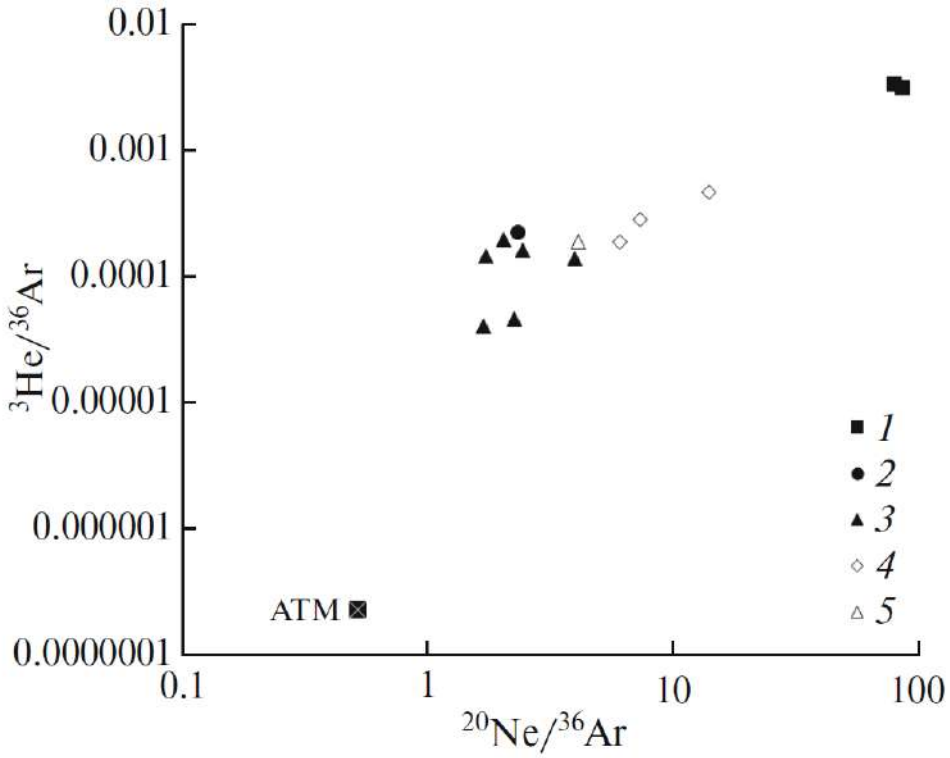

Fig. 67. Ratios of non-radiogenic isotopes of helium, neon, and argon (Akimova et al., 2017). Symbols: gneisses and metasomatites according to them: 1 – at a distance from Khitoostrov (samples NK11-037B/1, Ch-1), 2 – within Khitoostrov with a normal oxygen isotopic composition (NK13-065), 3 – within Khitoostrov with anomalous oxygen composition (NK11-071/1, Khi-006, Khi-007a, NK13-064/6, Ea16-002, Khi-008a, Khi-008b), 4 – amphibolized gabbro with normal oxygen isotopic composition (Khi-001, Khi-002, NK13-006/10) 5 – amphibolite after gabbro with anomalous oxygen isotopic composition (NK13-069). ATM is the ratio of isotopes in the atmosphere.

Fig. 68 shows that the decrease in the $^{3}He/^{36}Ar$ ratio is caused by a decrease in the concentrations of helium (hence, neon) in rocks from the permeable zone. On fig. 69, however, it is shown that the decrease in the $^{3}He/^{36}Ar$ ratio in the permeable zone is also associated with some increase in the ^{36}Ar concentration. However, the leading factor in the decrease in the values of $^{20}Ne/^{36}Ar$ and

$^{3}He/^{36}Ar$ in the permeable zone, compared to the host rocks, was a decrease in the concentrations of helium and neon (Akimova et al., 2017).

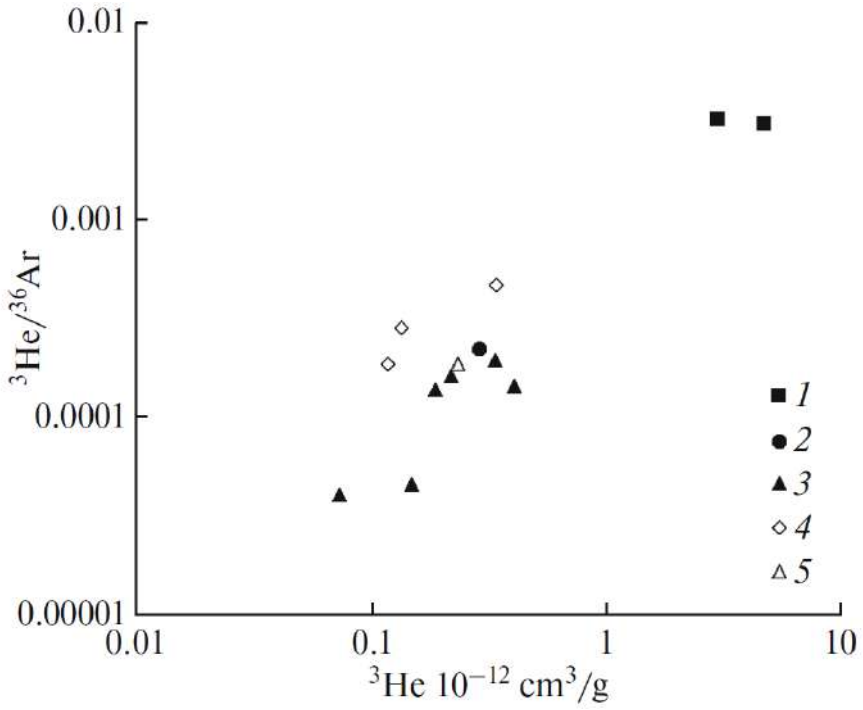

Fig. 68. Dependence of the $^{3}He/^{36}Ar$ ratio on the ^{3}He concentration (Akimova et al., 2017). Symbols are the same as in Fig. 67.

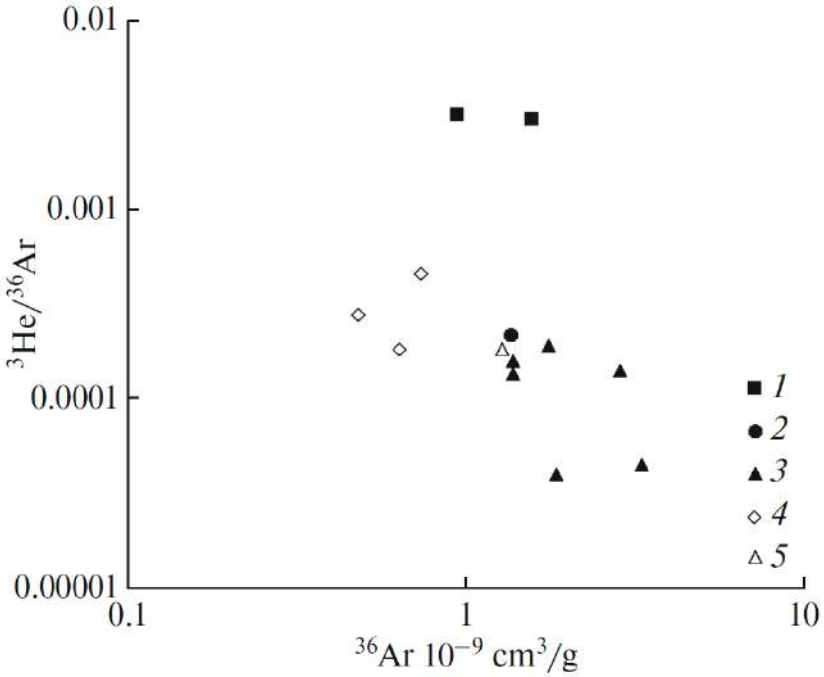

Fig. 69. Dependence of the $^{3}He/^{36}Ar$ ratio on the ^{36}Ar concentration (Akimova et al., 2017). Symbols are the same as in Fig. 67.

Fig. 70 shows the ratios of argon isotopes. As can be seen from a simple construction, in order to obtain the measured value $^{40}Ar/^{36}Ar$ = 4000–5000 in metasomatites, about 1 × 10^{-5} cm3/g of radiogenic ^{40}Ar should be added to argon in the composition of the hypothetical original clay rock with an age of 2750 Ma with $^{40}Ar/^{36}Ar$ = 750 (Akimova et al., 2017), which is unlikely.

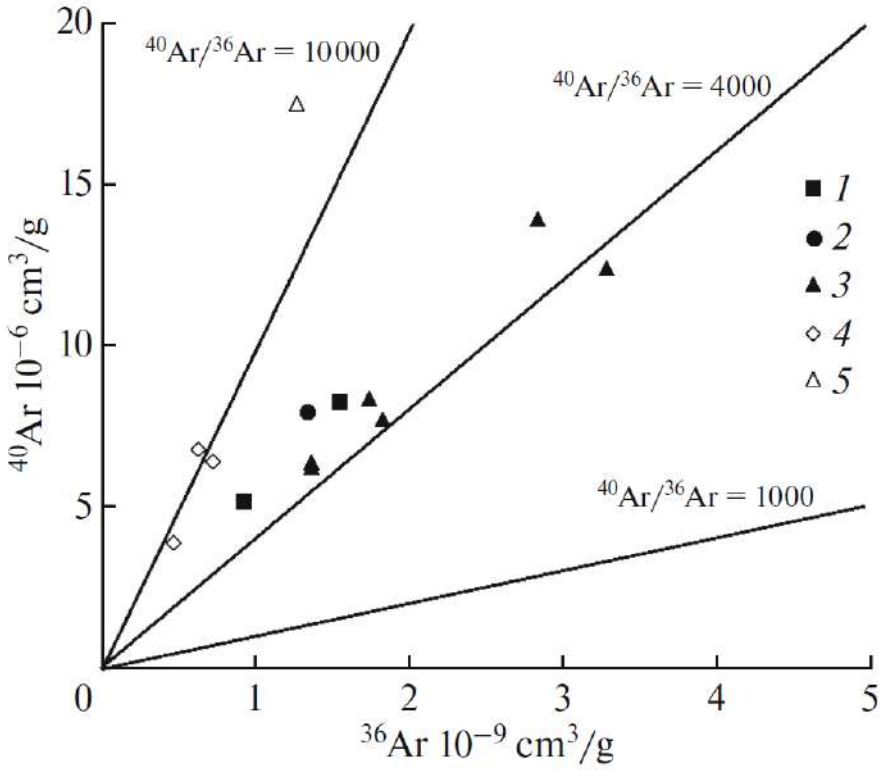

Fig. 70. Argon isotopes in rocks. Symbols are the same as in Fig. 67.

Fig. 71 shows the ratios of helium isotopes. Rocks with normal oxygen isotopic composition both outside the permeable zone and within it are characterized by a narrow range of values $^{3}He/^{4}He$ = (0.71–1.1) × 10^{-7}, and in metasomatites with anomalous oxygen isotopic composition, this value is increased and reaches (2.1–3.6) × 10^{-7}. This difference is due to the fact that, at a comparable concentration of 3He, they have a smaller amount of ^{4}He (Fig. 71). The increased $^{3}He/^{4}He$ ratio in rocks with anomalously light oxygen is apparently a characteristic feature of the metasomatic fluid that led to the formation of rocks with corundum (Akimova et al., 2017).

It should be noted that lower values of $^{3}He/^{36}Ar$ are described in the lower crustal xenoliths of the Belomorian mobile belt (Vetrin et al., 2007), where they are associated with the presence of mantle ^{3}He in the trapped fluid.

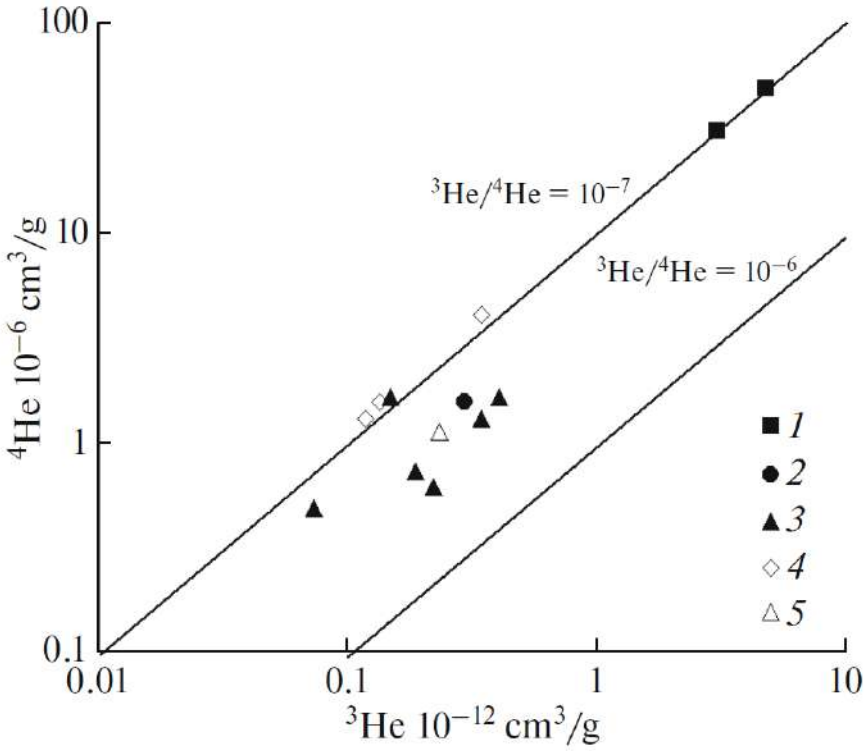

Fig. 71. Helium isotopes in rocks. Symbols are the same as in Fig. 67.

Fig. 72 shows the systematics of the ratios of non-radiogenic isotopes of neon, argon, as well as the isotopic composition of argon. Modern reservoirs of noble gases are clearly fixed in these coordinates: upper mantle, atmosphere, gases dissolved in surface water, gases from clay minerals (Ozima, Podosek, 2002; Harrison et al., 2003). In addition to the parameters of modern clays (point 1), the calculated values at the time of metamorphic transformations (1.89 billion years ago) are indicated for sedimentary rocks with a clay component, which have a sedimentation age of about 2.75 billion years and are characterized by the content of K_2O = 2%, H_2O = 10% (point 3, to the hypothesis of ancient weathering crusts with anomalous oxygen), as well as the calculated values for secondary minerals formed from the main rocks with an age of 2.45 billion years, characterized by the content of K_2O = 1%, H_2O = 10% (point 2, to the hypothesis of the protolith of corundum-bearing rocks as a result of low-temperature hydrothermal processing of basic rocks by melt water) (Akimova et al., 2017).

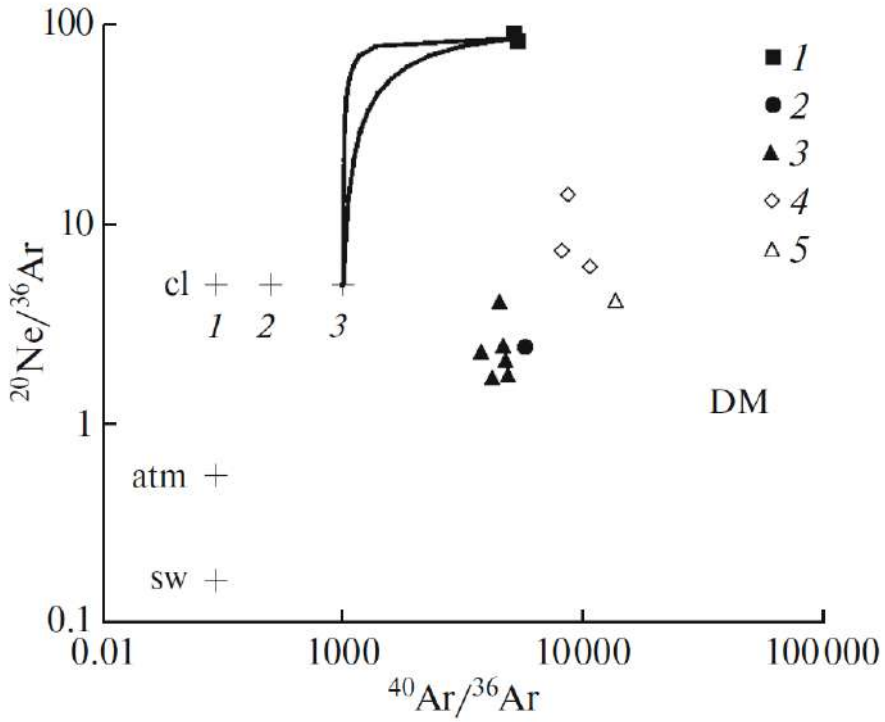

Fig. 72. Correlation between the isotopic composition of argon and the 20Ne/36Ar ratio in the fluid. Symbols are the same as in Fig. 67. Symbols of reservoirs: DM – upper mantle; atm – atmosphere; sw – surface water; cl – clay minerals (1 – modern, at a time of 1.89 Ga ago: 2 – formed after gabbroids with an age of 2.45 Ga, 3 – formed after rocks with a clay component aged 2.75 Ga). The solid curves show the mixing lines. DM, atm, sw and cl parameters from (Ozima, Podosek, 2002, Harrison et al., 2003).

The figurative points of the studied rocks occupy a specific field outside these reservoirs. As in the previous plots, it can be seen that the rocks in the permeable zone are characterized by a lower content of neon relative to argon, while the isotopic composition of argon differs little from that of the host rocks. Gases from the original host gneisses apparently fix the composition of the fluid during the regional metamorphism of the Chupa sequence under the conditions of the amphibolite facies (Akimova et al., 2017).

The possibility of the formation of a protolith with anomalously isotopically light oxygen due to ancient weathering crusts or due to low-temperature alteration of basic rocks is excluded, which is illustrated by the mixing lines shown in Fig. 72. The construction of mixing lines was carried out according to the known equations of two-component mixing (Faure, 1989). Mixing lines were calculated using data on noble gas contents in rock with a clay component (Ozima, Podosek, 2002; Harrison et al., 2003) and in metamorphic fluid (Lokhov, Levskii, 1995). The following isotope parameters of the end members are specified: in the fluid of gneisses of the Chupinskaya sequence, the concentration range of ^{36}Ar is 10^{-7} – 10^{-6} cm^3/mol H_2O (Lokhov et

al., 2016), $^{40}Ar/^{36}Ar$=5500, $^{20}Ne/^{36}Ar$=85; in rocks with a clay component and 10% water, the ^{36}Ar concentration is 2.5 × 10^{-6} cm^3/mol H_2O (Lokhov et al., 2016), $^{40}Ar/^{36}Ar$=1000, $^{20}Ne/^{36}Ar$=4.9 (Fig. 72). All experimental points lie far outside the field limited by hypothetical mixing lines for the case of ancient weathering crusts and secondary altered mafic rocks (no mixing lines were plotted for the latter) (Akimova et al., 2017).

The result of the analysis of noble gas isotopes in bulk samples can leave doubts and uncertainties. Thus, the fraction of argon and helium isotopes released from the intergranular space (although a fraction of 0.5–0.25 mm is analyzed, crystal intergrowths are also found) (Buikin et al., 2018) cannot be taken into account at all. Therefore, an additional study was made of the isotopic composition of noble gases by the method of stepwise crushing in corundum.

A monofraction of corundum 0.5–0.25 mm (sample 7.07 mg) was studied, as well as a crystal fragment not containing inclusions of biotite and amphibole (sample weight 33.25 mg). The intervals for the release of noble gases from the monofraction and the crystal fragment turned out to be similar, the differences are observed only in the amount of noble gases released, which is due to the difference in weights, therefore, the results obtained for the crystal fragment are given below.

At 100 strokes, a peak of release of ^{40}Ar ($4.93*10^{-7}$ g), ^{36}Ar ($0.02*10^{-8}$ g) and ^{4}He ($4.5*10^{-8}$ g) is recorded (Fig. 73, 74), and all of them are released simultaneously, therefore, are a component of the CO_2 fluid inclusions discussed earlier (see Chapter 5). The $^{40}Ar/^{36}Ar$ isotopic ratio is 1988, and the $^{4}He/^{40}Ar$ elemental ratio is 0.09. In general, these figures are in good agreement with those obtained earlier for bulk samples.

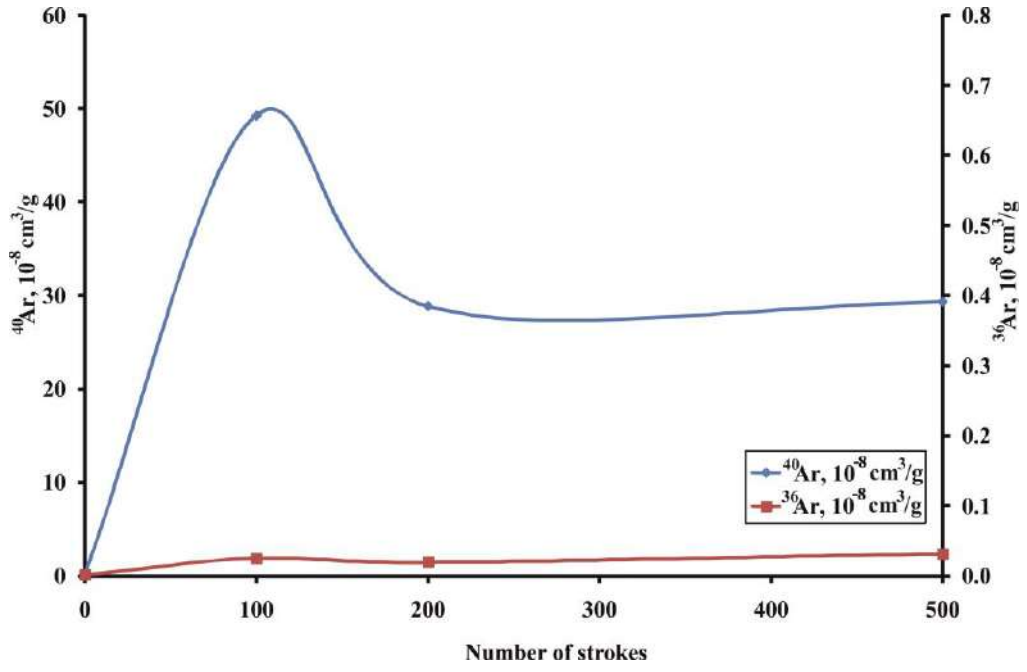

Fig. 73. Emission of argon isotopes from corundum during stepwise crushing

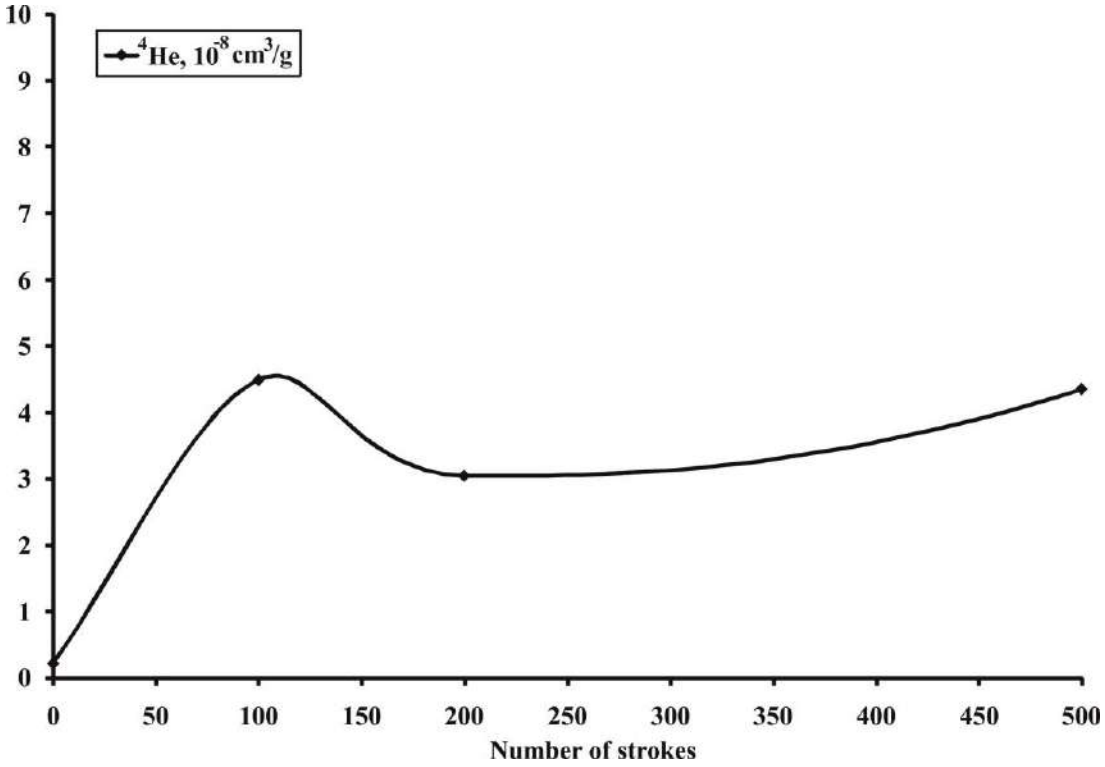

Fig. 74. Emission of ^{4}He from corundum during stepwise crushing

The reasons for the reduced ^{4}He/4^0Ar ratio, which is an order of magnitude lower than the production ratio, remain mysterious. Such a low ^{4}He/^{40}Ar ratio in inclusions in corundum may be the result of partial losses of ^{4}He (Verkhovsky, Shukoliukov, 1990). Could there be a partial loss of ^{4}He from corundum by diffusion during late low-temperature processes of rock alteration?

There are no experimental data in the literature necessary to calculate the rate of diffusion of helium from corundum, but recent data for hematite (Farley, 2018) are suitable for approximate estimates, since corundum and hematite are isostructural.

The helium loss fraction was calculated using the following initial data: Do = 5.17×10^{-5} m^2/c, Ea = 171 kJ/mol (Farley, 2018) according to formulas from work (Watson, Cherniak, 2013). The diffusion radius is set to 3 mm (grain size 6 mm), temperature 200°C, time 10 million years. At temperatures up to 200°C, the ^{4}He loss fraction is very small and does not reach 0.1, but a further increase in temperature leads to an increase in the ^{4}He loss fraction, so that at 300°C the loss fraction reaches 1 (Fig. 75).

This means that at low temperatures almost all of the helium will be retained in inclusions in corundum; therefore, late low-temperature processes cannot significantly affect the ^{4}He/^{40}Ar ratio. In this case, the diffusion of helium from fluid inclusions in corundum will be even more difficult, since for this helium must first dissolve in the mineral (but, as is known, the solubility of noble gases in solids is very low), and only then will its diffusion from the mineral become

possible. Apparently, the mineral-forming fluid already at the moment of capture of the inclusions was characterized by a reduced $^{4}He/^{40}Ar$ ratio. The literature contains examples of rocks characterized by similar $^{4}He/^{40}Ar$ ratios acquired in a hydrothermal process (Verkhovsky, Shukoliukov, 1990).

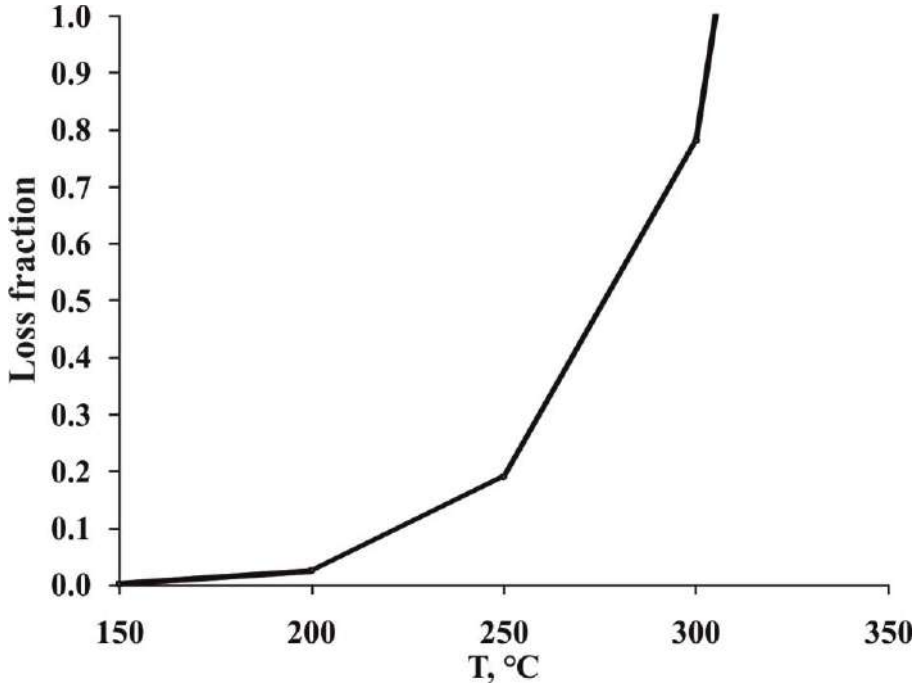

Fig. 75. Model of diffusion losses of ^{4}He from corundum during heating

The obtained data on the isotopic composition of noble gases in fluid inclusions in minerals of corundum-bearing rocks of the Khitoostrov occurrence allow us to conclude that endogenous fluid was involved in the mineral formation. This is evidenced, firstly, by a significant proportion of radiogenic argon, approximately the same as in the host kyanite-garnet-biotite gneisses of the Chupa sequence. And secondly, the addition of ^{3}He, which we interpret as mantle.

6.2. Rb-Sr and Sm-Nd isotope systematics of apatite

Apatite is a common accessory mineral of sedimentary, igneous and metamorphic rocks, widely used for dating and isotope-geochemical reconstructions using Rb-Sr, Sm-Nd, U-Pb isotope systematics (Spear, Pyle, 2002, Bruand et al., 2017, Henrich et al., 2018, O'Sullivan et al., 2020 and references there). In metamorphic rocks, apatite is a marker of the degree of metamorphism (Henrich et al., 2019), while apatite from metasomatic rocks provides valuable information about the sources, composition, and evolution of fluids (Spear, Pyle, 2002; Harlov, 2015; Zhao et al., 2015; Zirner et al., 2015; Mao et al., 2016; Adlakha et al., 2018; Li et al., 2021, 2022 etc.). Often, apatite retains a geochemical marker of the participation of surface

waters in mineral formation (Xiqiang et al., 2020). In this regard, it is of interest to study the Rb-Sr, Sm-Nd isotope systematics of apatite from corundum-bearing and host rocks.

The results of the analysis of the isotopic composition of the Rb-Sr and Sm-Nd systems in apatite are given in Table 5, 6.

Table 5. Results of the analysis of the isotopic composition of the Rb-Sr system in apatite

Rock	Sample	SiO_2, mas. %	Rb, ppm	Sr, ppm	$^{87}Rb/^{86}Sr$	$^{87}Sr/^{86}Sr$	$^{87}Sr/^{86}Sr(ini)$
Ky-Grt-Bt gneiss	Ch-1	26.9	3.63	184	0.0573	0.7268	0.7247
Crn rock	Ea16-005I	1.5	0.36	319	0.0033	0.70873	0.7086
Bt-Grt plagioclasite	Ea16-005II	7.4	0.52	283	0.0053	0.7088	0.7086
Grt amphibolites after gabbro	KHI-004	31.4	0.61	325	0.0054	0.70574	0.7055
Crn rock	KHI-008A	15.5	0.64	231	0.008	0.70893	0.7086
Crn rock	KHI-010	16.6	0.71	261	0.0079	0.70916	0.7089

Table 6. Results of the analysis of the isotopic composition of the Sm-Nd system in apatite

Rock	Sample	SiO_2, mas. %	Sm, ppm	Nd, ppm	$^{147}Sm/^{144}Nd$	$^{143}Nd/^{144}Nd$	εNd(T) 1.89Ga
Ky-Grt-Bt gneiss	Ch-1	26.9	126	243	0.3147	0.51361	-10
Crn rock	Ea16-005I	1.5	345	1420	0.1969	0.51231	-6.6
Bt-Grt plagioclasite	Ea16-005II	7.4	349	1618	0.1487	0.5116	-8.7
Grt amphibolites after gabbro	KHI-004	31.4	11.1	42.4	0.1269	0.51135	-8.1
Crn rock	KHI-008A	15.5	236	490	0.2904	0.51326	-10.7
Crn rock	KHI-010	16.6	415	1295	0.1937	0.51214	-9.1

As follows from the obtained data, corundum-bearing rocks hosting kyanite-garnet-biotite gneisses and garnet amphibolites are characterized by similar εNd, varying in a rather

narrow range (approximately from -7 to -11). At the same time, the $^{87}Sr/^{86}Sr$ ratio in corundum-bearing rocks is significantly lower against the background of host kyanite-garnet-biotite gneisses, while it is minimal in garnet amphibolites. In the 87Sr/86Sr – εNd diagram, the points of corundum-bearing rocks and garnet amphibolites are on the mixing line of the lower crustal and mantle sources, and the point of the enclosing kyanite-garnet-biotite gneisses is somewhat shifted towards the upper crustal source (Fig. 76).

The Sm-Nd age of apatite from all the studied rocks (Fig. 77) coincides within the error with the age of the last, Svecofennian stage of regional metamorphism (Skublov et al., 2017 and references therein) and with the age of corundum-bearing rocks determined by the U-Pb method according to zircons (Serebryakov et al., 2007).

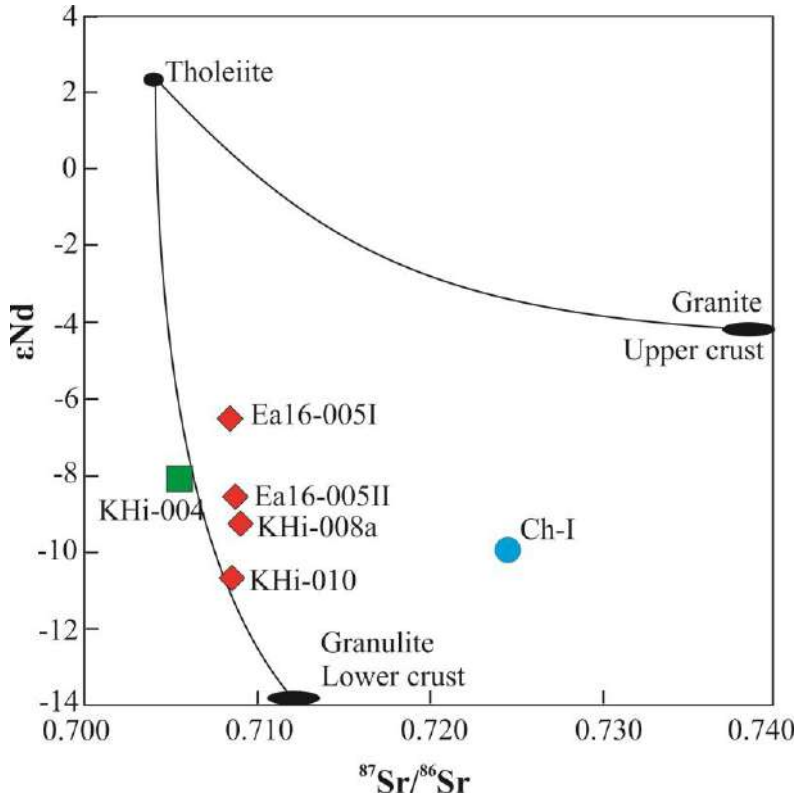

Fig. 76. Diagram $^{87}Sr/^{86}Sr$ – εNd with fields of possible fluid sources (mantle, lower crustal, upper crustal) and mixing lines between them (after Fore, 1981). The points of the studied rocks from Table 5, 6 are shown.

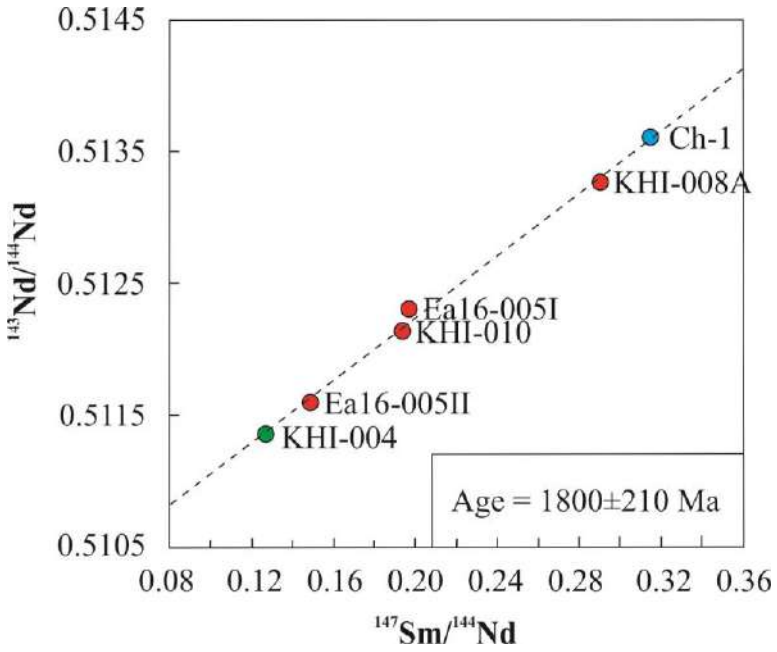

Fig. 77. Sm-Nd isochrone for the studied samples of apatite from Table 6.

Conclusions to chapter 6

Summarizing the data on the isotopic composition of noble gases and the Sr-Nd isotope systematics of apatite in corundum-bearing rocks of the Khitoostrov occurrence, we can conclude that the deep source of the fluid that led to the formation of corundum-bearing rocks. This is supported by the following indications:

– elevated contents of ^{3}He in the component of fluid inclusions of corundum-bearing rocks released as a result of crushing;

– low values of $^{87}Sr/^{86}Sr$, close to lower crustal values of εNd, as well as elevated contents of Sr, REE (see Chapter 4) in apatite from corundum-bearing rocks.

Chapter 7. Reconstruction of conditions of the formation of metasomatites

Based on the results of geological and mineralogical-petrographic studies of the rocks of the Khitoostrov occurrence, a number of features have been identified that testify in favor of the metasomatic nature of corundum-bearing rocks and associated clinozoisite amphibolites. Firstly, the complex zonal structure of the bodies of corundum-containing rocks, wide variations in the mineral and chemical composition. Secondly, multimineral associations with characteristic reaction structures (symplectites, rims, pseudomorphs) and atypical parageneses (staurolite + calcium amphibole). Thirdly, the appearance of unusual minerals that are not characteristic of host rocks (aspidolite, sodic gedrite, magnesian staurolite, Na-Ca-amphiboles), and a regular, directed change in the compositions of the main minerals from one association to another. Fourthly, the characteristic distribution of rare earth elements, indicating the mobile behavior of REE.

The discussed metasomatic nature of the studied rocks determines the use in this work of the approaches traditionally used for metasomatites. The study of metasomatic processes involves the construction and analysis of diagrams in the coordinates of intensive parameters (temperature, pressure, chemical potentials of perfectly mobile components (PMC)), as well as auxiliary composition diagrams for the selected system (Korzhinsky, 1973). Due to the lack of thermodynamic databases, the diagrams in the coordinates of intensive parameters were initially of a qualitative nature. With the advent of experimental data, it became possible to construct quantitative diagrams in the coordinates of PMC activities (references in Sverjensky et al., 1991).

Since the construction and analysis of diagrams in the coordinates of the chemical potentials of the PMC is possible only at constant temperature and pressure, thermodynamic modeling was carried out in two stages. The first is the determination of PT-parameters for the formation of metasomatites and host rocks by the pseudosection method. The second stage is the simulation of the behavior of the PMC already at a given temperature and pressure. In this approach, it is especially informative to compare the model variations in mineral compositions with natural ones.

The chemical potential was chosen as a measure of the mobile behavior of the components. The obtained values of $\mu(SiO_2)$ can be easily converted into $lga(SiO_2)$, and $\mu(Na_2O)$ and $\mu(K_2O)$ into A_R values, where R is Na, K (Kol'tsov, 2015), using the formula:

$$A_R = (\mu(R_2O) - 2G(R^+) - G(H_2O))/4.606RT \quad (1),$$

where $G(R^+)$, $G(H_2O)$ – reference values obtained from the database DEW17HP622ver_elements.dat, included in the software package Perplex. The values of $\mu(Na_2O)$, $\mu(K_2O)$ for all zones of model zoning of corundum-bearing metasomatites and the corresponding A_{Na}, A_K are given in Table 7.

The data obtained on the direction of the metasomatic process also make it possible to quantify the change in pH during metasomatism using the formula (Akimova, Kol'tsov, 2019):

$$\mu(R_2O)=2G(R^+) + G(H_2O) + 2RTln(aR^+/aH^+) \quad (2).$$

7.1. PT-conditions of host rock metamorphism

The simplified model system SiO_2-Al_2O_3-FeO-MgO-CaO-Na_2O-K_2O-H_2O-CO_2 is convenient for considering phase equilibria both in the host rocks (kyanite-garnet-biotite gneisses of the Chupa sequence and garnet amphibolites) and in the metasomatites developing over them.

Modeling of metamorphism of kyanite-garnet-biotite gneisses of the Chupa sequence

In kyanite-garnet-biotite gneisses, all components, except for H_2O and CO_2, are inert, SiO_2 is an excess component (quartz is present in the rocks). Mineral equilibria in such a system are expressed on a plane in the form of a T-P projection (Fig. 78). The diagram was calculated in the presence of carbon dioxide-water fluid with $X(CO_2) = 0.3$; this value makes it possible to reproduce the values of water activity characteristic of amphibolite facies metamorphism in calculations (Aranovich, Newton, 1999).

On the resulting pseudosection for a given composition of migmatized kyanite-garnet-biotite gneisses of the Chupa sequence (SiO_2 – 63.57, Al_2O_3 – 18.12, FeO – 6.43, MgO – 3.95, CaO – 2.54, Na_2O – 2.96, K_2O – 2.44 вес. %) (Myskova, 2001) it can be seen that the *Pl + Bt + Grt + Ky + Qz* association observed in kyanite–garnet–biotite gneisses hosting corundum-bearing rocks is stable in the temperature range of 590–750°C and pressures from 6.4 to 11.2 kbar. At higher pressures, as well as at lower temperatures, muscovite appears in gneisses, at lower pressures kyanite disappears and sillimanite appears. With an increase in temperature and pressure, partial melting processes begin. With a decrease in temperature and pressure, staurolite-containing associations can form, but the range of conditions for their formation is rather narrow: temperatures 560–620°C, pressure no more than 7.6 kbar; this can explain their rarity in the rocks of the Chupa sequence (Shurkin et al., 1962).

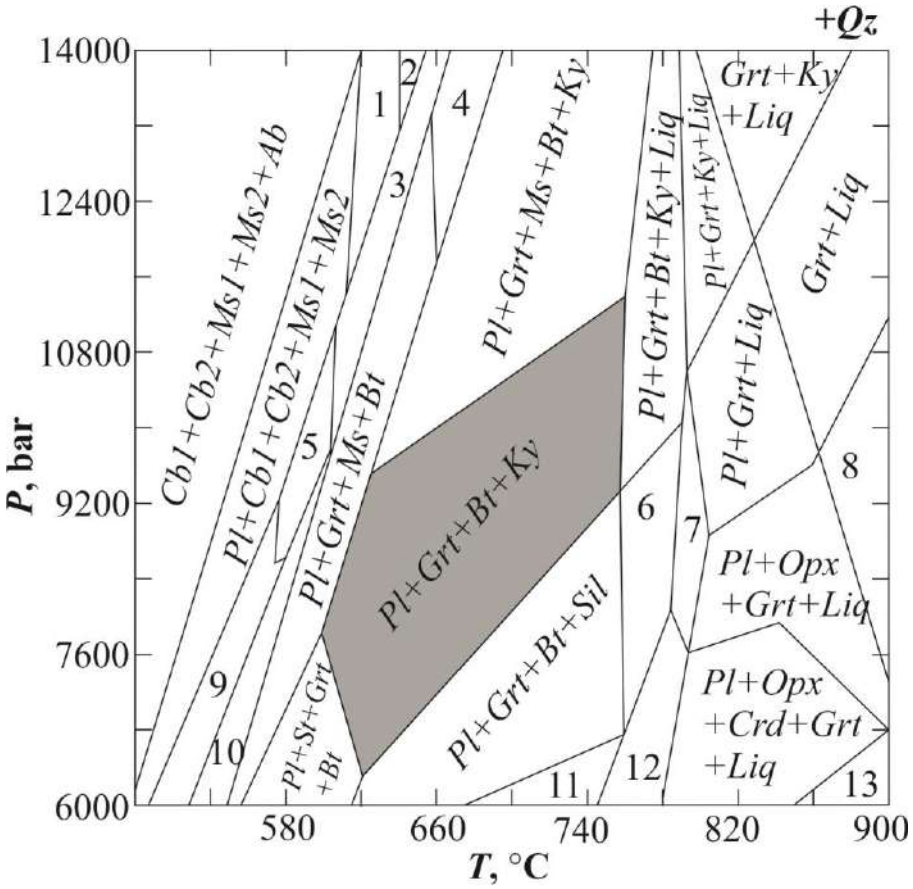

Fig. 78. P–T pseudosection for a given composition of migmatized kyanite-garnet-biotite gneisses of the Chupa sequence (composition 1 in Table 1 in Appendix 2) with the mineral association *Pl + Qz + Bt + Grt + Ky*. X(CO_2) = 0.3. The gneiss field is marked in grey. Associations are marked with numbers: *1 – Pl + Cb1 + Cb2 + Ms1 + Ms2 + Cam, 2 – Cb1 + Cb2 + Ms1 + Ms2 + Cam, 3 – Cb1 + Cb2 + Ms + Bt + Cam, 4 – Pl + Grt + Ms1 + Ms2 + Bt, 5 – Pl + Cb1 + Cb2 + Ms + Bt + Cam, 6 – Pl + Grt + Bt + Sil + Liq, 7 – Pl + Grt + Bt + Liq, 8 – Opx + Grt + Liq, 9 – Pl + Cb1 + Cb2 + Ms + Bt, 10 – Pl + Cb + Ms + Bt + Cam, 11 – Pl + Crd + Grt + Bt + Sil, 12 – Pl + Crd + Grt + Bt + Liq, 13 – Pl + Opx + Crd + Liq.*

Modeling of the metamorphism of garnet amphibolites

In garnet amphibolites, all components, except for H_2O and CO_2, are also inert, but SiO_2 is not an excess component (quartz may or may not be present in rocks). Mineral equilibria in such a system are expressed on a plane in the form of a T-P projection (Fig. 79).

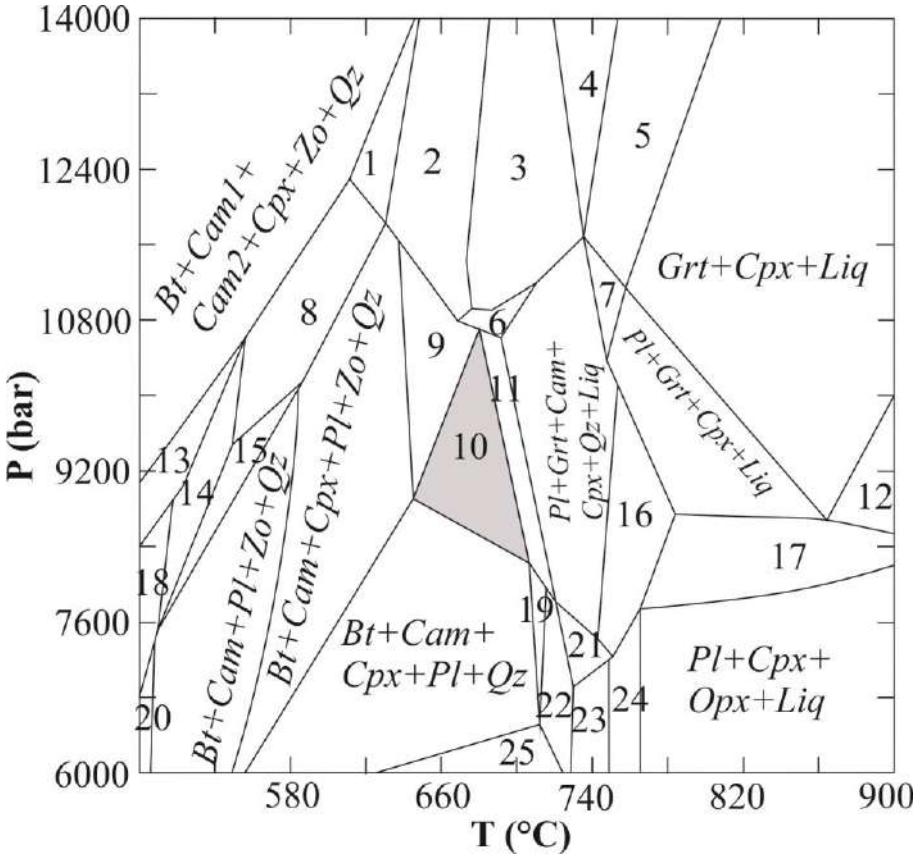

Fig. 79. P–T pseudosection for a given composition of migmatized garnet amphibolites (sample Khi008g in Table 1 in Appendix 2) with the mineral association *Pl + Qz + Bt + Grt + Cam + Cpx*. X(CO_2) = 0. The field of amphibolites is marked in gray. Associations are marked with numbers: *1 – Cam1 + Cam2 + Cpx + Bt + Zo + Qz + Liq, 2 – Grt + Cpx + Bt + Cam + Zo + Qz + Liq, 3 – Grt + Cpx + Cam + Zo + Qz + Liq, 4 – Grt + Cpx + Zo + Qz + Liq, 5 – Cpx + Grt + Qz + Liq, 6 – Grt + Cpx + Cam + Pl + Zo + Qz + Liq, 7 – Pl + Grt + Cpx + Qz + Liq, 8 – Cam + Cam + Pl + Bt + Cpx + Zo + Qz, 9 – Pl + Grt + Cpx + Bt + Cam + Zo + Qz, 10 – Pl + Grt + Cpx + Bt + Cam + Qz, 11 – Pl + Cpx + Bt + Cam + Grt + Qz + Liq, 12 – Opx + Grt + Cpx + Liq, 13 – Cam1 + Cam2 + Ms + Bt + Pl + Zo + Qz, 14 – Cam1 + Cam2 + Pl + Bt + Zo + Qz, 15 – Pl + Bt + Cam + Chl + Zo + Qz, 16 – Pl + Grt + Cam + Cpx + Liq, 17 –Pl + Opx + Grt + Cpx + Liq, 18 – Pl + Bt + Cam1 + Cam2 + Chl + Zo + Qz, 19 – Pl + Cam + Bt + Cpx + Qz+ Liq, 20 – Pl + Bt + Cam + Chl + Zo + Qz, 21 – Pl + Cam + Grt + Qz + Liq, 22 – Pl + Cam + Opx + Qz + Liq, 23 – Pl + Cam + Opx + Liq, 24 – Pl + Cpx + Opx + Cam + Liq, 25 – Pl + Cam + Bt + Qz.*

The obtained pseudosection for the given composition of migmatized garnet amphibolites shows that the *Pl + Bt + Grt + Cam + Qz + Cpx* association observed in garnet amphibolites is stable in the temperature range of 650–710°C and pressures from 7.8 to 10.8 kbar. At higher

pressures and/or lower temperatures, zoisite appears in garnet amphibolites and then garnet disappears. As the temperature rises, partial melting processes begin. When the pressure drops, the garnet disappears.

7.2. PT-conditions of the formation of metasomatites

Previously, for the corundum-bearing rocks of Khitoostrov, P-T parameters of their formation were already determined by several methods:

- temperatures obtained by decrepitation of gas-liquid inclusions: 660–900°C for primary inclusions and 300–500°C for secondary inclusions (Busheva, 1983);
- using the method of classical mineral geothermobarometry (Grt-Bt, Grt-Hbl, Grt-St geothermometers in the GeoPath program, Ti and Mg in the Bt geothermometer), temperatures of 600 - 700°C were obtained, pressures were estimated at 6 - 8 kbar (Serebryakov, 2004);
- temperatures of 400–475°C for rocks with corundum, 375–500°C for rocks without corundum were obtained by oxygen isotope thermometry (Ustinov et al., 2008, Krylov, Glebovitsky, 2017).
- using the thermodynamic modeling method in the Selector-S program, it was found that the formation temperatures of corundum-bearing rocks are at least 720°C, and pressures are at least 10 kbar (Vysotsky et al., 2008).

It can be seen that the data on temperature and pressure during the formation of corundum-bearing rocks, obtained by different methods, differ greatly, there is no information about the parageneses for which they were obtained. Data for clinozoisite amphibolites are completely absent in the literature.

We need our own estimates of PT-parameters, for which the method of pseudosections is chosen, which is usually used in cases where rocks with complex, multi-mineral associations and reaction relationships of minerals are studied. Staurolite-containing associations are the most informative for estimating PT-parameters, since the stability field of staurolite is quite narrow and staurolite is considered an indicator mineral of metamorphic rocks (Fedkin, 1975). Therefore, first of all, the pseudosection was constructed for varieties of corundum-bearing rocks with stable staurolite (zone 2).

As can be seen from the resulting pseudosection (Fig. 80), the stability field of staurolite in corundum-bearing rocks is indeed not very wide: 620–660°C and 4.5–10.5 kbar. At lower temperatures chlorite is stable, at higher temperatures staurolite disappears. At lower pressures,

associations with cordierite appear, and at higher pressures, associations with muscovite and calcium amphibole appear.

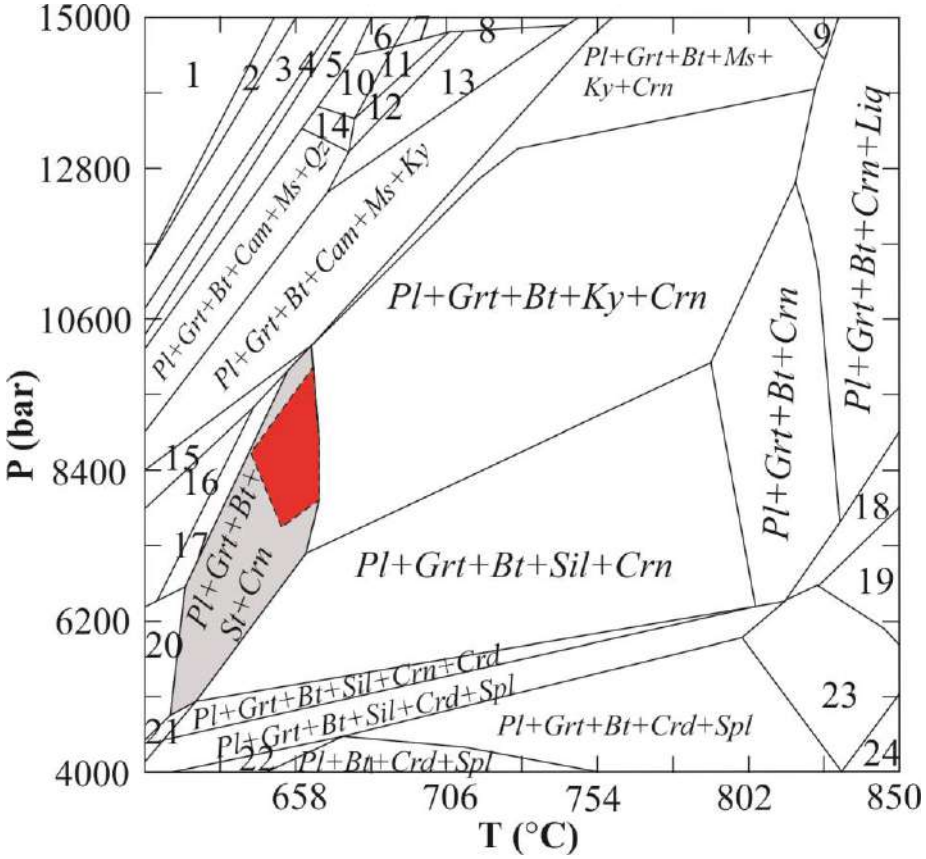

Fig. 80. P–T pseudosection for a given composition of corundum-bearing rocks, zone 2 (areal microprobe analysis data) with the mineral association *Pl + Bt + Grt + St*. X(CO_2) = 0.3. The field of the desired association is marked in gray. Red shows the overlap field with the *Pl + Cam + Grt + Bt + Crn* paragenesis. Associations are marked with numbers: *1 – Ms + Ky + Qz + Cal + Dol, 2 – Grt + Ms + Ky + Qz + Dol + Cal, 3 – Ms + Grt + Qz + Cal + Dol, 4 – Ms + Grt + Bt + Qz + Dol + Cal, 5 – Grt + Ms + Bt + Cam + Pl + Qz + Dol, 6 – Pl + Grt + Cpx + Ms1 + Ms2 + Cam + Qz, 7 – Ms1 + Ms2 + Grt + Pl + Cpx + Cam, 8 – Pl + Ms + Grt + Bt + Cam + Cpx, 9 – Grt + Pl + Ms + Bt + Crn, 10 – Pl + Grt + Cam + Ms + Ms + Qz, 11 – Ms1 + Ms2 + Grt + Cam + Pl, 12 – Grt + Bt + Cam + Pl + Ms1 + Ms2, 13 – Bt + Cam + Grt + Ms + Pl, 14 – Pl + Grt + Bt + Ms1 + Ms2 + Cam + Qz, 15 – Pl + Grt + St + Ms + Cam + Bt, 16 – Bt + Pl + Cam + St + Grt, 17 – Pl + Grt + Bt + Cam + St + Crn, 18 – Pl + Grt + Spl + Bt + Crn + Liq, 19 – Pl + Grt + Spl + Bt + Sap + Liq, 20 – Pl + St + Grt + Chl + Bt + Crn, 21 – Pl + St + Crd + Grt + Bt + Crn, 22 – Pl + Crd + Spl + Bt + Sil, 23 – Pl + Crd + Spl + Grt + Bt + Liq, 24 – Pl + Opx + Crd + Spl + Bt + Liq.*

Note that corundum is also present in the *Pl + Bt + Grt + St* association field; the reason for its appearance will be discussed below.

In addition, a pseudosection was constructed for corundum-bearing rocks of zone 4. As can be seen from the resulting pseudosection (Fig. 81), the stability field of the *Pl + Cam + Grt + Crn* association is quite wide: 630–830°C and 8–10.5 kbar.

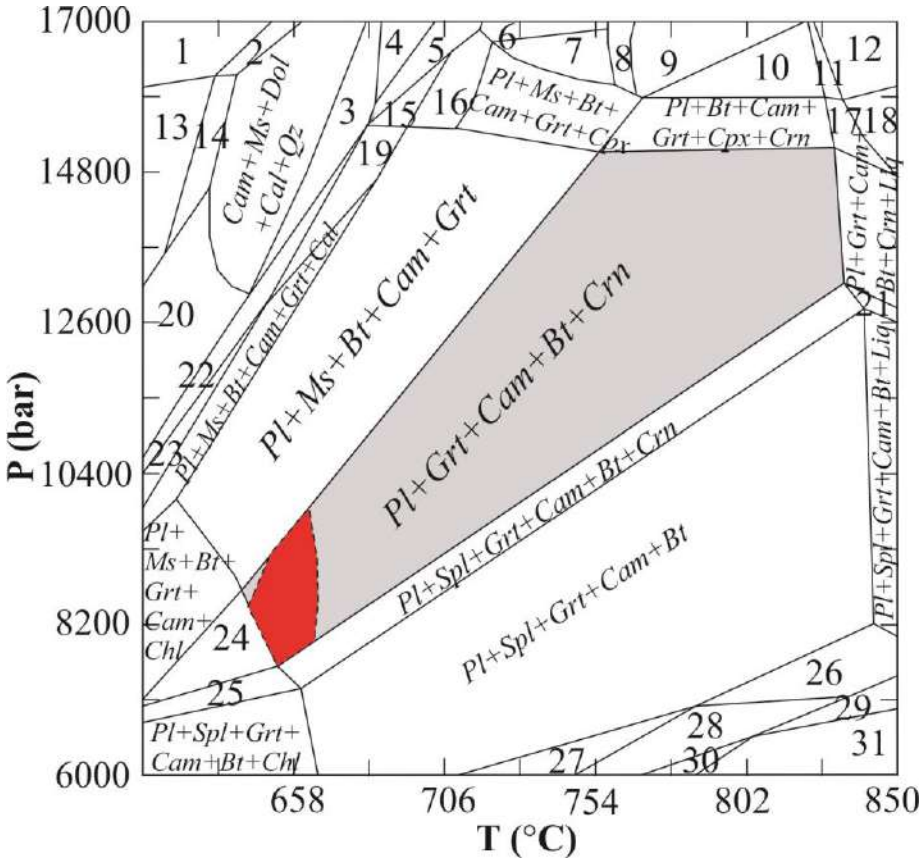

Fig. 81. P–T pseudosection for a given composition of corundum-bearing rocks, zone 4 (average composition of corundum-bearing rocks according to 4 analyzes, analyzes 7–10 in Table 1 in Appendix 2) with the mineral association *Pl + Cam + Grt + Crn*. X(CO_2) = 0.3. The field of the desired association is marked in gray. Red shows the overlap field with the *Pl + Grt + Bt + St + Crn* paragenesis. Associations are marked with numbers: *1 – Ms + Cpx + Qz + Cal + Dol, 2 – Cam + Cpx + Ms + Qz + Dol + Cal, 3 – Cam + Ms + Grt + Qz + Dol + Cal, 4 – Cam + Ms + Grt + Cpx + Qz + Cal, 5 – Cam + Grt + Ms + Cpx + Qz, 6 – Grt + Ms + Cpx + Pl, 7 – Cpx + Pl + Ms + Bt + Grt, 8 – Pl + Grt + Cpx + Ms + Bt + Ky, 9 – Grt + Bt + Pl + Cpx + Ky, 10 – Bt + Grt + Pl + Cpx + Crn, 11 – Grt + Bt + Cpx + Pl + Crn + Liq, 12 – Bt + Cpx + Grt + Crn + Liq, 13 – Ms + Ab + Qz + Cal + Dol, 14 – Cam + Ms + Ab + Qz + Dol + Cal, 15 – Cam + Cam + Ms + Grt + Pl + Cpx, 16 – Pl + Grt + Cpx + Ms + Cam, 17 – Pl + Grt + Cpx + Bt + Cam + Crn + Liq, 18 – Cpx + Grt + Cam + Bt + Crn + Liq, 19 – Cam1 + Cam2 + Pl + Grt + Ms, 20 – Ms + Cam + Pl + Qz + Dol + Cal, 21 – Grt + Pl + Spl + Bt + Cam + Crn + Liq, 22 – Pl + Grt + Ms + Qz + Cal + Dol, 23 – Pl + Grt + Ms + Bt + Cam + Qz + Cal, 24 – Bt + Cam + Chl + Pl + Grt + Crn, 25 – Pl + Spl + Grt + Bt + Cam + Chl + Crn, 26 – Ol + Spl + Grt + Cam + Bt + Pl, 27 – Pl + Grt + Bt + Spl + Cam + Opx, 28 – Pl + Opx + Ol + Spl + Grt + Bt +*

Cam, 29 – Pl + Opx + Ol + Spl + Bt + Grt, 30 – Pl + Opx + Ol + Bt + Cam + Spl, 31 – Opx + Spl + Pl + Ol + Bt.

At lower temperatures, chlorite is stable, at higher temperatures, partial melting processes begin. At higher pressures, associations with clinopyroxene appear, and at lower pressures, associations with spinel. Muscovite appears at higher pressures and lower temperatures.

The field of the *Pl + Cam + Grt + Crn* association contains biotite, which, according to petrographic data, is replaced by calcium amphibole.

Staurolite and biotite in the field of the sought associations of corundum-bearing rocks arose because PT-pseudosections are constructed in a closed system, when all components are inert. The available geological, petrographic and mineralogical data, which testify to the metasomatic nature of corundum-bearing rocks, make it necessary to move on to modeling the process of their formation in an open system. To do this, it is necessary to set constant temperature and pressure.

Despite the wide field of stability of the *Pl + Cam + Grt + Crn* association, due to the fact that relic and even stable staurolite is present in this and other associations, we cannot consider options with temperatures and pressures that go beyond its stability limits. Therefore, the most informative field is the overlap of the *Pl + Grt + Bt + St + Crn* and *Pl + Cam + Grt + Bt + Crn* parageneses.

Thus, for further thermodynamic modeling, the following estimate of the PT parameters for the formation of corundum-bearing rocks was chosen: T = 650ºC, P = 8 kbar. It is in good agreement with the estimation of PT-parameters by classical thermobarometry methods (Serebryakov, 2004). This estimate also does not contradict the estimates of the conditions of Early Svecofennian metamorphism (during which corundum-bearing rocks were formed): T = 640–765ºC, P = 8–11.7 kbar (Kozlovsky et al., 2016, 2020). Justification of the selected values of $X(CO_2)$ - see further in the text and in fig. 91–93.

A pseudosection was also constructed for clinozoisite amphibolites, which are closely spatially associated with corundum-bearing rocks (Fig. 82).

The field of the *Pl + Cam + Bt + Grt + Zo* association observed in clinozoisite amphibolites is small. At lower temperatures and higher pressures, quartz appears. At higher temperatures, associations with clinopyroxene are stable. At lower pressures and temperatures, the garnet-free association *Pl + Cam + Bt + Zo* is stable. Note that, according to petrographic data, garnet in clinozoisite amphibolites is replaced by plagioclase-amphibole symplectites.

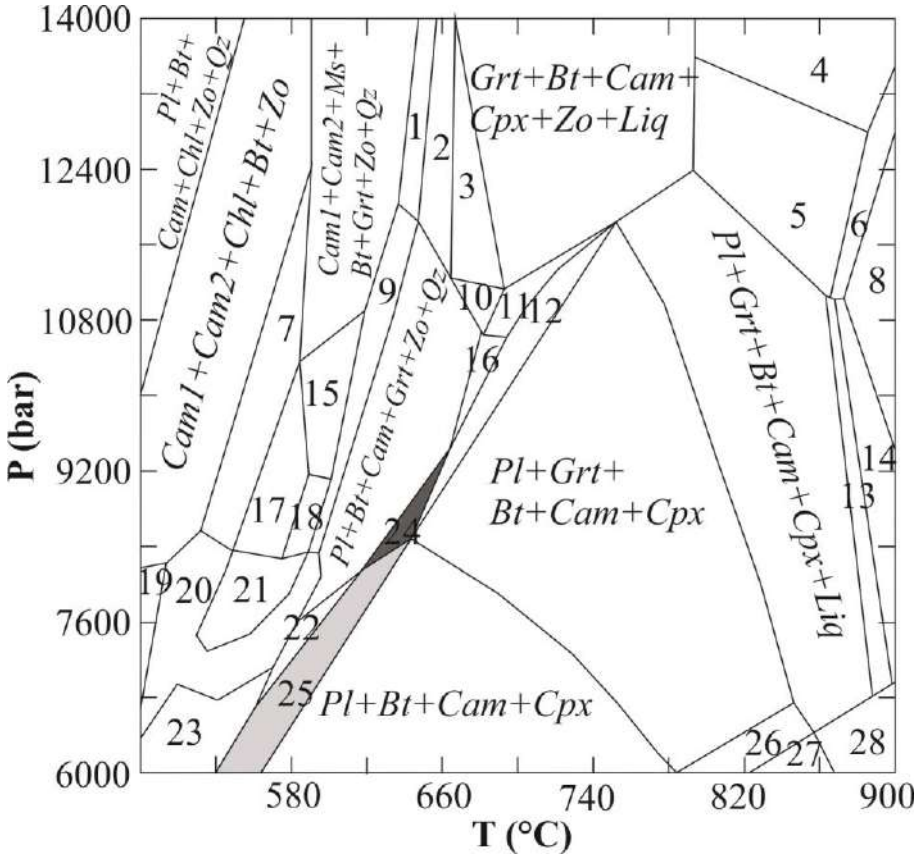

Fig. 82. P–T pseudosection for a given composition of clinozoisite amphibolites (sample Khi008d in Table 1 in Appendix 2). $X(CO_2) = 0$. The field of the *Pl + Cam + Bt + Grt + Zo* association observed in clinozoisite amphibolites is marked in dark gray; the field of association *Pl + Cam + Bt + Zo* is marked in light gray. Explanations are in the text. Associations are marked with numbers:

1 – Grt + Ms + Bt + Cam + Zo + Qz + Liq, 2 – Bt + Cam + Grt + Zo + Qz + Liq, 3 – Grt + Cam + Bt + Zo + Liq, 4 – Grt + Cpx + Bt + Crn + Liq, 5 – Cpx + Cam + Grt + Bt + Crn + Liq, 6 – Spl + Cpx + Grt + Bt + Crn + Liq, 7 – Cam + Cam + Bt + Ms + Chl + Zo + Qz, 8 – Grt + Bt + Spl + Cpx + Liq, 9 – Cam + Grt + Ms + Bt + Zo + Qz, 10 – Cam + Grt + Pl + Bt + Zo + Liq, 11 – Grt + Pl + Bt + Cam + Cpx + Zo + Liq, 12 – Pl + Grt + Cpx + Cam + Bt + Liq, 13 – Pl + Spl + Grt + Cpx + Bt + Cam + Liq, 14 – Cpx + Grt + Spl + Pl + Bt + Liq, 15 – Cam + Grt + Ms + Bt + Zo + Qz, 16 – Pl + Grt + Cpx + Bt + Cam + Zo + Qz, 17 – Cam + Ms + Bt + Chl + Zo + Qz, 18 – Cam + Ms + Bt + Zo + Qz, 19 – Cam1 + Cam2 + Pl + Bt + Chl + Zo, 20 – Cam1 + Cam2 + Bt + Pl + Chl + Zo + Qz, 21 – Cam + Pl + Ms + Bt + Zo + Qz, 22 – Pl + Cam + Bt + Zo + Qz, 23 – Pl + Bt + Cam + Chl + Zo + Qz, 24 – Pl + Cam + Bt + Grt + Zo, 25 – Pl + Cam + Bt + Zo, 26 – Pl + Cam + Opx + Cpx + Bt + Grt, 27 – Pl + Cam + Ol + Bt + Cpx, 28 – Pl + Bt + Ol + Cpx + Cam + Liq.

It is important to note that the PT-parameters of metasomatism in this case are somewhat lower than the PT-parameters of the host garnet amphibolite metamorphism and the PT-parameters of the formation of corundum-bearing metasomatites.

For further thermodynamic modeling, the following estimate of the PT parameters for the formation of clinozoisite amphibolites was chosen: T = 620°C, P = 8 kbar. $X(CO_2)$ was set equal to zero (pure water fluid), since, according to thermodynamic modeling data, the effect of CO_2 addition on the position and shape of the stability fields of mineral associations in amphibolites is negligible.

7.3. Thermodynamic modeling of the formation of metasomatites

Thermodynamic modeling of the process of formation of corundum-bearing rocks. To consider phase equilibria in zone 1 of corundum metasomatites, the following model system was chosen: CaO, FeO, MgO are virtual inert components, Al_2O_3 is an excess component, K_2O, Na_2O are isolated components (K_2O is present only in biotite, Na_2O is present only in plagioclase), SiO_2 is a mobile component. Subsequently, isolated Na_2O and then K_2O become mobile.

In such systems, it is convenient to consider the relationships of minerals on triangular composition diagrams (Fig. 83).

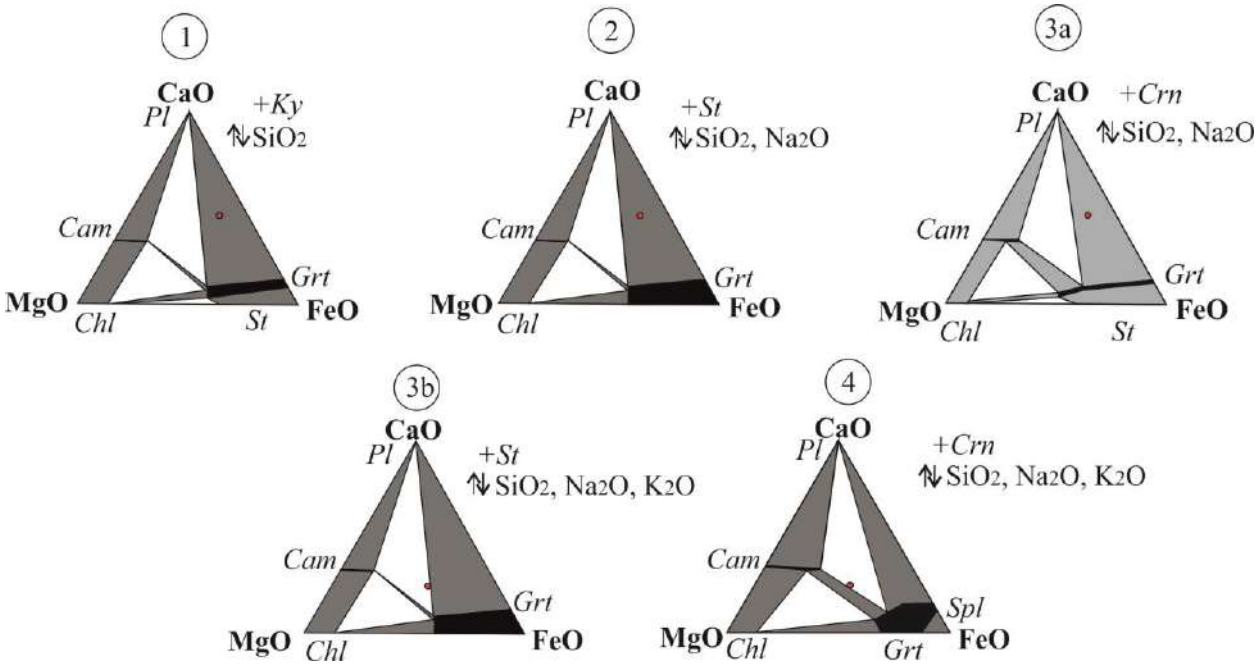

Fig. 83. Composition diagrams in addition to pseudosections in coordinates $\mu(SiO_2)$–$\mu(Na_2O)$. The red dot shows the composition of the kyanite-garnet-biotite gneiss of the Chupa sequence. The numbers in the circles correspond to the numbers of the metasomatic zones and the

corresponding fields on the pseudosections for which the CD was constructed. In the diagrams for zones 3b and 4, the gneiss point is shifted due to the partial deduction of K_2O.

In the frontal zone (zone 1) of mineral zoning of apogneissic corundum-bearing rocks, quartz disappears, which is described by a simple reaction:

$$Qz = SiO_2(aq) \quad (3)$$

This reaction corresponds to the transition of SiO_2 to the mobile state. As can be seen in the T-μ(SiO_2) diagram (Fig. 84), on the left, below the silica saturation line in kyanite-garnet-biotite gneisses, the *Pl + Bt + Grt + Ky* paragenesis appears, noted in zone 1 of the mineral zoning of apogneissic corundum-bearing rocks.

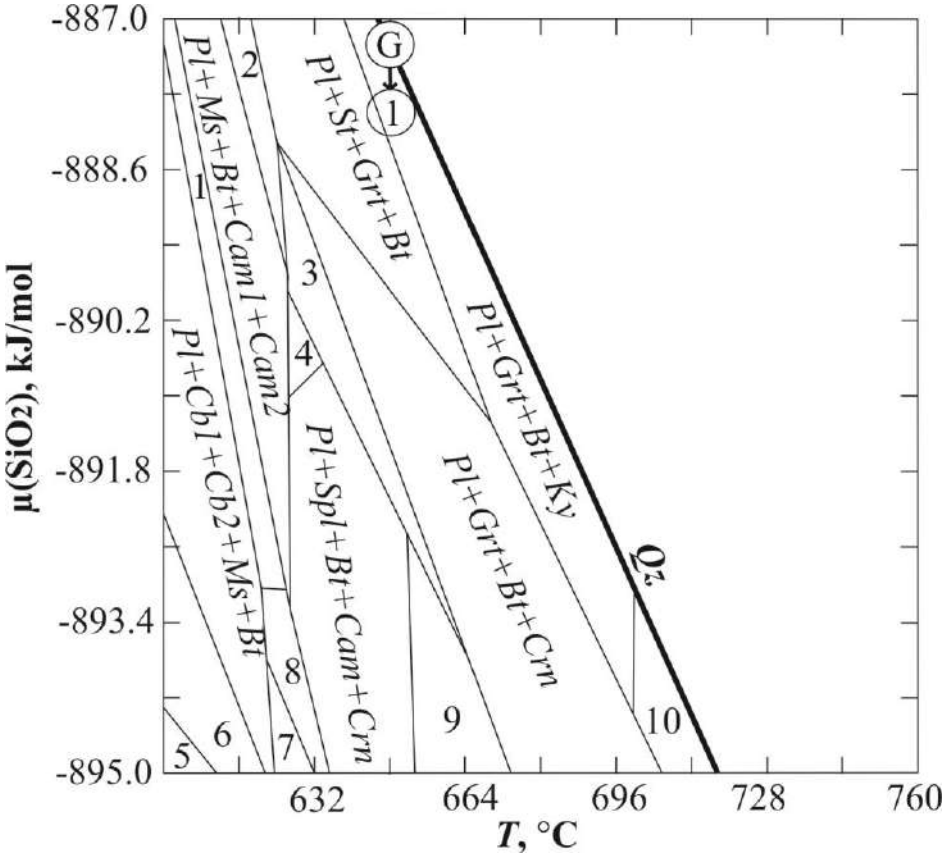

Fig. 84. T–μ(SiO_2) pseudosection for a given composition of migmatized kyanite-garnet-biotite gneisses of the Chupa sequence (composition 1 in Table 1 in Appendix 2). P = 8 kbar, X(CO_2) = 0.3. The number 1 in the circle corresponds to zone 1 with the corresponding composition diagram. Letter G denotes the position of paragenesis of kyanite-garnet-biotite gneisses. Associations are marked with numbers: *1 – Pl + Cb + Ms + Bt + Cam1 + Cam2, 2 – Pl + Grt + Ms + Bt + Cam, 3 – Pl + Grt + Bt + Cam + Crn, 4 – Pl + Spl + Bt + Cam1 + Cam2 + Crn, 5 – Cb1 + Cb2 + Bt + Nph + Crn, 6 – Cb1 + Cb2 + Ms + Bt + Nph, 7 – Pl + Cb + Spl + Ms + Bt, 8 – Pl + Cb + Spl + Ms + Bt + Cam, 9 – Pl + Spl + Bt + Cam, 10 – Pl + Grt + Bt + Sil.*

In the second zone of metasomatic zoning (indicated by number 2 in Fig. 85), large kyanite crystals are replaced by staurolite-plagioclase symplectites (indicating the participation of plagioclase in mineral transformations) after the complete disappearance of quartz. Here, Na2O passes into the mobile state, which is evidenced by the appearance of aspidolite, sodic gedrite, and Na-Ca amphibole in the inner zones of metasomatites. The pseudosection in the coordinates $\mu(SiO_2)$–$\mu(Na_2O)$ (Fig. 85) shows that, upon transition to the mobile state of Na_2O against the background of ongoing desilication, the *Pl + Bt + Grt + Ky* paragenesis is replaced by the *Pl + Bt + Grt + St* paragenesis. This transition is described by the reaction:

$$Ky + Grt + Na_2O + H_2O = Pl + St + SiO_2 \quad (4)$$

According to the results of thermodynamic modeling, the course of this reaction provides an increase in the volume percentage of plagioclase by 1.5% and, at the same time, a decrease in the volume percentage of garnet by 6% and the appearance of 16% staurolite (Fig. 86). In the composition-paragenesis diagrams (Fig. 83), this process is expressed in the fact that staurolite becomes the carrier of excess alumina instead of kyanite.

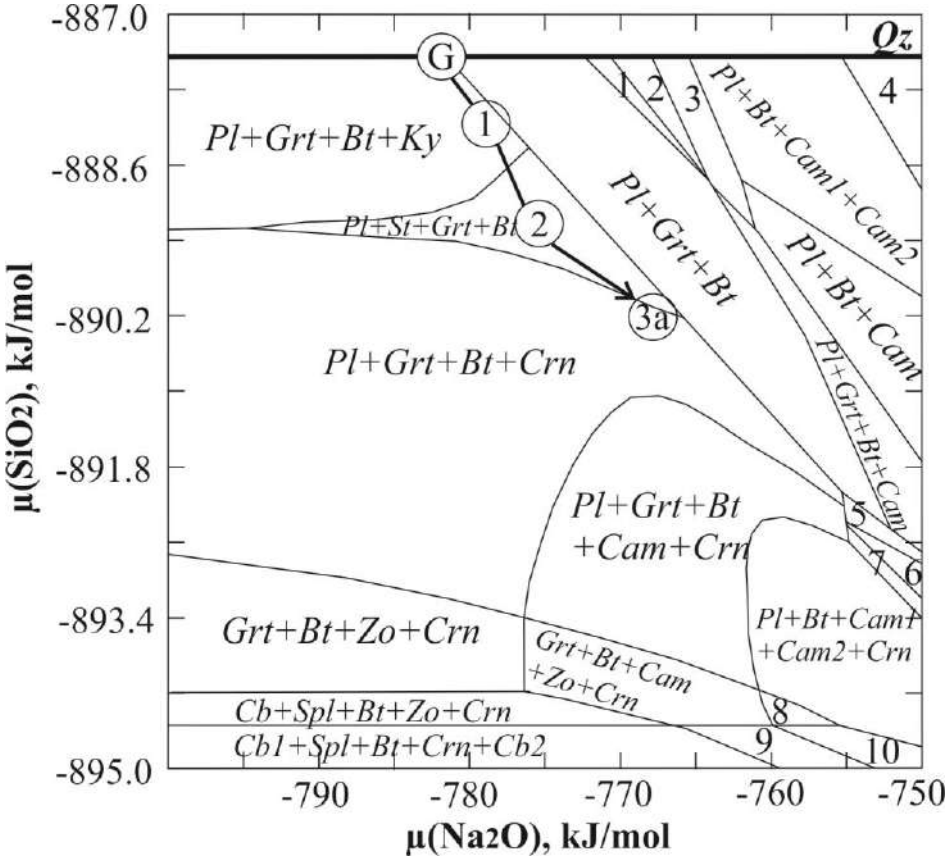

Fig. 85. $\mu(SiO_2)$–$\mu(Na_2O)$ pseudosection for a given composition of migmatized kyanite-garnet-biotite gneisses of the Chupa Unit (composition 1 in Table 1 in Appendix 2) with the mineral association *Pl + Qz + Bt + Grt + Ky*. T = 650°C, P = 8 kbar, $X(CO_2)$ = 0.3. Numbers in circles correspond to zones with corresponding composition diagrams. Letter G denotes the position of

paragenesis of kyanite-garnet-biotite gneisses. Associations are marked with numbers: *1 – Pl + Opx + Grt + Bt, 2 – Pl + Opx + Bt + Cam, 3 – Pl + Opx + Bt + Cam1 + Cam2, 4 – Pl + Cpx + Bt + Cam1 + Cam2, 5 – Pl + Spl + Grt + Bt + Cam, 6 – Pl + Spl + Bt + Cam, 7 – Pl + Spl + Bt + Cam + Crn, 8 – Bt + Cam + Cam + Zo + Crn, 9 – Spl + Bt + Cam + Crn + Cal, 10 – Bt + Cam1 + Cam2 + Crn + Cal*.

A significant part of the pseudosection (Fig. 85) is also occupied by the association observed in amphibole-free corundum-bearing rocks – *Pl + Bt + Grt + Crn* (zone 3a).

As can be seen in the diagrams with isomodes (isolines of quantitative ratios of minerals), an increase in μ(Na_2O) leads to a rapid increase in the content of plagioclase in the rock, but the amount of corundum and garnet decreases just as quickly (Fig. 86).

In this zone, corundum-plagioclase symplectites are formed in place of staurolite, and then large crystals of corundum appear in the rocks. On the pseudosection, the transition from the *Pl + Bt + Grt + St* paragenesis to the *Pl + Bt + Grt + Crn* paragenesis occurs according to the reaction:

$$Pl + St = Crn + Grt + Na_2O + SiO_2 + H_2O \quad (5),$$

and taking into account the direction of the metasomatic process - as a result of ongoing desilication, accompanied by Na-alkaline metasomatism. The opposite behavior of Na_2O in reactions (4) and (5) corresponds to the mutually opposite slope of the lines of these equilibria, which limit the field *Pl + Bt + Grt + St* on Fig. 85.

According to the results of thermodynamic modeling, the reaction (5) provides an increase in the volume percentage of garnet content by 2% and, at the same time, a decrease in the volume percentage of plagioclase content by 3.5% and the appearance of 5% corundum (Fig. 86). In the composition diagrams (Fig. 83), this process is expressed in the fact that corundum becomes the carrier of excess alumina instead of staurolite.

Although the discussed parageneses (*Pl + Bt + Grt + Ky*, *Pl + Bt + Grt + St*, and *Pl + Bt + Grt + Crn*) were also present in the T–μ(SiO_2) diagram, the μ(SiO_2)–μ(Na_2O) diagram adds the possibility of changing the plagioclase composition, which actually takes place.

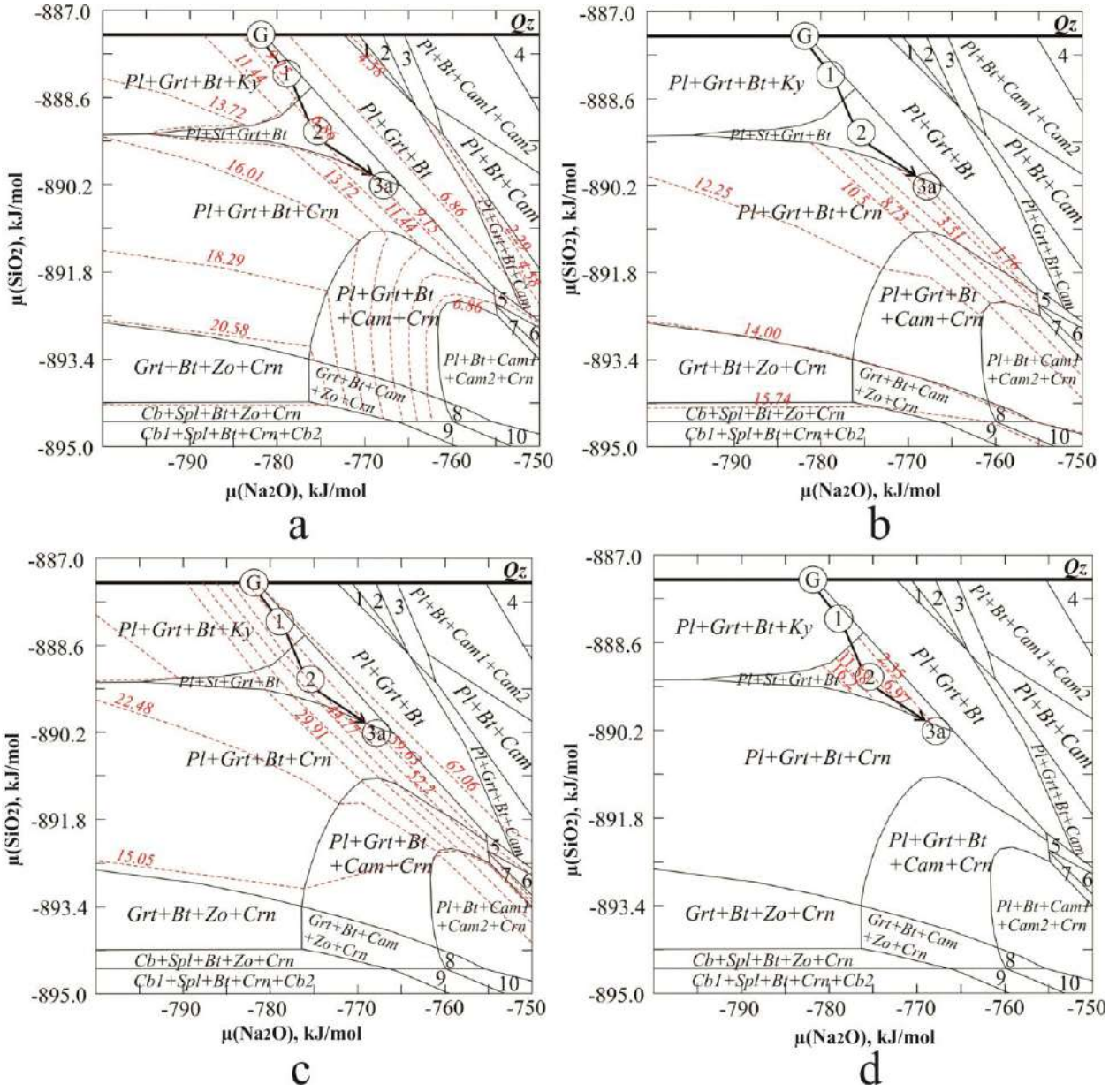

Fig. 86. Isomodes to the μ(SiO_2)–μ(Na_2O) pseudosection: a – for garnet, b – for corundum, c – for plagioclase, d – for staurolite.

According to petrographic data, calcium amphibole begins to appear already in those varieties where staurolite-plagioclase symplectites around kyanite are noted (zone 3b). All these data indicate that K_2O in the inner zones of corundum-bearing metasomatites passes into a mobile state.

In the perfectly mobile state of K_2O, the phase relations in the system under study are shown in the diagram μ(SiO_2)–μ(K_2O) (Fig. 87).

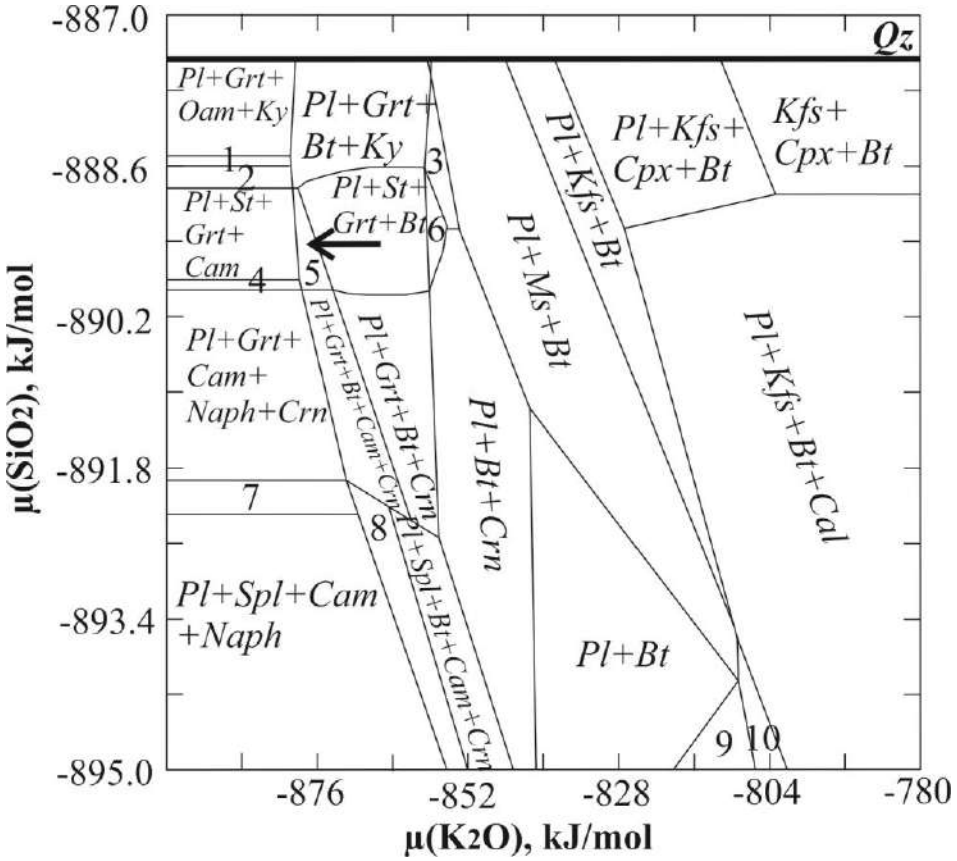

Fig. 87. $\mu(SiO_2)$–$\mu(K_2O)$ pseudosection for a given composition of migmatized kyanite-garnet-biotite gneisses of the Chupa sequence (composition 1 in Table 1 in Appendix 2). T = 650°C, P = 8 kbar, $X(CO_2)$ = 0.3. The arrow shows the direction of the process. Associations are marked with numbers: *1 – Pl + Grt + Oam + Cam + Ky, 2 – Pl + Grt + Cam + Ky , 3 – Pl + Bt + Ky, 4 – Pl + St + Grt + Cam + Naph, 5 – Pl + St + Grt + Bt + Cam, 6 – Pl + Grt + Cam + Ky, 7 – Pl + Spl + Grt + Cam + Naph, 8 – Pl + Spl + Bt + Cam, 9 – Pl + Bt + Cal, 10 – Pl + Ms + Bt + Cal. Naph* – Na-phlogopite.

As can be seen from the resulting diagram, a decrease in the chemical potential of K_2O leads to the appearance of calcium amphibole in biotite-containing associations, and then to the disappearance of biotite. Thus, the course of the reaction:

$$Pl + Bt + Grt = Cam + SiO_2 + K_2O \quad (6)$$

ultimately ensures the transition from the *Pl + Bt + St + Grt* paragenesis to the *Pl + St + Grt + Cam* paragenesis in the amphibole zone. According to the results of thermodynamic modeling, the occurrence of this reaction ensures the appearance of 6.5–7% calcium amphibole (Fig. 88).

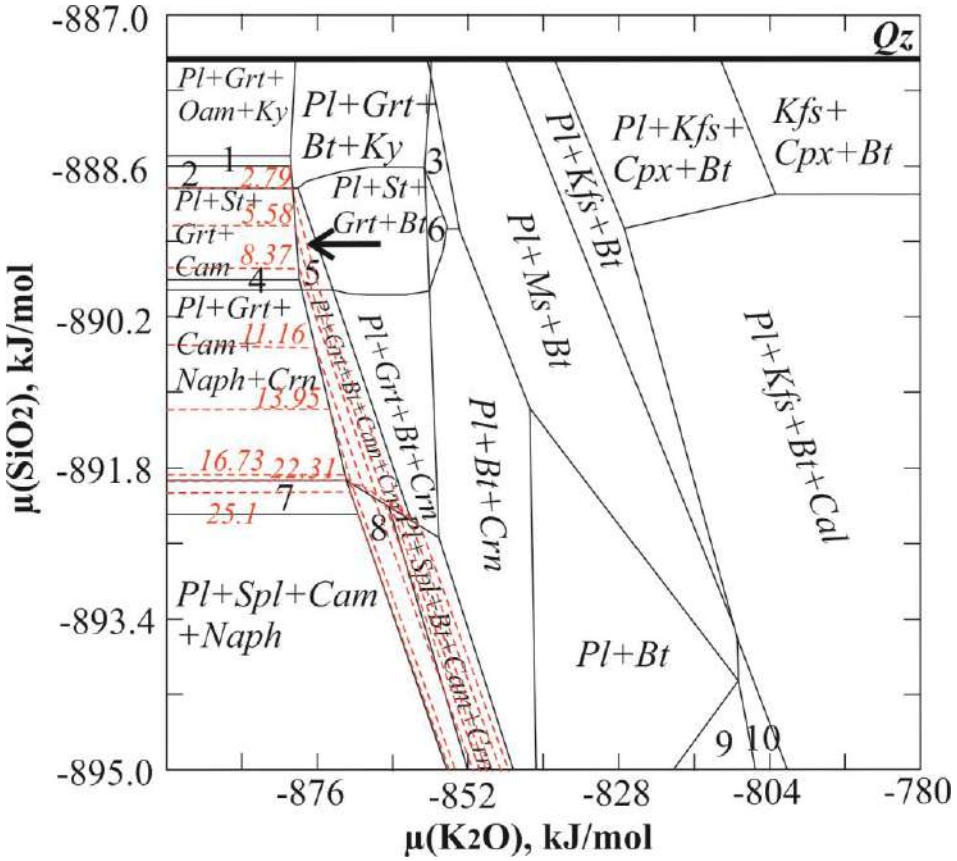

Fig. 88. Diagram with calcium amphibole isomodes for pseudosection $\mu(SiO_2)$–$\mu(K_2O)$.

The Perplex software package does not allow modeling metasomatism with more than two fully mobile components. To take into account the mobile behavior of K_2O and the decrease in its chemical potential in the simulation, the amount of K_2O in the initial composition was reduced to 0.87 wt % (this value corresponds to the chemical potential of K_2O in the *Pl + St + Grt + Cam* paragenesis field in the $\mu(SiO_2)$–$\mu(K_2O)$ diagram). A decrease in the amount of K_2O in the initial composition leads, in particular, to a shift in the point of kyanite-garnet-biotite gneiss on the composition diagrams (diagrams 3 and 4 in Fig. 83) due to the subtraction of biotite from the rock composition.

The conditions for the formation of associations of amphibole-bearing rocks with staurolite and corundum (zones 3b, 4) are reflected in the $\mu(SiO_2)$–$\mu(Na_2O)$ pseudosection with a reduced amount of K_2O in the initial composition (Fig. 89).

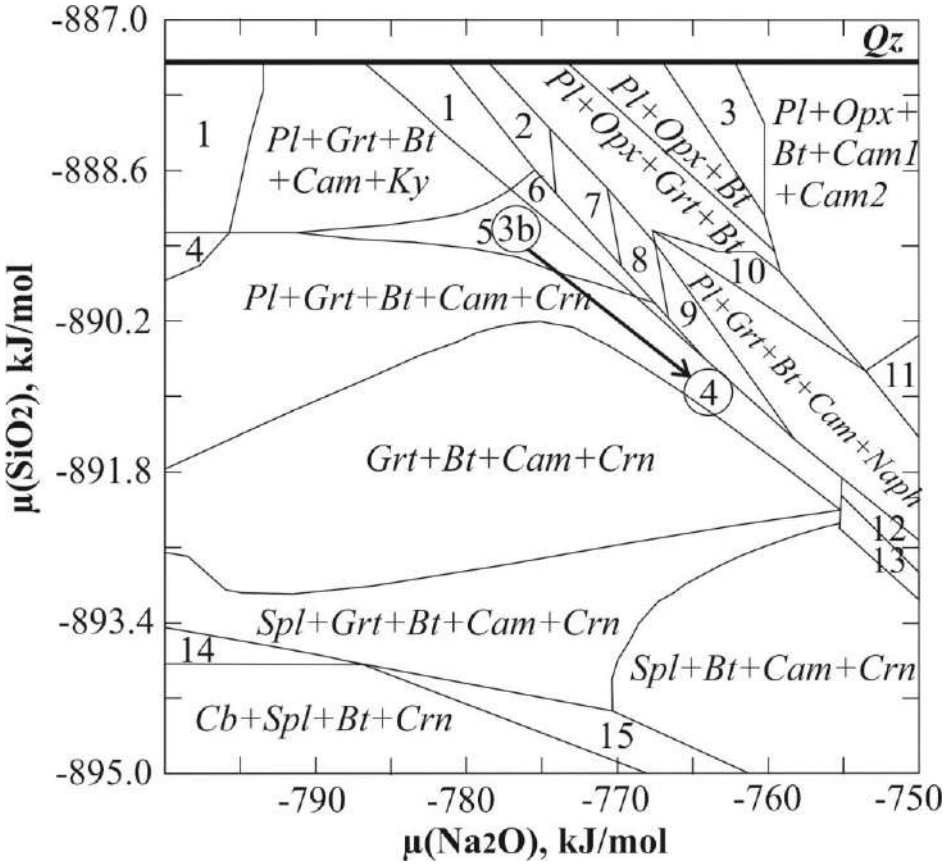

Fig. 89. $\mu(SiO_2)$–$\mu(Na_2O)$ pseudosection for a given composition of migmatized kyanite-garnet-biotite gneisses of the Chupa sequence (composition 1 in Table 1 in Appendix 2). T = 650°C, P = 8 kbar, $X(CO_2)$ = 0.3. The amount of K_2O in the initial composition was reduced to 0.87 wt.%. Numbers 3 and 4 in circles correspond to the corresponding composition diagrams. Associations are marked with numbers: *1 – Pl + Grt + Bt + Ky, 2 – Pl + Grt + Bt, 3 – Pl + Opx + Bt + Cam, 4 – Pl + Grt + Bt + Crn, 5 – Pl + St + Grt + Bt + Cam, 6 – Pl + St + Grt + Bt, 7 – Chl + Pl + Grt + Bt, 8 – Pl + Grt + Bt + Cam, 9 – Pl + Grt + Bt + Naph, 10 – Pl + Opx + Grt + Bt + Cam, 11 – Pl + Bt + Cam + Cam + Naph, 12 – Pl + Spl + Bt + Cam, 13 – Pl + Spl + Bt + Cam + Crn, 14 – Cb + Spl + Grt + Bt + Crn, 15 – Cb + Spl + Bt + Cam + Crn.*

The growth of the field of calcium amphibole ensures its appearance in the staurolite paragenesis at the same chemical potentials $\mu(SiO_2)$–$\mu(Na_2O)$ as in zone 2.

At the same time, biotite is still present on the obtained pseudosection, since the amount of K_2O sufficient for its formation is present in the initial composition. However, upon further transition to the mobile K_2O state, biotite will become unstable and finally disappear, which will lead to the formation of the *Pl + Grt + St + Cam* paragenesis. Turning to the data of multiequilibrium thermobarometry (Akimova, Skublov, 2021), we note that it was not possible to obtain converging constructions with biotite, due to the fact that biotite is not in equilibrium with calcium amphibole.

The *Pl + Grt + St + Cam* paragenesis will be replaced by the *Pl + Grt + Cam + Crn* paragenesis with a decrease in $\mu(SiO_2)$ and an increase in $\mu(Na_2O)$, which corresponds to reaction (5), which in this case proceeds in the presence of calcium amphibole rather than biotite.

Thus, the *Pl + Grt + Cam + Crn* paragenesis noted in zone 4 of corundum-bearing rocks was formed during the ongoing desilication of kyanite-garnet-biotite gneisses, accompanied by Na-alkaline metasomatism, after the transition of K_2O to the mobile state.

As can be seen from the diagrams with isomodes (Fig. 90), the transition to the mobile state of K_2O leads to the appearance of parageneses with a very significant amount of calcium amphibole – up to 35%, while wide variations in the content of calcium amphibole and plagioclase in the rock are provided, since the isomodes in the area of interest of the pseudosection are very close together.

The positions of circles with zone numbers and composition diagrams on all pseudosections correspond to the parameters of rock formation in these zones and were determined based on model variations in mineral compositions (see below).

Note that all pseudosections (Fig. 78, 84–89) were plotted at a given $X(CO_2) = 0.3$, and the question arises whether this value could take place in reality, or whether it is worth taking into account wide variations in $X(CO_2)$ in a natural fluid. To do this, consider pseudosections similar to the diagram in Fig. 89, but at a given $X(CO_2) = 0.1$ (Fig. 91), $X(CO_2) = 0.2$ (Fig. 92), $X(CO_2) = 0.4$ (Fig. 93).

The resulting diagrams show that if $X(CO_2)$ decreases to 0.1, then the chlorite stability field expands greatly, and the *Pl+Grt+Bt+Cam+Crn* association field almost disappears (Fig. 91). And if $X(CO_2)$ increases to 0.4, then the *Pl+Grt+Bt+Cam+Crn* association field expands, but the staurolite field almost disappears (Fig. 93). Thus, the possible range of $X(CO_2)$ in the fluid at given RT is from 0.2 to 0.3.

Note that the estimates obtained are valid only at the given temperature and pressure, since a decrease in temperature is equivalent to an increase in the proportion of water in the fluid.

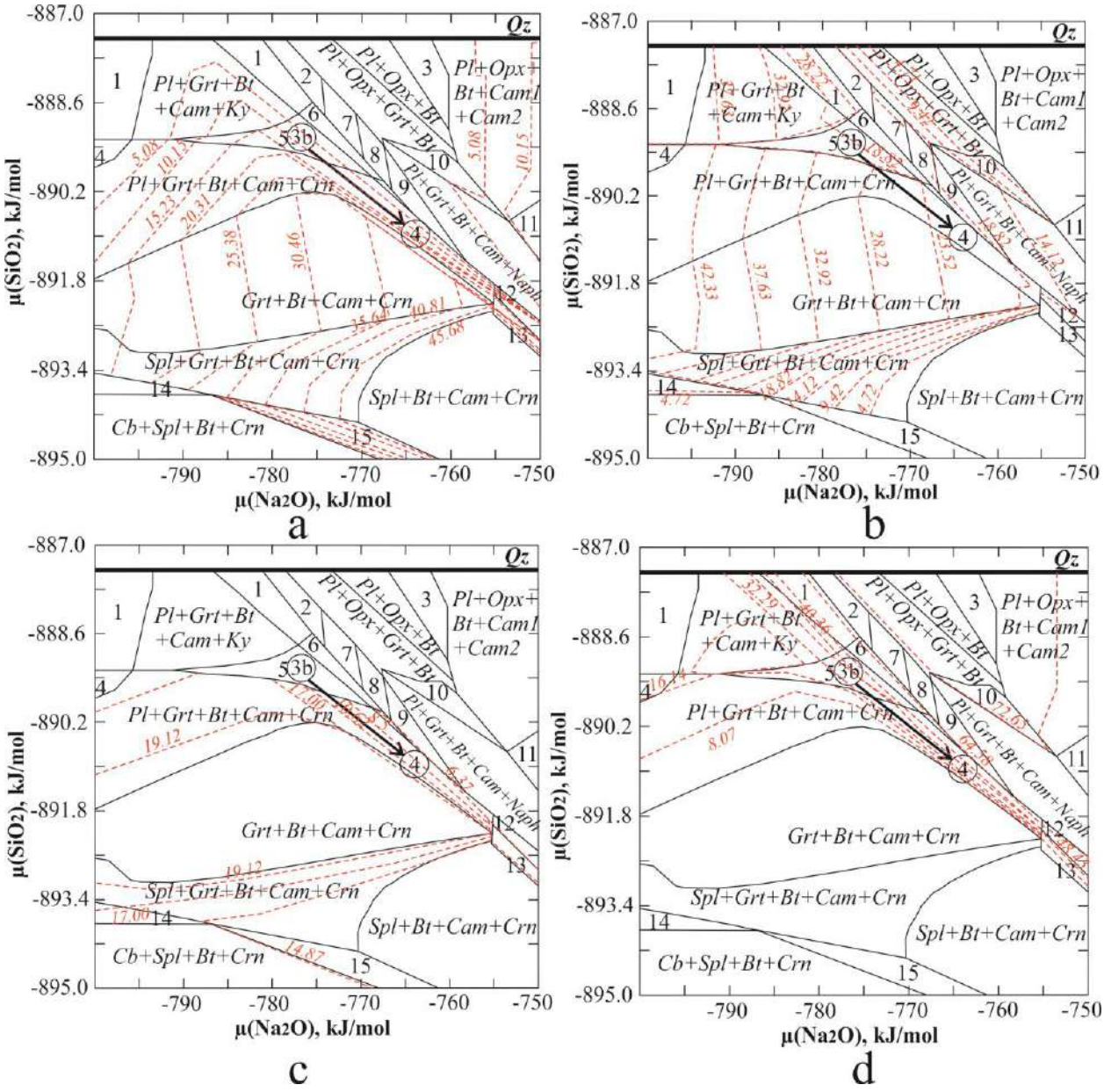

Fig. 90. Isomodes to the μ(SiO_2)–μ(Na_2O) pseudosection with the amount of K_2O reduced to 0.87 wt % in the initial composition: a – for calcium amphibole, b – for garnet, c – for corundum, and d – for plagioclase.

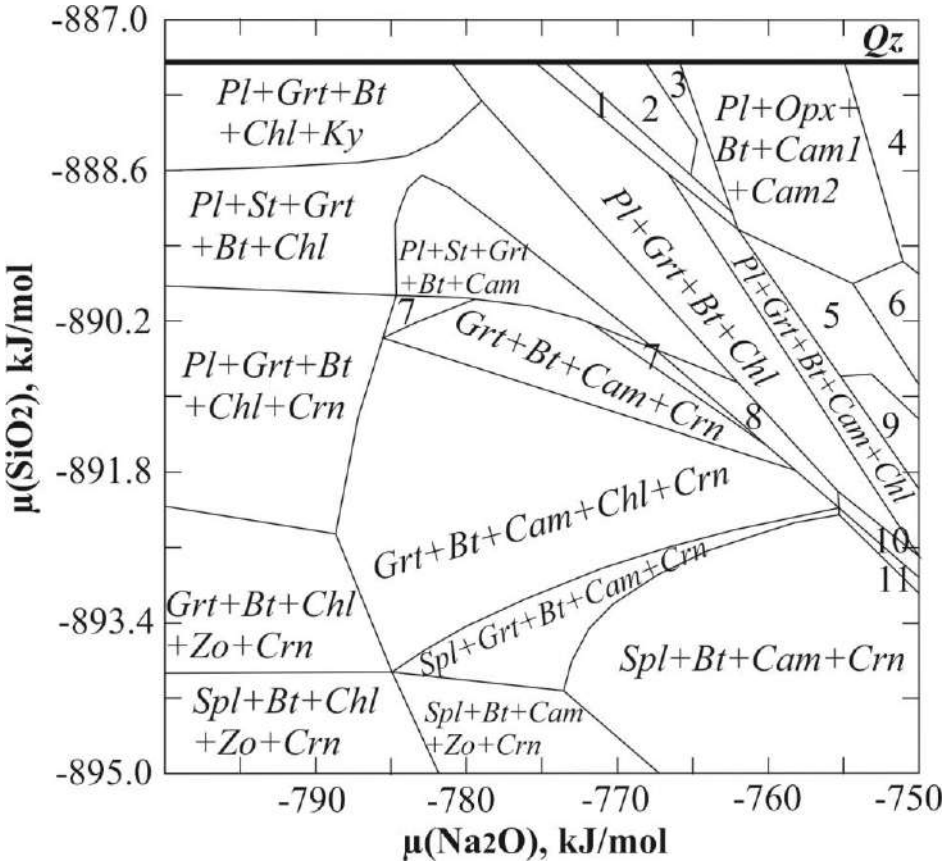

Fig. 91. $\mu(SiO_2)$–$\mu(Na_2O)$ pseudosection for a given composition of migmatized kyanite-garnet-biotite gneisses of the Chupa sequence (composition 1 in Table 1 in Appendix 2). T = 650°C, P = 8 kbar, $X(CO_2)$ = 0.1. The amount of K_2O in the initial composition was reduced to 0.87 wt %. Associations are marked with numbers: *1 – Pl + Opx + Grt + Bt, 2 – Pl + Opx + Bt, 3 – Pl + Opx + Bt + Cam, 4 – Pl + Bt + Cam1 + Cam2, 5 – Pl + Bt + Cam1 + Cam2 + Chl, 6 – Pl + Bt + Cam1 + Cam2 + Naph, 7 – Pl + Grt + Bt + Cam + Crn, 8 – Pl + Grt + Bt + Chl + Crn, 9 – Pl + Bt + Cam + Chl, 10 – Pl + Spl + Bt + Cam + Chl, 11 – Pl + Spl + Bt + Cam + Crn.*

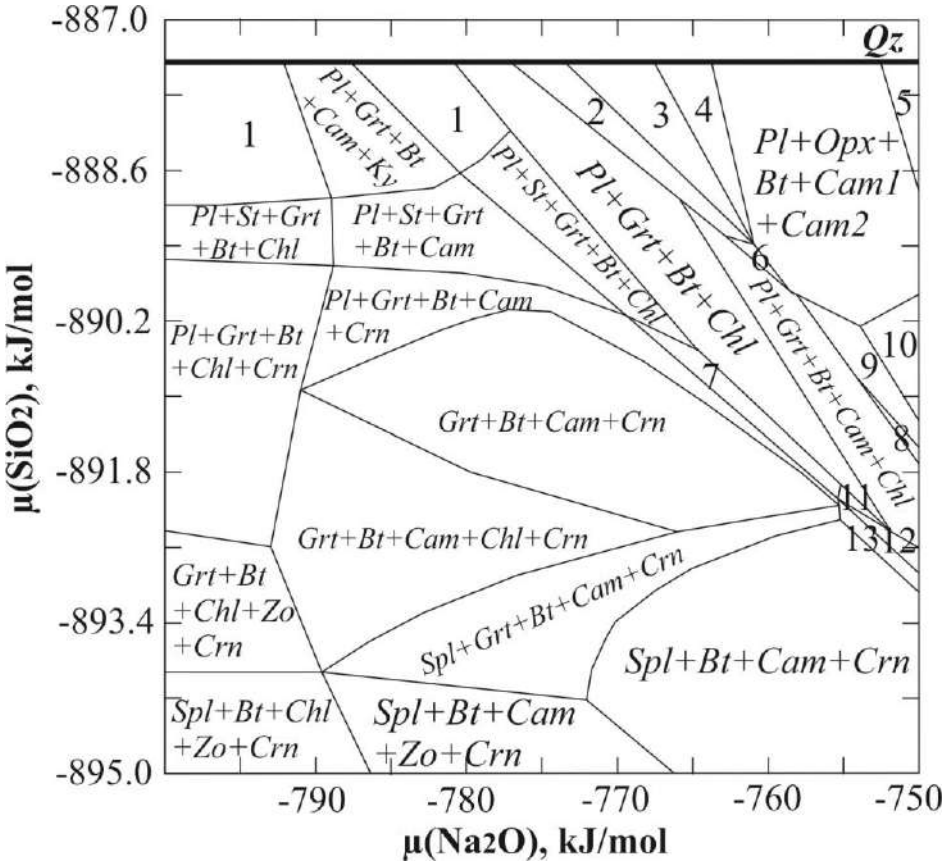

Fig. 92. $\mu(SiO_2)$–$\mu(Na_2O)$ pseudosection for a given composition of migmatized kyanite-garnet-biotite gneisses of the Chupa sequence (composition 1 in Table 1 in Appendix 2). T = 650°C, P = 8 kbar, $X(CO_2)$ = 0.2. The amount of K_2O in the initial composition was reduced to 0.87 wt %. Associations are marked with numbers: *1 – Pl + Grt + Bt + Chl + Ky, 2 – Pl + Opx + Grt + Bt, 3 – Pl + Opx + Bt, 4 – Pl + Opx + Bt + Cam, 5 – Pl + Bt + Cam1 + Cam2, 6 – Pl + Opx + Grt + Bt + Cam, 7 – Pl + Grt + Bt + Chl + Crn, 8 – Pl + Bt + Cam + Chl, 9 – Pl + Bt + Cam1 + Cam2 + Chl, 10 – Pl + Bt + Cam1 + Cam2 + Naph, 11 – Pl + Spl + Grt + Bt + Chl, 12 – Pl + Spl + Bt + Cam + Chl, 13 – Pl + Spl + Bt + Cam + Crn.*

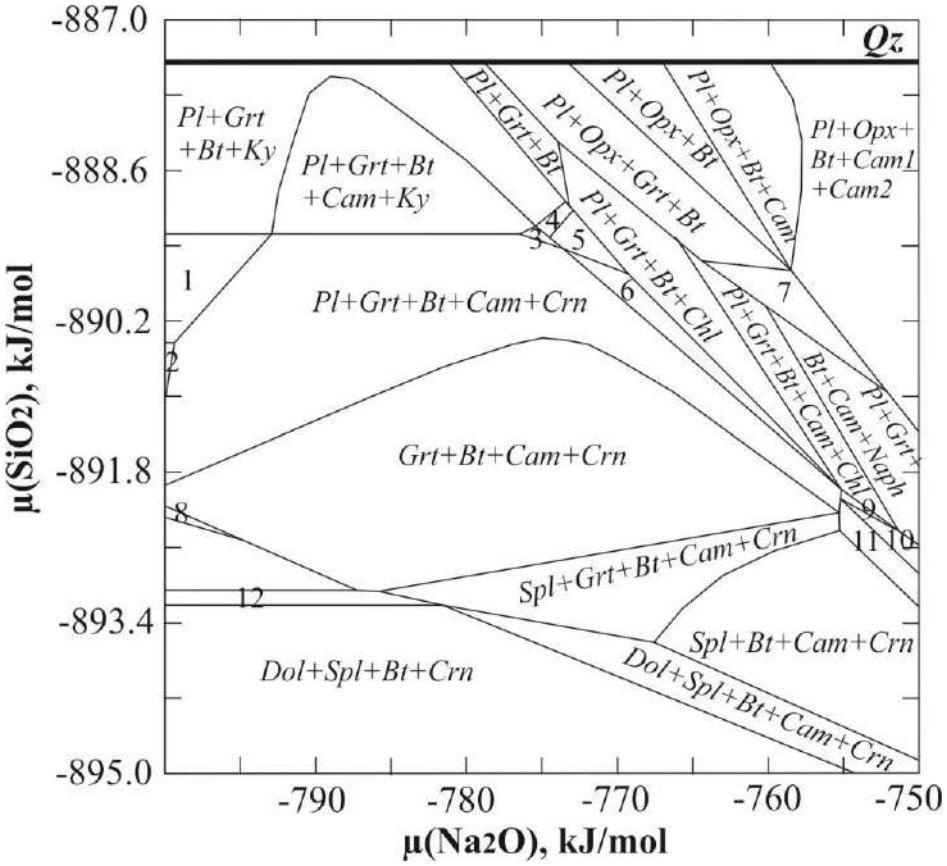

Fig. 93. $\mu(SiO_2)$–$\mu(Na_2O)$ pseudosection for a given composition of migmatized kyanite-garnet-biotite gneisses of the Chupa sequence (composition 1 in Table 1 in Appendix 2). T = 650°C, P = 8 kbar, $X(CO_2)$ = 0.4. The amount of K_2O in the initial composition was reduced to 0.87 wt %. Associations are marked with numbers: *1 - Pl + Grt + Bt + Crn, 2 - Pl + Grt + Bt + Chl + Crn, 3 - Pl + St + Grt + Bt + Cam, 4 - Pl + St + Grt + Bt, 5 - Pl + St + Grt + Bt + Chl, 6 - Pl + Grt + Bt + Chl + Crn, 7 - Pl + Opx + Grt + Bt + Cam, 8 - Grt + Bt + Cam + Chl + Crn, 9 - Pl + Spl + Grt + Bt + Cam, 10 - Pl + Spl + Bt + Cam, 11 - Pl + Spl + Bt + Cam + Crn, 12 - Dol + Spl + Grt + Bt + Crn.*

It is also necessary to consider the mobile behavior of CaO (together with Na_2O), discussed in the works of colleagues (Serebryakov, Rusinov, 2004). The petrochemical data indicate a slight increase in the amount of CaO in corundum-bearing rocks compared to the host kyanite-garnet-biotite gneisses (Table 1 in Appendix 2), which can be explained both by the supply of CaO (i.e., its mobile behavior) and the participation of a protolith somewhat enriched in CaO in the metasomatic process.

Let us consider the first of the possible scenarios, which allows the mobile behavior of CaO. The transition of CaO into a mobile state is most probable at the boundary of zones 1 and 2, where kyanite is replaced by staurolite-plagioclase symplectites and, in this case, the grossular

component in garnet increases, while plagioclase becomes somewhat more basic. Let us turn to the pseudosection in the coordinates μ(SiO_2)–μ(CaO) for zones 1-2 (Fig. 94).

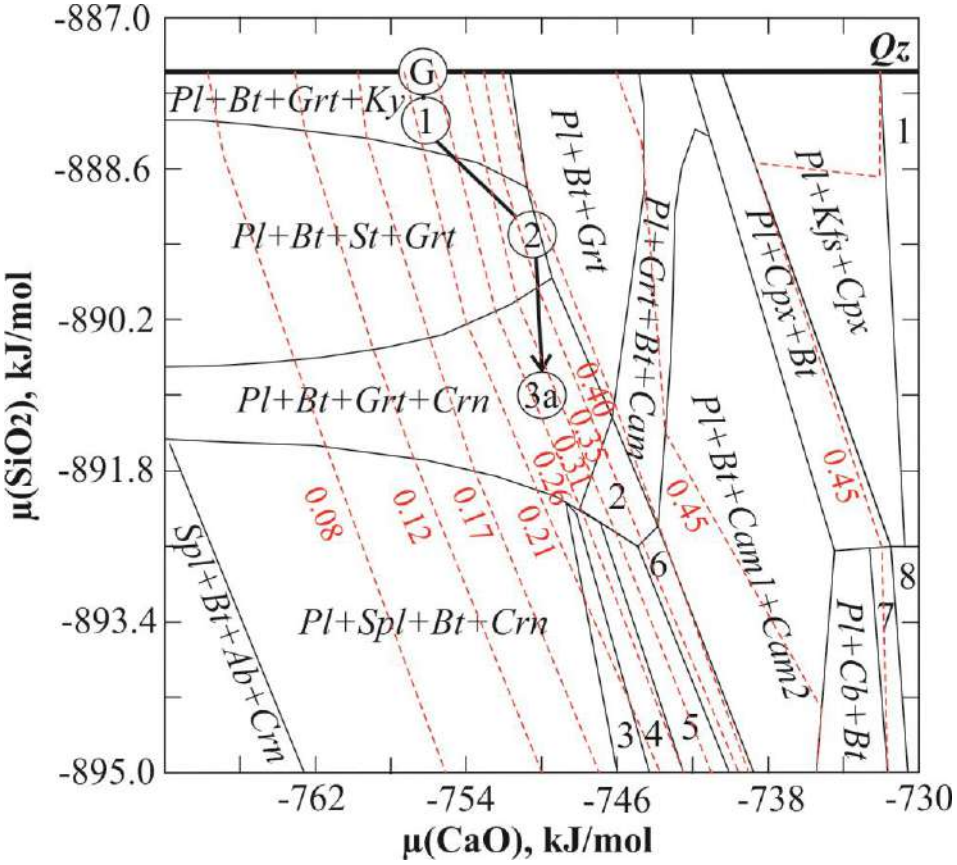

Fig. 94. μ(SiO_2)–μ(CaO) pseudosection for a given composition of migmatized kyanite-garnet-biotite gneisses of the Chupa sequence (composition 1 in Table 1 in Appendix 2). T = 650°C, P = 8 kbar, X(CO_2) = 0.3. Red dotted lines are isopleths reflecting model variations in the anorthite component in plagioclase in zones 1–3a. Associations are marked with numbers: *1 – Pl + Kfs + Cpx + Zo, 2 – Pl + Grt + Bt + Cam + Crn, 3 – Pl + Spl + Bt, 4 – Pl + Spl + Bt + Cam, 5 – Pl + Spl + Bt + Cam + Crn, 6 – Pl + Bt + Cam1 + Cam2 + Crn, 7 – Pl + Dol + Bt + Zo, 8 – Pl + Kfs + Dol + Zo.*

The obtained pseudosection shows the fields of the same parageneses of corundum-bearing metasomatites as on μ(SiO_2)–μ(Na_2O): *Pl + Grt + Bt + Ky, Pl + Bt + St + Grt, Pl + Bt + Grt + Crn, Pl + St + Grt + Bt + Cam, Pl + Grt + Bt + Cam + Crn*. The trend reconstructed from the isolines of the plagioclase composition allows a significant change in μ(CaO) only when moving from zone 1 to zone 2.

But Na_2O here still remains inert, which is obviously not the case in reality. In order to take into account the mobile behavior of three components at once - SiO_2, CaO and Na_2O, let us consider the projection of the three-dimensional diagram μ(SiO_2)–μ(CaO)–μ(Na_2O) onto the μ(CaO)–μ(Na_2O) plane for the Na_2O-CaO-Al_2O_3-SiO_2 system with inert Al_2O_3 (Fig. 95).

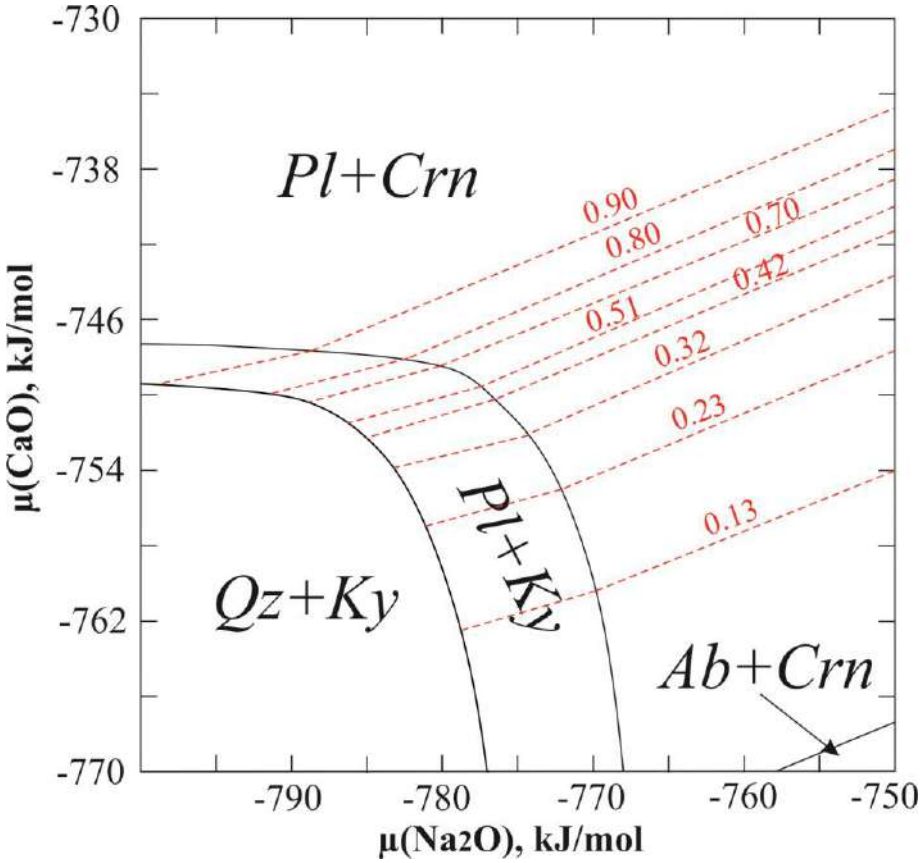

Fig. 95. Projection of the three-dimensional diagram $\mu(SiO_2)$–$\mu(CaO)$–$\mu(Na_2O)$ onto the $\mu(CaO)$–$\mu(Na_2O)$ plane for the CaO-Na_2O-Al_2O_3-SiO_2 system with inert Al_2O_3. T = 650°C, P = 8 kbar, $X(CO_2)$ = 0.3. Red dotted lines show plagioclase isopleths.

In the Na_2O-CaO-Al_2O_3-SiO_2 subsystem, in the presence of coexisting Crn and Pl, there are two degrees of freedom, one of which is due to SiO_2. Hence, the second PMC can be either Na_2O or CaO. If Na_2O is mobile, then the plagioclase composition uniquely determines the CaO potential, and *vice versa*. That is why the $\mu(SiO_2)$–$\mu(CaO)$ diagram, where the same parageneses are present at the same Pl compositions, as in the $\mu(SiO_2)$–$\mu(Na_2O)$ diagram.

If SiO_2, Na_2O, and CaO are mobile at the same time, then the *Crn+Pl* association is unstable. In corundum-bearing rocks, taking into account the mobile behavior of Na_2O, CaO, SiO_2, and K_2O (Al_2O_3, FeO, and MgO are inert here), a three-mineral paragenesis should appear, either *Crn + Grt + Cam* or *Pl + Grt + Cam*. However, such three-mineral parageneses were not observed in thin sections.

Thus, Na_2O and CaO in the case of corundum-bearing rocks could not be mobile simultaneously (within one metasomatic column).

Let us consider the possibility that the increased content of CaO was a feature of the protolith, along which corundum-bearing metasomatites developed. Variations in the composition of the kyanite–garnet–biotite gneisses of the Chupa sequence allow elevated CaO

contents, up to 4.54 wt % (Volodichev, 1990, Myskova, 2001). Let us turn to the pseudosection in the coordinates $\mu(SiO_2)$–$\mu(Na_2O)$ with the addition of CaO in the initial composition (Fig. 96).

If we compare the resulting pseudosection with $\mu(SiO_2)$–$\mu(Na_2O)$ without CaO addition (Fig. 89), we can notice some changes. Firstly, the line

$$2Abss = Crn + Na_2O + 6SiO_2 \quad (7)$$

moved noticeably to the left. Secondly, the field of paragenesis *Pl + Grt + Bt + Cam + Crn* has significantly expanded (as a result, the field of plagioclase-free paragenesis *Grt + Bt + Cam + Crn* has disappeared). As can be seen from the isolines of the plagioclase composition, the plagioclase in the *Pl + Grt + Bt + Cam + Crn* paragenesis became, on the whole, more basic. Here, the same trend of metasomatic reworking is still relevant as on $\mu(SiO_2)$–$\mu(Na_2O)$ without the addition of CaO (Fig. 89). However, it has substantially approached the line marking the transformation of corundum into plagioclase.

The content of calcium amphibole in zone 4 here, according to the results of thermodynamic modeling, is 18 vol %, and with an increase in the intensity of desilication with Na-alkaline metasomatism, it will very quickly increase up to 32% at $\mu(Na_2O)$ = -760 kJ/mol, $\mu(SiO_2)$ = -892 kJ/mol (Fig. 97).

Thus, the scenario with a CaO-enriched protolith is realistic and makes it possible to explain, firstly, the occurrence of corundum-bearing rocks enriched in calcium amphibole, and secondly, the absence of three-mineral parageneses corresponding to the mobile behavior of SiO_2, Na_2O, K_2O, and CaO simultaneously.

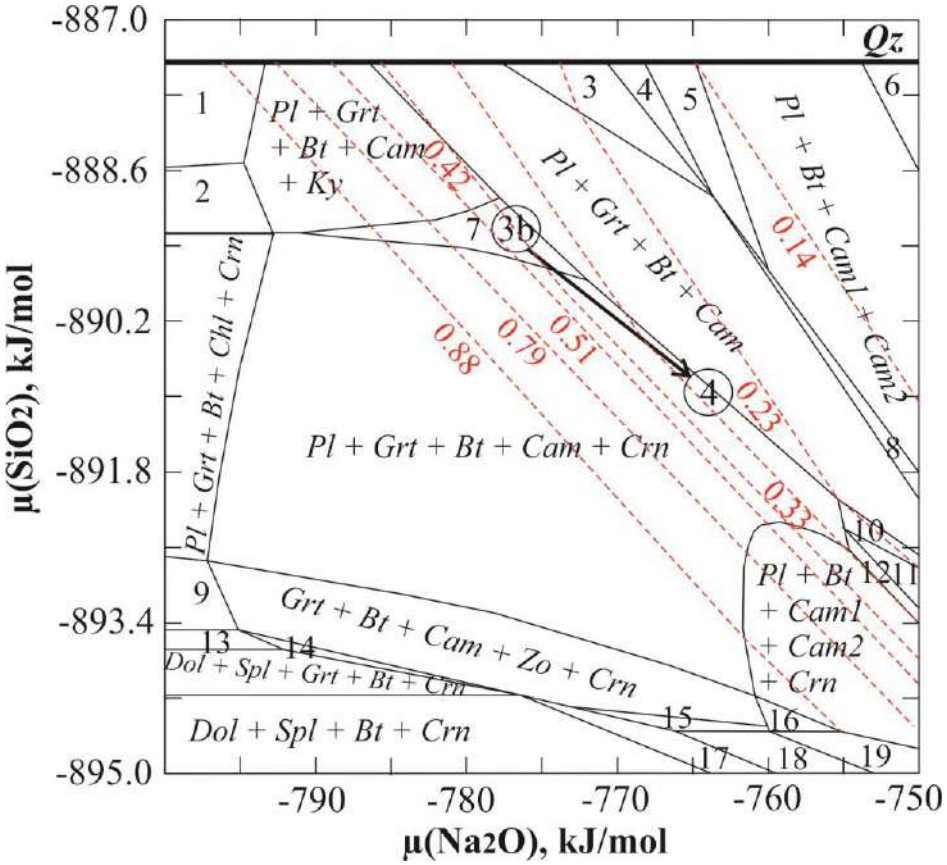

Fig. 96. $\mu(SiO_2)$–$\mu(Na_2O)$ pseudosection for a given composition of migmatized kyanite-garnet-biotite gneisses of the Chupa sequence (composition 1 in Table 1 in Appendix 2). T = 650°C, P = 8 kbar, $X(CO_2)$ = 0.3. The amount of K_2O in the initial composition was reduced to 0.87 wt %, while the amount of CaO was increased to 4.54 wt %. Red dotted lines are isopleths reflecting model variations in the anorthite component in plagioclase in zones 3b–4. Associations are marked with numbers: *1 – Pl + Grt + Bt + Ky, 2 – Pl + Grt + Bt + Chl + Ky, 3 – Pl + Opx + Grt + Bt + Cam, 4 – Pl + Opx + Bt + Cam, 5 – Pl + Opx + Bt + Cam1 + Cam2, 6 – Pl + Cpx + Bt + Cam + Cam, 7 – Pl + St + Grt + Bt + Cam, 8 – Pl + Grt + Bt + Cam1 + Cam2, 9 – Grt + Bt + Chl + Zo + Crn, 10 – Pl + Spl + Grt + Bt + Cam, 11 – Pl + Spl + Bt + Cam, 12 – Pl + Spl + Bt + Cam + Crn, 13 – Dol + Grt + Bt + Chl + Crn, 14 – Dol + Grt + Bt + Cam + Crn, 15 – Spl + Bt + Cam + Zo + Crn, 16 – Bt + Cam1 + Cam2 + Zo + Crn, 17 – Dol + Spl + Bt + Cam + Crn, 18 – Spl + Bt + Cam + Crn + Cal, 19 – Bt + Cam1 + Cam2 + Crn + Cal.*

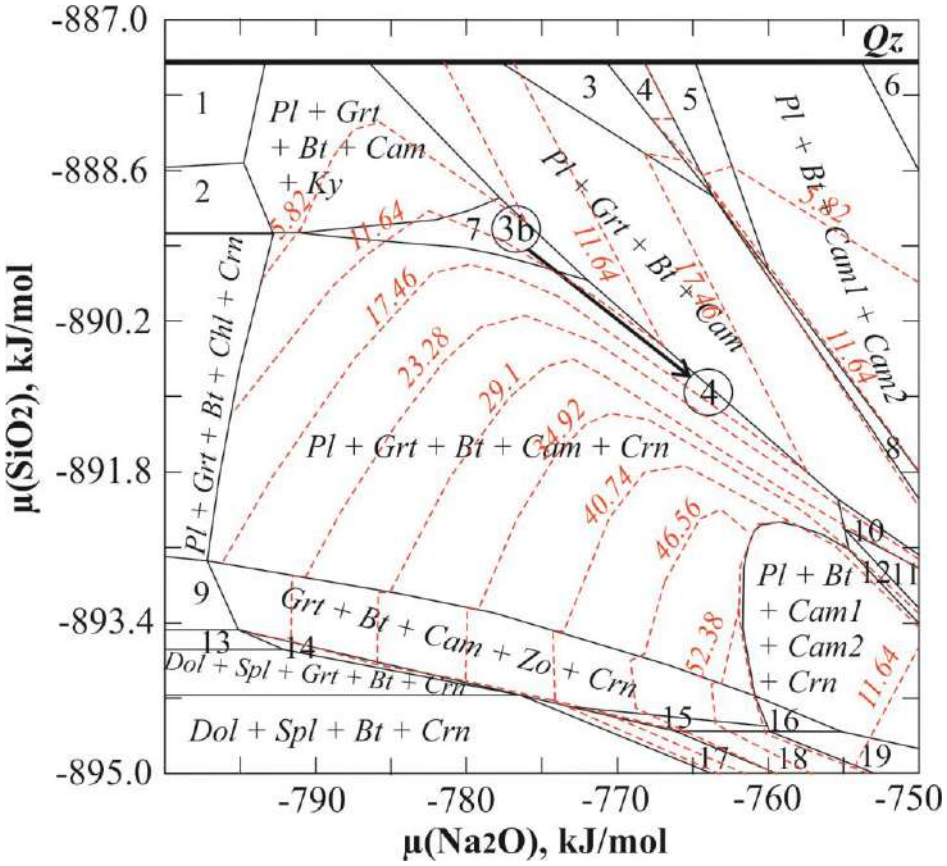

Fig. 97. Diagram with isomodes of calcium amphibole for $\mu(SiO_2)$–$\mu(Na_2O)$ pseudosection with the amount of K_2O reduced to 0.87 wt % and the amount of CaO increased to 4.54 wt % in the initial composition.

Table 7 summarizes the quantitative data on the mobile behavior of the components during metasomatism.

Table 7. The values of $\mu(SiO_2)$, $\mu(Na_2O)$, $\mu(K_2O)$ and their corresponding $lga(SiO_2)$, A_{Na}, A_K for zones of model zoning of corundum-bearing metasomatites.

	$\mu(SiO_2)$, J/mol	$lga(SiO_2)$	$\mu(Na_2O)$, J/mol	A_{Na}	$\mu(K_2O)$, J/mol	A_K
Zone 1	-888500	-0.05766	-780000	4.378010	-863662	3.353453
Zone 2	-889500	-0.11424	-776000	4.491178	-863022	3.371560
Zone 3a	-891000	-0.19912	-762000	4.887267	-864602	3.326859
Zone 3b	-889500	-0.11424	-776000	4.491178	-870454	3.161294
Zone 4	-891000	-0.19912	-762000	4.887267	-872156	3.113141

It follows from the data obtained that the corundum-bearing rocks were formed under conditions of a decrease in lga(SiO_2) from -0.06 to -0.2) with an increased activity of Na (A_{Na} increases from 4.38 to 4.88) and a decreased activity of K (A_K decreases from 3.35 to 3.11).

To assess the change in pH during metasomatism, we denote the chemical potential of Na_2O in the original rock as $\mu(Na_2O)_0$, and in the inner zone of metasomatites, as $\mu(Na_2O)_1$. Then:

$$\mu(Na_2O)_0 - \mu(Na_2O)_1 = 2RT(lnaH^+_1 - lnaH^+_0) \qquad (8),$$

and in this case, we can express the change in pH during metasomatism, denoting it $\Delta pH = pH_1 - pH_0$, as

$$\Delta pH = - 0.43429(lnaH^+_1 - lnaH^+_0) \qquad (9),$$

or, passing to chemical potentials, as

$$\Delta pH = - 0.43429(\mu(Na_2O)_0 - \mu(Na_2O)_1)/2RT \qquad (10).$$

Thus, in the case of corundum-bearing rocks of the occurrence Khitoostrov, where T = 923 K, $\mu(Na_2O)_0$ = -780 kJ/mol (in the original gneiss), $\mu(Na_2O)_1$ = -762 kJ/mol (in zone 4), ΔpH = 0.51. That is, in this case, the pH value slightly increased during metasomatism, which determined the subalkaline character of metasomatism.

Model variations of mineral compositions. Modeling variations in the compositions of minerals in Perplex is a somewhat more difficult task due to a number of limitations associated with the imperfection of thermodynamic models of solid solutions. Firstly, it is impossible to take into account the entry of Na into the K position in biotite, which is controlled by the changing ratio of $\mu(Na_2O)$ and $\mu(K_2O)$. Secondly, the presence of sodic gedrite in mineral associations is not taken into account. Thirdly, the existing models of a calcium amphibole solid solution do not allow us to take into account the possibility of the formation of amphiboles with ^{T}Al > 2 f.c. and ^{B}Na > 0.5 f.c. under simulated conditions. Nevertheless, a quantitative assessment of the nature of the process is impossible without model variations in the compositions of minerals.

Fig. 98 (a, b) shows that the composition of plagioclase is controlled by both the process of desilication and Na-alkaline metasomatism, i.e. the predominance of desilication will lead to a shift in the composition of plagioclase towards more basic (which is noted in zone 2), while Na-alkaline metasomatism may contribute to maintaining the constancy of the composition of plagioclase or even its shift towards more acidic (which is observed in zones 3–4).

The mobility of SiO_2 and Na_2O also affects the garnet composition: desilication will lead to an increase in calcium content (X_{Ca} = Ca/(Ca + Mg + Fe)) (which is observed in zone 2), and Na-alkaline metasomatism will decrease it (which occurs in zones 3b–4) (Fig. 98 c, d).

At the same time, desilication has a rather weak effect on the alumina content of biotite (Fig. 98 e), and an increase in $\mu(Na_2O)$ leads to the maintenance of a constant ^{T}Al content. This explains the absence of significant variations in the composition of biotite in corundum-bearing rocks.

An increase in $\mu(Na_2O)$ also leads to an increase in the Na content in the calcium amphibole (Fig. 98 f), but the model variations turn out to be somewhat narrower than natural ones due, as already mentioned, to the imperfection of solid solution models.

Comparison of model variations in the composition of plagioclase, and then other minerals (see Fig. 98 a-f) with natural ones (see Appendix 3) made it possible to determine the position of the zones of the metasomatic column of corundum-bearing metasomatites on pseudosections (Fig. 85, 89) and the direction of the trend of the metasomatic process.

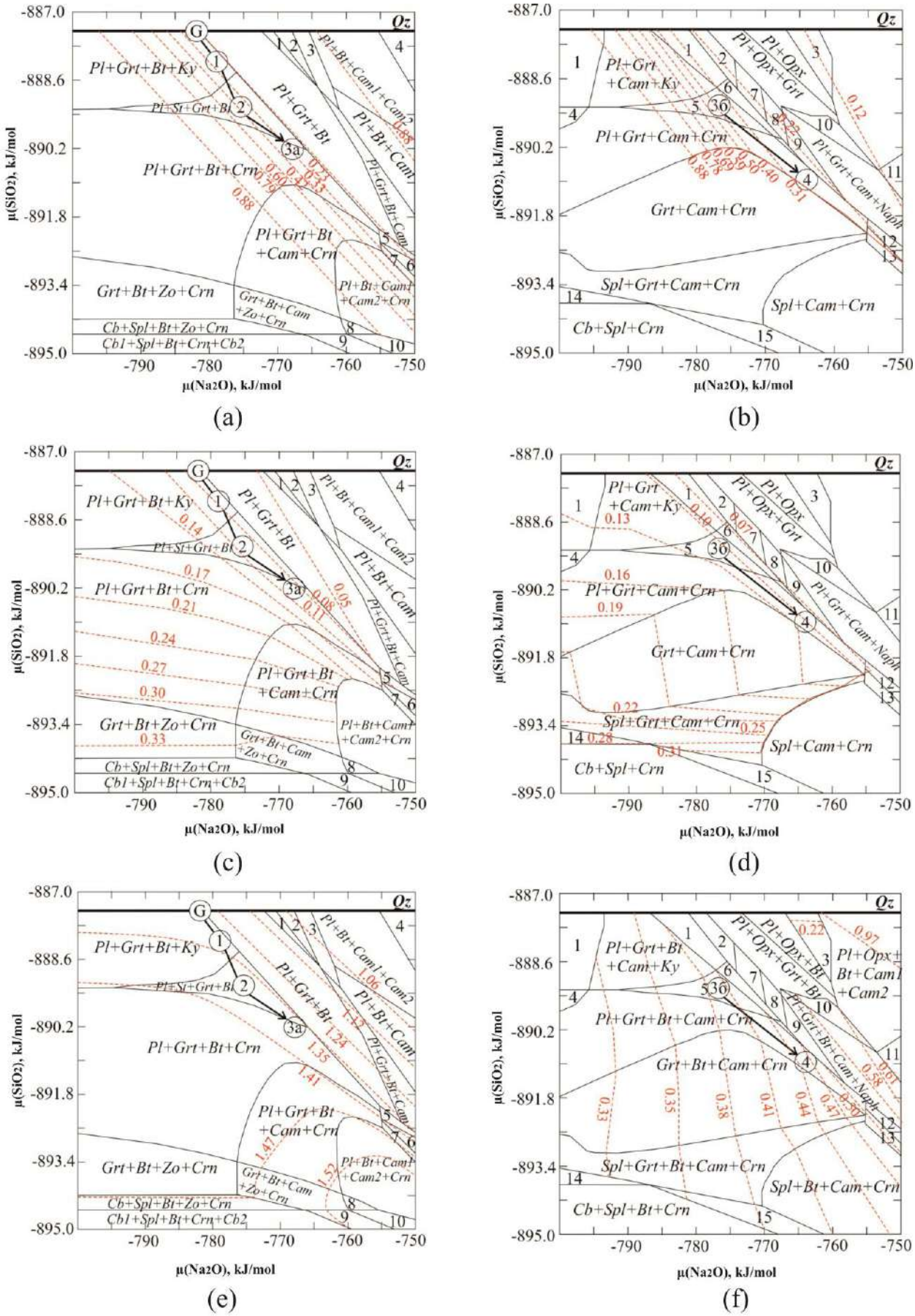

Fig. 98. Diagrams with isopleths showing model variations: anorthite component in plagioclase in zones 1–3a (a), anorthite component in plagioclase in zones 3b–4 (b), Ca/(Ca + Mg + Fe) in

garnet in zones 1–3a (c), Ca/(Ca + Mg + Fe) in garnet in zones 3b–4 (d), ^{IV}Al in biotite (e), Na in calcium amphibole (f).

Thermodynamic modeling of the process of formation of clinozoisite amphibolites. The disappearance of quartz in clinozoisite amphibolites, the development of more aluminous biotite and amphibole are evidence of desilication of host garnet amphibolites. In this case, the appearance of basic plagioclase is possible both as a result of desilication and as a result of a decrease in $\mu(Na_2O)$ (Fig. 99). The appearance of zoisite in this case could be facilitated by both a decrease in temperature and the effect of desilication and a decrease in $\mu(Na_2O)$. The replacement of garnet with plagioclase-amphibole symplectites in this case is apparently associated with a decrease in temperature.

Note that the resulting pseudosection does not contain corundum. Its formation is hindered by the high content of bases in amphibolites. Probably, the appearance of corundum in clinozoisite amphibolites at other manifestations is facilitated by the subsequent transition to the mobile state of the bases, but this issue requires further research.

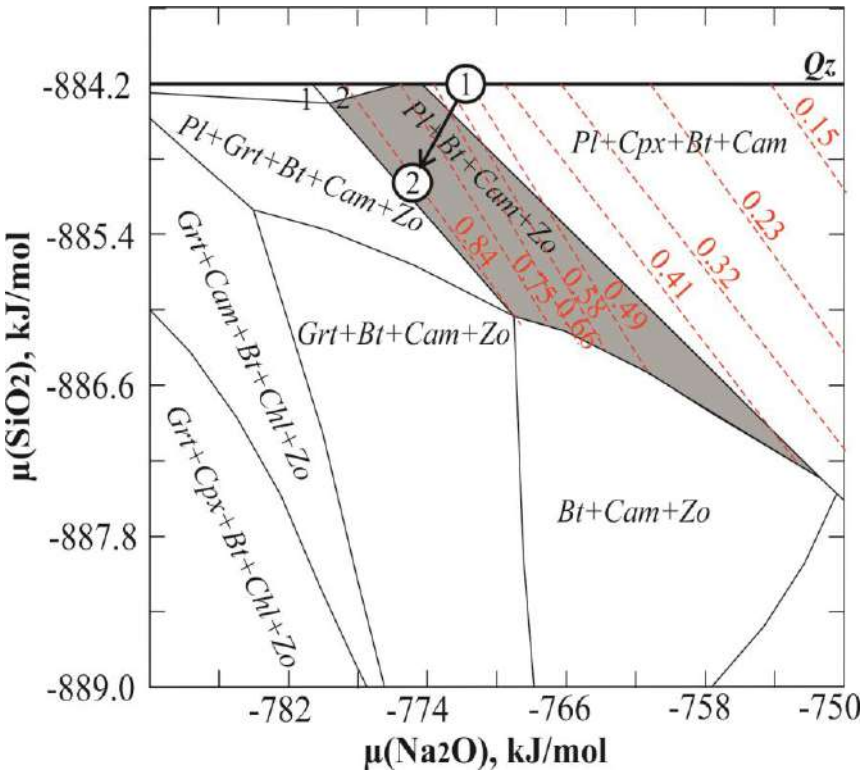

Fig. 99. $\mu(SiO_2)$–$\mu(Na_2O)$ pseudosection for a given composition of migmatized garnet amphibolites (sample Khi008g in Table 1 in Appendix 2). T = 620°C, P = 8 kbar, $X(CO_2) = 0$. Numbers indicate associations: *1 – Grt + Cam + Bt + Pl, 2 - Cam + Bt + Pl*. Red dotted lines with red numbers are isopleths reflecting the composition of plagioclase (content of the anorthite component). Numbers in circles: 1 – compositional point of host garnet amphibolite, 2 –

compositional point of clinozoisite amphibolite. The arrow shows the assumed trend of metasomatic reworking.

Finally, it should be noted that the stability of associations with clinozoisite-epidote, and not with zoisite, is due to a higher fO_2 (Fig. 100): the fields of associations with zoisite are mostly located below the QFM buffer, and the fields of associations with clinozoisite-epidote are above the QFM buffer.

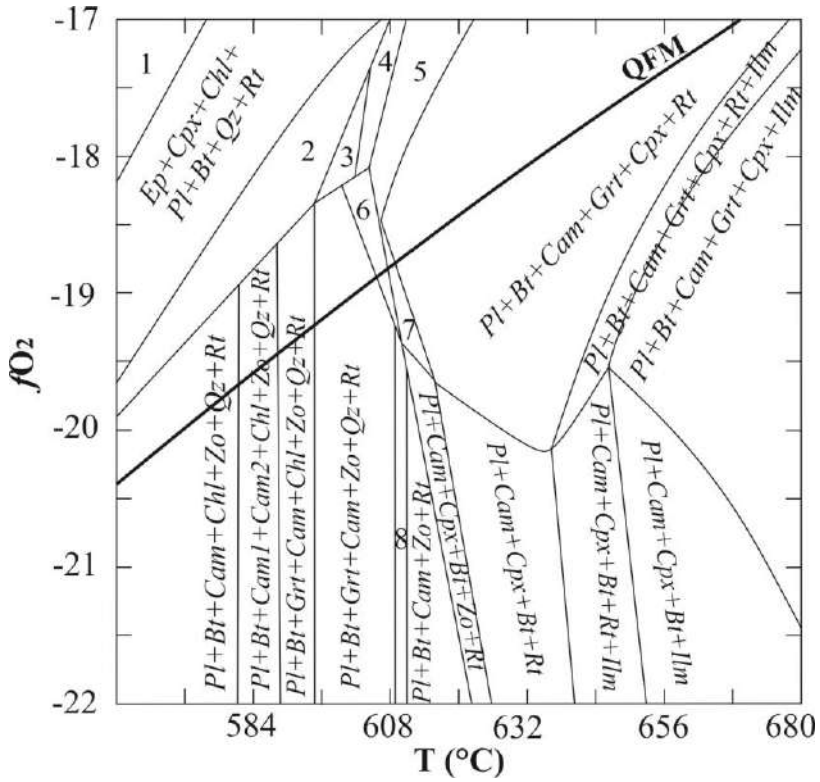

Fig. 100. T–fO_2 pseudosection for a given composition of clinozoisite amphibolites (sample Khi008d in Table 1 in Appendix 2). P = 8 kbar. Associations are marked with numbers: *1 – Chl + Cpx + Ms + Ep + Bt + Qz + Rt, 2 – Cam + Pl + Ep + Bt + Chl + Qz + Rt, 3 – Pl + Ep + Grt + Bt + Cam + Qz + Rt, 4 – Pl + Grt + Cpx + Bt + Cam + Ep + Qz + Rt, 5 – Pl + Cam + Grt + Bt + Cpx + Qz + Rt, 6 – Pl + Grt + Bt + Cam + Cpx + Zo + Qz + Rt, 7 – Pl + Cam + Grt + Cpx + Bt + Zo + Rt.*

7.4. Genesis of corundum-bearing rocks

The genesis of corundum-bearing rocks has long been discussed in the literature, but still remains debatable. To date, hypotheses and scenarios of the formation of Crn rocks in the metamorphic strata of the BMB have been proposed with varying degrees of validity.

1. Corundum-bearing rocks were formed as a result of metamorphism of aluminous sediments.

2. The rocks with corundum are metasomatites formed as a result of desilication of the gneisses of the Chupa sequence and amphibolites at the contact with gabbroid intrusions.

3. Associations with corundum were formed in the process of migmatization.

4. Corundum-bearing rocks are the result of metamorphism of hydrothermally transformed rocks (blackwall type).

5. Corundum-bearing rocks (as well as associated clinozoisite amphibolites, plagioclasites, etc.) are metasomatites that formed synchronously with regional metamorphism.

The obtained data on the structure of bodies of corundum-bearing and associated rocks, mineral compositions, isotope-geochemical characteristics of the mineral-forming medium and the results of thermodynamic modeling allow the author to make some of his own observations and conclusions about the genetic nature of these formations.

Based on field observations, corundum-bearing rocks are controlled by shear deformation zones associated with the Svecofennian stage of regional metamorphism in the Belomorian mobile belt. Often, rock bodies with corundum are located at the contact of intrusions of mafic rocks (gabbroids), but such an arrangement can be accidental, since contacts of rocks with different rheologies during deformation usually turn out to be permeable to fluids. It should be noted that the contacts of the gabbroid intrusion with the host rocks on Khitoostrov are tectonic (Babarina et al., 2017), the metamorphosed gabbro has been transformed into boudine.

The bodies of corundum-bearing rocks are characterized by a complex internal structure: a regular mineral zoning is observed in them, within which some minerals are replaced by others.

These data, together with the results of thermodynamic modeling and mineralogical and petrographic data, make it possible to reconstruct the metasomatic zoning of corundum-bearing rocks of the Khitoostrov occurrence (Table 8), separating relict minerals from the rest.

Table 8. Scheme of mineral zoning of corundum-bearing metasomatites after kyanite-garnet-biotite gneisses (Khitoostrov occurrence)

Zone	1	2	3a	3b	4
Paragenesis	*Pl + Grt + Bt + Ky*	*Pl + Grt + Bt + St*	*Pl + Grt + Bt + Crn*	*Pl + Grt + Cam + St*	*Pl + Grt + Cam + Crn*
Relic minerals	-	*Ky*	*Ky, St*	*Bt, Ky*	*St, Bt*
Reaction minerals	-	*St*	*Crn*	*Cam*	*Cam/Crn*

Mobile components	SiO_2	SiO_2, Na_2O	SiO_2, Na_2O	SiO_2, Na_2O, K_2O	SiO_2, Na_2O, K_2O

In the advanced zones, kyanite appears and quartz disappears; in the intermediate zones, staurolite appears in paragenesis with calcium amphibole. As the process continues, associations with corundum also arise, and with further development of the process, plagioclase-free associations of melanocratic corundum amphibolites, known from some manifestations that were not considered in the work, may form.

A characteristic feature of the studied rocks of both manifestations are multimineral associations, which include from three to four to seven to eight minerals (excluding ore, accessory and secondary minerals). Moreover, associations with different amounts of minerals can be difficult to combine even within a thin section. This distinguishes the studied rocks from rather homogeneous host metamorphic rocks, where the amount of minerals is relatively constant.

The main problem of the proposed concept of the metasomatic origin of corundum-bearing rocks was previously that it was problematic to separate different zones: instead of the reference metasomatic zoning, which is familiar to geologists, with a decrease in the number of minerals from the outer zones to the rear, strange mineral associations arise in the column, where the amount of minerals not only does not decrease, but even tends to increase. Such an increase in the amount of minerals was traditionally allowed only in the outer zones of metasomatites, where enrichment in the displaced inert component can occur (Glebovitsky, Bushmin, 1983).

It is known that the classical metasomatic zoning with a decrease in the number of minerals is formed under strictly defined conditions, which are not always realized in nature: the rock must be homogeneous and finely porous, uniformly impregnated with a solution, the rate of reactions of substitution of some minerals by others must be higher than the rate of solution (Korzhinsky, 1982). If all conditions are met, and the column is isothermal, then the replacement of some minerals by others occurs instantly at the boundaries of metasomatic zones (Metasomatism and metasomatic ..., 1998), as a result of which the number of phases is constant within a particular zone.

The condition of homogeneity and fine porosity of the rocks is obviously not satisfied for the kyanite-garnet-biotite gneisses of the Chupa sequence, which by the time of the Svecofennian metamorphism had already been twice metamorphosed, migmatized, and complexly deformed.

If the process was very fast or there was not enough fluid, reaction structures are observed: pseudomorphoses, rims, symplectites (Metasomatism and metasomatic ..., 1998), which are very characteristic of corundum-bearing rocks.

None of the conditions for the emergence of classical metasomatic zoning is met, which means that zoning will become more complicated: some minerals will be preserved in the following zones (relict minerals). The literature describes many cases of significant complication of the zoning of skarns, greisens, and other formations, the metasomatic nature of which is not questioned (Gramenitsky, 2012, Metasomatism and metasomatic…, 1998). Most metasomatites are formed under conditions of decreasing or increasing temperatures and pressures, which complicates their zoning to varying degrees.

In addition, reaction minerals (which are staurolite, sodic gedrite, calcium amphibole, corundum) will form in each zone. Due to the presence of reaction minerals, the number of phases in different zones of the metasomatic column can remain constant (Metasomatism and metasomatic..., 1998). And the presence of relic minerals can even lead to an increase in the number of phases from the outer zone to the inner. Which, apparently, is typical for corundum-bearing metasomatites of the Belomorian mobile belt: the number of mobile components and relict minerals increases, but there are still four minerals in the paragenesis.

In metasomatic zoning, the alumina content of rock-forming minerals increases and the content of silica in them decreases. This pattern of changes in the composition of minerals is common to all occurrences of corundum in the Belomorian mobile belt (Serebryakov, 2004). In addition, the content of calculated Fe^{3+} in calcium amphibole increases in metasomatic zoning.

Due to the alkaline nature of the process, rare and unusual minerals appear in corundum-bearing rocks: sodic gedrite (Serebryakov, 2004), aspidolite, and barroisite. Sodic gedrite occurs in some hydrothermal veins and granulites, as part of symplectites (Damman, 1988, Kanazawa et al., 2009, Tsunogae et al., 2007, Moulas et al., 2013), in coronal structures between plagioclase and olivine in dolerites (Otten, 1984), and also in alkaline metasomatites among metapelites (Dasgupta et al., 1999). Na-biotite is known in some volcanics (Spear et al., 1981, Anthony et al., 2001).

The presence of sodic gedrite, aspidolite, and Na-Ca-amphibole (barroisite) in corundum-bearing rocks is evidence that the desilication of kyanite-garnet-biotite gneisses was accompanied by an increase in alkalinity, while the replacement of biotite by calcium amphibole and aspidolite reflects an increase in Na/K in the fluid. The combination of desilication with an increase in Na/K in the fluid led to the formation of an unusual *Pl + Grt + St + Cam* paragenesis, where staurolite is in equilibrium with calcium amphibole.

Using the equilibrium of plagioclase with corundum (or kyanite), it is easy to understand how the intensity of desilication and alkaline sodic metasomatism correlate with each other:

$$2Ab = Crn + Na_2O + 6SiO_2 \qquad (14)$$

Since the composition of plagioclase in corundum-bearing rocks remains almost the same as in gneisses, it can be concluded that with a decrease in the chemical potential of SiO_2, the potential of Na_2O increased six times faster. At the same time, in the outer staurolite zone, the increase in alkalinity was somewhat weaker in relation to desilication, which led here to a slight deviation of the plagioclase composition towards a more basic one.

Based on the foregoing, we can conclude that corundum-bearing rocks were formed in the course of metasomatic reworking of host kyanite-garnet-biotite gneisses. The impact of the fluid led to the desilication of rocks with Na-alkaline metasomatism against the background of a decrease in the chemical potential of K_2O.

Note that the obtained schemes of metasomatic zoning (Tables 5, 6) do not show any similarity with the zoning of contact-metasomatic formations (plumazites and kyshtymites) (Korzhinsky, 1955, Kolesnik, 1976). And this means that, most likely, corundum-bearing rocks are not contact-metasomatic formations.

Thus, according to the author, the most likely mechanism for the formation of corundum-bearing metasomatites is metasomatism against the background of metamorphism, which coincides with the opinion of most previous researchers who have studied these same objects (Glebovitsky, Bushmin, 1983, Serebryakov, Rusinov, 2004, Terekhov, 2007, Astafiev et al., 2020, Khodorevskaya, Varlamov, 2018).

There are many examples in the literature when similar formations are formed in the course of metasomatic processes associated with metamorphism.

Rocks with *Bt+Pl+Crn+St+Rt*, *Bt+Pl+Grt+Crn+Ilm* parageneses are formed as a result of metasomatic processing of gneisses at contact with dunite bodies in ruby deposits in Greenland (van Hinsberg et al., 2021). Corundum-bearing leucosomes are formed in the migmatites of the Skattora complex in northern Norway as a result of incongruent melting of plagioclase and an increase in the alumina content of the melt during the removal of Ca, Mg, and Fe from rocks by aqueous fluid enriched in K, Rb, and Ba (Kullerud et al., 2012). Corundum and sapphirine are formed during Mg metasomatism of scapolized gabbro in the Bamble sector in Southern Norway (Engvik, Austrheim, 2010). Amphibolites with corundum, kyanite, and sapphirine are formed as a result of metasomatism of troctolites in the Central French Variscan Massif with the addition of Ca and Al, and then Mg and Si (Berger et al., 2010).

Some works postulate the mobile behavior of aluminum in the fluid that led to the formation of rocks with corundum (Kisin et al., 2020, Terekhov, Akimov, 2013, Berger et al., 2010, Yakymchuk, Szilas, 2018), including in the application to corundum-bearing rocks of the Belomorian belt (Terekhov, 2007, Khodorevskaya, Varlamov, 2018). It follows from experimental studies that the solubility of corundum increases significantly with increasing pressure (up to 10 kbar and higher) and temperature (up to 800°C) (Tropper, Manning, 2007). Aluminum is transported by acidic fluoride solutions or, conversely, by rather alkaline fluids with pH≥8 (Zaraisky, 2007). The presence of Si and Na in the fluid also contributes to an increase in the geochemical mobility of aluminum, which forms Si–Al and Na–Al complexes with them (Newton, Manning, 2008). In this case, it is traditionally assumed that aluminum, like titanium, is an inert component that tends to accumulate in the rock rather than migrate in the fluid (Korzhinsky, 1955). In this case, we are talking about the thermodynamic mobility of the components, which is not identical to the geochemical one (Kol'tsov, 2008), therefore, speaking about aluminum as an inert component, we cannot exclude the possibility that aluminum was geochemically mobile and was introduced in the process of metasomatism.

The plagioclasites of the Khitoostrov manifestation, although always closely associated with corundum-bearing rocks, are not associated with them by gradual transitions: they are marked by the abrupt disappearance of all minerals except plagioclase, and their boundaries with corundum-bearing rocks are sharp and clear. On the basis of geological and petrographic data, we can assume that plagioclasites are leukosomes desilicated during metasomatism, which were already present in the host kyanite-garnet-biotite gneisses.

Closely spatially associated with corundum-bearing rocks at the Khitoostrov occurrence, clinozoisite amphibolites differ from the host garnet amphibolites in their increased content of bases and high alumina content, low content of SiO_2 and alkalis, and their composition does not correspond to the igneous protolith.

Clinozoisite amphibolites are characterized by an unusual composition of minerals in terms of the main components against the background of host garnet amphibolites: biotites and calcium amphiboles from clinozoisite amphibolites are characterized by increased alumina content, and plagioclase in them is more basic compared to host rocks.

Reaction structures are widespread in clinozoisite amphibolites: the replacement of large garnet porphyroblasts by plagioclase-amphibole symplectites, the replacement of calcium amphibole by clinozoisite.

All these features, together with the anomalously light isotopic composition of oxygen and hydrogen in the minerals of clinozoisite amphibolites, indicate that these rocks are metasomatites, which could have been formed when the host garnet amphibolites were exposed

to a fluid similar to that that led to the formation of corundum-bearing metasomatites among the kyanite-garnet-biotite gneisses of the Chupa sequence.

Answering the question of whether the metasomatic alteration of garnet amphibolites at the Khitoostrov occurrence could have been caused by the same fluid that led to the formation of corundum-bearing metasomatites, we can conclude based on the results of thermodynamic modeling that the formation of clinozoisite amphibolites was caused by the action of a somewhat different, much less alkaline fluid, which led not to Na-alkaline metasomatism, but to an insignificant removal of Na_2O in combination with desilication.

7.5. Characteristics of the fluid involved in mineral formation

The obtained results of thermodynamic modeling, data on the distribution of REE in minerals, and data on the isotope composition of noble gases in fluid microinclusions in minerals provide us with a lot of valuable information about the composition and properties of the metasomatizing fluid.

As follows from the results of thermodynamic modeling, the fluid that affected the rocks was undersaturated in silica, contributed to the removal of K_2O from the rocks, and μNa_2O could increase or decrease at different occurrences.

In order to understand which rocks could serve as a source of such fluid, the $\mu(SiO_2)$ – $\mu(Na_2O)$ and $\mu(SiO_2)$ – $\mu(K_2O)$ diagrams (Figs. 101–102) were plotted with points of compositions of different rocks taken from the literature data (Table 9).

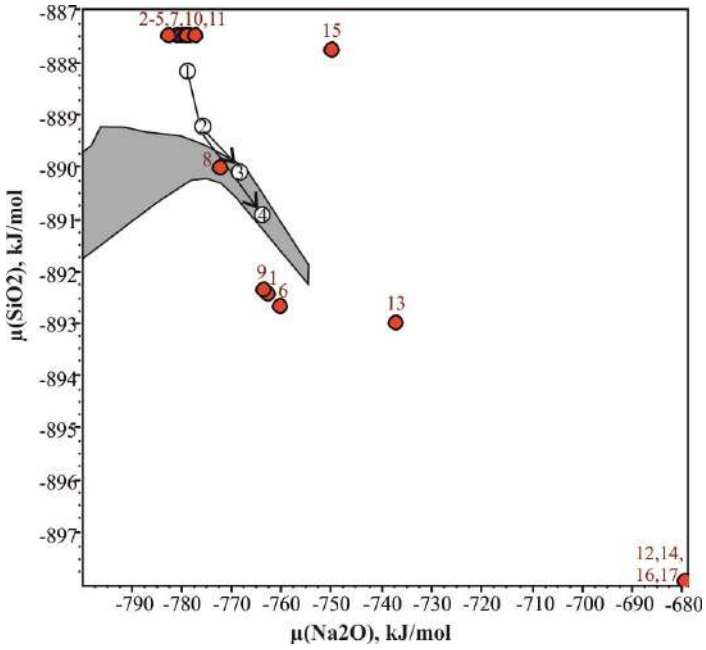

Fig. 101. Diagram $\mu(SiO_2)$ – $\mu(Na_2O)$ with plotted dots of rock composition – possible sources of metasomatizing fluid. The field of corundum-bearing rocks is shown in gray. The red circles

show the compositions of the source rocks. The corresponding numbers of compositions are in Table 9.

Based on the position of the points in the considered diagrams, the most likely source of the fluid seems to be metamorphosed ultramafic rocks, which are quite widespread in the Belomorian mobile belt (Slabunov et al., 2019). Apparently, during the Svecofennian metamorphism, a fluid was separated from these rocks, which was significantly depleted in silica and not too rich in alkalis.

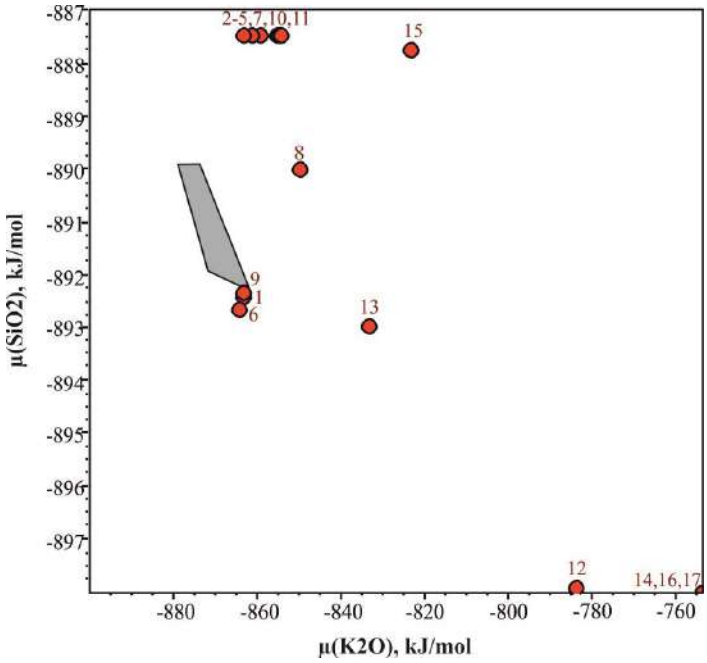

Fig. 102. Diagram $\mu(SiO_2) – \mu(K_2O)$ with plotted dots of rock composition – possible sources of metasomatizing fluid. The field of corundum-bearing rocks is shown in gray. The red circles show the compositions of the source rocks. The corresponding numbers of compositions are in Table 9.

Table 9. Coordinates of rock composition points - possible sources of metasomatizing fluid for Fig. 124, 125.

Point number	Rock type	$\mu(SiO_2)$, kJ/mol	$\mu(Na_2O)$, kJ/mol	$\mu(K_2O)$, kJ/mol
1	metaperidotites (Slabunov et al., 2019)	-892.401	-763.084	-863.481
2	"green" amphibolites (Slabunov et al., 2019)	-887.473	-781.227	-859.121
3	"brown" amphibolites (Slabunov et al., 2019)	-887.481	-780.479	-855.59

4	amphibolites (Shcherbakova, Terekhov, 2008)	-887.481	-778.622	-854.67
5	gabbroids (Stepanova et al., 2017)	-887.481	-779.563	-861.436
6	ultramafic rocks (Stepanova et al., 2017)	-892.673	-760.332	-864.551
7	metabasalts (Myskova, 2001)	-887.481	-778.955	-854.902
8	metaanorthosites (Volodichev, 1990)	-890.007	-772.535	-849.628
9	ultrabasites (Volodichev, 1990)	-892.341	-763.656	-863.251
10	Ky-eclogites, Gridino (Volodichev, 1990)	-887.481	-782.893	-863.251
11	eclogites, Gridino (Volodichev, 1990)	-887.48	-777.352	-854.02
12	ultramafic foidolites (Dubrovsky, 2018)	-897.933	-679.501	-783.779
13	alkaline gabbroids (Dubrovsky, 2018)	-892.977	-737.418	-833.079
14	basic foidolites (Dubrovsky, 2018)	-898.388	-679.913	-754.393
15	alkaline syenites (Dubrovsky, 2018)	-887.773	-750.024	-823.154
16	basic feldspathoidic syenites (Dubrovsky, 2018)	-898.388	-679.913	-754.393
17	feldspathoid syenites of the middle group (Dubrovsky, 2018)	-898.388	-679.913	-754.393

Comparison of the distribution spectra of rare earth elements in the minerals of corundum-bearing rocks, clinozoisite amphibolites, and host rocks (kyanite-garnet-biotite of the Chupa sequence and garnet amphibolites after gabbro) shows that all the main rock-forming minerals of metasomatites, in comparison with the minerals of host rocks, are enriched in LREE to varying degrees. Note also that LREE enrichment is also recorded in the outer shells of zircon grains from corundum-bearing rocks (Krylov et al., 2012). Therefore, it is difficult to relate such LREE mineral enrichment to the geochemical features of the sedimentary protolith.

This effect cannot be attributed to the difference between the PT-parameters of the formation of corundum-bearing rocks and amphibolites after gabbro, although they are quite different: changes in temperature and pressure only lead to a local redistribution of elements between minerals.

Apparently, LREE were at least partially introduced by the fluid during metasomatism and concentrated during recrystallization in all minerals. However, calcium amphibole was the main LREE concentrating mineral, in which LREE enrichment is most pronounced.

It is known that rare earth elements are conditionally inert during high-temperature metamorphism, but become mobile during infiltration metasomatism, when the fluid/rock ratios reach 102–103 (Bau, 1991), which is confirmed by experimental data (Louvel et al., 2015). Moreover, under certain conditions, even highly charged elements become mobile during metasomatism (Jiang et al., 2005). Therefore, the observed mineral enrichment of corundum-bearing rocks in LREE is evidence of the participation of significant amounts of fluid in the mineral formation – sufficient for LREE to become mobile.

Currently, many different variants of the behavior of rare earth elements during metasomatism are known: REEs can remain inert or acquire mobility; while light REEs, medium REEs and/or heavy REEs can become mobile; there may be an input, output, or local redistribution of REE (Ague, 2017 and references there). Thus, fluid processing of the rocks of the Dabi-Sulu complex (UHP–eclogites and granite gneisses), known for their anomalously isotopically light oxygen ($\delta^{18}O$ to -12‰), led to the introduction of not only LREE, but also HREE (Huang and Xiao, 2015 and references therein).

The behavior of certain rare earth elements in a fluid is affected by the composition of the fluid and the alkalinity of the medium. REE transport can be mediated by the formation of chloride, fluoride, and hydroxide complexes under acidic, neutral, and alkaline pH conditions, respectively (Haas et al., 1995). At the same time, in hydrothermal solutions, the main ligands transporting REE are chloride and sulfate, while fluoride complexes contribute to the precipitation of fluid-displaced REE (Migdisov et al., 2016).

Fractionation of REE in fluid is a complex and poorly understood process. First, REE fractionation can be carried out due to the difference in the distribution coefficients of REE between the fluid and minerals, which, in turn, is due to the crystal chemical features of the minerals. In addition, REE fractionation may occur due to differences in the stability of LREE and HREE as an aqueous chloride complex (Migdisov et al., 2016). Therefore, it is not yet possible to answer the question of which particular feature of the fluid that participated in the mineral formation led to the enrichment of the minerals of corundum-bearing rocks in LREE.

Obviously, the formation of corundum-bearing rocks was not caused by the same fluid that caused the amphibolization of gabbroids; in apogabbro garnet amphibolites, enrichment of LREE minerals is not recorded. Estimates of P-T parameters support this conclusion: the corundum-bearing rocks were formed at slightly lower temperatures and at much lower pressures than the apogabbro amphibolites, probably somewhat later than them, during the decline of

metamorphism. The fact that corun-bearing rocks were formed at lower pressures, in particular, is due to their confinement to a fluid-permeable zone of shear deformations.

The anomaly of the oxygen isotopic composition recorded in the marginal parts of the boudins of the migmatized apogabbro amphibolites is most likely the result of a weak influence of the metasomatizing fluid on the rocks, which led to the formation of corundum-bearing rocks after amphibolization.

Within the Belomorian mobile belt, LREE enrichment is also established in eclogites after amphibolites, eclogite-like rocks, and plagiomigmatites, where it is associated with the impact of alkaline fluid on the amphibolite-gneiss complex during the Svecofennian tectonic-metamorphic activation (Kozlovsky, Bychkova, 2016). Apparently, the participation of metamorphogenic fluids in the mineral formation, which determined the mobility of rare earth elements and led to the formation of various metasomatites, including corundum-bearing, is a specific feature of the Svecofennian stage of metamorphism of the rocks of the Belomorian mobile belt.

In the case of corundum-bearing rocks of the Khitoostrov occurrence, the impact of subalkaline carbon dioxide-water fluid containing Na and Ca chlorides on kyanite-garnet-biotite gneisses led to the mobilization (input) of LREE (Akimova, Skublov, 2021, Akimova, 2022). Probably, in the case of clinozoisite amphibolites, the formation of chloride complexes also contributed to the mobilization and redistribution of LREE.

The problem of the fluid source that led to the formation of corundum-bearing and associated rocks deserves special attention, in particular, in connection with the identification of an oxygen isotope anomaly in them.

The data on the behavior of noble gas isotopes in the mineral-forming fluid, and on the distribution of REE and Sr-Nd on the isotopic systematics of apatite in corundum-bearing rocks of the Khitoostrov occurrence indicate that the metasomatic fluid separated from a deep source external to the rocks. At the same time, the relationship between the data obtained and the data on the isotopic composition of oxygen in rocks is still not obvious.

Further studies and experiments will allow us to answer the question whether rocks with an unusual isotopic composition of oxygen and hydrogen were formed with the participation of a surface fluid enriched in light oxygen and hydrogen isotopes, or under endogenous conditions under the influence of thermal diffusion, kinetic effects, or some other mechanism.

Conclusions to chapter 7

1. Corundum-bearing metasomatites of the Khitoostrov occurrence were formed by desilication of kyanite-garnet-biotite gneisses during the Svecofennian stage of regional metamorphism

(lga(SiO_2) decreases from -0.06 to -0.2), which proceeded with increased Na activity (A_{Na} increased from 4.38 to 4.88) and decreased K activity (A_K decreased from 3.35 to 3.11), ΔpH = 0.51 (subalkaline metasomatism).

2. The trend towards the preservation and even increase in the number of minerals in the zoning of corundum-bearing metasomatites is explained by the non-equilibrium of mineral associations. This is, firstly, the preservation of relic minerals, and secondly, the emergence of new, reactionary minerals. The occurrence of reactive minerals in all zones leads to a constancy of the number of minerals, and the simultaneous preservation of relict minerals leads to an increase in the number of minerals.

3. The mobility of the LREE was provided by the specific composition of the fluid involved in the mineral formation. A possible source of the fluid that led to the formation of metasomatites is ultramafic rocks.

Conclusion

Summing up the geological, petrographic, petrological, geochemical and isotope-geochemical data, we can draw the following conclusions:

1. The corundum-bearing rocks of the Khitoostrov occurrence are an integral part of a complex zonal body confined to the kyanite-garnet-biotite gneisses of the Chupa sequence. On the northwestern flank of this body, rocks with parageneses *Pl + Grt + Bt + Ky, Pl + Grt + Bt + Crn* (zones 1, 3a) are common; on the southeastern flank, rocks with parageneses *Pl + Grt + Bt + St, Pl + Grt + St + Cam* (zones 2, 3b); in the central part of the body, rocks with the *Pl + Grt + Cam + Crn* paragenesis (zone 4).

2. The zoning of the body of corundum-bearing rocks is due to the regular change of parageneses: at first, quartz disappears in kyanite-garnet-biotite gneisses and kyanite crystals become coarser; then staurolite appears, developing as plagioclase-staurolite symplectites around kyanite, then corundum appears, first as corundum-plagioclase symplectites, and then as large porphyroblasts; biotite is replaced by calcium amphibole, and staurolite is replaced by sodic gedrite-corundum-plagioclase symplectites.

3. In the corundum-bearing rocks of the Khitoostrov occurrence, in association with corundum pyrope-almandine garnet, plagioclase №26–39, phlogopite and aspidolite, Ca-amphiboles of the tschermakite-sadanagaite series, Na-Ca-amphibole (barroisite) and Mg-Fe orthorhombic amphibole – sodic gedrite, magnesian staurolite, paragonite, muscovite, ilmenite, rutile were found.

4. In association with corundum-bearing rocks, there are plagioclasites and clinozoisite amphibolites. The latter are also associated with the host rocks (garnet amphibolites) by a gradual transition: quartz disappears in garnet amphibolites, then amphibole-plagioclase symplectites after garnet, clinozoisite-plagioclase symplectites are formed, then calcium amphibole is replaced by clinozoisite. The clinozoisite amphibolites contain ferruginous phlogopite containing more Al than the ferruginous phlogopite from the host garnet amphibolites; calcium amphibole of the tschermakite-pargasite-sadanagaite series; garnet, clinozoisite, epidote, titanite; basic plagioclase, which is absent in the host rocks, and margarite appear.

5. Minerals of corundum-bearing rocks (garnet, calcium amphibole, apatite) and associated clinozoisite amphibolites are enriched to varying degrees in LREE against the background of host rocks – garnet amphibolites after gabbro, as well as kyanite-garnet-biotite gneisses of the Chupa sequence (Skublov, 2005). It should be noted that, in total, corundum-bearing rocks and

clinozoisite amphibolites contain a higher LREE content than kyanite-garnet-biotite gneisses of the Chupa sequence (Myskova et al., 2000; Terekhov, 2007) and garnet amphibolites, respectively. In clinozoisite metasomatites associated with corundum ones, the effect of inheritance of the REE distribution was established when garnet was replaced by Ca-amphibole and clinozoisite. The mobility of the LREE was provided by the specific composition of the fluid involved in the mineral formation.

6. Data on the study of fluid inclusions indicate that the corundum-bearing rocks were formed with the participation of carbon dioxide-water fluid. At the same time, the minerals of corundum-bearing and host rocks were found to contain water-salt inclusions similar in salt composition containing NaCl and $CaCl_2$. Apparently, such inclusions are also characteristic of other rocks of the Belomorian mobile belt; additional studies are needed to resolve this issue. The similarity of the salt composition of fluid inclusions in corundum-bearing and host rocks indicates that these rocks were formed in a single process (the Svecofennian stage of regional metamorphism). The fact that fluid inclusions in the minerals of corundum-bearing rocks are characterized by a somewhat higher total salinity indicates that a fluid (a solution of Ca and Na chlorides) could be in equilibrium with the minerals of corundum-bearing metasomatites, which differed in composition from the pore fluid of the host gneisses of the Chupa sequence and garnet amphibolites – characterized by a higher concentration of salts, in particular, $CaCl_2$.

7. The data on the isotopic composition of noble gases and the Sr-Nd isotopic systematics of apatite in corundum-bearing rocks of the Khitoostrov occurrence allow us to conclude that the source of the fluid that led to the formation of corundum-bearing rocks was a deep source. This is supported by increased ^{3}He contents in the component of fluid inclusions of corundum-bearing rocks released as a result of crushing, as well as reduced $^{87}Sr/^{86}Sr$ values close to the lower crustal values of εNd, as well as increased Sr and REE contents in apatite from corundum-bearing rocks.

8. The corundum-bearing rocks of the Khitoostrov occurrence are metasomatites that were formed by desilication of kyanite-garnet-biotite gneisses during the Svecofennian stage of regional metamorphism ($lga(SiO_2)$ decreases from -0.06 to -0.2), which proceeded with increased Na activity (A_{Na} increases from 4.38 to 4.88) and decreased K activity (A_K decreases from 3.35 to 3.11), $\Delta pH = 0.51$ (subalkaline metasomatism). The trend towards the preservation and even increase in the number of minerals in the zoning of corundum-bearing metasomatites is explained by the non-equilibrium of mineral associations. This is, firstly, the preservation of relic minerals, and secondly, the emergence of new, reactionary minerals. The occurrence of reactive minerals in all zones leads to a constancy of the number of minerals, and the simultaneous preservation of relict minerals leads to an increase in the number of minerals.

Bibliography

1. Ague J.J. (2017) Element mobility during regional metamorphism in crustal and subduction zone environments with a focus on the rare earth elements (REE). American Mineralogist. V. 102. P. 1796–1821.

2. Akimova E.Yu., Kozlov E.N., Lokhov K.I. (2017) Origin of corundum rocks of the Belomorian mobile belt: Evidence from noble gas isotope geochemistry. Geochemistry International. V. 55. № 11. P. 1000–1009.

3. Akimova E.Yu., Azimov P.Ya., Serebryakov N.S. (2019) Rare and unusual minerals of corundum-bearing rocks of Khitoostrov (Northern Karelia). Proceedings of the Kola Scientific Center of the Russian Academy of Sciences. № 6 (10). P. 9–15.

4. Akimova E.Yu., Skublov S.G. (2021) Distribution of rare earth elements in rock-forming minerals of corundum-bearing rocks of the Khitoostrov deposit (Northern Karelia). Bulletin of St. Petersburg State University. Earth Sciences. V. 66. № 4. P. 686–705.

5. Akimova E.Yu., Kol'tsov A.B. (2022) Thermodynamic modeling of the formation of corundum-bearing metasomatic rocks in the Belomorian mobile belt, Fennoscandian shield. Petrology. V. 30. № 1. P. 60–81.

6. Akimova E.Yu., Skublov S.G. (2023) Mineralogy of clinozoisite amphibolites in the Khitoostrov occurrence of corundum-bearing rocks (Fenno-Scandinavian shield). Zapiski RMO. V. CLII. № 3. P. 59–81.

7. Altherr R., Okrusch M., Bank H. (1982) Corundum- and kyanite-bearing anatexites from the Precambrian of Tanzania. Lithos. V. 15. P. 191–197.

8. Anthony J.W., Bideaux R.A., Bladh K.W., Nichols M.C. Handbook of Mineralogy / Chantilly, VA (USA): Mineralogical Society of America, 2001. – URL: http://www.handbookofmineralogy.org

9. Adlakha E., Hanley J.J., Falck H., Boucher B. (2018) The origin of mineralizing hydrothermal fluids recorded in apatite chemistry at the Cantung W-Cu skarn deposit, NWT, Canada. Eur. J. Mineral. V. 30. P. 1095–1113.

10. Aranovich L.Y., Newton R.C. (1999) Experimental determination of CO2–H2O activity–composition relations at 600–1000 °C and 6–14 kbar by reversed decarbonation and dehydration reactions. Am Mineral. V. 84. P. 1319–1332.

11. Armbruster T. H., Bonazzi P., Akasaka M. et al. (2006) Recommended nomenclature of epidote-group minerals. Eur. J. Miner. V. 18. P. 551–567.

12. Astafiev B.Yu., Voinova O.A. (2020) Klimovsky metasomatic complex of the Belomorian mobile belt: composition, age, geological position. Geotectonics. № 1. P. 23–40.

13. Awalt M.B., Whitney D.L. (2018) Petrogenesis of kyanite- and corundum-bearing mafic granulite in a meta-ophiolite, SE Turkey. J Metamorph Geol. V. 36. P. 881–904.

14. Babarina I.I., Stepanova A.V., Azimov P.Ya., Serebryakov N.S. (2017) Heterogeneity of basement reworking in the Paleoproterozoic Lapland-Kola collisional orogen, Belomorian province of the Fennoscandian Shield. Geotectonics. № 5. P. 3–19.

15. Bakker R.J. (2018) AqSo_NaCl: Computer program to calculate p-T-V-x properties in the H2O-NaCl fluid system applied to fluid inclusion research and pore fluid calculation. Computers & Geosciences. V. 115. 122–13.

16. Baksheev I.A., Ustinov V.I., Dolgova O.S., Balitsky V.S., Ekimenkova I.A. (2006) The isotopic composition of oxygen is an indicator of the genesis of corundum. Bulletin of the Earth Sciences Branch of the Russian Academy of Sciences. V. 1(24).

17. Balagansky V. V., Bogdanova M. N., Kozlova N. E. Structural-metamorphic evolution of the North-Western White Sea. Apatity, 1986. 100 p.

18. Baldwin J. A., Powell R., White R. W., Stípská P. (2015) Using calculated chemical potential relationships to account for replacement of kyanite by symplectite in high pressure granulites: An example from the Snowbird tectonic zone, Canada. Journal of Metamorphic Geology. V. 33. P. 311–330.

19. Ballentine C.J., Burnard P. (2002) Production, Release and Transport of Noble Gases in the Continental Crust. Reviews in Mineralogy and Geochemistry. V. 47. P. 481–538.

20. Baolei M., Jian S., Guanyu W., Guohan Y, Yongfu A. (1997) A skarn-type lead-zinc deposit related to low ^{18}O magma. Chinese Science Bulletin V. 42. № 19. 1997. P. 1636–1640.

21. Bau M. (1991). Rare-earth element mobility during hydrothermal and metamorphic fluid-rock interaction and the significance of the oxidation state of europium. Chemical Geology. V. 93. P. 219–230.

22. Beach A. (1973) The mineralogy of high-temperature shear zones at Scourie, NW Scotland. Journal of Petrology. V. 14. 231–48.

23. Belousova E. A., Griffin W. L., O'Reilly S. Y., Fisher N. I. (2002) Apatite as an indicator mineral for mineral exploration: trace-element compositions and their relationship to host rock type. J. Geochem. Explor. V. 76. P. 45–69.

24. Berger J., Femenias O., Ohnenstetter D., Plissart G., Mercier J.C.C. (2010) Origin and tectonic significance of corundum–kyanite–sapphirine amphibolites from the Variscan French Massif Central. Journal of Metamorphic Geology. V. 28 (3). P. 341–360.

25. Bibikova E.V., Sheld T., Bogdanova S.V., Drugova G.M., Lobach-Zhuchenko S.B. (1993) Geochronology of Belomorids: interpretation of multi-stage geological history. Geochemistry. № 10. P. 1393–1411.

26. Bibikova E. V., Skiold T., Bogdanova S. V. (1996) Age and geodynamic aspects of the oldest rocks in the Precambrian Belmorian Belt of the Baltic (Fennoscandian) Sheild. *From* Brewer, T. S. (ed.), Precambrian Crustal Evolution in the North Atlantic Region, Geological Society Special Publication. V. 112. P. 69–90.

27. Bibikova E.V., Borisova E.Yu., Drugova G.M., Makarov V.A. (1997) Metamorphic history and age of aluminous gneisses of the Belomorian belt of the Baltic Shield. Geochemistry International. № 9. P. 883–893.

28. Bibikova E.V., Claesson S., Glebovitsky V.A., Sedova I.S., Ruchyev A.M. (2001) Isotope dating of the Belomorian belt of the Baltic Shield. Geochemistry. № 10. P. 1023–1026.

29. Bibikova E.V., Bogdanova S.V., Glebovitsky V.A., Klaisson S., Sheld T. (2004) Evolutionary stages of the Belomorian mobile belt according to U-Pb zircon geochronology (Nordsim ion microprobe), Petrology. V. 12. № 3. P. 227–244.

30. Bindeman, I.N., Schmitt, A.K., Evans, D.A.D. (2010) Origin of the lowest-known $\delta^{18}O$ silicate rock on Earth in Paleoproterozoic Karelian rift: Geology. V. 38. P. 631–634.

31. Bindeman I.N., Serebryakov N.S. (2011) Geology, Petrology and O and H isotope geochemistry of remarkably ^{18}O depleted Paleoproterozoic rocks of the Belomorian Belt, Karelia, Russia, attributed to global glaciation 2.4 Ga. Earth and Planetary Science Letters, V. 306. P. 163–174.

32. Bindeman I.N., Lundstrom C.C., Bopp C., Huang F. (2013) Stable isotope fractionation by thermal diffusion through partially molten wet and dry silicate rocks. Earth and Planetary Science Letters. V. 365. P. 51–62.

33. Bindeman I.N., Serebryakov N.S., Schmitt A.K., Vazquez J.A., Guan Y., Azimov P.Ya., Astafiev B.Yu., Palandri J., Dobrzhinetskaya L. (2014) Field and microanalytical isotopic investigation of ultradepleted in ^{18}O Paleoproterozoic “Slushball Earth” rocks from Karelia, Russia. Geosphere. V. 10. P. 308–339.

34. Bogdanova S. V., Bibikova E. V. (1993) The 'Saamian' of the Belomorian Mobile Belt: new geochronological constraints. Precambrian Research. V. 64. P. 131–152.

35. Borisenko A.S. (1977) Study of the salt composition of solutions of gas-liquid inclusions in minerals by cryometry. Geology and Geophysics. № 8. P. 16–27.

36. Bruand E., Fowler M., Storey C., Darling J. (2017) Apatite trace element and isotope applications to petrogenesis and provenance. Am. Mineral. V. 102. P. 75–84.

37. Bucher K., De Capitani C., Grapes R. (2005) The development of a margarite-corundum blackwall by metasomatic alteration of a slice of mica schist in ultramafic rock, Kvesjöen, Norwegian Caledonides. Can Mineral. V. 43. P. 129–156.

38. Budnitsky S.Yu. New potassium-argon geochronology of rare and unique geological and archaeological objects. Abstract of thesis ....cand. geol-min. sciences, Vladivostok. 2013. 22 p.

39. Buikin, A.I., Kamaleeva A.I., Sorokhtina N.V. (2018) On the issue of the efficiency of separation of trapped and formed in situ components of noble gases during the crushing of samples in vacuum. Geochemistry International. № 6. P. 586–593.

40. Bukanov V.V., Lipovsky Yu.O. New finds of noble corundum in the eastern part of the Baltic Shield. Samotsvety. L.: 1980. P. 110–115.

41. Bulakh A. G., Zolotarev A. A., Krivovichev V. G. Structure, isomorphism, formulas, classification of minerals. St. Petersburg: St. Petersburg University Publishing House. 2014. 133 p.

42. Burtseva M.V., Ripp G.S., Posokhov V.F., Murzintseva A.E. (2015) Nephrites of Eastern Siberia: geochemical features and problems of genesis. Geology and Geophysics. V. 56. № 3. P. 516–527.

43. Busheva N.L. (1983) Genetic features of the corundum deposit in North Karelia. Izvestiya vuzov. Geology and exploration. Moscow. P. 90.

44. Bushmin S.A. (1987) Mineral facies of metasomatites associated with regional metamorphism. Zap. Vseross. mineral. society. № 5. P. 585–601.

45. Bushmin S.A., Glebovitsky V.A. (2016) Scheme of mineral facies of metamorphic rocks and its application to the Fennoscandian shield with representative sites of orogenic gold mineralization. Transactions of KarRC RAS. V. 2. P. 3–27.

46. Cao M., Li G., Qin K., Seitmuratova E.Y., Liu Y. (2011) Major and trace element characteristics of apatites in granitoids from central Kazakhstan: implications for petrogenesis and mineralization. Resour. Geol. V. 62. P. 63–83.

47. Chowdhury P., Talukdar M., Sengupta P. et al. (2013) Controls of P–T path and element mobility on the formation of corundum pseudomorphs in Paleoproterozoic high-pressure anorthosite from Sittampundi, Tamil Nadu, India. Am Mineral. V. 98. P. 1725–1737.

48. Connolly J.A.D. (2005) Computation of phase equilibria by linear programming: A tool for geodynamic modeling and its application to subduction zone decarbonation. Earth and Planetary Science Letters. V. 236. P. 524–541.

49. Daly J. S., Balagansky V. V., Timmerman M. J., Whitehouse M. J. (2006) The Lapland-Kola Orogen: Paleoproterozoic collision and accretion of the northern Fennoscandian

lithosphere. European Lithosphere Dynamics. Eds.: Gee D. G. and Stephenson R. A. Geological Society of London, Memoir. V. 32. P. 579–598.

50. Damman A. (1988) Hydrothermal subsilicic sodium gedrite from the Gåsborn area, West Bergslagen, central Sweden. Min. Mag. V. 52. P. 193–200.

51. Dasgupta S., Sengupta P., Sengupta P., Ehl J., Raith M. (1999) Petrology of gedrite-bearing rocks in mid-crustal ductile shear zones from the Eastern Ghats Belt, India. Journal of Metamorphic Geology. V. 17 (6). P. 765–778.

52. Dokukina K.A., Konilov A.N., Van K.V., Mints M.V. Dumortierite- and corundum-bearing quartz-feldspar-mica pegmatoid rocks of the Belomorian eclogite province: an example of phengite+quartz melting. Reports of the Academy of Sciences. 2017. V. 477. № 3. P. 377–341.

53. Drake M. (1975) The oxidation state of europium as an indicator of oxygen fugacity. Geochim. Cosmochim. Acta. V. 39. P. 55–64.

54. Drugova G.M. (1996) Peculiarities of Early Precambrian metamorphism in the Belomorian fold belt (Baltic Shield). Zapiski of the Russian Mineralogical Society. № 2. P. 24–37.

55. Drugova G.M. (1999) The main stages of the evolution of the Chupinskaya strata of the Belomorian folded belt. Zapiski of the Russian Mineralogical Society. № 3. P. 49–57.

56. Dubinina E.O., Perchuk A.L., Korepanova O.S. (2012) Oxygen isotopic effects during dehydration of glaucophane shale: experimental data at P-T parameters of the subduction zone. Reports of the Academy of Sciences. V. 444. № 5. P. 1–5

57. Dubrovsky, M. I. Systematics and petrogenesis of magmatic undersaturated SiO_2 and Al_2O_3 ("alkaline") rocks. Geological Institute of the Kola Scientific Center of the Russian Academy of Sciences. Apatity: KSC RAN. 2016. 456 p.

58. Dufour M.S., Koltsov A.B., Zolotarev A.A., Kuznetsov A.B. (2007) Corundum-bearing metasomatites of the Central Pamirs. Petrology. V. 15. № 2. P. 1–18.

59. Dutrow B.L., Henry D.J., Sun Z. (2019) Origin Of Corundum–Tourmaline–Phlogopite Rocks From Badakhshan, Northeastern Afghanistan: A New Type Of Metasomatism Associated With Sapphire Formation. European Journal of Mineralogy. V. 31(4). P. 739–753.

60. Early Precambrian of the Baltic Shield. Ed. Glebovitsky V.A. St. Petersburg: Nauka, 2005. 711 p.

61. Engvik A.K., Austrheim H (2010) Formation of sapphirine and corundum in scapolitised and Mg-metasomatised gabbro. Terra Nova 22. P. 166–171.

62. Facies of metamorphism in the eastern part of the Baltic Shield / Ed. V.A. Glebovitsky. L.: Nauka, 1990. 144 p.

63. Farley K.A., Libarkin J., Mukhopadhyay S., Amidon W. (2006) Cosmogenic and nucleogenic ^{3}He in apatite, titanite, and zircon. Earth Planet. Sci. Lett. V. 248. P. 451–461.

64. Farley K.A. (2018) Helium diffusion parameters of hematite from a single-diffusion-domain crystal. Geochim. Cosmochim. Acta. V. 231. P. 117–129.

65. Faure G. Principles of isotope geology. M.: Mir, 1989. 590 p.

66. Fed'kin V.V. Staurolite. M.: Nauka, 1975. 272 p.

67. Fernando G.W.A.R., Dharmapriya, P.L., Baumgartner, L.P. (2017) Silica-undersaturated reaction zones at a crust-mantle interface in the Highland Complex, Sri Lanka: mass transfer and melt infiltration during high-temperature metasomatism. Lithos. V. 284-285. P. 237–256.

68. Filina M.I., Sorokina E.S., Botcharnikov R. et al. (2019) Corundum Anorthosites-Kyshtymites from the South Urals, Russia: A Combined Mineralogical, Geochemical, and U-Pb Zircon Geochronological Study. Minerals. V. 9. 234.

69. Földvári M. Handbook of thermogravimetric system of minerals and its use in geological practice. Budapest: Geol. inst. of Hungary. 2011. 180 p.

70. Frezzotti M.L., Tecce F., Casagli A. (2012) Raman spectroscopy for fluid inclusion analysis. Journal of Geochemical Exploration. V. 112. P. 1–20.

71. Fu B., Kita N. T., Wilde S. A., Liu X., Cliff J., Greig A. (2013) Origin of the Tongbai-Dabie-Sulu Neoproterozoic low-δ^{18}O igneous province, east-central China. Contributions to Mineralogy and Petrology. V. 165(4). P. 641–662.

72. Geology and pegmatite content of Belomorides / ed. K.O. Kratz. L.: Nauka, 1985. 251 p.

73. Giuliani G. Groat L.A., Fallick A.E. et al. (2020) Ruby Deposits: A review and geological classification. Minerals. V. 10. 597.

74. Glebovitsky V.A., Bushmin S.A. Post-migmatite metasomatism. L.: Nauka, 1983. 216 p.

75. Glebovitsky V.A., Miller Yu.V., Drugova G.M., Milkevich R.I., Vrevsky A.B. (1996) Structure and metamorphism of the Belomorian-Lapland collision zone. Geotectonics. № 1. P. 63–75.

76. Glebovitsky V.A., Sedova I.S. (2005) Specificity of the Late Paleoproterozoic ultrametamorphism in the Belomorian allochthon. Reports of the Academy of Sciences. V. 401. № 1. P. 1–5.

77. Glebovitsky V.A., Sedova I.S., Larionov A.N., Berezhnaya N.G. (2017) Isotopic periodization of igneous and metamorphic events at the turn of the Archean and Paleoproterozoic in the Belomorian belt, Fennoscandian Shield. Reports of the Academy of Sciences. V. 476. № 4. P. 435–439.

78. Goncalves P., Oliot E., Marquer D., Connolly J.A.D. (2012) Role of chemical processes on shear zone formation: an example from the Grimsel metagranodiorite (Aar massif, Central Alps). J. Metamorph. Geol. V. 30. P. 703–722.

79. Gorokhov I.M., Kuznetsov A.B., Melezhik V.A. (1998) Strontium isotopic composition in the Upper Yatulian dolomites of the Tulomozero Formation, Southeast Karelia. Reports of the Academy of Sciences. V. 360. № 4. P. 533–536.

80. Gorokhov I.M., Kuznetsov A.B., Ovchinnikova G.V. (2016) Pb, Sr, O, and C isotopic composition in metacarbonate rocks of the Derba Formation (Eastern Sayan): chemostratigraphic and geochronological significance. Stratigraphy. Geol. correlation. V. 24. № 1. P. 1–20.

81. Gramenitsky E.N. Petrology of Metasomatic Rocks: Textbook. M.: INFRA-M, 2012. 221 p.

82. Grodnitsky L.L. Granite pegmatites of the Baltic Shield. L.: Nauka, 1982. 295 p.

83. Grodnitsky L.L., Sibelev O.S. (1995) Late Svecofennian stage of regional metamorphism, matasomatosis, pegmatite and ore formation on the territory of Karelia and the southwestern part of the Kola Peninsula. Notes of the Russian Mineralogical Society. V. 124 (3). P. 26–32.

84. Gromov A.V. (1993) Pink corundum from the Khitostrovsky occurrence in North Karelia. World of Stones. № 2. P. 24.

85. Haapala I., Siivola J., Ojanpera P., Yletyienen V. (1971) Red corundum, sapphirine and kornerupine from Kittila, Finnish Lapland. Bull. Geol. Soc. Finland. V. 43. P. 221–231.

86. Haas, J., Shock, E.L., Sassani, D. (1995) Rare earth elements in hydrothermal systems: estimates of standard partial molal thermodynamic properties of aqueous complexes of the rare earth elements at high pressures and temperatures, Geochimica et Cosmochimica Acta. V. 59. P. 4329–4350.

87. Harlov D.E. (2015) Apatite: a fingerprint for metasomatic processes. Elements. V. 11 (3). P. 171–176.

88. Harrison D., Burnard P., Trieloff M., Turner G. (2003) Resolving atmospheric contaminants in mantle noble gas analyses. Geochem. Geophys. Geosyst. V. 4(3). P. 1–17.

89. Hawthorne F.C., Oberti R., Harlow G.E., Martin R.F., Schumacher J.C., Welch M.D. (2012) Nomenclature of the amphibole supergroup. American Mineralogist. V. 97. № 11–12. P. 2031–2048.

90. Henrichs I.A., O'Sullivan G.J., Chew D.M., Mark C., Babechuk M.G., McKenna C., Emo R. (2018) The trace element and U-Pb systematics of metamorphic apatite. Chem. Geol. V. 483. P. 218–238.

91. Henrichs I.A., Chew D.M., Sullivan G.J.O. et al. (2019) Trace element (Mn-Sr-Y-Th-REE) and U-Pb isotope systematics of metapelitic apatite during progressive greenschist- to amphibolite-facies Barrovian metamorphism. Geochem. Geophys. Geosyst. V. 20 (8). P. 4103–4129.

92. Herwartz D., Pack A., Krylov D., Xiao Y., Muehlenbachs K., Sengupta S., Di Rocco T. (2015) Revealing the climate of snowball Earth from $\delta^{17}O$ systematics of hydrothermal rocks. Proceedings of the National Academy of Sciences of the United States of America (PNAS). V. 112. № 17. P. 5337–5341.

93. Hoefs J. Stable Isotope Geochemistry. 8-th ed., Berlin, Springer. 2018. 389 p.

94. Holland T.J.B., Powell R. (1991) A Compensated-Redlich-Kwong (CORK) equation for volumes and fugacities of CO_2 and H_2O in the range 1 bar to 50 kbar and 100–1600°C. Contrib. Mineral. Petrol. V. 109. P. 265–273.

95. Holland T.J.B., Powell R. (1998) An internally-consistent thermodynamic dataset for phases of petrological interest. Journal of Metamorphic Geology. V. 16. P. 309–344.

96. Holland T.J.B., Powell R. (2011) An improved and extended internally consistent thermodynamic dataset for phases of petrological interest, involving a new equation of state for solids. J. Metamorphic Geol., V. 29. № 3. P. 333–383

97. Huang J., Xiao Y. (2015) Element mobility in mafic and felsic ultrahigh-pressure metamorphic rocks from the Dabie UHP Orogen, China: insights into supercritical liquids in continental subduction zones. International Geology Review. V. 57. P. 1103–1129.

98. Izbrodin I.A., Ripp G.S., Doroshkevich A.G., Posokhov V.F. (2014) Isotopic composition of oxygen and hydrogen in metamorphosed high-alumina rocks of southwestern Transbaikalia. Reports of the Academy of Sciences. V. 459. № 3. P. 352–356.

99. Jiang S. Y., Wang R. C., Xu X. S. et al. (2005) Mobility of high field strength elements (HFSE) in magmatic-, metamorphic- and submarine-hydrothermal systems. Physics and Chemistry of the Earth. V. 30. P. 1020–1029.

100. Kanazawa T., Tsunogae T., Sato K., Santosh M. (2009) The stability and origin of sodicgedrite in ultrahigh-temperature Mg-Al granulites: a case study from the Gondwana suture in southern India. Contributions to Mineralogy and Petrology. V 157. № 1. P. 95–110.

101. Karmakar S., Mukherjee S., Sanyal S., Sengupta P. (2017) Origin of peraluminous minerals (corundum, spinel, and sapphirine) in a highly calcic anorthosite from the Sittampundi Layered Complex, Tamil Nadu, India. Contrib Mineral Petrol. V. 172. 67.

102. Karmakar S., Mukherjee S., Dutta U. (2020) Origin of corundum within anorthite megacrysts from anorthositic amphibolites, Granulite Terrane, Southern India. American Mineralogist. V 105. P. 1161–1174.

103. Keulen N., Schumacher J.C., Næraa T., Kokfelt T.F., Scherstén A., Szilas K., Van Hinsberg V.J., Schlatter D.M., Windley B.F. (2014) Meso- and Neoarchaean geological history of the Bjørnesund and Ravns Storø Supracrustal Belts, southern West Greenland: Settings for gold enrichment and corundum formation. Precambrian Research. V. 254. P. 36–58.

104. Keulen N., Thomsen T. B., Schumacher J.C. et al. (2020) Formation, origin and geographic typing of corundum (ruby and pink sapphire) from the Fiskenæsset complex, Greenland. Lithos. V. 366–367. 105536.

105. Khodorevskaya L.I., Varlamov D.A. (2018) High-temperature metasomatism in the Kiyostrovsky mafic-ultramafic layered massif of the Belomorian belt. Geochemistry International. № 6. P. 541–558.

106. Kievlenko E.Ya., Chuprov V.I., Dramsheva E.E. Decorative collection minerals. M.: Nedra, 1987. 223 p. (P. 179–180).

107. Kissin A.Yu., Murzin V.V., Tomilina A.V., Smirnov V.N., Pritchin M.E. (2020) Ruby mineralization in the Murzinsko-Aduisky metamorphic complex (Middle Urals). Geology of ore deposits. V. 62. № 4. P. 369–388.

108. Kolesnik Yu.N. High-temperature metasomatism in ultrabasic massifs. Novosibirsk: Nauka, 1976. 239 p.

109. Kolodyazhny S.Yu. Structural-kinematic evolution of the southeastern part of the Baltic Shield in the Paleoproterozoic. M.: GEOS. 2006. 332 p.

110. Kolodyazhny S.Yu. Structural and kinematic features of the evolution of the central part of the Belomoran-Lapland belt in the Paleoproterozoic. Geotectonics. 2007. № 3. P. 46–68.

111. Kol’tsov A.B. (2008) Mass transfer and replacement of minerals during infiltration metasomatism, Geochem. № 8. P. 836–849.

112. Kol’tsov A.B. (2015) Influence of sources and evolution paths of solutions on the composition of metasomatites. Geochemistry International. № 2. P. 144–161.

113. Korzhinsky D.S. Essay on metasomatic processes. On Sat. "Main problems in the study of magmatogenic ore deposits" M.: AN SSSR, 1955. P. 335–457.

114. Korzhinsky D.S. Theoretical foundations for the analysis of mineral paragenesis. M.: Nauka, 1973. 288 p.

115. Korzhinsky D.S. The theory of metasomatic zoning. M.: Nauka, 1982. 104 p.

116. Korikovsky S.P. Facies of metapelite metamorphism. M.: Nauka, 1979. 263 p.

117. Korpechkov D.I. (2009) Klimovskoe corundum occurrence, North Karelia: some petrographic features. Materials of XX Ros. conf. young scientists dedicated to memory of Corresponding Member USSR Academy of Sciences K.O. Kratz. Petrozavodsk: Karelian Scientific Center of the Russian Academy of Sciences. P. 94–97.

118. Kozlovsky V.M., Bychkova Ya.V. (2016) Geochemical evolution of amphibolites and gneisses of the Belomorian mobile belt during Paleoproterozoic metamorphism. Geochemistry International. № 6. P. 543–557.

119. Kozlovsky V.M., Travin V.V., Korpechkov D.I., Zaitseva M.N., Kurdyukov E.B., Travin A.V. Terentyeva L.B., Savatenkov V.M. (2016) Geological structure, age and P-T-conditions for the formation of gentle shearing zones of the Belomorian mobile belt. Geotectonics. № 6. P. 52–74.

120. Kozlovsky V.M., Travin V.V., Travin A.V., Savatenkov V.M. (2018) The first data on the age and PT-conditions for the formation of flat gneiss zones in the Belomorian mobile belt. Reports of the Academy of Sciences. V. 480. № 2. P. 204–209.

121. Kozlovsky V.M., Travin V.V., Savatenkov V.M. (2020) Thermobarometry of Paleoproterozoic metamorphic events in the central part of the Belomorian mobile belt, North Karelia. Petrology. V. 28. № 2. P. 184–209.

122. Krupenin M.T., Kuznetsov A.B., Chervyakovskaya M.V., Gulyaeva T.Ya., Konstantinova G.V. (2021) Source of ore-bearing fluids and Sm-Nd age of siderites of the largest Bakal deposit, Southern Urals. Geology of ore deposits. V. 63. № 4. P. 336–353.

123. Krylov D.P., Glebovitsky V.A. (2007) Oxygen isotopic composition and fluid nature during the formation of high-alumina corundum-bearing rocks of Dyadina Gora (Northern Karelia). Reports of the Academy of Sciences. V. 412. № 5. P. 679–681.

124. Krylov D.P. (2008) Anomalous ratios $^{18}O/^{16}O$ in corundum-bearing rocks of Khitoostrov (Northern Karelia). Reports of the Academy of Sciences. V. 419. № 4. P. 533–536.

125. Krylov D.P., Salnikova E.B., Fedoseenko A.M., Yakovleva S.Z., Plotkina Yu.V., Anisimova I.V. (2011) Age and origin of corundum-bearing rocks of Khitoostrov Island, North Karelia. Petrology. V. 19. № 1. P. 80–88.

126. Krylov D.P., Glebovitsky V.A., Skublov S.G., Tolmacheva E.V. (2012) Rare-earth and trace elements in zircons of different ages from corundum-bearing rocks of Khitoostrov (Northern Karelia). Reports of the Academy of Sciences. V. 443. № 3. P. 352–357.

127. Krylov D.P., Glebovitsky V.A. (2017) Local distribution of oxygen isotopes and fluid exchange during the formation of corundum-bearing rocks of Khitoostrov. Reports of the Academy of Sciences. V. 473. № 5. P. 593–595.

128. Kulikov V.S., Kulikova V.V. (1990) On geology of the Kiyostrovsky archipelago of the White Sea. Oper-inform. materials for 1989. Petrozavodsk. P. 3–6.

129. Kullerud K, Nasipuri P, Ravna EJK, Selbekk RS (2012) Formation of corundum megacrysts during H_2O-saturated incongruent melting of feldspar: P–T pseudosection-based

modelling from the Skattøra migmatite complex, North Norwegian Caledonides. CMP. V. 164. P. 627–641.

130. Lanari P., Duesterhoeft E. (2019) Modeling Metamorphic Rocks Using Equilibrium Thermodynamics and Internally Consistent Databases: Past Achievements, Problems and Perspectives. Journal of Petrology. V 60. 1. P. 19–56.

131. Leake B.E. Woolley A.R., Arps C.E.S., Birch W.D., Gilbert M.C., Grice J.D., Hawthorne F.C., Kato A., Kisch H.J., Krivovichev V.G., Linthout K., Laird J., Mandarino J.A., Maresch W.V., Nickel E.H., Rock N.M.S., Schumacher J.C., Smith D.C., Stephenson N.C.N., Ungaretti L., Whittaker E.J.W., Youzhi G. (1997) Nomenclature of amphiboles: Report of the Subcommittee on Amphiboles of the International Mineralogical Association, Commission on New Minerals and Mineral Names.The Canadian Mineralogist. V. 35. 1. P. 219–246.

132. Leake B. E., Woolley A. R., Birch W. D., Burke E. A.J., Ferraris G., Grice J. D., Hawthorne F. C., Kisch H. J., Krivovichev V. G., Schumacher J. C., Stephenson N. C.N., Whittaker E. J.W. (2004) Nomenclature of amphiboles: Additions and revisions to the International Mineralogical Association's amphibole nomenclature. Amer. Miner. V. 89. P. 883–887.

133. Lebedev V.K., Kalmykova N.A., Nagaytsev Yu.V. (1974) Corundum-staurolite-hornblende schists of the Belomorian complex. Soviet Geology. № 9. P. 78–89.

134. Levitsky V.I. Petrology and geochemistry of metasomatism during the formation of the continental crust. Novosibirsk: GEO, 2005. 324 p.

135. Li Y., Yang Y., LiuY.-C., Groppo C., Rolfo F. (2020) Muscovite dehydration melting in silica-undersaturated systems: acase study from corundum-bearing anatectic rocks in the Dabie orogen. Minerals. V. 10. 213.

136. Li X.-C., Harlov D. E., Zhou M.-F., Hu H. (2022) Experimental investigation into the disturbance of the Sm-Nd isotopic system during metasomatic alteration of apatite. Geochim. Cosmochim. Acta. V. 330. P. 191–208.

137. Li X.-C., Harlov D. E., Zhou M.-F., Hu H. (2022) Metasomatic modification of Sr isotopes in apatite as a function of fluid chemistry. Geochim. Cosmochim. Acta. V. 323. P. 123–140.

138. Liu P., Massonne H.-J., Jin Z. et al. (2017) Diopside, apatite, and rutile in an ultrahigh pressure impure marble from the Dabie Shan, eastern China: A record of eclogite facies metasomatism during exhumation. Chem. Geol. V. 466. P. 123–139.

139. Liu Y., Fan Y., Zhou T. et al. (2020) Hydrothermal fluid characteristics and implications of the Makou IOA deposit in Luzong Basin, eastern China. Ore Geology Reviews. V. 127. 103867.

140. Lobach-Zhuchenko S. B., Chekulaev V. P., Stepanov V. C., Slabunov A. I., Arestova N. A. (1998) Belomorian Belt – Late Archean Accretion-Collision Zone of the Baltic Shield. Reports of the Academy of Sciences. V. 358. № 2. P. 226–229.

141. Locock A. J. (2014) An Excel spreadsheet to classify chemical analyses of amphiboles following the IMA 2012 recommendations. Computers & Geosciences. V. 62. P. 1–11.

142. Lokhov K.I., Levsky L.K. (1995) Carbon and isotopes of heavy noble gases in metamorphic fluids. Geochemistry International. № 6. P. 829–842.

143. Lokhov K.I., Prasolov E.M., Akimova E.Yu., Lokhov D.K., Bushmin S.A. (2016) Isotopic and elemental fractionated He, Ne, and Ar in the fluid Inclusions of minerals from metamorphic rocks of the Northern Karelia with anomalous isotopic light oxygen: isotopic fractionation in endogenous fluid by thermodiffusion with cascading. Bulletin of St. Petersburg State University, Series 7: Geology and Geography. № 1. P. 29–47.

144. Louvel, M., Bordage, A., Testemale, D. et al. (2015) Hydrothermal controls on the formation of REE deposits: insights from in situ XAS study of REE (Nd, Gd, Yb) solubility and speciation in high temperature fluids (T < 600 °C). SGA conference materials.

145. Lubnina N.V., Zakharov V.S., Novikova M.A., Vorontsova V.P. (2015) Paleoproterozoic magnetization reversal in the Belomorian mobile belt (Karelia): petropaleomagnetic evidence and supercomputer modeling. Moscow University Bulletin. Series 4. Geology. 2015. №2. P. 10–21.

146. Lubnina N.V., Slabunov A.I., Stepanova A.V., Bubnov A.Yu., Kosevich N.I., Novikova M.A., Tarasov N.A. (2016) Magnetization reversal trend in the rocks of the Belomorian mobile belt in the Paleoproterozoic: paleomagnetic and geological evidence. Bulletin of the Moscow University. Series 4. Geology. № 4. P. 3–14.

147. Lutkovskaya T.A. (1971) On the issue of kyanite formation at the Lyagkomina deposit. Proceedings of the Institute of Geology of the Karelian branch of the USSR Academy of Sciences. № 7. "Mineralogy and geochemistry of the Precambrian of Karelia". P. 68–78.

148. Manning C.E. (2013) Thermodynamic modeling of fluid-rock interaction at mid-crustal to upper-mantle conditions. Rev Mineral Geochem. V. 76. P. 135–164.

149. Mao M., Rukhlov A.S., Rowins S.M. et al. (2016) Detrital Apatite Trace-Element Compositions: a Robust New Tool for Mineral Exploration. Economic Geology. V. 111. P. 1187–1222.

150. McDonough W.F., Sun S.S. (1995) The composition of the Earth. Chemical Geology. V. 120. P. 223–253.

151. Metasomatism and metasomatic rocks / ed. V.A. Zharikov, V.L. Rusinov. M.: Scientific world, 1998. 492 p.

152. Migdisov A., Williams-Jones A.E., Brugger J. et al. (2016) Hydrothermal transport, deposition, and fractionation of the REE: Experimental data and thermodynamic calculations. Chemical Geology. V. 439. P. 13–42.

153. Migmatization and granite formation in various thermodynamic regimes. (Glebovitsky V.A., Zinger T.F., Kozakov I.K. and others) / Ed. Mitrofanov F.P. L.: Nauka, 1985. 310 p.

154. Miller Yu.V., Lvov A.B., Myskova T.A., Milkevich R.I. (1995) Position of the Early Proterozoic drusites in the folded cover structure of the Belomorian mobile belt. Bulletin of St. Petersburg State University. Ser. 7. № 4 (28). P. 63–71.

155. Miller Yu.V., Milkevich R.I. (1995) Cover-fold structure of the Belomorian zone and its correlation with the Karelian granite-greenstone region. Geotectonics. № 6. P. 80–93.

156. Miller Yu.V. (1997) Late Archean cover structure of the Belomorian mobile belt. Bulletin of St. Petersburg State University. Ser. 7. № 3(21). P. 28–40.

157. Miller Yu.V., Glebovitsky V.A., Myskova T.A., Lvov A.B. (1999) New data on the structural position and geotectonic significance of the Chupa nappe of the Belomorian mobile belt. Reports of the Academy of Sciences. V. 366. № 3. P. 379–383.

158. Miller Yu.V. (2006) Belomorian mobile belt of the Fennoscandian shield. Regional geology and metallogeny. № 27. P. 5–14.

159. Moiseeva O.A. (2002) Peculiarities of the genesis of corundums in North Karelia. Mineralogical Museums. Proceedings of the IV International Symposium. St. Petersburg. P. 110–112.

160. Moskovchenko N.I., Turchenko S.I. Metamorphism of kyanite-sillimanite type and sulfide mineralization. L., 1975. 139 p.

161. Moulas E., Kostopoulos D., Connolly J.A.D., Burg J.P. (2013) P-T estimates and timing of the sapphirine-bearing metamorphic overprint in kyanite eclogites from Central Rhodope, northern Greece. Petrology. V 21. 5. P. 507–521.

162. Myskova T.A., Milkevich R.I., Lvov A.B., Miller Yu.V. (2000) The origin of the Chupa gneisses of the Belomorian region in the light of new lithological and geochemical data. Lithology and Mineral Resources. № 6. P. 653–664.

163. Myskova T.A. Aluminous gneisses of the Belomorian region: chemical composition, origin, conditions of formation. Abstract of the thesis. PhD St. Petersburg, 2001. 24 p.

164. Myskova T.A. (2002) Conditions of Late Archean metamorphism of aluminous gneisses of the Chupa Complex of the Belomorian Region. Zapiski of the Russian Mineralogical Society, V. 131. № 4. P. 12–22.

165. Myskova T.A., Glebovitsky V.A., Miller Yu.V., Lvov A.B., Kotov A.B., Kovach V.P., Zagornaya N.Yu. (2003) Supracrustal sequences of the Belomorian mobile belt: primary composition, age and origin. Stratigraphy. geological correlation. V. 11. № 6. P. 3–19.

166. Nagaytsev Yu.V. Petrology of metamorphic rocks of the Ladozhsky and Belomorian complexes. L., 1974. 160 p.

167. Nasedkina V.Kh. Deposits of corundum and spinel rocks of the southwestern slope of the Batenevsky Ridge. M.: Nauka, 1977. 107 p.

168. Newton R.C., Manning C.E. (2008) Solubility of corundum in the system Al_2O_3–SiO_2–H_2O–NaCl solutions at 800 °C and 10 kbar. Chemical Geology. 249. P. 250–261.

169. Niedermann S. (2002) Cosmic-Ray-Produced Noble Gases in Terrestrial Rocks: Dating Tools for Surface Processes. Reviews in Mineralogy and Geochemistry. V. 47. P. 731–784.

170. Nozaka T., Meyer R., Wintsch R.P., Wathen B. (2016) Hydrothermal spinel, corundum and diaspore in lower oceanic crustal troctolites from the Hess Deep Rift. Contrib. Miner. Petrol. V. 171 (53). P. 1–14.

171. O'Sullivan G., Chew D., Kenny G., Henrichs I. Mulligan D. (2020) The trace element composition of apatite and its application to detrital provenance studies. Earth-Sci. Rev. V. 201. 103044.

172. Otten M.T. (1984) Na–Al-rich gedrite coexisting with hornblende in a corona between plagioclase and olivine. Am Mineral. V. 69. P. 458–464.

173. Owens B. E., Belkin H. E., Zerolis J. M. (2013) Margarite, corundum, gahnite and zincohögbomite in a blackwall, Raleigh Terrane, Eastern Piedmont Province, USA. Mineralogical Magazine. V. 77. 7. P. 2913–2930.

174. Ozima M., Podosek F.A. Noble Gas Geochemistry, 2nd ed. Cambridge Univ. Press, 2002. 286 p.

175. Pajunen M., Poutiainen M. (1999) Palaeoproterozoic prograde metasomatic-metamorphic overprint zones in Archaean tonalitic gneisses eastern Finland. Bull of the Geol Soc. of Finland. V. 71(1). P. 73–132.

176. Pinaeva N.I. Rare parageneses in the rocks of the kolchedan formation of North Karelia. Regional metamorphism and metamorphogenic ore formation. L.: Nauka, 1970. P. 117–123.

177. Prasolov E.M., Lokhov K.I., Krupenik V.A. (2011) Isotopic composition of helium and argon in halite. In book "Paleoproterozoic Onega structure (geology, tectonics, deep structure and mineralogy" (Edited by L.V. Glushanin, N.V. Sharov, V.V. Shchiptsov), Petrozavodsk,

publishing house of the Karelian Scientific Center of the Russian Academy of Sciences. 2011. P. 248–250.

178. Precambrian high grade mobile belts. Belomorian mobile belt in the eastern Fennoscandian Shield. Field Guidebook. Petrozavodsk: KRC RAS. 2014. 99 p.

179. Raith M. M., Rakotondrazafy R., Sengupta P. (2008) Petrology of corundum-spinel-sapphirine-anorthite rocks (‘sakenites’) from the type locality in southern Madagascar. Journal of Metamorphic Geology. V. 26. P. 647–667.

180. Raith M.M., Srikantappa C., Sengupta P., Kooijman E., Upadhyay D. (2010) Corundum–leucosome-bearing aluminous gneiss from Ayyarmalai, Southern Granulite Terrain, India: A textbook example of vapor phase-absent muscovite-melting in silica undersaturated aluminous rocks. American Mineralogist. V. 95. P. 897–907.

181. Redder E. Fluid inclusions in minerals: in 2 volumes. M.: Mir, 1987. V. 1. 557 p.

182. Rieder M., Cavazzini M. G., D'yakonov Y.S., Frank-Kamenetskii V.A., Gottardi G., Guggenheim S., Koval’ P.V., Müller G., Neiva A.M.R., Radoslovich E.W., Robert J.-L., Sassi F.P., Takeda H., Weiss Z., Wones D.R. (1998) Nomenclature of the micas. The Canadian Mineralogist. V. 36. 3. P. 905–912.

183. Riesco M., Stuwe K., Reche J. (2005) Formation of corundum in metapelites around ultramafic bodies. An example from the Saualpe region, Eastern Alps. Mineralogy and Petrology. V. 83. 1–25.

184. Ruchev A.M. (1998) On some features of paragneisses of the Chupa Formation (Belomorian Complex). Geology and Minerals of Karelia. Petrozavodsk. № 1. P. 73–81.

185. Ruchev A.M. (2000) On the protolith of North Karelian gneisses of the Chupa Formation of the Belomorian Complex. Geology and Minerals of Karelia. Petrozavodsk. № 2. P. 12–25.

186. Ruchev A.M. Paragneisses of the Chupa belt in the area of the settlement of Tedino (Slyudovarakka). Belomorian mobile belt and its analogues. Geological tour guide. Petrozavodsk, 2005. P. 25–31.

187. Ruchev A.M. (2010) Formation of kyanite gneisses in the tectonophysical aspect (Belomorsky complex of rocks of the Baltic Shield). Geology and minerals of Karelia. № 13. Petrozavodsk: KarRC RAS. P. 13–27.

188. Rybakov S.I., Golubev A.I., Slyusarev V.D., Stepanov V.S., Lavrov M.M., Trofimov N.N. (2000) Proterozoic rifting and its role in the formation of the Belomorian mobile zone. Geology and Minerals of Karelia. Petrozavodsk. № 2. P. 4–11.

189. Schumacher J.C., Robinson P. (1987) Mineral Chemistry and Metasomatic Growth of Aluminous Enclaves in Gedrite-Cordierite-Gneiss from Southwestern New Hampshire, USA. Journal of Petrology. V. 28. 6. P. 1033–1073.

190. Sedova I. S., Glebovitsky V. A. (2005) Peculiarities of Late Archean granitization and migmatite formation in the Belomorian belt. Zapiski of the Russian Mineralogical Society. V. 134. № 3. P. 1–24.

191. Sengupta P., Raith M.M., Levitsky V.I. (2004) Compositional characteristics and paragenetic relations of magnesiohögbomite in aluminous amphibolites from the Belomorian complex, Baltic Shield, Russia. Amer. Miner., V. 89. P. 819–831.

192. Serebryakov N.S., Gladysheva A.P., Aristov Vs.V. (2001) Faceted microrelief of corundum crystals (Khitostrovsky corundum occurrence, Karelia). Izv. Universities: Geology and exploration. № 2. P. 30–35.

193. Serebryakov N.S., Aristov Vs.V. (2004) Localization conditions for manifestations of collection corundum in the rocks of the Chupa sequence of the Belomorian complex of North Karelia. Izvestiya vuzov. Geology and exploration. № 4. P. 36–42.

194. Serebryakov N.S., Rusinov V.L. (2004) High-temperature high-pressure calcium-sodium metasomatism and corundum formation in the Precambrian Belomorian mobile belt (Karelia). Reports of the Russian Academy of Sciences. V. 395. № 4. P. 529–533.

195. Serebryakov N.S. Petrology of corundum-bearing rocks of the Chupa sequence of the Belomorian mobile belt (on the example of the Chupa segment). Diss. cand. geol-min. sciences. M., 2004. 161 p.

196. Serebryakov N.S. (2006) Genesis of high-alumina sapphirine from corundum-bearing metasomatites in the metabasites of the Chupa sequence of the Belomorian mobile belt. Geology, Minerals and Geoecology of the North-West of Russia. Materials of the XVII Youth Scientific Conference dedicated to the memory of K.O. Kratz. Petrozavodsk. KarRC RAS. P. 109–111.

197. Serebryakov N.S., Astafiev B.Yu., Voinova O.A., Presnyakov S.L. (2007) The first local Th-U-Pb dating of zircon from metasomatites of the Belomorian mobile belt. Reports of the Academy of Sciences. V. 413. № 3. P. 388–392.

198. Serebryakov N.S. (2007) Corundum-bearing rocks of the Peruselka manifestation, Murmansk region. Geology and minerageny of the Kola region. Proceedings of the All-Russian Scientific Conference and the IV Fersman Scientific Session. Apatity. P. 127–129.

199. Serebryakov N.S., Korpechkov D.I. (2009) Evolution of acidity-alkalinity during the formation of corundum-bearing metasomatites in the metabasites of the Chupa strata of the Belomorian mobile belt. Physico-chemical factors of petro- and ore genesis: new frontiers. Conf. dedicated 110th anniversary of D.S. Korzhinsky. Moscow, IGEM RAS. P. 360–363.

200. Shcherbakova T.F., Terekhov E.N. (2004) Geochemical characteristics of aluminous plagiogneisses: on the origin of kyanite-bearing rocks of the Belomorian belt. Geochemistry International. № 6. P. 611–631.

201. Shcherbakova T.F., Terekhov E.N. (2008) Amphibolites and basic metasomatites of the Belomorian belt: similarities and differences. Geochemistry International. № 3. P. 302–322.

202. Shevchenko S.S., Akhmedov A.M., Krupenik V.A., Sveshnikova K.Yu. (2009) Late Archean noble-metal metasomatites of the Chupino-Loukha fragment of the Belomorian mobile zone (North Karelia). Region. geol. and metallogeny. № 37. P. 106–120.

203. Shurkin K.A., Gorlov N.V., Salie M.E. and others. The Belomorian complex of North Karelia and the southwest of the Kola Peninsula (Geology and pegmatite content). M.; L.: Publishing House of the Academy of Sciences of the USSR, 1962. 306 p.

204. Sibelev O.S. Late Svekofennian (PR1) stage of metamorphism (SW part of the Kola Peninsula and North Karelia). Abstract of the thesis. dis. cand. geol.-miner. sciences. M., 1998. 21 p.

205. Skublov S., Drugova G. (2003) Patterns of trace-element distribution in calcic amphiboles as a function of metamorphic grade. Canadian Mineralogist. V. 41. P. 383–392.

206. Skublov, S.G. (2005) Geochemistry of rare earth elements in rock-forming metamorphic minerals. St. Petersburg: Science. 147 p.

207. Skublov S.G., Levsky L.K., Marin Yu.B. Gembitskaya I.M., Azimov P.Ya., Larionov A.N. (2009) Age, geochemistry of minerals and formation conditions of the Shueretskoye garnet deposit (Belomorsky belt). Reports of the Academy of Sciences. V. 429. № 5. P. 661–667.

208. Skublov S.G., Azimov P.Ya., Li S.Kh., Glebovitsky V.A., Melnik A.E. (2017) Polymetamorphism of the Chupa sequence of the Belomorian mobile belt (Fennoscandia) according to the isotope-geochemical (U-Pb, REE, O) study of zircon. Geochemistry International. № 1. P. 3–16.

209. Skublov, S.G., Bushmin, S.A., Kuznetsov, A.B. and others (2020). Oxygen isotope composition in zircon from corundum-bearing metasomatites of the Dyadina Gora ore occurrence, Belomorian mobile belt. Reports of the Academy of Sciences. V. 491. № 2. P. 71–76.

210. Slabunov A.I. Geology and geodynamics of the Archean mobile belts (on the example of the Belomorian province of the Fennoscandian shield). Petrozavodsk, KarRC RAS publishing house. 2008. 296 p.

211. Slabunov A.I., Azimov P.Ya., Glebovitsky V.A., Zhang L., Kevlich V.I. (2016) Archean and Paleoproterozoic migmatization of rocks of the Belomorian province of the Fennoscandian Shield: petrology, geochronology, geodynamic consequences. Reports of the Academy of Sciences. V. 467. № 1. P. 71–74.

212. Slabunov A.I., Shchipansky A.A., Stepanov V.S., Babarina I.I. (2019) A relic of the Mesoarchean oceanic lithosphere in the structure of the Belomorian province of the Fennoscandian Shield. Geotectonics. № 2. P. 46-71.

213. Spear F.S., Hazen R.M., and Rumble D. (1981) Wonesite: a new rock-forming silicate from the Post Pond volcanics, Vermont. American Mineralogist. V. 66. P. 100–105.

214. Spear F.S., Pyle J.M. (2002) Apatite, Monazite, and Xenotime in Metamorphic Rocks. Rev. Mineral. Geochem. V. 48. P. 293–335.

215. Steele-MacInnis M., Bodnar R.J., Naden J. (2011) Numerical model to determine the composition of H_2O-NaCl-$CaCl_2$ fluid inclusions based on microthermometric and microanalytical data. Geochimica et Cosmochimica Acta. V. 75. P. 21–40.

216. Stepanov V.S. The main magmatism of the Precambrian of the Western White Sea. M.; L., 1981. 215 p.

217. Stepanova A.V., Larionov A.N., Bibikova E.V., Stepanov V.S., Slabunov A.I. (2003) Early Proterozoic (2.1 Ga) Fe-tholeiitic magmatism of the Belomorian province of the Baltic Shield: geochemistry, geochronology. Reports of the Academy of Sciences. V. 390. № 4. P. 528–532.

218. Stepanova A.V., Stepanov V.S. (2005) Coronitic gabbro of the Belomorian mobile belt. Geology and minerals of Karelia. № 8. Petrozavodsk. P. 29–39.

219. Stepanova A.V. Stepanov V.S. (2010) Paleoproterozoic mafic dyke swarms of the Belomorian Province, eastern Fennoscandian Shield. Precambrian Research. V.183. P. 602–616.

220. Stepanova A.V., Stepanov V.S., Slabunov A.I. (2011) Achievements and problems in the study of the basic magmatism of the Belomorian province of the Fennoscandian shield. Geology of Karelia from the Archean to the present day. Institute of Geology KarRC RAS. P. 79–90.

221. Stepanova A. V., Stepanov V. S., Larionov A. N., Azimov P. Ya., Egorova S. V., Larionova Yu. O. (2017) 2.5 Ga gabbro-anorthosites in the Belomorian province of the Fennoscandian Shield: petrology and tectonic position. Petrology. V. 25. № 6. P. 581–608.

222. Stepanova, A.V., Stepanov, V.S., Larionov, A.N., Salnikova, E.B., Samsonov, A.V., Azimov, P., Egorova, S.V., Larionova, Y.O., Sukhanova, M.A., Kervinen, A.V., Maksimov, O.A. (2022) Relicts of Palaeoproterozoic LIPs in the Belomorian Province, eastern Fennoscandian Shield: barcode reconstruction for a deeply eroded collisional orogen. Spec. Publ.

223. Sverjensky D.A., Hemley J.J., D'Angelo W.M. (1991) Thermodynamic assessment of hydrothermal alkali feldspar mica-aluminosilicate equilibria. Geochim Cosmochim Acta. 55. P. 989–1004.

224. Terekhov E.N., Levitsky V.I. (1991) Geological and structural regularities of the distribution of corundum mineralization in the North-Western White Sea. Izvestiya vuzov. Geology and exploration. № 6. P. 3–13.

225. Terekhov E.N. (2007) Peculiarities of REE distribution in corundum-bearing and other metasomatites of the period of rise to the surface of metamorphic rocks of the Belomorian belt (Baltic shield). Geochemistry. № 4. P. 411–428.

226. Terekhov E.N., Akimov A.P. (2013) Tectonic position and genesis of deposits of jewelry corundum in High Asia. Lithosphere. № 5. P. 122–140.

227. Tropper P., Manning C.E. (2007) The solubility of corundum in H_2O at high pressure and temperature and its implication for Al mobility in the deep crust and upper mantle. Chemical Geology. V. 240. P. 54–60.

228. Tsunogae T., Santosh M., Shimpo M. (2007) Sodicgedrite in ultrahigh-temperature Mg-V. Al-rich rocks from the Palghat-Cauvery Shear Zone system, southern India. J Mineral Petrol Sci. 102. P. 39–43.

229. Ustinov V.I., Baksheev I.A. Serebryakov N.S. (2008) Oxygen isotope composition of mineral-forming fluids of corundum-bearing metasomatites of the Khitoostrovsky and Varatsky occurrences, North Karelia. Geochemistry International. № 11. P. 1245–1248.

230. van Hinsberg V., Yakymchuk C., Jepsen A.T.K., Kirkland C.L., Szilas K. (2021) The corundum conundrum: Constraining the compositions of fluids involved in ruby formation in metamorphic melanges of ultramafic and aluminous rocks. Chemical Geology. V. 571. 120180.

231. Vakhrusheva N.V., Ivanov K.S., Stepanov A.E., Shokalsky S.P., Azanov A.N., Hiller V.V., Shiryaev P.B. (2016) Plagioclasites from chromite-bearing ultramafic rocks of the Rai-Iz massif. Litosphere. № 5. P. 134–145.

232. Verkhovsky A.B., Shukolyukov Yu.A. (1991) Elemental and isotopic fractionation of noble gases in nature. Moscow: Nauka, 293 p.

233. Verchovsky A.B., Sephton M.A., Wright I.P., Pillinger C.T. (2002) Separation of planetary noble gas carrier from bulk carbon in enstatite chondrites during stepped combustion. Earth Planet. Sci. Lett. V. 199. P. 243–255.

234. Vernon R.H. and Clarke G.L. (2008) Principles of Metamorphic Petrology. Cambridge University Press.

235. Vetrin V.R., Kamensky I.L., Ikorsky S.V. (2007) Helium and argon isotopes in xenoliths of the lower crust of the Belomorian mobile belt. Petrology. V. 15. № 3. P. 324–336.

236. Volodichev O.I. Metamorphism of disthene gneiss facies (on the example of the Belomorian complex). L.: Nauka, 1975. 170 p.

237. Volodichev O.I. Belomorsky complex of Karelia. Geology and petrology. L.: Nauka, 1990. 246 p.

238. Volodichev O.I., Korol N.E., Kuzenko T.I., Sibelev O.S. (2011) Metamorphism of the Early Precambrian complexes of the eastern part of the Fennoscandian shield. Geology of Karelia from the Archean to the present day. Institute of Geology KarRC RAS. P. 49–54.

239. Vysotsky S.V., Ignatiev A.V., Yakovenko V.V., Karabtsov A.A. (2008) Abnormally light oxygen isotopic composition of minerals in corundum-bearing formations of northern Karelia. Reports of the Academy of Sciences. V. 423. № 1. P. 85–88.

240. Vysotsky S.V., Ignatiev A.V., Levitsky V.I., Budnitsky S.Yu., Velivetskaya T.A. (2011) New data on stable isotopes of minerals from corundum-bearing formations in northern Karelia (Russia). Reports of the Academy of Sciences. V. 439. № 1. P. 95–98.

241. Vysotsky S.V., Ignatiev A.V., Levitsky V.I., Nechaev V.P., Velivetskaya T.A., Yakovenko V.V. (2014) Geochemistry of stable isotopes of oxygen and hydrogen in corundum-bearing rocks and minerals of North Karelia as an indicator of unusual conditions for their formation. Geochemistry International. № 9. P. 843–853.

242. Vysotsky S.V., Yakovenko V.V., Ignatiev A.V., Velivetskaya T.A., Nechaev V.P. (2014) Oxygen isotopic composition as an indicator of the genesis of rubies and sapphires. Bulletin of the Far Eastern Branch of the Russian Academy of Sciences. № 4. P. 25–31.

243. Wang K.K., Graham I.T., Lay A., Harris S.L., Cohen D.R. (2017) The origin of a new pargasite-schist hosted ruby deposit from Paranesti, Northern Greece. The Canadian Mineralogist. V. 55. P. 535–560.

244. Watson E.B., Cherniak D.J. (2013) Simple equations for diffusion in response to heating. Chemical Geology. V. 335. P. 93–104.

245. Whitney D.L., Evans B.W. (2010) Abbreviations for names of rock-forming minerals. American Mineralogist. V. 95. P. 185–187.

246. Yakovenko V.V. Isotope-geological systematics of corundums and their genesis. Abstract of thesis ....cand. geol-min. sciences, Vladivostok, 2013. 22 p.

247. Yakymchuk C., Szilas K. (2018) Corundum formation by metasomatic reactions in Archean metapelite, SW Greenland: exploration vectors for ruby deposits within high-grade greenstone belts. Geoscience Frontiers. V. 9 (3). P. 727–749.

248. Yui T.-F., Kwon S.-T. (2002) Origin of a Dolomite-Related Jade Deposit at Chuncheon, Korea. Economic Geology. V 97. P. 593–601.

249. Yuzhanova V.V. (1975) Staurolite from aluminous gneisses of the Archean Chupa Formation. Proceedings of the Institute of Geology of the Karelian Branch of the Academy of Sciences of the USSR. № 27. P. 143–145.

250. Zack T., von Eynatten H., Kronz A. (2004) Rutile geochemistry and its potential use inquantitative provenance studies. Sediment. Geol. V. 171. P. 37–58.

251. Zakharov D.O., Bindeman I.N., Slabunov A.I., Ovtcharova M., Coble M.A., Serebryakov N.S., Schaltegger U. (2017) Dating the Paleoproterozoic snowball Earth glaciations using contemporaneous subglacial hydrothermal systems. Geology. V. 45. № 7. P. 667–670.

252. Zakharov D.O., Bindeman I.N., Serebryakov N.S. et al. (2019) Low $\delta^{18}O$ rocks in the Belomorian belt, NW Russia, and Scourie dikes, NW Scotland: A record of ancient meteoric water captured by the early paleoproterozoic global mafic magmatism. Precambrian Research. V. 333. 105431.

253. Zaraisky G.P. An experiment in solving the problems of metasomatism. M.: GEOS, 2007. 136 p.

254. Zhao X.F., Zhou M.F., Gao J.F. et al. (2015) In situ Sr isotope analysis of apatite by LA-MC-ICPMS: Constraints on the evolution of ore fluids of the Yinachang Fe-Cu-REE deposit, Southwest China. Miner. Deposita. V. 50. P. 871–884.

255. Zirner A.L.K., Marks M.A.W., Wenzel T. et al. (2015) Rare earth elements in apatite as a monitor of magmatic and metasomatic processes: Th Ilímaussaq complex, South Greenland. Lithos. V. 228–229. P. 12–22.

Appendices

Appendix 1. Map of actual material with sampling points

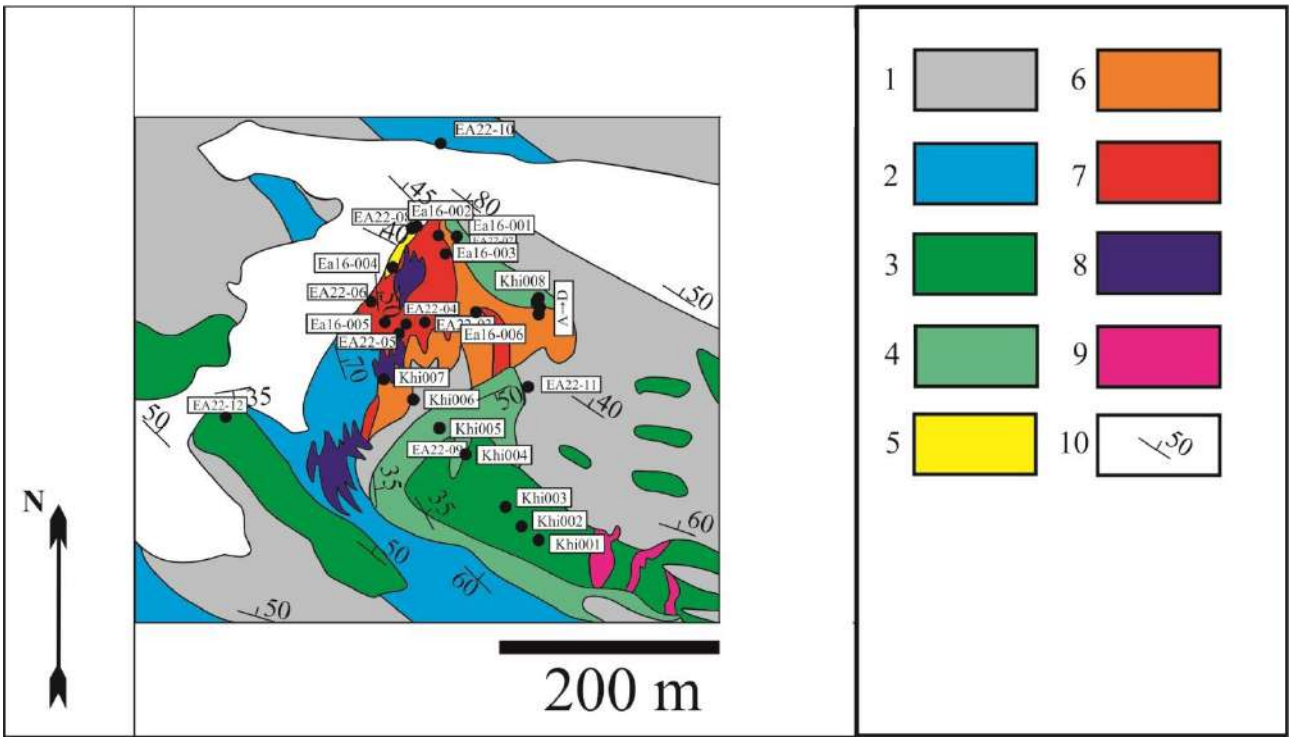

Symbols: 1, 2 – gneisses of the Chupa sequence (1 – garnet-biotite, 2 – kyanite-garnet-biotite); 3 – metagabbro; 4 – migmatized garnet amphibolites; 5 – rocks with parageneses *Pl* + *Grt* + *Bt* + *Ky*, *Pl* + *Grt* + *Bt* + *Crn* (zones 1, 3a) (Akimova, Kol'tsov, 2022); 6 – rocks with parageneses *Pl* + *Grt* + *Bt* + *St*, *Pl* + *Grt* + *St* + *Cam* (zones 2, 3b); 7 – rocks with *Pl* + *Grt* + *Cam* + *Crn* paragenesis (zone 4); 8 – plagioclasites; 9 – pegmatites; 10 – occurrence elements.

Appendix 2. Petrochemical Data

Table 1. Chemical composition of the rocks of the Khitoostrov occurrence

Components	Rocks											
	Ky-Grt-Bt gneisses	Crn-metasomatites, zone 1			Crn-metasomatites, zone 3a		Crn-metasomatites, zone 3b		Crn-metasomatites, zone 4			
	1	2	Khi006	Khi008b	3	4	5	6	7	8	9	10
SiO_2	62.84	48.30	58.90	52.80	47.40	45.80	47.25	45.90	47.16	49.36	46.26	50.36
TiO_2	0.93	1.13	0.59	0.93	1.20	1.16	1.40	1.14	1.28	1.11	1.16	0.95
Al_2O_3	17.91	21.90	21.80	21.70	22.20	25.50	22.50	21.90	23.84	23.56	24.09	24.25
Fe_2O_3	7.06	1.55	0.87	1.97	1.00	11.86	1.00	1.00	10.73	10.07	11.91	8.57
FeO	-	8.69	2.88	5.15	9.62	-	9.50	12.83	-	-	-	-

MnO	0.07	0.03	0.09	0.07	0.12	0.11	0.17	0.11	0.07	0.06	0.07	0.05
MgO	3.90	5.05	7.61	3.95	6.12	5.74	6.12	6.12	5.79	4.88	6.01	4.19
CaO	2.51	2.57	10.10	4.84	2.75	2.16	4.95	5.53	4.74	4.89	4.79	4.98
Na_2O	2.93	4.80	1.80	5.09	4.20	3.85	4.21	3.36	4.89	5.28	4.62	5.64
K_2O	2.41	3.97	0.88	2.18	3.49	3.14	1.67	0.76	0.41	0.28	0.53	0.32
P_2O_5	-	0.08	0.09	0.10	0.02	0.05	0.08	0.06	0.06	0.07	0.04	0.06
LOI	-	-	0.38	0.59	-	0.72	-	-	1.12	0.09	0.75	0.66
Total	100.56	98.07	106.00	99.37	98.12	100.09	98.85	98.71	100.09	99.65	100.23	100.03

Note: 1 – data from T.A. Myskova, 2–12 data from E.N. Terekhov, N.S. Serebryakov. Samples marked with Khi are author's data.

Continuation of Table 1

Components	Rocks								
	Metagabbro	Grt amphibolites			Gr amphibolite (leucosome)	Czo amphibolite	Plagioclasites		
	Khi001	Khi004	Khi005	Khi008g	Khi008v	Khi008d	11	12	Khi007
SiO_2	53.20	59.40	53.90	56.70	74.60	44.50	59.78	62.03	61.70
Al_2O_3	16.75	13.89	13.94	15.50	12.40	22.00	0.29	0.07	0.03
TiO_2	1.34	0.64	0.74	0.62	0.40	0.63	22.98	22.33	23.70
Fe_2O_3	10.80	8.93	10.40	7.71	2.87	9.08	2.65	1.20	<0.3
FeO	-	-	-	-	-	-	-	-	0.57
MnO	0.09	0.24	0.09	0.10	0.06	0.03	0.02	0.01	0.01
MgO	4.11	5.08	7.61	5.91	1.57	6.83	1.04	0.39	0.38
CaO	7.82	8.76	10.10	9.79	4.16	13.10	4.36	3.62	3.55
Na_2O	4.88	2.01	1.80	2.43	3.21	1.91	8.29	8.95	8.80
K_2O	0.68	0.68	0.88	0.72	0.40	0.98	0.15	0.40	0.69
P_2O_5	0.07	0.07	0.09	0.07	<0.05	0.04	0.11	0.09	<0.05
LOI	0.20	0.28	0.38	0.31	0.22	0.85	0.34	0.49	0.62
Total	99.94	99.98	99.94	99.86	99.89	99.95	100.01	99.58	100

Note: 1 – data from T.A. Myskova, 2–12 – data from E.N. Terekhov, N.S. Serebryakov. Samples marked with Khi are author's data.

Appendix 3. Composition of minerals

Table 1. Chemical composition (wt. %) and coefficients in the crystal chemical formulas of amphiboles in the rocks of Khitoostrov.

	Rocks					
	Crn-metasomatites					
	Zone 3b		Zone 4			
Components	Ts	Na-Ged	Ts	Brs	Sd	Na-Ged
SiO_2	44.01	42.04	41.87	42.56	41.39	40.17
TiO_2	1.08	0.28	1.12	1.14	1.08	0.43
Al_2O_3	16.95	22.04	19.74	19.88	20.09	22.83
FeO^{tot}	12.68	15.78	12.39	11.81	12.27	17.48
MgO	12.07	16.92	11.38	11.69	10.89	15.67
CaO	10.85	0.46	10.47	9.50	11.03	0.46
Na_2O	1.96	2.48	2.76	3.13	3.03	2.95
K_2O	0.39		0.26	0.29	0.22	
Total	100.00	100.00	100.00	100.00	100.00	100.00
Coefficients calculated for 13 cations						
Si	6.12	5.88	5.82	5.88	5.81	5.69
Al	1.88	2.13	2.18	2.12	2.19	2.31
∑T	8.00	8.00	8.00	8.00	8.00	8.00
Ti	0.11	0.03	0.12	0.12	0.11	0.05
Al	0.91	1.51	1.06	1.11	1.13	1.50
Fe^{3+}	1.12		1.20	1.28	0.86	
Fe^{2+}	0.40		0.25	0.13	0.58	0.14
Mg	2.50	3.47	2.36	2.39	2.28	3.31
∑C	5.00	5.00	5.00	5.00	5.00	5.00
Fe^{2+}		1.84				1.93
Mg	0.08	0.06	0.06	0.04		
Ca	1.62	0.07	1.56	1.41	1.66	0.07
Na	0.37	0.03	0.44	0.58	0.34	0.00
∑B	2.00	2.00	2.00	2.00	2.00	2.00
Na	0.16	0.65	0.31	0.26	0.48	0.81
K	0.07		0.05	0.05	0.04	
∑A	0.22	0.65	0.35	0.31	0.52	0.81
O^{2-} (except W)	22.00	22.00	22.00	22.00	22.00	22.00
OH^-	1.78	1.94	1.76	1.76	1.77	1.91
O^{2-}	0.23	0.06	0.24	0.24	0.23	0.09

∑W	2.00	2.00	2.00	2.00	2.00	2.00
T,C,B,A sum	15.22	15.64	15.34	15.31	15.52	15.81

Note: The compositions of amphiboles were calculated using the ACES-9 program (Lokock, 2014). The contents of the components in the oxide form are given to 100%. Ts – tschermakite, Na-Ged – sodic gedrite, Brs – barroisite, Sd – sadanagaite, Hbl – magnesian hornblende, Prg – pargasite.

Continuation of Table 1

	Rocks			
		Czo amphibolite		
	Grt amphibolite	Matrix	Symplectites	
Components	Hbl	Prg	Sd	Ts
SiO_2	46.03	42.80	40.83	41.02
TiO_2	0.83	0.91	0.68	0.44
Al_2O_3	13.03	16.30	18.40	19.17
FeO^{tot}	13.17	14.84	17.59	17.53
MgO	12.34	10.20	7.71	7.35
CaO	12.27	12.27	12.01	11.90
Na_2O	1.39	1.65	1.71	1.56
K_2O	0.95	1.04	1.07	1.03
Total	100.00	100.00	100.00	100.00
Coefficients calculated for 13 cations				
Si	6.55	6.15	5.96	5.95
Al	1.46	1.85	2.04	2.05
∑T	8.00	8.00	8.00	8.00
Ti	0.09	0.10	0.04	0.03
Al	0.73	0.92	1.12	1.24
Fe^{3+}	0.43	0.49	0.49	0.48
Fe^{2+}	1.13	1.29	1.66	1.65
Mg	2.62	2.19	1.68	1.59
∑C	5.00	5.00	5.00	5.00
Fe^{2+}				
Mg				
Ca	1.87	1.89	1.88	1.85
Na	0.13	0.11	0.12	0.15
∑B	2.00	2.00	2.00	2.00
Na	0.25	0.35	0.36	0.29
K	0.17	0.19	0.20	0.19
∑A	0.43	0.54	0.56	0.48

O^{2-} (except W)	22.00	22.00	22.00	22.00
OH^-	1.82	1.80	1.92	1.94
O^{2-}	0.18	0.20	0.08	0.06
∑W	2.00	2.00	2.00	2.00
T,C,B,A sum	15.42	15.54	15.56	15.48

Note: The compositions of amphiboles were calculated using the ACES-9 program (Lokock, 2014). The contents of the components in the oxide form are given to 100%. Ts – tschermakite, Na-Ged – sodic gedrite, Brs – barroisite, Sd – sadanagaite, Hbl – magnesian hornblende, Prg – pargasite.

Table 2. Chemical composition (wt. %) and coefficients in the crystal chemical formulas of micas in the rocks of Khitoostrov

	Rocks						
		Crn-metasomatites					
	Ky-Grt-Bt gneiss	Zone 1	Zone 2	Zone 3a			Zone 3b
Components	Phl	Phl	Phl	Phl	Ms	Pg	Phl
SiO_2	38.91	39.44	38.31	38.62	47.72	48.51	39.73
TiO_2	2.51	2.32	2.88	2.08	0.54		2.02
Al_2O_3	19.59	19.99	19.13	20.02	38.21	41.83	19.30
FeO^{tot}	16.47	14.84	14.76	15.12	1.36	0.55	12.48
MgO	11.81	14.01	14.88	14.25	0.85		17.03
CaO						0.52	
Na_2O	0.32		0.56	0.45	1.14	5.97	0.62
K_2O	10.38	9.40	9.47	9.46	10.19	2.61	8.83
Total	100	100	100	100	100	100	100
Coefficients calculated for 22 charges							
Si	2.80	2.79	2.74	2.75	3.01	2.97	2.78
Ti	0.14	0.12	0.16	0.11	0.03		0.11
Al	1.06	1.08	1.10	1.14	0.96	1.03	1.11
∑T	4.00	4.00	4.00	4.00	4.00	4.00	4.00
Al	0.60	0.59	0.51	0.54	1.88	1.99	0.48
Fe^{2+}	0.99	0.88	0.88	0.90	0.07	0.03	0.73
Mg	1.27	1.48	1.59	1.51	0.08		1.78
Ca						0.03	
∑D	2.86	2.95	2.98	2.95	2.03	2.05	2.99
Na	0.05		0.08	0.06	0.14	0.71	0.08
K	0.95	0.85	0.86	0.86	0.82	0.20	0.79
Ca							
∑A	1.00	0.85	0.94	0.92	0.96	0.91	0.87

Total	7.86		7.80	7.92	7.87	6.99	6.96	7.86
*x*Mg	0.56		0.63	0.64	0.63			0.71

Note: the contents of the components in the oxide form are given to 100%. *x*Mg = Mg/(Mg+Fe), where Mg, Fe are f.c. When calculating, a correction for isomorphic substitution was introduced $M^{2+} + 2OH^- = Ti^{4+} + 2O^{2-}$. Asp – aspidolite, Pg – paragonite, Mrg – margarite.

Continuation of Table 2

	Rocks					
	Crn- metasomatites			Grt amphibolite	Czo amphibolite	
	Zone 4					
Components	Phl	Pg	Asp	Phl	Phl	Mrg
SiO_2	39.07	48.21	40.10	39.56	37.72	45.41
TiO_2	1.85		1.99	2.86	1.54	
Al_2O_3	20.99	43.24	21.64	17.80	19.34	24.40
FeO^{tot}	10.60		9.71	15.11	19.08	0.61
MgO	18.07		18.97	14.98	12.71	
CaO		0.84				29.57
Na_2O	0.98	6.76	5.49			
K_2O	8.44	0.95	2.09	9.69	9.62	
Total	100	100	100	100	100	100
Coefficients calculated for 22 charges						
Si	2.71	2.93	2.71	2.83	2.73	3.01
Ti	0.10		0.10	0.15	0.08	
Al	1.20	1.07	1.19	1.02	1.19	0.99
∑T	4.00	4.00	4.00	4.00	4.00	4.00
Al	0.52	2.03	0.53	0.48	0.46	0.91
Fe^{2+}	0.61		0.55	0.90	1.16	0.03
Mg	1.87		1.91	1.60	1.37	
Ca		0.06				1.06
∑D	3.00	2.08	2.98	2.98	2.99	2.00
Na	0.13	0.80	0.72			
K	0.75	0.07	0.18	0.88	0.89	
Ca						1.04
∑A	0.88	0.87	0.90	0.88	0.89	1.04
Total	7.87	6.95	7.88	7.86	7.88	7.04
*x*Mg	0.76		0.78	0.64	0.55	

Note: the contents of the components in the oxide form are given to 100%. *x*Mg = Mg/(Mg+Fe), where Mg, Fe are f.c. When calculating, a correction for isomorphic substitution was introduced $M^{2+} + 2OH^- = Ti^{4+} + 2O^{2-}$. Asp – aspidolite, Pg – paragonite, Mrg – margarite.

Table 3. Chemical composition (wt. %) and coefficients in the crystal chemical formulas of garnet in the rocks of Khitoostrov

Components	Rocks							
	Ky-Grt-Bt gneiss	Crn-metasomatites					Grt amphibolite	Czo amphibolite
		Zone 1	Zone 2	Zone 3a	Zone 3b	Zone 4		
SiO_2	37.36	37.91	37.92	37.63	38.78	38.66	38.34	38.00
Al_2O_3	20.84	21.04	21.58	21.45	21.99	21.94	21.76	21.50
FeO^{tot}	32.84	31.42	28.44	31.34	26.22	26.95	24.25	23.60
MnO	1.28	1.10	0.77	0.82	0.33	0.39	1.99	1.84
MgO	4.39	5.83	5.61	5.80	8.13	8.48	4.03	4.11
CaO	3.29	2.69	5.67	2.96	4.56	3.58	9.62	10.96
Total	100.00	100.00	100.00	100.00	100.00	100.00	100.00	100.00
Coefficients calculated for 8 cations								
Si	2.97	3.00	2.97	2.96	2.99	2.98	3.00	2.97
Al	0.03	0.00	0.03	0.04	0.01	0.02	0.00	0.03
∑T	3.00	3.00	3.00	3.00	3.00	3.00	3.00	3.00
Al	1.95	1.96	1.99	1.99	2.00	1.99	2.00	1.94
Fe^{3+}	0.07	0.04	0.04	0.05	0.03	0.04		0.09
∑B	2.02	2.00	2.03	2.04	2.03	2.03	2.00	2.03
Fe^{2+}	2.09	2.04	1.79	1.98	1.65	1.68	1.59	1.45
Mn	0.09	0.04	0.05	0.05	0.01	0.02	0.13	0.12
Mg	0.52	0.69	0.65	0.68	0.93	0.97	0.47	0.48
Ca	0.28	0.23	0.48	0.25	0.38	0.3	0.81	0.92
∑A	2.98	3.00	2.97	2.96	2.97	2.97	2.99	2.97
Total	8.00	8.00	8.00	8.00	8.00	8.00	8.00	8.00

Note: The ratio of Fe^{2+} and Fe^{3+} is calculated based on the stoichiometry of the mineral and the rule of electroneutrality of the formula. The contents of the components in the oxide form are given to 100%.

Table 4. Chemical composition (wt. %) and coefficients in the crystal chemical formulas of plagioclase in the rocks of Khitoostrov

Components	Rocks								
	Ky-Grt-Bt gneiss	Crn-metasomatites					Plagioclasite	Grt amphibolite	Czo amphibolite	
		Zone 1	Zone 2	Zone 3a	Zone 3b	Zone 4			Pl1	Pl2

SiO_2	60.35	62.56	58.79	60.94	58.13	60.65	60.91	59.97	53.40	46.51
Al_2O_3	24.83	23.80	26.13	24.42	26.20	24.78	25.00	25.59	29.90	34.40
FeO^{tot}			0.31	0.47	0.41	0.33				
CaO	7.08	5.30	7.75	5.74	7.88	6.08	6.19	6.92	11.74	17.44
Na_2O	7.65	8.34	7.02	8.06	6.86	7.94	7.90	7.51	4.96	1.65
K_2O	0.09			0.36	0.52	0.22				
Total	100.00	100.00	100.00	100.00	100.00	100.00	100.00	100.00	100.00	100.00
Coefficients calculated for 5 cations										
Si	2.69	2.78	2.63	2.70	2.60	2.69	2.71	2.67	2.41	2.13
Al	1.30	1.25	1.38	1.28	1.38	1.30	1.31	1.35	1.59	1.86
Fe^{2+}				0.02	0.02	0.01				
Fe^{3+}			0.01	0.01		0.01				
Ca	0.34	0.25	0.37	0.28	0.38	0.29	0.30	0.33	0.57	0.86
Na	0.66	0.72	0.61	0.69	0.60	0.69	0.68	0.65	0.43	0.15
K	0.01			0.02	0.03	0.01				
Total	5.00	5.00	5.00	5.00	5.00	5.00	5.00	5.00	5.00	5.00
№Pl	34.00	25.77	37.76	28.57	38.78	29.59	30.25	33.74	56.71	85.36

Note: The ratio of Fe^{2+} and Fe^{3+} is calculated based on the stoichiometry of the mineral and the rule of electroneutrality of the formula. The contents of the components in the oxide form are given to 100%.

Table 5. Chemical composition (wt. %) and coefficients in the crystal-chemical formulas of staurolite from corundum-bearing rocks of Khitoostrov

	Crn-metasomatites			
Components	Zone 2	Zone 3a	Zone 3b	Zone 4
SiO_2	26.79	27.58	27.74	27.57
TiO_2	0.78	0.68	0.53	0.75
Al_2O_3	55.53	55.42	55.98	55.12
FeO^{tot}	13.47	12.75	12.33	12.29
MgO	2.62	2.76	3.42	3.92
Na_2O	0.20	0.11		0.06
ZnO	0.61	0.69		0.28
Total	100	100	100	100
Coefficients calculated for 15 cations				

Si	3.70	3.80	3.79	3.77
Ti	0.08	0.07	0.05	0.08
Al	9.02	8.99	9.02	8.89
Fe^{2+}	0.99	1.16	1.06	0.91
Fe^{3+}	0.57	0.32	0.39	0.50
Mg	0.54	0.57	0.70	0.80
Na	0.05	0.03		0.02
Zn	0.06	0.07		0.03
Total	15	15	15	15
*x*Mg	0.35	0.33	0.40	0.47

Note: The ratio of Fe^{2+} and Fe^{3+} is calculated based on the stoichiometry of the mineral and the rule of electroneutrality of the formula. The contents of the components in the oxide form are given to 100%.

Table 6. Chemical composition (wt. %) and coefficients in the crystal chemical formulas of minerals of the epidote group

Components	Rocks									
	Czo-amphibolites									
	Khi-008D									
	Czo								Fep	Ep
	1	2	3	4	5	6	7	8	9	10
SiO_2	39.71	39.53	39.91	39.50	39.94	39.21	39.65	39.26	38.98	39.25
Al_2O_3	33.04	29.24	30.86	28.39	28.73	28.92	28.95	28.84	21.12	27.38
FeO^{tot}	2.02	6.70	4.12	7.27	6.82	7.20	6.89	6.97	16.12	8.46
CaO	25.23	24.53	25.11	24.84	24.52	24.67	24.51	24.93	23.78	24.91
Total	100	100	100	100	100	100	100	100	100	100
Coefficients calculated for 8 cations										
Si	2.96	2.99	2.99	2.99	3.02	2.97	3	2.97	3.03	2.98
∑T	2.96	2.99	2.99	2.99	3.02	2.97	3	2.97	3.03	2.98
Al	2.00	2.00	2.00	2.00	2.00	2.00	2.00	2.00	1.94	2.00
Fe^{3+}									0.06	
∑M1, M2	2.00	2.00	2.00	2.00	2.00	2.00	2.00	2.00	2.00	2.00
Al	0.90	0.60	0.73	0.53	0.56	0.58	0.58	0.57	0.00	0.45
Fe^{3+}	0.13	0.42	0.26	0.46	0.43	0.46	0.43	0.44	0.98	0.54
∑M3	1.03	1.03	0.99	0.99	0.99	1.04	1.00	1.01	0.98	0.99

Ca	2.01	1.99	2.02	2.02	1.99	2.00	1.99	2.02	1.98	2.03
∑A	2.01	1.99	2.02	2.02	1.99	2.00	1.99	2.02	1.98	2.03
Total	8.00	8.00	8.00	8.00	8.00	8.00	7.99	8.00	8.00	8.00

Note: The ratio of Fe^{2+} and Fe^{3+} is calculated based on the stoichiometry of the mineral and the rule of electroneutrality of the formula. The contents of the components in the oxide form are given to 100%.

Table 7. Chemical composition (wt. %) and coefficients in the crystal chemical formulas of titanite

	Rocks							
	Grt amphibolite			Czo amphibolite				
	Khi-008G			Khi-008D				
Components	1	2	3	4	5	6	7	8
SiO_2	31.13	32.44	32.00	30.45	30.59	29.95	29.84	29.75
TiO_2	38.60	33.63	32.69	38.71	38.57	39.23	39.14	39.46
Al_2O_3	1.76	4.23	5.44	1.90	1.63	1.52	1.73	1.69
FeO^{tot}	0.00	1.79	2.10	0.32	0.42	0.42	0.40	0.49
MgO	0.00	0.99	1.88	0.00	0.00	0.00	0.00	0.00
CaO	28.51	26.92	25.90	28.61	28.79	28.88	28.89	28.62
Total	100	100	100	100	100	100	100	100
Coefficients calculated for 3 cations								
Si	1.01	1.03	1.01	0.99	0.99	0.97	0.97	0.97
Ti	0.94	0.8	0.77	0.94	0.94	0.96	0.95	0.96
Al	0.07	0.16	0.2	0.07	0.06	0.06	0.07	0.07
Fe^{2+}		0.03	0.02	0.01				
Fe^{3+}		0.02	0.03		0.01	0.01	0.01	0.01
Mg		0.05	0.09					
Ca	0.99	0.92	0.87	0.99	1.00	1.00	1.00	1.00
Total	3.00	3.00	3.00	3.00	3.00	3.00	3.00	3.00

Note: The ratio of Fe^{2+} and Fe^{3+} is calculated based on the stoichiometry of the mineral and the rule of electroneutrality of the formula. The contents of the components in the oxide form are given to 100%.

Table 8. Chemical composition (wt. %) of apatite

	Rocks						
	Ky-Grt-Bt gneiss	Grt amphibolite	Crn rock	Crn rock	Crn rock	Plagioclasite	Lower Limits
Elements	Ch-1	KHI-004	Ea16-005I	KHI-008A	KHI-010	Ea16-005II	
Na_2O	0.10	0.2	0.16	1.05	0.97	0.27	0.01

MgO	0.07	0.17	0.10	0.21	0.15	0.38	0.01
Al_2O_3	15.5	1.81	0.51	3.26	8.72	4.19	0.01
SiO_2	13.1	11.7	0.95	8.74	7.52	2.86	0.01
K_2O	0.31	0.03	<0.01	0.07	0.04	0.02	0.01
TiO_2	0.11	8.98	0.18	2.79	1.77	0.56	0.001
MnO	0.03	0.02	0.02	0.01	0.01	0.01	0.0002
Fe_2O_3	0.33	0.57	0.55	0.50	0.44	0.86	0.01
Na	0.04	0.07	0.06	0.39	0.36	0.10	
Ti	0.07	5.38	0.11	1.67	1.06	0.34	

Appendix 4. Rare element composition of minerals

Table 1. The content of rare earth elements in garnet from the rocks of Khitoostrov (ppm)

	Garnet amphibolite after gabbro (Khi004)								
Elements	2 rim	3 middle	4 middle	5 core	9 rim	10 middle	11 middle	12 middle	13 core
La	0.03	0.02	0.06	0.04	0.02	0.04	0.04	0.54	0.02
Ce	0.07	0.04	0.06	0.04	0.02	0.01	0.01	0.89	0.02
Pr	0.08	0.06	0.07	0.03	0.03	0.03	0.08	0.66	0.04
Nd	0.41	0.26	0.20	0.07	0.20	0.10	0.10	0.70	0.22
Sm	3.64	2.50	2.26	1.54	2.37	0.89	0.84	3.41	1.97
Eu	6.85	5.90	5.24	3.32	3.96	2.65	1.58	4.08	3.18
Gd	15.6	14.0	11.1	8.18	10.5	6.98	5.41	10.8	10.3
Dy	48.9	46.6	38.7	32.8	38.2	27.9	29.0	37.6	45.4
Er	70.7	68.7	68.4	58.5	60.9	51.2	67.7	101	119
Yb	51.3	56.4	60.9	57.0	59.4	56.6	78.7	147	172
Lu	41.6	42.0	47.1	45.1	41.5	41.6	51.5	120	144

Continuation of Table 1

	Crn-metasomatite (KHI-010-5)							
Elements	24 rim	24a rim	25 core	30 rim	31 middle	32 middle	33 core	34 middle
La	0.17	0.31	0.06	0.06	0.18	0.19	0.08	0.36
Ce	0.23	0.50	0.11	0.15	0.12	0.08	0.07	0.32
Pr	0.36	0.60	0.32	0.49	0.39	0.24	0.25	0.33
Nd	1.39	1.64	1.32	2.01	1.98	1.40	1.21	1.37
Sm	14.3	10.8	12.0	16.6	13.2	14.6	14.0	12.7
Eu	10.8	11.8	9.60	12.3	10.7	11.1	10.5	9.45
Gd	38.1	34.0	33.2	38.4	40.7	39.3	37.7	34.3
Dy	40.4	44.1	38.6	31.5	66.5	55.0	78.9	83.0
Er	49.0	49.7	41.3	14.4	65.9	49.3	82.4	122
Yb	56.2	51.4	55.1	10.1	61.4	41.9	80.8	125
Lu	51.0	53.9	54.4	17.9	46.6	45.6	67.3	106

Continuation of Table 1.

Elements	Czo amphibolite (KHi008D)				
	22 core	23 middle	24 middle	25 rim	27 rim
La	0.01	b.d.l.	-	-	-
Ce	0.02	0.02	0.03	0.03	0.02
Pr	b.d.l.	-	b.d.l.	b.d.l.	n.d.
Nd	0.06	0.03	0.04	0.07	0.03
Sm	0.08	0.15	0.11	0.12	0.12
Eu	0.06	0.04	0.06	0.08	0.05
Gd	0.81	1.01	1.09	1.09	1.44
Tb	0.41	0.46	0.48	0.52	0.55
Dy	4.86	5.25	6.10	6.30	6.56
Ho	1.56	1.61	1.71	1.98	2.16
Er	6.50	6.81	7.59	8.73	9.46
Yb	8.76	8.66	9.64	11.3	13.4
Lu	1.12	1.25	1.24	1.45	1.73

Table 2. The content of rare earth elements in amphiboles from the rocks of Khitoostrov (ppm)

Elements	Grt amphibolite after gabbro (Khi004)		Crn-metasomatite (KHI-010-5)				
	Cam		Cam			Na-Ged	
	1	6	18	22	23	29	19
La	3.78	2.27	7.7	15.7	10.2	0.49	0.03
Ce	4.44	2.99	27.8	42.3	28.9	0.55	0.06
Pr	5.29	3.80	76.5	80.8	65.9	0.39	0.07
Nd	5.62	5.41	147	126	125	0.43	0.23
Sm	5.86	8.22	204	163	213	1.67	0.76
Eu	12.6	13.2	87.8	73.2	83.0	1.02	0.02
Gd	7.37	7.86	145	109	143	3.62	0.46
Dy	6.69	7.87	44.8	34.2	53.8	3.46	2.91
Er	6.03	7.35	15.4	11.3	25.1	4.18	3.84
Yb	4.39	5.56	14.2	7.40	21.5	3.81	4.68
Lu	5.21	7.44	23.4	19.9	31.4	4.59	4.08

Continuation of Table 2

Elements	Czo amphibolite (KHi008D)		
	Cam1	Cam2	
	18	31	35
La	0.31	0.04	0.03
Ce	0.87	0.06	0.04
Pr	0.21	0.01	0.02

Nd	1.85	0.21	0.18
Sm	0.82	0.36	0.17
Eu	0.29	0.14	0.15
Gd	1.64	1.20	1.47
Tb	0.28	0.50	0.61
Dy	2.18	6.31	8.87
Ho	0.44	2.23	2.66
Er	1.54	9.16	10.9
Yb	1.58	12.2	13.6
Lu	0.22	1.51	1.77

Table 3. The content of rare earth elements in plagioclase from the rocks of Khitoostrov (ppm)

	Grt amphibolite after gabbro (Khi004)		Crn-metasomatite (KHI-010-5)		Czo amphibolite (Khi008D)	
Elements	7	8	15	26	19	20
La	0.37	0.27	7.55	3.88	0.02	0.03
Ce	0.18	0.15	6.68	3.19	0.03	0.03
Pr	0.09	0.06	5.53	2.60	-	0.01
Nd	0.06	0.05	4.88	2.96	b.d.l.	0.04
Sm	0.14	-	1.96	0.98	b.d.l.	0.02
Eu	2.33	2.52	18.2	18.1	0.05	0.09
Gd	0.16	0.10	-	0.40	0.03	0.02
Tb	-	-	-	-	-	0.01
Dy	0.12	0.25	0.07	0.15	0.03	0.03
Ho	-	-	-	-	0.02	0.01
Er	0.22	0.11	0.55	0.59	0.04	0.02
Yb	0.09	0.22	0.13	0.16	b.d.l.	0.02
Lu	0.31	-	-	-	b.d.l.	b.d.l.

Table 4. The content of rare earth elements in biotite from the rocks of Khitoostrov (ppm)

	Crn-metasomatite (KHI-010-5)			Czo amphibolite (Khi008D)	
Elements	21	27	28	28	34
La	13.9	7.35	6.22	2.28	2.23
Ce	2.19	1.07	0.35	0.05	0.07
Pr	1.83	0.98	0.39	0.01	0.01
Nd	1.69	0.77	0.22	0.06	0.05
Sm	0.84	0.32	0.63	0.10	0.19
Eu	-	-	-	n.d.	n.d.
Gd	0.45	0.07	0.23	b.d.l.	0.03
Tb	-	-	-	0.03	0.01
Dy	1.86	1.93	2.16	0.91	0.90
Ho	-	-	-	0.82	0.80

Er	0.84	1.8	1.78	0.39	0.24
Yb	0.08	0.35	0.22	0.06	0.04
Lu	1.08	0.64	1.06	0.03	0.03

Table 5. Content of rare earth elements in clinozoisite and titanite from clinozoisite amphibolites of Khitoostrov (ppm)

	Czo amphibolite (Khi008D)				
	Czo			Ttn	
Elements	29	30	36	32	33
La	0.01	1.67	0.02	11.1	7.41
Ce	0.02	7.55	0.07	65.6	33.6
Pr	n.d.	1.89	0.02	15.1	8.60
Nd	0.05	12.0	0.25	107	58.7
Sm	0.27	6.56	0.48	48.1	23.6
Eu	0.18	3.90	1.93	7.68	5.87
Gd	0.09	13.3	2.79	55.6	25.9
Tb	0.06	2.81	1.74	-	-
Dy	1.14	31.7	26.6	58.7	37.2
Ho	0.63	8.73	9.55	-	-
Er	5.14	36.2	45.2	17.0	11.0
Yb	14.3	45.8	58.2	10.2	6.72
Lu	1.89	5.27	6.63	2.60	1.85

Table 6. The content of trace elements in rutile from the rocks of Khitoostrov (ppm)

	Crn-metasomatite (KHI-010-5)		Czo amphibolite (Khi008D)	
Elements	14	20	21	26
Cr	1900	844	647	663
Fe	1470	996	2760	3667
Zr	470	624	457	413
Mo	56.7	37.7	49.9	52.3
Sb	0.187	0.156	0.64	0.39
Ta	84.3	39.3	57.44	73.0
Th	0.0163	0.00595	0.03	0.07
U	14.9	15.3	0.03	0.10
W	0.81	0.765	72.2	63.4
Hf	14.5	17.2	6.04	5.78
Sn	27.1	27.8	13.8	17.2
Nb	2840	815	2196	3046
Mn	6.74	3.08	11.3	24.2
V	2080	1590	1736	1349
Al	129	60.5	166	381

Table 7. The content of rare and rare earth elements in apatite from the rocks of Khitoostrov, ppm

	Rocks						Lower Limits
	Ky-Grt-Bt gneiss	Grt amphibolite	Crn rock	Crn rock	Crn rock	Plagioclasites	
Elements	Ch-1	KHI-004	Ea16-005I	KHI-008A	KHI-010	Ea16-005II	
Cr	159	24.0	1.39	18.2	108	68.2	1
Sr	124	267	302	252	260	251	1
Y	462	246	269	116	193	155	0.1
Nb	0.87	96.6	1.62	53.5	34.4	8.50	0.5
Ba	45.4	12.3	10.1	23.6	33.9	23.6	3
La	179	91.1	2392	549	646	460	0.01
Ce	255	143	2925	636	784	760	0.01
Pr	334	191	3105	748	963	1045	0.01
Nd	413	229	2891	916	1182	1259	0.01
Sm	660	293	1902	1209	1392	1007	0.005
Eu	137	269	466	216	302	271	0.005
Gd	735	254	1036	745	910	555	0.01
Tb	832	281	572	321	521	329	0.005
Dy	535	215	291	122	231	159	0.01
Ho	337	170	182	68	128	110	0.005
Er	224	125	132	47.7	75.5	69.5	0.01
Tm	160	89.4	102	36.1	51.0	49.8	0.005
Yb	129	65.9	95.9	42.0	48.2	43.8	0.01
Lu	104	46.9	76.0	35.4	41.3	34.6	0.005
Hf	2.12	8.23	4.70	9.2	3.41	1.99	0.01
Ta	0.12	15.4	0.19	0.76	0.60	0.42	0.1
Pb	5.63	4.35	11.0	13.1	7.72	9.04	1
Th	3.85	3.50	27.5	44.9	16.2	2.28	0.1
U	19.6	18.9	105	42.2	60.9	58.1	0.1
LREE	532	295	4320	1216	1507	1431	
REE	935	457	4681	1432	1802	1625	
HREE+Y	865	408	630	333	488	349	
Sr/Y	0.27	1.09	1.12	2.17	1.35	1.62	
La/Sm	0.42	0.48	1.95	0.7	0.72	0.71	
Mn	201	132	132	68.9	71.3	41.0	
Mn/Sr	1.62	0.49	0.44	0.27	0.27	0.16	
Eu/Eu*	0.20	0.98	0.32	0.22	0.26	0.35	
Ce/Ce*	0.99	1.02	1.06	0.98	0.98	1.01	

Appendix 5.

Table 1. Microthermometric data for fluid inclusions from corundum-bearing rocks of the Khitoostrov occurrence, North Karelia

Sample	Rock	Mineral	Type	Tml	Tmf	wt% NaCl	wt% $CaCl_2$	X_{NaCl}	X_{CaCl2}
B752-9	Garnet-biotite plagioclasite	Garnet	ps (H_2O) L with calcite	-44	-39	2.37	26.02	0.01	0.06
				-47	-37	1.95	25.69	0.01	0.05
				-47	-32	1.83	24.05	0.01	0.05
				-45	-36	2.15	25.21	0.01	0.05
				-42	-36	2.62	24.87	0.01	0.05
				-45	-33	2.07	24.23	0.01	0.05
				-46	-35	2.01	24.98	0.01	0.05
				-44	-32	2.17	23.78	0.01	0.05
				-42	-32	2.48	23.53	0.01	0.05
				-45	-34	2.1	24.56	0.01	0.05
				-47	-35	1.91	25.06	0.01	0.05
				-46	-36	2.03	25.3	0.01	0.05
				-44	-34	2.23	24.46	0.01	0.05
				-42	-32	2.48	23.53	0.01	0.05
				-40	-30.5	2.82	22.67	0.01	0.05
B 755-1	Garnet-biotite plagioclasite	Garnet	ps (H_2O) L	-47	-34	1.88	24.73	0.01	0.05
KHI-010	Crn-rock	Garnet	ps (H_2O) L with calcite	-38	-29	3.28	21.7	0.01	0.04
				-44	-36	2.29	25.11	0.01	0.05
				-41	-24	2.32	20.35	0.01	0.04
				-40	-38	3.13	25.15	0.01	0.05
				-48	-32	1.74	24.12	0.01	0.05
B 745-10	Leucocratic corundum-bearing garnet-biotite-plagioclase rock with St	Garnet	ps (H_2O) L with calcite?	-46	-36	2.03	25.3	0.01	0.05
				-45	-29	1.95	22.8	0.01	0.05
				-46	-34	1.98	24.65	0.01	0.05
				-45	-33	2.07	24.23	0.01	0.05
				-48	-26	1.58	21.88	0.01	0.04
				-44	-34	2.23	24.46	0.01	0.05
				-47	-32	1.83	24.05	0.01	0.05
				-45	-30	1.98	23.16	0.01	0.05
				-44	-35	2.26	24.79	0.01	0.05

				-47	-31.8	1.82	23.98	0.01	0.05
				-48	-31.6	1.73	23.98	0.01	0.05
B 750-5	Melanocratic kyanite-garnet-plagioclase-biotite rock with Crn	Garnet	ps H_2O	-44	-32	2.17	23.78	0.01	0.05
				-51	-30	1.48	23.57	0.01	0.05
				-53	-38				
		Plagioclase	s? H_2O	-35	-17	3.35	15.83	0.01	0.03
				-30	-13.4	5.12	11.75	0.02	0.02
				-34	-10	2.73	11.37	0.01	0.02
				-30	-14	5.25	12.05	0.02	0.02
				-30	-12.9	5.	11.48	0.02	0.02
				-25	-17	11.33	8.27	0.04	0.02
				-21	-11				
				-19	-13				
				-20	-13				
				-29	-10	4.81	9.24	0.02	0.02
				-27	-13	7.32	9.27	0.03	0.02

Note: Tml is the eutectic temperature, Tmf is the melting point of ice.